University of Cyprus
Department of Civil and Environmental Engineering

MSc Thesis

SPATIAL DISTRIBUTION OF WINKLER SPRING STIFFNESS FOR THE STRUCTURAL ANALYSIS OF EMBEDDED RECTANGULAR MAT FOUNDATIONS

by

ANDREA LEONIDOU

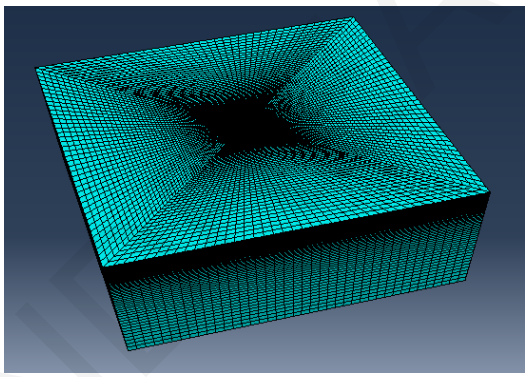

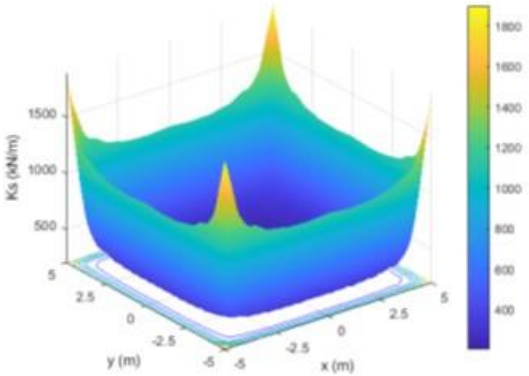

MAY 2021

SPATIAL DISTRIBUTION OF WINKLER SPRING STIFFNESS FOR THE STRUCTURAL ANALYSIS OF EMBEDDED RECTANGULAR MAT FOUNDATIONS

MSc Thesis

by

ANDREA LEONIDOU

SUPERVISOR

DIMITRIOS LOUKIDIS, Associate Professor

Department of Civil and Environmental Engineering

University of Cyprus

EXAMINATION COMMITEE

PANOS PAPANASTASIOU, Professor

Department of Civil and Environmental Engineering

University of Cyprus

DIMOS CHARMPIS, Associate Professor

Department of Civil and Environmental Engineering

University of Cyprus

DIMITRIOS LOUKIDIS, Associate Professor

Department of Civil and Environmental Engineering

University of Cyprus

To my parents Konstantino and Thekla

and to my little girl Vasiliki who came

into the world very recently

ACKNOWLEDGEMENTS

I would like to thank the supervising professor of my Master's Thesis, Dr. Dimitrios Loukidis, for the continuous guidance and assistance he provided me, as well as for the excellent cooperation throughout the research. I would also like to thank the members of the three-member examination committee, Dr. Panos Papanastasiou and Dr. Dimos Charmpis, for the time they allocated for the evaluation of my dissertation.

Finally, I would like to thank my parents, my sisters and brother, Irini, Styliani and Theodoros, as well as the father of my child for their support, encouragement and advices during my studies at the University of Cyprus.

SUMMARY

The topic of the present dissertation is the structural analysis of mat foundations. A mat foundation is a type of shallow foundation in the form of a single large concrete slab. This research examines the appropriate spatial distribution of Winkler spring stiffness for the static analysis of mat foundations with and without embedment based on the pseudo-coupled method. Three-dimensional finite element parametric analyses were performed with the software Abaqus to calculate the settlements and deflections of a mat resting on an elastic continuum representing the ground. The settlement values are then entered into an algorithm that determines the corresponding equivalent Winkler spring stiffness values at each mat node by solving the spring-supported plate problem inversely. Based on these results, a general equation is proposed for determining the distribution of Winkler spring stiffness coefficients for rectangular mat foundations which takes into account the effects of foundation embedment and soil stiffness variation with depth. It is shown that the use of the proposed equation in the analysis of mat foundations produces more accurate results than the Winkler spring stiffness distributions widely used in practice, which lead to non-conservative estimates of bending moments.

Table of Contents

CHAPTER 1: INTRODUCTION

1.1 Foundation types

Geotechnical engineering is the branch of civil engineering that takes into account the behavior of earth materials. It has also applications in military, mining, petroleum and other engineering disciplines. A major branch of geotechnical engineering is foundation engineering. Nowadays, in the island of Cyprus there is a rampant development of high-rise buildings, a fact that renders the highly accurate and reliable foundation design an absolute necessity**.** In the case of tall structures, engineers usually apply mat or pile foundations because of the high loads that must be transferred to the ground.

Generally, there are two categories of foundations: shallow and deep foundations (piles). The first category consists of three types of foundations, the isolated footings (Figure 1.1a), the combined and strip footings (Figure 1.2b) and the mat foundations (Figure 1.1c).

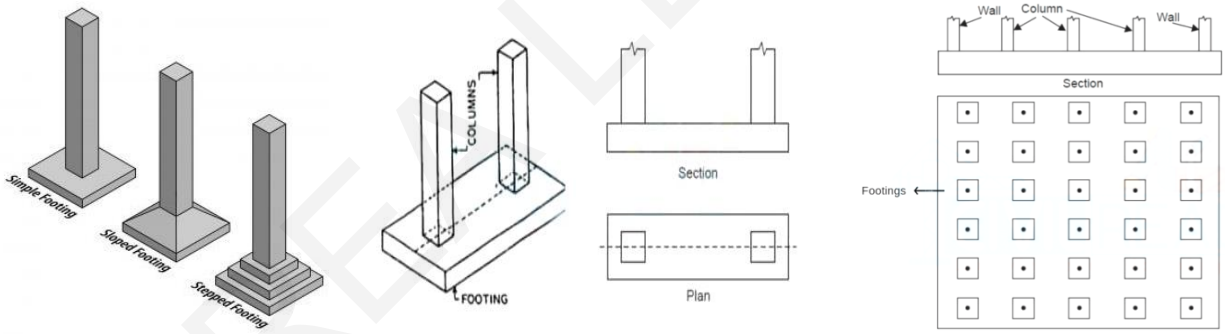

(a) (b) (c)

Figure 1.1: Types of shallow foundations: (a) isolated footing, (b) combined footing, (c) mat foundation (source: https://civilread.com/different-types-footings/)

Isolated footing is a form of spread foundation in the form of a rectangle, square or sometimes circular concrete 'pad' that supports localized single-point loads such as structural columns. This load is then spread by the pad to the bearing layer of soil or rock below.

Combined footings are preferred when the distance between two columns is small or when one column is close to a property line or sewer pipe. In the latter case, the center of gravity

of the column on the horizontal plane will not coincide with that of an isolated footing. In such cases, it is necessary to combine this footing with that of an adjacent internal column. The combined footing may be rectangular, trapezoidal or T-shaped in plan view. Strip footings support an entire row of the building columns and can be constructed in both horizontal directions, thus forming a grid of foundation beams. It is important to note that combined and strip footings reduce the possibility of differential settlements that can lead to problems of functionality and integrity of the building.

Mat foundations are the third and most massive type of shallow foundations. The mat foundations are large concrete slabs which can support all the vertical members of the superstructure. The thickness of the slab depends on the superstructure loads and usually falls in the 0.5m-2m range. The larger the superstructure loads are, the larger the thickness of the slab has to be. This type of foundation is often used in residential buildings, public buildings, tanks, water towers and silos. The mat foundation is the preferred type of foundation in the following cases (Coduto, 2011):

- Mat foundations are preferred when the loads of the structure are too large or the soil below is too soft and of low bearing capacity, and thus the footings must be extremely big. Generally, when the footings occupy a surface more than 50% of the whole planar area of the structure, then the most economical solution is that of the mat foundation (Salgado, 2008).

- Another reason for choosing this type of foundation is the rigidity that it offers, which reduces the possibility of differential settlement due to variation of the loads that are carried by nearby columns or because of lateral non-homogeneity of the ground. This way, cracking and other serious problems, like damage of underground pipes, are avoided.

- When swelling clays are present, such as the case of the Nicosia marl, causing differential heave of the ground when it gets wet and differential settlement when it loses moisture. As a result, structures supported by isolated or strip footings on swelling soils face serious problems in their lifetime. Hence, engineers often choose to exploit the rigidity of the mat foundation and mitigate these problems to a significant extent.

- Underground water conditions also play a significant role in the choice of the foundation type. During the excavation at the site, part of the soil profile may be below the water table. In this case, the ground water will seep into the building if the building is not waterproofed properly. The mat foundation can protect the

building from the ground water by using a waterproofing membrane which can be placed very easily to the site right underneath the mat. In addition, the weight of the mat foundation resists the hydrostatic loads of the underground water.

- It is also worth mentioning that mat foundations are the most commonly used shallow type of foundations nowadays in Cyprus, since they save time and money. They save time because formwork is applied more easily in contrast to the other two types of shallow foundations, and they save money since less workhours are needed.

1.2 Mat structural analysis

The structural design of mat foundations is based on the calculation of the settlements and internal forces (moments and shear forces) of the whole slab. So far, many methods are available for mat design, which can be separated in two categories: the ‘‘rigid’’ and the ‘‘non-rigid’’ methods of analysis.

The rigid methods approach the problem in a rather simplistic way. These methods assume that the mat foundation does not flex at all and, hence, its settlement is uniformly distributed. For the calculations of the internal shear forces and moments of the slab, it is assumed that the distribution of contact pressure under the mat foundation is also uniform (Figure 1.2a) and its magnitude depends solely on the loads that are applied to the slab by the columns and the self-weight of the slab. The structural analysis is based on that of a bending member in which there are reaction supports (hinges) at the positions of columns and the uniform contact pressure is considered as an external load. This method, although simple and fast, is known to be very inaccurate for mat foundations and is thus nowadays abandoned. The rigid method, with its consideration of uniform distribution of contact pressure, is acceptable for the structural design of isolated footings, in which case ratio of width to thickness is small enough (Coduto, 2001).

On the other hand, “non-rigid” methods are more accurate and realistic in predicting the stresses and deformations of mat foundations. This happens because during the analysis the deformations of the mat foundations and the effect that they have on the distribution of the contact pressure, which in reality is not uniform (Figure 1.2b), are taken into account. However, the disadvantage of non-rigid methods is that they are more computationally complicated, since they consider the interaction between the soil and the foundation.

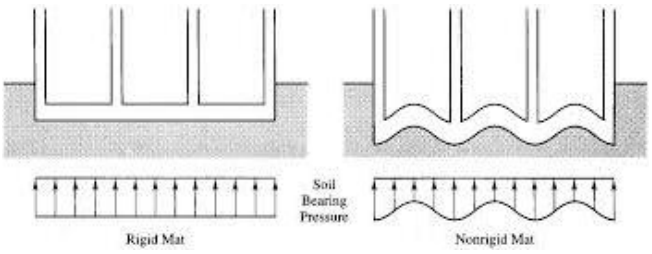

(a) (b)

Figure 1.2: Distribution of contact pressure: (a) for rigid method of analysis, (b) for non-rigid method of analysis (source: Coduto 2001)

The interaction between the soil and the mat can be modeled using the concept of the coefficient of vertical subgrade reaction k_s, which is simply expressed as:

$$k_s = \frac{q}{\delta} \tag{1.1}$$

where:

k_s = coefficient of vertical subgrade reaction (kN/m^3)

q = vertical pressure applied to the soil (kPa)

δ = deflection resulting from the application of q (m)

The coefficient of vertical subgrade reaction multiplied by the influence area of a mat node gives the stiffness coefficient K_{el} of a vertical linearly elastic spring, known as Winkler spring, connected to the specific node (Winkler, 1867). Winkler springs have been used for many decades for the simulation of the interaction between the soil and the foundation elements.

The calculation of the coefficient of vertical subgrade reaction is not simple because k_s is not a fundamental property of the soil like the Young modulus. It is a function of the stiffness parameters of the soil (i.e. the elastic constants), but depends also on the geometrical characteristics of the foundation (Coduto, 2001).

More specifically, the magnitude of k_s is affected by the following parameters:

- The shape of the loaded surface. For example, a mat foundation with one dimension much larger than the other distributes its stresses with depth through the soil differently from a square mat foundation (Figure 1.3).

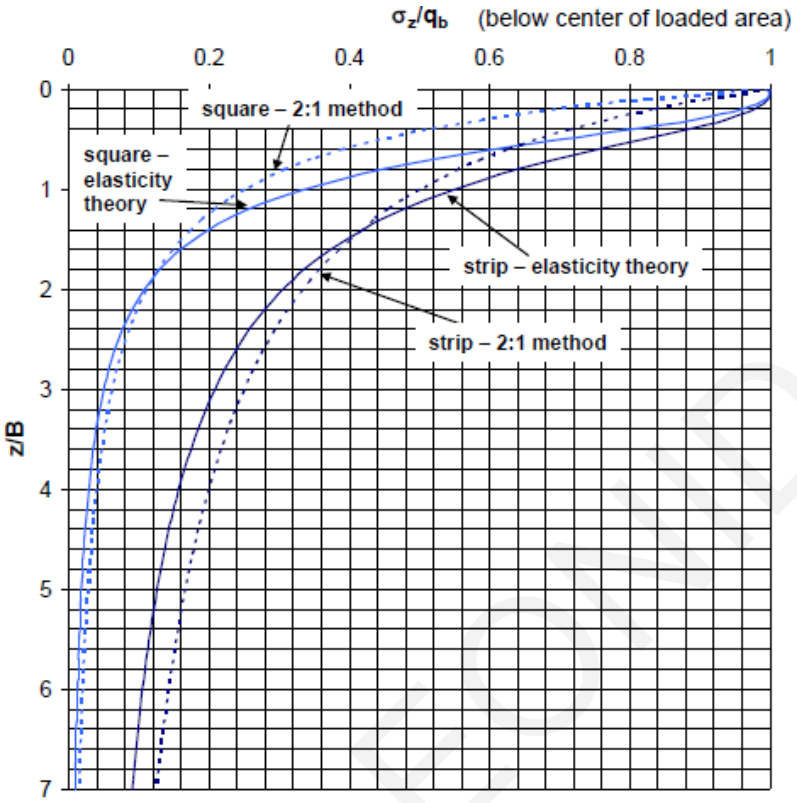

Figure 1.3: Stress distribution below center of loaded area of different shapes.

- The width of the loaded surface. A mat foundation with large width will develop larger settlement than another with smaller width, for the same average contact pressure. So, the larger the mat width is, the smaller the coefficient of vertical subgrade reaction k_s.

- The depth of the loaded surface below the surface of the ground, i.e. the foundation embedment. As the foundation depth from the ground surface increases, the settlement becomes smaller and therefore the vertical subgrade reaction k_s is larger.

- The position along the mat foundation. Researchers have pointed out that k_s is smaller at the center of the mat and larger near its edges (Ulrich, 1991; Bowles, 1996; Coduto, 2001; Loukidis & Tamiolakis, 2017). The present thesis examines in particular this aspect.

- The time and the type of the soil. If below the mat foundation there is a soft soil (e.g. normally consolidated clay), consolidation settlements will develop in the long term. Taking into account both long- and short-term settlements would render k_s smaller.

1.3 Objective of thesis

The aim of this Master's thesis is the determination of the proper spatial distribution of the stiffness coefficient K_{el} of Winkler springs below a mat foundation and its dependence on several parameters such as the foundation embedment, the increase of the Young's modulus of the soil with depth, the dimensions of the foundation, the Poisson's ratio, the column load distribution, and the thickness of the deformable soil layer. Moreover, the case of a two-layered soil profile with different Young's modulus values is examined. For that purpose, series of finite element analyses were carried out to examine the influence of the aforementioned parameters. This was done by using the commercial finite element software Abaqus to calculate the settlements and deflections of mat foundations and then using a MATLAB script to back-calculate the stiffness coefficient K_{el} of the equivalent Winkler springs.

At the end, these results were used to derive an equation for the calculation of the appropriate stiffness coefficient K_{el} at any point of the mat foundation that would allow to calculate with accuracy the internal moments and forces during the structural design. It is worth mentioning, that although many researchers have examined rigid foundations, very few studies have dealt with the determination of stiffness coefficient K_{el} for non-rigid foundations. Chapter 2 presents information for the existing methods for the design of mat foundations and pertinent concepts. Chapter 3 presents the methodology that was followed in order to perform the analysis with the finite element method in Abaqus and the back-calculation of Winkler springs in Matlab. In Chapter 4, the results of the analyses are presented in detail, processed and discussed. Finally, Chapter 5 summarizes the main conclusions and outcomes of this research effort.

CHAPTER 2: KNOWLEDGE BACKGROUND

Mat foundations (also called raft foundations) are nowadays the most common type of foundation in Cyprus that structural engineers design for residential and office buildings, both high- and low-rise. However, scanning through the international technical literature, one notices that the designer of raft foundations has very little information readily available on how to properly perform analysis for the estimation of differential settlements and bending moments, in contrast with other geotechnical and structural topics. This chapter presents the methods which have been proposed so far for the analysis of mat foundations, along with pertinent research studies.

2.1 Semi-analytical studies of rectangular rafts

Semi-analytical methods are the most accurate methods available and, hence, they are presented first in this Chapter. These methods exploit well-known analytical solutions from the Theory of Elasticity in order to calculate the support reaction provided by the soil. Nonetheless, they lack versatility and are so far used in research studies.

The first satisfactory solutions for square rafts of arbitrary flexibility were obtained by Cheung and Zienkiewicz (1965). The stiffness of the soil was derived based on the Boussinesq equation and was combined with the plate bending finite elements to form a stiffness matrix for the whole system. The method of Cheung and Zienkiewicz (1965) was improved by Svec and Gladwell (1973) by assuming a continuous contact pressure distribution, which was given by a third degree polynomial below each plate finite element.

Wardle and Fraser (1974) extended the approach of Cheung and Zienkiewicz (1965) to a multi-layered soil system, investigating also the effects of a finite homogeneous soil layer and a soil modulus that increased linearly with depth. They programmed their method in a computer program named FOCALS (Wardle and Fraser, 1975). The computer program performs a static elastic analysis of rafts of arbitrary rigidity and variable thickness resting on a layered soil mass. By using integral transform techniques and therefore a semi-analytical solution for the soil (Gerrard and Harrison, 1971), the ground surface settlements due to uniformly loaded rectangular areas are obtained, and then the surface element stiffness matrix is derived. The accuracy of the solutions was found to depend markedly on the degree of discretization used (Fraser and Wardle, 1976). The effect that varying the

number of plate elements has on the convergence in terms of displacements and bending moments is illustrated in Fig.2.1 for a rigid square raft on a semi-infinite soil mass.

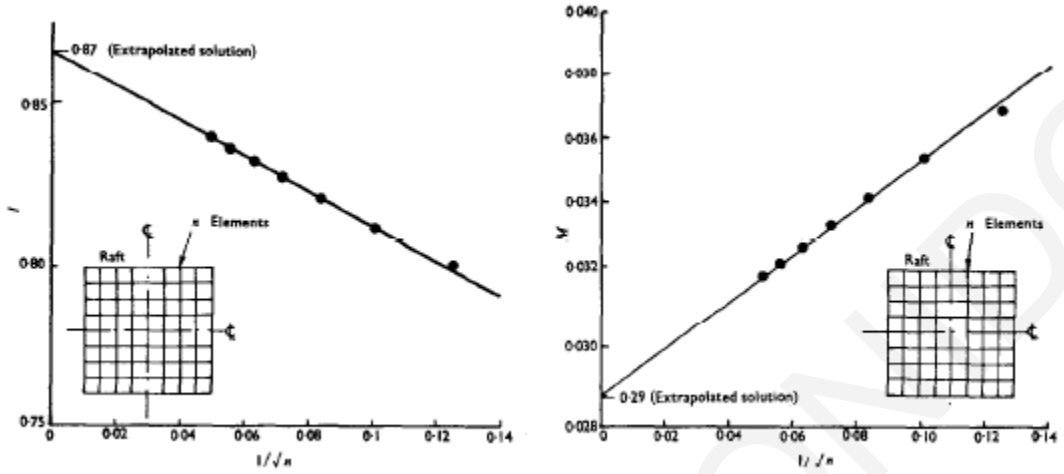

(a) (b)

Figure 2.1: Convergence of solution for rigid square raft: (a) settlement and (b) maximum bending moment (from Fraser & Wardle, 1976).

In the above charts, the results are plotted with respect to $n^{-1/2}$, where *n* is the number of plate elements discretizing the mat. For n>10000 ($n^{-1/2} < 0.01$), the exact solution for both settlement and maximum bending moment is practically attained (error less than 1%).

According to Fraser and Wardle (1976), the relative stiffness between the mat and the supporting soil can be quantified by the following factor:

$$K = \frac{4}{3} \times \frac{E_r(1-\nu_s^2)\times t^3}{E_S\times(1-\nu_r^2)\times b^3} \tag{2.1}$$

where E_r is the modulus of elasticity of the raft material, ν_r is the Poisson's ratio of the raft material, E_s is th modulus of elasticity of the soil, ν_s is the Poisson's ratio of the soil, *t* is the raft thickness and *b* is the raft width.

The settlements ρ of a foundation are traditionally calculated using an equation of the following form:

$$\rho = pb\frac{(1-\nu_s^2)}{E_s} I \tag{2.2}$$

where *p* is the applied contact pressure (assumed uniform) and *I* is the influence factor. Fraser and Wardle (1976) provide solutions for the factor *I* for the center (point A), the edge midpoint (point B) and the corner (point C) of a uniformly loaded square mat for various relative stiffness values (Fig. 2.2). It can be seen that as the relative stiffness factor *K* increases, the settlement becomes the same at the three characteristic points, while as *K* approaches zero, the settlement at the center of the mat tends to become double that at the corner (as expected based on the Theory of Elasticity).

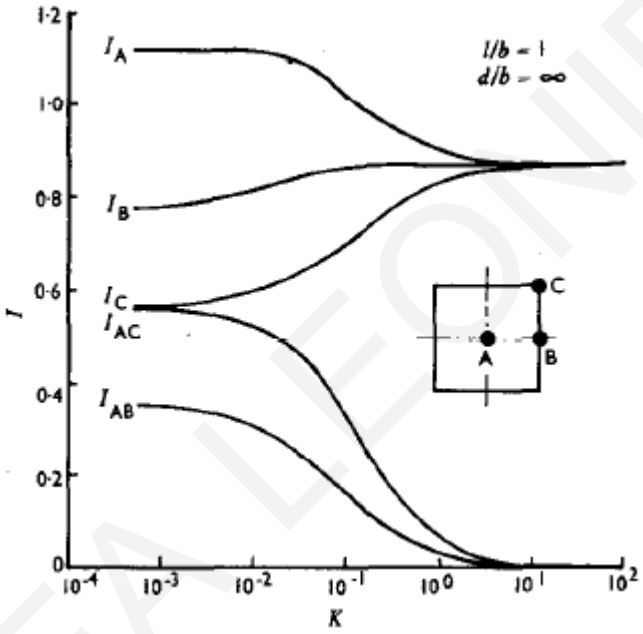

Figure 2.2: Settlement influence factor I for square mat on elastic half-space (from Fraser & Wardle, 1976).

Fig. 2.3 gives the factor *M* for the estimation of the maximum bending moment *m* per unit width using the equation

$$m = plbM \tag{2.3}$$

where *l* is the raft length.

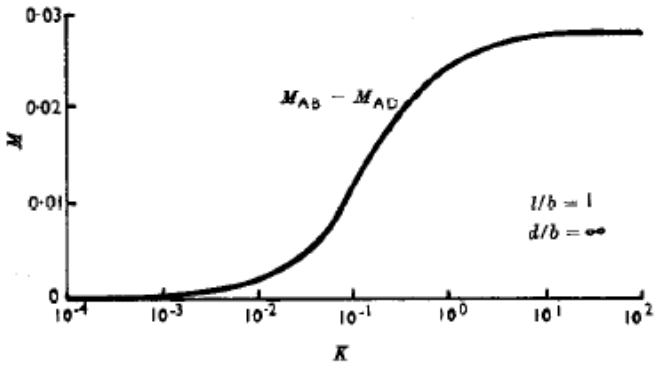

Figure 2.3: Bending moment influence factor M for square mat on elastic half-space (from Fraser & Wardle, 1976).

Fraser & Wardle (1976) provide charts also for length to width ratio equal to 2. In case the soil is not assumed to extend infinitely with depth (i.e. elastic half-space) but has a finite thickness *d*, the settlement is calculated by multiplying the settlement for the case of an elastic half-space with a correction factor *S*:

$$\rho = S\rho^{sI} \tag{2.4}$$

where ρ^{sl} is the displacement for an elastic half-space calculated using eq. (2.2). Similarly, the maximum bending moment is given by:

$$m = Rm^{sI} \tag{2.5}$$

where m^{sl} is the maximum bending moment in the case of the elastic half-space and *R* is a correction factor accounting for the effect of the finite layer thickness *d.* The correction factors are shown in Fig. 2.4.

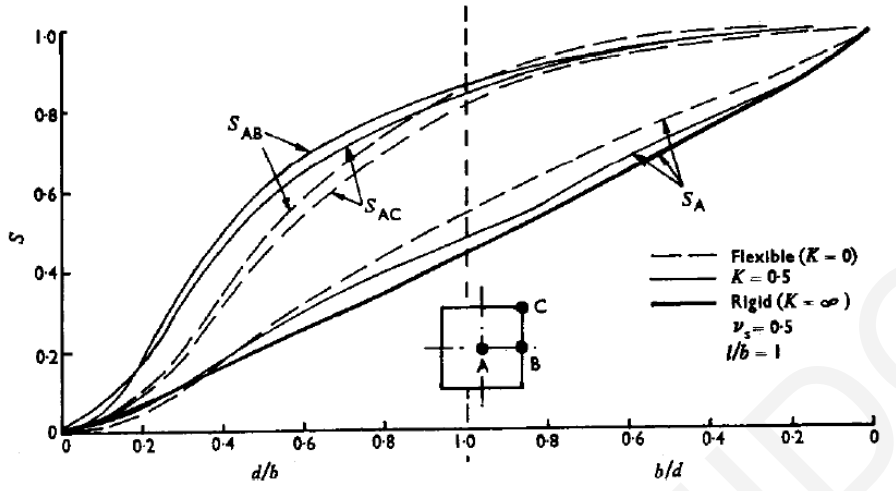

(a)

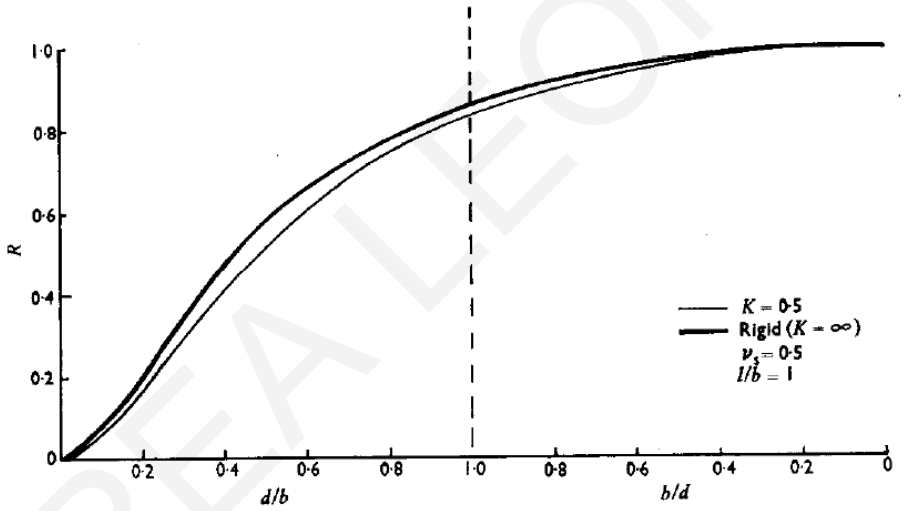

(b)

Figure 2.4: Settlement (a) and moment (b) correction factors for square mat on soil layer with finite thickness and ν_S=0.5 (from Fraser and Wardle, 1976).

Chow (1987) extended the work of Fraser and Wardle (1976) to the case of a mat foundation of an arbitrary shape. Moreover, he improved the computational efficiency of the methodology, allowing to attain the necessary accuracy with a smaller number of elements, thus reducing the required computational cost.

2.2 Winkler spring method

Winkler springs (Winkler, 1867) constitute the oldest available method, which has been used for many decades for the simulation of the interaction between the soil and the foundation. The Winkler spring stiffness coefficient K_{el} can be obtained by multiplying the coefficient of vertical subgrade reaction with the influence area of the mat node to which the spring is attached (Fig. 2.5).

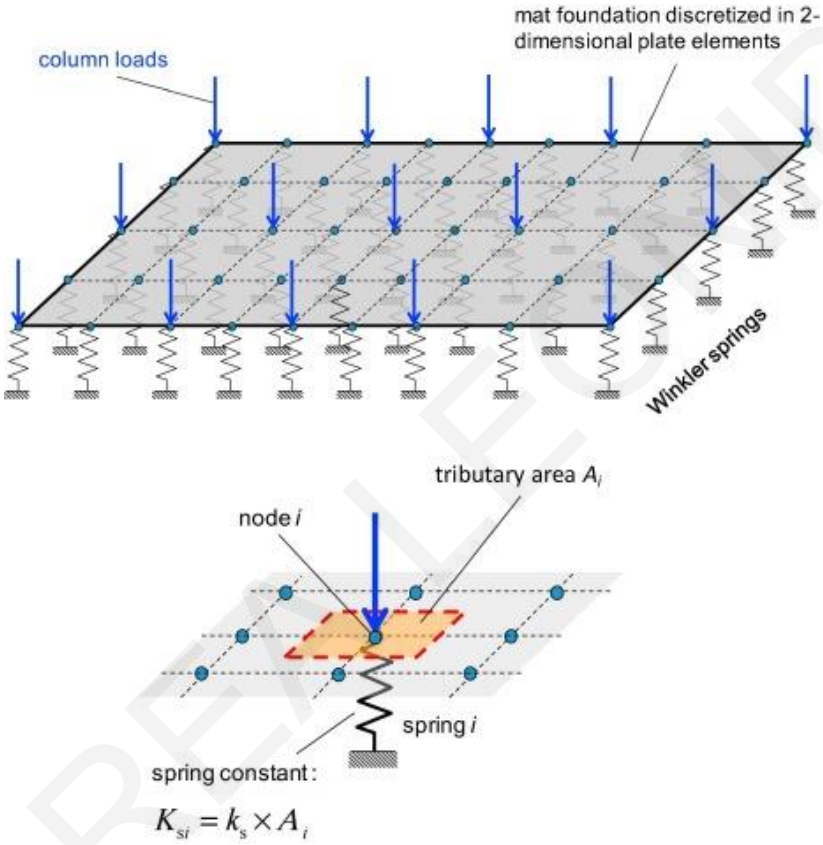

Figure 2.5: Winkler springs below mat foundation for the simulation of soil-foundation interaction (from Loukidis and Tamiolakis, 2017)

Ideally, an infinite number of springs should be used under the base of the foundation. However, for the practical purposes of a structural model, there will be only a finite number of springs (Horvath and Colasanti, 2011) which depends on the mat discretization in plate of shell elements. The Winkler spring method is easy to implement in a structural analysis model, as it requires to simply attach linear springs to the foundation nodes. The springs are only affecting the structure in the vertical direction. Winkler's method assumes that every

single spring acts independently from the others. In a static analysis of a structure, the approach of using Winkler springs is definitely an improvement to the rigid method, since the Winkler spring method is able to predict the fact that the contact pressure under the columns is larger than in the midspans. However, the classical Winkler spring method is still far away from the reality of the interaction between the mat foundation and the soil. This happens because of the assumed independence between the springs, i.e. the force which is developed inside the spring depends only on the settlement of the slab at the point where the spring is connected. In reality, due to the shear stiffness and resistance of the soil, the reaction that the soil offers at a given location under the mat depends also on the settlement of the neighboring points. This effect is particularly strong near the perimeter of the mat. So, in fact, the springs should not act independently but they should be coupled. Using coupled springs in a model means that the contact pressure, which is applied at a point i of the mat foundation must cause settlement not only at the point i but also at the nearby points (i+1, i-1, etc.) of the soil, even if these points lie outside the area covered by the mat .

The drawback of the uncoupled Winkler spring method can be clearly illustrated through the example of a very flexible mat loaded by uniform pressure and overlying a completely uniform soil. In that case, the uncoupled Winkler spring method predicts that the settlement of the slab will be uniform, i.e. there will be no differential settlements at all. It is well known from the theory of elasticity that the settlement at the center of a uniformly loaded area will be substantially larger than that at the edges. This happens because the stresses that develop inside the soil below the central region of the loaded area are bigger than those at the edges, as depicted by the stress bulb. Therefore, in order to represent correctly the settlement distribution of a very flexible mat, either the springs need to be somehow coupled or the coefficient of vertical subgrade reaction k_s near the perimeter of the mat must be considered to be larger than at its center. In other words, in the latter approach, which is called pseudo-coupled Winkler spring method, the k_s values are increased near the edges of the slab, so that the settlements at these points will be smaller than those at the center.

The independence of the springs that the classical Winkler's method considers leads also to errors in the calculations of the internal forces, i.e. moments and shear forces (Horvilleur & Patel 1995). These facts were recognized by several researchers, leading to the development of either fully coupled methods or pseudo-coupled approaches.

2.3 Coupled springs method

The coupled springs method constitutes a significant improvement over the classical Winkler spring approach. By interrelating the soil reaction of one node to the settlements at the neighboring nodes, the coupled approach is like having both vertical and diagonal springs (Fig. 2.6).The most direct and obvious effect of coupling versus non-coupling is that a coupled springs analysis of a flexible uniformly loaded mat will produce a dishing profile across the slab (as opposed to the constant settlement in the absence coupling).

Nonetheless, the actual mathematical formulation of the coupled models is quite more complex than the simple schematic of Fig. 2.6. Moreover, it is not clear how their input parameters should be established by the engineer based on standard soil properties (Coduto 2001).

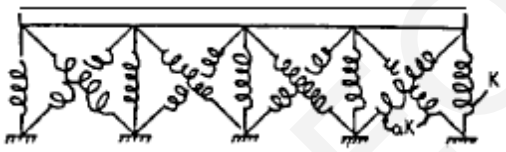

Figure 2.6: Coupled springs (source: ACI Committee 336).

An example of coupled methods are the multi-parameter models (Horvath, 2002). In the multiple parameter models the variation in the coefficient of subgrade reaction does not have to be assumed beforehand. The reason is that the soil shear (spring coupling) that is inherently missing from Winkler hypothesis is incorporated explicitly in the mathematical formulation (even in the simplest multiple-parameter models). For example, the model by Horvath (2002) relies on the following general equation:

$$\mathrm{p(x,y)} - \mathrm{c_{p1}}\nabla^2\mathrm{p(x,y)} + \mathrm{c_{p2}}\nabla^4\mathrm{p(x,y)} = \mathrm{c_{w1}w(x,y)} - \mathrm{c_{w2}}\nabla^2\mathrm{w(x,y)} + \mathrm{c_{w3}}\nabla^4\mathrm{w(x,y)} \qquad (2.6)$$

where

p(x,y): contact pressure

w(x,y): vertical displacement of the nodes of the mat foundation

c_{pi}, c_{wi}: model parameters (constants).

Depending on the order of the model considered, some of these constants may be assumed to be zero in some cases. If all parameters are assumed equal to zero except c_{w1}, the above model is reduced to the classical Winkler approach, with c_{w1} being the modulus of subgrade reaction k_s.

It is important to note that multi-parameter models come at a high mathematical complexity and computational cost. They can be visualized as containing two or more layers of springs compared to the single one used in the classical Winkler hypothesis. Depending on the particular model used, there are two or more model parameters whose values must be determined by the engineer. This turns out to be a significant problem, since the conceptual and numerical relationships between these and the fundamental soil properties, such as Young's modulus and Poisson's ratio, is not obvious.

Moreover, special treatment is required regarding boundary conditions. This is because spring coupling results in subgrade displacements beyond the edge of the foundation. This issue does not arise with the Winkler approach because due to the lack of spring coupling the subgrade displacements always end abruptly at the edge of the mat foundation. The number and complexity of boundary conditions that must be considered increases with the order and sophistication of the multi-parameter model chosen.

As a result, coupled multiple parameter methods have seen very little penetration in engineering practice. Moreover, with few exceptions, they have not been implemented in the structural analysis computer programs used in practice.

2.4 Pseudo-coupled approach

The pseudo-coupled approach is simply a return to the general form of Winkler's hypothesis. It appears that the predominant reason for the pseudo-coupled approach is its ability to be readily used in the framework of commercially available structural analysis software. The potential improvement that the pseudo-coupled concept offers comes simply from allowing the coefficient of subgrade reaction to vary underneath the foundation elements. Because this variation in the coefficient of subgrade reaction is dictated, in part, by the vertical shearing that develops in actual subgrade materials, using variable Winkler springs under a foundation creates the appearance or an end-result of spring coupling without explicitly doing so mathematically (Horvath, 2002), i.e. without increasing the analytical complexity, a fact that renders the approach very attractive for use in standard engineering practice.

Vertical springs with constants that vary in magnitude from point to point can easily be used in popular structural analysis software, such as SAP2000, ETABS, e.t.c. However, published pseudo-coupled methods rarely highlight several key facts:

- ❖ Winkler's hypothesis is still being used as the subgrade model. This means that the entire burden for estimating the effects of spring (pseudo-)coupling is borne by the engineer performing the analysis.
- ❖ The proper variation of the coefficient of subgrade reaction across the mat is not a unique property and it is not well established. To date, there is a multitude of proposed variations of the modulus of subgrade reaction, most notably those of Liao (1995), the books of Bowels (1996) and Coduto (2001) and the ACI 2002 code.

The aforementioned issues inherent in the pseudo-coupled concept have not deterred its use in recent practice worldwide, and especially in the U.S.A. Generic variations proposed to date assume an increase in the modulus of subgrade reaction near the edges of the foundation. The simplest suggestion is to double the constant of the Winkler springs along the edges of the foundation (ACI Committee 336 1998; Bowles 1988). This suggestion gives good results when the slab is uniformly loaded or it supports one or two point loads. A somewhat more sophisticated version of this is to use a variation in the modulus of subgrade reaction that is based on the theory of linear elasticity. Typically, this gives a modulus of subgrade reaction that is also about twice as large around the edges of a mat compared to its base value at the center, but with gradual, curved pattern of variation in between (ACI Committee 336 (1988, 1989) and Bowles (1988, 1996)).

Coduto (2001) provides a version for the distribution of k_s according to which the mat foundation is divided in two or more zones, as presented in Figure 2.7. The internal zone has half the width and the length of the slab. Every zone has a specific value of modulus of subgrade reaction k_s, with the inner zone value being the smallest and k_s increasing progressively toward the edges. For example, if the slab is separated in three zones, the coefficient k_{sC} of the external zone of the slab must be double ($k_{sC}=2k_{sA}$) that of the central zone k_{sA}. Moreover, the coefficient k_{sB} of the middle zone is equal 1.5 times that of the central zone A (Figure 2.7).

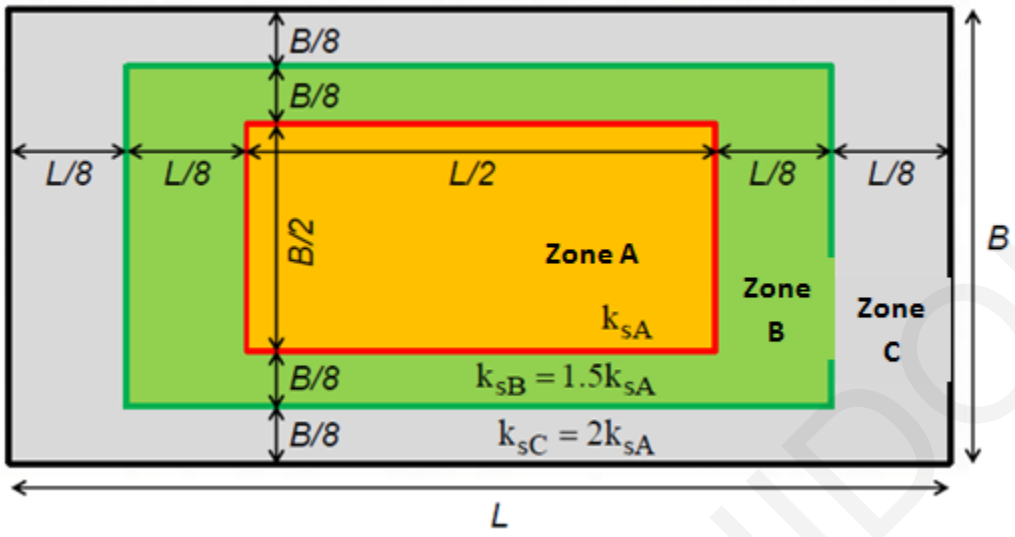

Figure 2.7: Mat foundation divided in zones for pseudo-coupled analysis based on Coduto (2001).

In order to find the values of the modulus of subgrade reaction in each zone, the following equation (2.7) must be solved, where A_i is the area of the zone i:

$$k_{s,ave} \times (A_A + A_B + A_C) = k_{sA} \times A_A + k_{sB} \times A_B + k_{sC} \times A_C \qquad (2.7)$$

By substituting k_{sB} and k_{sC} as multiples of k_{sA} in Fig. 2.7, the equation can be solved with respect to a single unknown k_{sA}:

$$k_{sA} = k_{s,ave} \times \frac{A_A + A_B + A_C}{A_A + 1.5A_B + 2A_C} \qquad (2.8)$$

In the above equation, $k_{s,ave}$ is the average modulus of subgrade reaction, which is equal to the ratio of the average pressure applied by the slab to the average settlement that it produces. Hence, $k_{s,ave}$ can be easily established through classical geotechnical computations of foundation settlement.

A method for estimating the proper distribution of the k_s for plane strain conditions was proposed by Liao (1995). This new method was developed using results from plane strain finite element analyses of a loaded beam or slab resting on the surface of a homogeneous linear elastic soil layer. It is applicable in practice to the design of cut-and-cover tunnel slabs or other similar elongated structures since it is derived on the assumption of plane strain conditions. Liao (1995) examined the effect of certain problem variables on the distribution of the modulus of subgrade reaction. These variables are the soil Young's modulus and Poisson's ratio, the slab stiffness, the thickness of the soil layer relative to the slab width and the pattern of column loads.

The modulus of subgrade reaction was extracted from the results of parametric finite element analyses using the algorithm illustrated in Fig.2.8, which shows a close-up schematic of the finite element mesh directly beneath the slab. The modulus of subgrade reaction is calculated at nodal points 1 through 10 by dividing the nodal displacement *d* by the average of the vertical stresses *p* in the adjacent elements. The computation of k_s at node 11 is complicated because of edge effects. In order to obtain an appropriate value of pressure, Liao (1995) used the basic principles of static force equilibrium, as shown in Figure 2.8. It is important to note that this procedure shown in Figure 2.8 is only suitable for symmetric loading conditions.

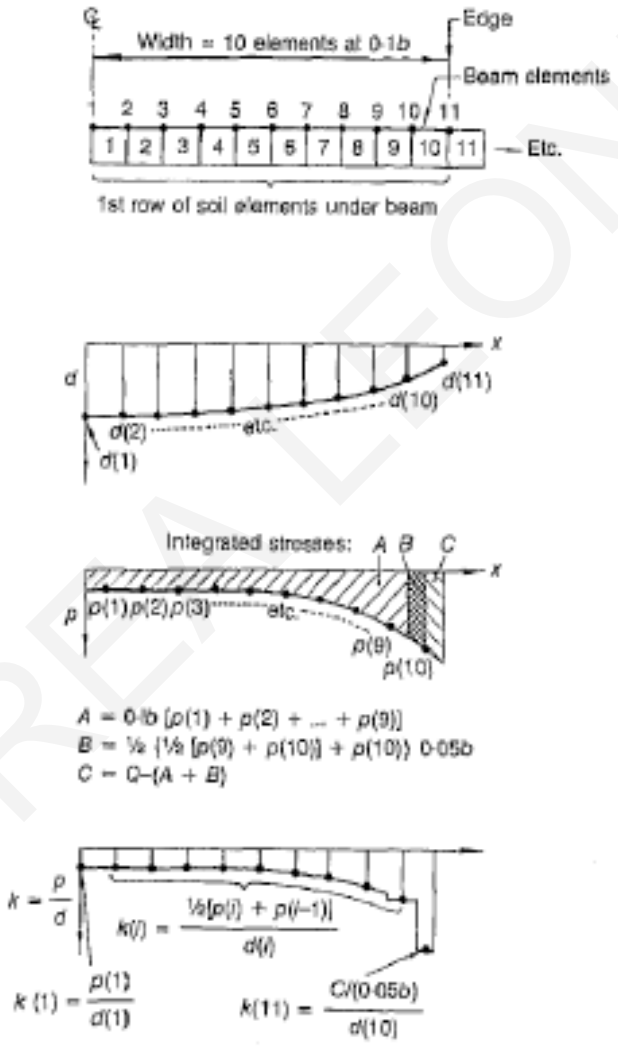

Figure 2.8: Schematic of procedure for calculating k_s from plane strain finite element results (Liao 1995).

In Figure 2.8, one can see the nodes and their corresponding deflections. Below the diagram of deflections is the diagram of the pressure developed by the soil (reaction). At the edge points, we have large reaction by the soil, while the corresponding settlement of the slab is disproportionally small. Hence, using simple mathematics it can be discerned that the resulting values of k_s increase sharply towards the edges of the foundation slab.

In order to plot his results and make them easy to compare, Liao (1995) used a normalized modulus of subgrade reaction k' defined as:

$$k' = \frac{kb}{E_s} \tag{2.9}$$

where *b* is the half-width of the foundation slab and E_s is the Young's modulus of the soil.

Effect of soil layer thickness

The thickness of the deformable soil layer has the most significant influence on the magnitude of k'. From Figure 2.9, it is clear that, by reducing H (depth to hard layer or bedrock) in the finite element model, the k' decreases. This effect becomes particularly strong in the case H is less that the slab width (H/b<2.0).

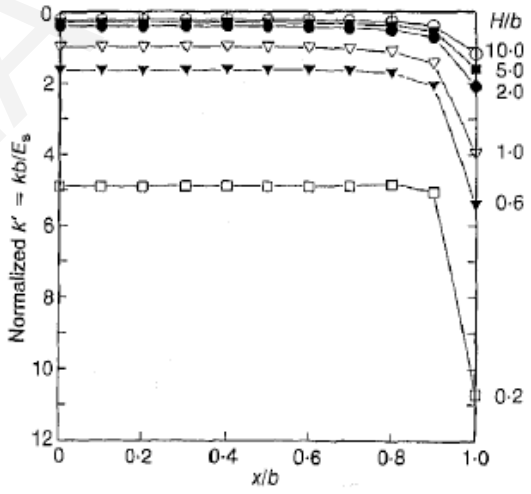

Figure 2.9: Effect of depth of hard layer on the distribution of k' (Liao 1995).

Effect of Poisson's ratio

In Figure 2.10, it is observed that higher values of the soil Poisson's ratio v_s generally lead to higher values of k', which makes sense since higher values of v_s are associated with more volumetrically incompressible materials. It is worth mentioning that the changes in k_s are relatively minor compared to the changes associated with the variation of the layer thickness H (Fig. 2.9).

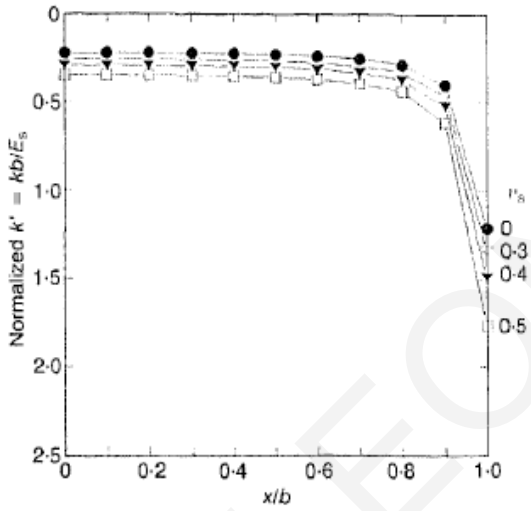

Figure 2.10: Effect of Poisson's ratio on the distribution of k' (Liao 1995).

Effect of slab stiffness

Liao (1995) used in his investigation the notion of relative stiffness ratio SR which is defined as:

$$SR = \frac{E_b \times I_b}{E_s \times b^3}$$

where E_b is the slab Young's modulus, I_b is the slab moment of inertia, E_s is the Young's modulus of the soil and b the slab half-width.

Looking at Figure 2.11, we can see that the k' distribution is relatively insensitive to the relative stiffness and always exhibits a sharp increase near the edge of the slab, with the exception of the perfectly flexible foundation (SR=0). In most cases, the proper value of the modulus of subgrade reaction at the slab edge is 5 times larger than that in the central region.

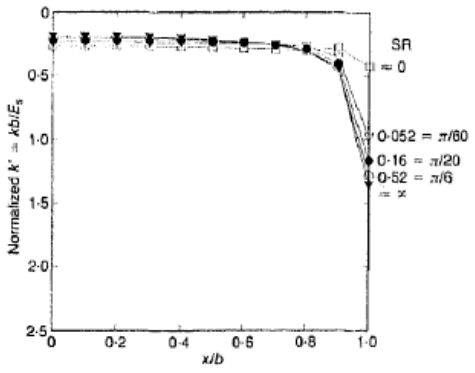

Figure 2.11: Effect of relative stiffness ratio on the distribution of k' (Liao 1995).

Effect of loading pattern on the distribution of k'

In Figure 2.12, Liao (1995) examined the effect of the loading pattern on the coefficient of subgrade reaction distribution for different relative stiffness SR values. The loading in all cases is symmetric with respect to the slab center. The results show that, for a relatively flexible slab (very thin slab or slab resting on rock), when the loading is central (line load at x=0) the k' is decreasing towards the edge. On the contrary, when the loading is symmetrically placed at or closer to the edges of the flexible slab (line loads at x=±0.5b or ±1.0b), we see that the k' increases sharply towards the slab edge (Figure 2.12a). For a relatively stiff slab (which is the case most of the time in geotechnical practice), Liao (1995) observed very little differential settlements but a strongly non-uniform k' distribution (Figure 2.12(b)), as expected due to the effect of the shear force that develops between the soil and the edges of the slab. Most importantly, for relatively rigid slabs, the shape of the modulus of subgrade reaction distribution turns to be quite insensitive to the loading configuration. This is an important observation because it allows the establishment of generic k_s distributions to be used in foundation engineering practice.

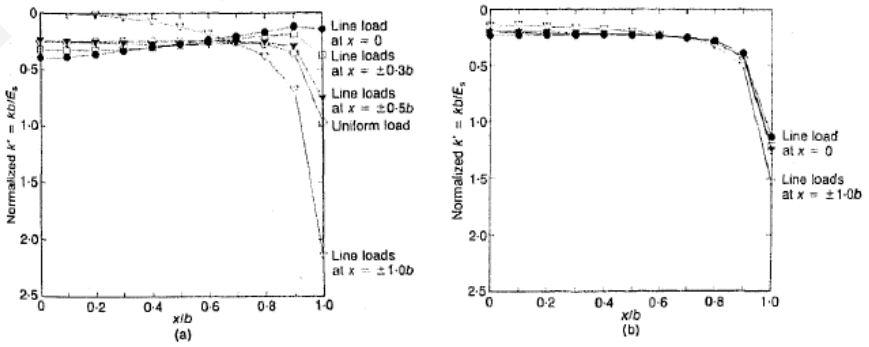

Figure 2.12: Effect of type of loading on the distribution of k' (Liao 1995): (a) relatively flexible slab (SR=0.05, H/b=10, v_s=0), (b) relatively stiff slab (SR=0.5, H/b=10, v_s=0)

Effect of non-symmetric loading

The results for the relatively flexible beam (SR=0.05) and for the relatively stiff slab (SR=0.5) are shown in Fig 2.13(a) and 2.13(b) for line load located at x/b=0, 0.2 and 0.3 (increasing load eccentricity). For both the relatively stiff and the relatively flexible slab, the value of k' increases to the right, i.e. towards where the line load is applied. Hence, the distributions of k' as a function x/b becomes non-symmetric for non-symmetric (eccentric) loading.

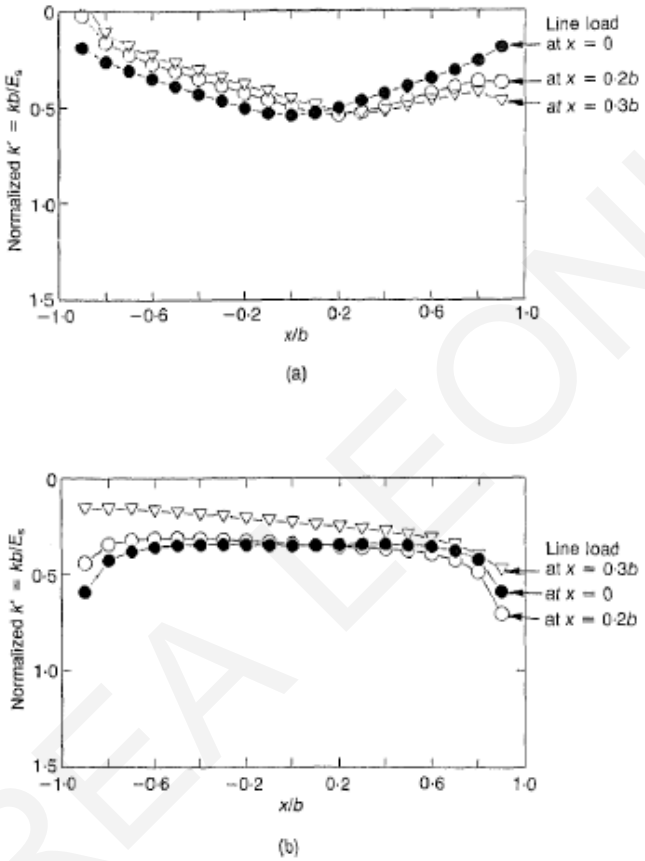

Figure 2.13: Effect of eccentric loading on the distribution of k' (Liao 1995): (a) relatively flexible slab (SR=0.05, H/b=10, v_s=0) and (b) relatively stiff slab (SR=0.5,H/b=10, v_s=0).

2.5 Discrete area method

The discrete area method is an iterative pseudo-coupled method proposed by Ulrich (1991) that gives the advantage to the engineer to properly model the subgrade response for any soil-foundation-superstructure system without relying on prescribed generic k_s distributions. The computational steps are the following:

- In the first step, the engineer performs an analysis of a mat on Winkler springs for a uniform modulus of subgrade reaction.
- Secondly, the mat is divided into small discrete areas of almost equal contact pressures (Fig 2.14).
- In the third step, the engineer computes the soil surface deflection for the idealized system of loaded areas using the Boussinesq theory.
- Then the subgrade response is compared to the mat deflections (compatibility check) and wherever there are discrepancies new values of modulus of subgrade reaction are computed by dividing the contact pressures to the produced (Boussinesq-based) soil deflections.
- The mat static analysis is repeated using the new spring coefficients. As before, new contact pressures and deflections are calculated, and the mat is again divided into areas of equal contact pressures. Nonetheless, the geometry of these new areas might be different from those in the previous trial. The procedure continues until compatibility is achieved between mat and soil deflections, i.e. the analysis converges to a final solution.

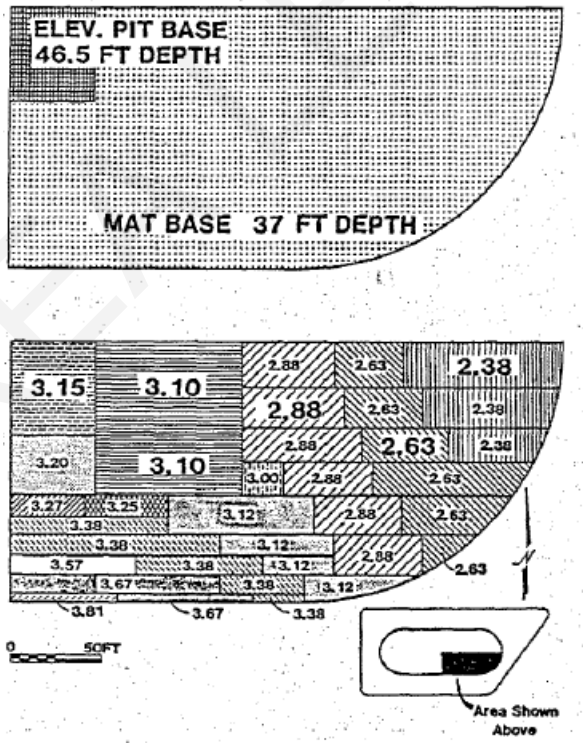

Figure 2.14: Division of the mat in discrete areas according to the contact pressure (Ulrich 1991).

2.6 Three-dimensional finite element analysis (3D-FEA)

Nowadays, three-dimensional finite element analysis is the computational method that permits the study of mat foundation - soil interaction with the highest possible level of fidelity. In such analysis, the soil is represented by a large block of 3D solid elements ("bricks") extending far away horizontally and in depth, while the mat foundation is represented either by shell or plate elements or even (less frequently) by also 3D solid elements. The subdivision of a whole domain into smaller simpler parts, i.e. the finite elements, has several advantages over the previously presented methods:

- Accurate representation of complex geometry
- Inclusion of dissimilar material properties
- Capturing of local effects
- Possibility of considering material non-linearity

The finite element method is the most realistic approach available to date, but its accuracy depends on how much dense is the finite element mesh. Hence, accurate 3D FEA has a very high computational cost and therefore a powerful workstation and expensive FEM software is needed, like Plaxis 3D or Abaqus. A single analysis run may last over one hour, and this will be only for one loading combination and structure configuration, a fact that renders this method unsuitable for routine design of mat foundations. Hence, the analysis using the finite element method is usually done for research purposes or for special construction projects.

Loukidis & Tamiolakis (2017) extended the work of Liao (1995) by using 3D finite element analysis for back-calculating the appropriate Winkler spring stiffness distribution under square and slightly elongated mats resting on the free surface of a uniform elastic soil layer. The mat foundation - soil interaction FEM analyses were performed using the program Abaqus. They found that the proper spring stiffness distribution rises sharply towards the mat edges and increases to even higher levels at the mat corners. Moreover, they verified that the Liao (1995) findings for plane strain conditions with respect to the effects of soil thickness, soil Poisson's ratio, relative stiffness and loading pattern apply also for full three-dimensional conditions (e.g. square mats). Based on their results, they proposed a 6^{th}-degree polynomial equation describing the variation of the spring stiffness along the mat.

CHAPTER 3: METHODOLOGY

3.1 Introduction

The purpose of this thesis is to determine the appropriate distribution of the Winkler spring stiffness coefficient K_{el} across embedded mat foundations and mat foundations resting on non-uniform soils, so that the pseudo-coupled method yields the most accurate results possible. In order to achieve this objective, 3-dimensional parametric analyses of slabs on an elastic medium were performed using the Abaqus finite element software. The settlements resulting from the Abaqus analyses were inputted into a script written in MATLAB (Tamiolakis, 2012) that solves a reverse slab-on-spring problem to determine the equivalent K_{el} values. The purpose of this study is to define a new equation which will give the distribution of the K_{el} stiffness coefficient applicable to mats placed at depth inside the soil and mats resting on soil profile with non-uniform stiffness.

3.2 The finite element model

A series of FE analyses were carried out in Abaqus, which will be presented in greater detail in the following paragraphs, by changing each time the parameters of the problem. These parameters were the following: the foundation embedment (D), the increase rate of the Young's modulus of the soil with the depth (ρ), the dimensions of the foundation, the soil Poisson's ratio (v), the mat loading pattern, the Young's modulus of a second layer of soil below the foundation soil layer, the thickness of the foundation soil layer (H_1), the thickness of the mat foundation (d), the thickness of the deformable model below the mat (H).

3.2.1 Model set-up

The finite element model in Abaqus comprises two parts: 1) the continuous medium representing the ground and 2) the plate representing a mat foundation resting on the continuous medium. For each of the two parts, certain characteristics must be defined, such as the type of finite elements to be used for the plate and the continuous medium, the manner in which each finite element is to be integrated, the constitutive model and the material properties, the type of interaction between the two parts, as well as the boundary conditions that have to be placed on the sides and the bottom of the continuous medium.

In the case of embedment, the mat is placed inside a trench having vertical walls with their own boundary conditions.

For the discretization of the soil medium, the finite elements used (code C3D8) were isoparametric hexahedral finite element with 8 nodes (Figure 3.1) and full Gauss integration. The behavior of the soil material was defined as linear elastic, with input material parameters the values of the Young's modulus and Poisson's ratio. The boundary conditions imposed on the sides of the soil sector and its bottom are total fixities (Figure 3.2), blocking the displacements in all three directions. On the trench walls (in the cases of embedded foundation), only the displacement in the normal direction is restrained, as if there are basement walls that are perfectly smooth. In reality, there will be a certain friction developing between the basement walls and the soil.

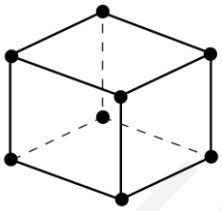

Figure 3.1 : Isoparametric hexahedral finite element with 8 nodes.

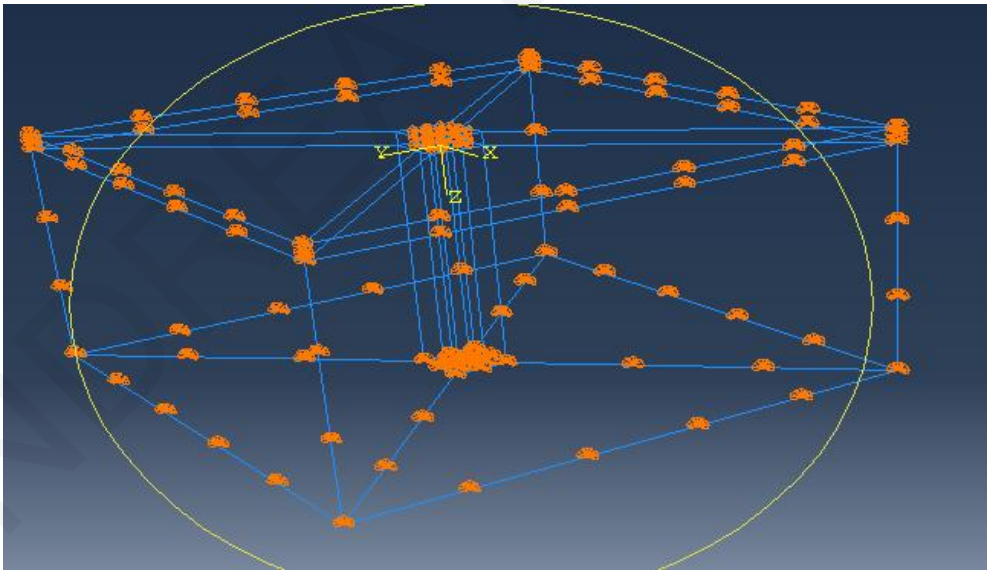

Figure 3.2 Fixities placed on the boundaries of the soil sector.

For the mat foundation, the finite elements used (code S4R5) were 4-noded shell elements with 5 degrees of freedom at each node (3 translational and 2 out-of-plane rotational), with

reduced Gauss integration. The behavior of the plate material was also defined as elastic, with input parameters the Young's modulus and Poisson's ratio of the mat. An equally important parameter in the case of the shell elements is the value of mat thickness d.

For the type of interaction of the two parts, the complete tie was chosen, which means that the nodes of the two parts are firmly connected to each other with respect to the translational degrees of freedom and there is no possibility of slippage or separation between soil and mat foundation.

In total, 50 parametric finite element analyses were performed. The detailed catalogue of parametric analyses is given in the following table (Table 3.1).

Table 3.1: List of parametric analyses.

	ANALYSES											
	Model thickness under the mat	Mat width	Length to width ratio	Embedment	Growth rate of E_1 with depth (E_1=10000+ρz)	Young modulus of the lower layer	Thickness of top layer	Poisson ratio of the soil	Young modulus of the top layer	Loading type	Column load spacing S	Plate thickness
#	H/B	B(m)	L/B	D(m)	ρ (kPa/m)	E_2 (kPa)	H_1(m)	ν	E_1(kPa)	-	(m)	d(m)
1	10	10	1	6	0	-	-	0.3	10000	C1	5	0.75
2	10	10	1	6	0	-	-	0.49	10000	C1	5	0.75
3	10	10	1	6	0	-	-	0.49	1000	C1	5	0.75
4	10	10	1	6	0	-	-	0.49	100000	C1	5	0.75
5	10	10	1	3	0	-	-	0.49	10000	C1	5	0.75
6	10	10	1	9	0	-	-	0.49	10000	C1	5	0.75
7	10	10	1	12	0	-	-	0.49	10000	C1	5	0.75
8	10	16	1	6	0	-	-	0.49	10000	C1	8	0.75
9	10	16	1	9	0	-	-	0.49	10000	C1	8	0.75
10	10	16	1	12	0	-	-	0.49	10000	C1	8	0.75
11	10	16	1	3	0	-	-	0.3	10000	C1	8	0.75
12	10	16	1	9	0	-	-	0.3	10000	C1	8	0.75
13	10	16	1	12	0	-	-	0.3	10000	C1	8	0.75
14	10	10	2	9	0	-	-	0.49	10000	C8	5	0.75
15	10	10	2	12	0	-	-	0.49	10000	C8	5	0.75
16	10	10	1	6	0	-	-	0.49	10000	C1	5	0.5
17	10	10	1	6	0	-	-	0.49	10000	C1	5	1.0
18	1	16	1	6	0	-	-	0.49	10000	C1	8	0.75
19	0.5	16	1	6	0	-	-	0.49	10000	C1	8	0.75
20	10	10	1	6	0	-	-	0.49	10000	C2	5	0.75
21	10	10	1	6	0	-	-	0.49	10000	C3	5	0.75
22	10	10	1	6	0	-	-	0.49	10000	C4	5	0.75
23	10	10	1	6	0	-	-	0.49	10000	C5	5	0.75
24	10	16	1	6	0	-	-	0.49	10000	C6	4	0.75
25	10	10	1	6	0	-	-	0.49	10000	C7	5	0.75
26	10	10	2	6	0	-	-	0.49	10000	C8	5	0.75
27	10	10	1	6	0	-	-	0.49	10000	C9	-	0.75
28	10	10	2	6	0	-	-	0.49	10000	C10	5	0.75
29	10	10	1	0	0	-	-	0.49	10000	C1	5	0.75
30	10	10	1	0	1000	-	-	0.49	10000+1000z	C1	5	0.75
31	10	10	1	0	2000	-	-	0.49	10000+2000z	C1	5	0.75
32	10	10	2	0	0	-	-	0.49	10000	C8	5	0.75

Table 3.1 (continued)

	Model thickness under the mat	Mat width	Length to width ratio	Embedment	Growth rate of E_1 with depth (E_1=10000+ρz)	Young modulus of the lower layer	Thickness of top layer	Poisson ratio of the soil	Young modulus of the top layer	Loading type		Plate thickness
#	H/B	B(m)	L/B	D(m)	ρ (kPa/m)	E_2 (kPa)	H_1(m)	ν	E_1(kPa)	-		d(m)
33	10	10	2	0	1000	-	-	0.49	10000+1000z	C8	5	0.75
34	10	10	2	0	2000	-	-	0.49	10000+2000z	C8	5	0.75
35	10	10	2	6	1000	-	-	0.49	10000+1000z	C8	5	0.75
36	10	10	2	6	2000	-	-	0.49	10000+2000z	C8	5	0.75
37	10	10	2	0	2000	-	-	0.49	10000+2000z	C10	5	0.75
38	10	10	1	0	2000	-	-	0.49	10000+2000z	C7	5	0.75
39	10	10	2	0	2000	-	-	0.49	10000+2000z	C8	5	0.5
40	10	10	2	0	2000	-	-	0.49	10000+2000z	C8	5	1.0
41	10	10	1	0	0	20000	10	0.49	10000	C1	5	0.75
42	10	10	1	0	0	5000	10	0.49	10000	C1	5	0.75
43	10	10	1	0	0	2500	10	0.49	10000	C1	5	0.75
44	10	16	1	0	0	2500	16	0.49	10000	C1	5	0.75
45	10	10	2	0	0	2500	16	0.49	10000	C8	5	0.75
46	10	10	1	0	0	2500	16	0.49	10000	C7	5	0.75
47	10	10	1	0	0	2500	5	0.49	10000	C1	5	0.75
48	10	10	1	0	0	20000	5	0.49	10000	C1	5	0.75
49	10	10	1	0	0	2500	20	0.49	10000	C1	5	0.75
50	10	10	1	0	0	20000	20	0.49	10000	C1	5	0.75

In the following paragraphs, the process of the creation of the models is described in detail and Analysis #1 is used as an example.

Module Parts

1) The creation of the parts of the soil and the plate with dimensions 200m x 200m x 100m and 10mx10m, respectively, was done with the command create part. It is important to note that the dimensions of the soil were initially chosen to be 100m x 100m x 100m (width x length x height), but later it was discovered that larger extent was required to obtain adequately accurate results in the case of v=0.49.

2) The depth of 100m of the soil part was given with the command Edit base extrusion.

3) In the 3rd step, the command Partition Face was used to create separations of the parts to sectors, in order to facilitate the meshing procedure and allow better control of the local mesh density and element size.

4) The 4th step consists of extrusion of the top surfaces around the mat to create the foundation embedment (of 6m in the case of analysis 1), as seen in Figures 3.3 and 3.4.

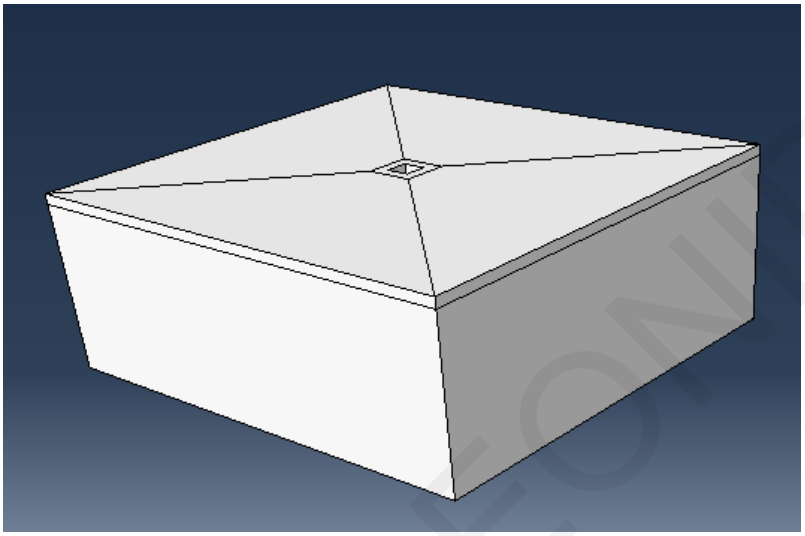

Figure 3.3: Creation of the soil part using extrusion.

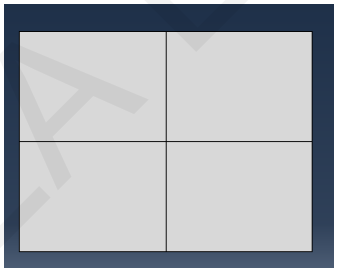

Figure 3.4: Part representing the mat foundation.

Module Property

5) The creation of the materials is done in the module Property. For the soil, the elastic properties were E_1=10000KPa and Poisson's ratio v=0.3 for analysis 1, while for the foundation plate, which is made out of concrete, E=32000000kPa and v=0.2 (Figure 3.5). It should be noted that, for analyses 41 through 50 (Table 3.1), the soil block is further partitioned into two layers of soil with two different Young modulus values, E_1 (upper or foundation layer) and E_2 (bottom layer).

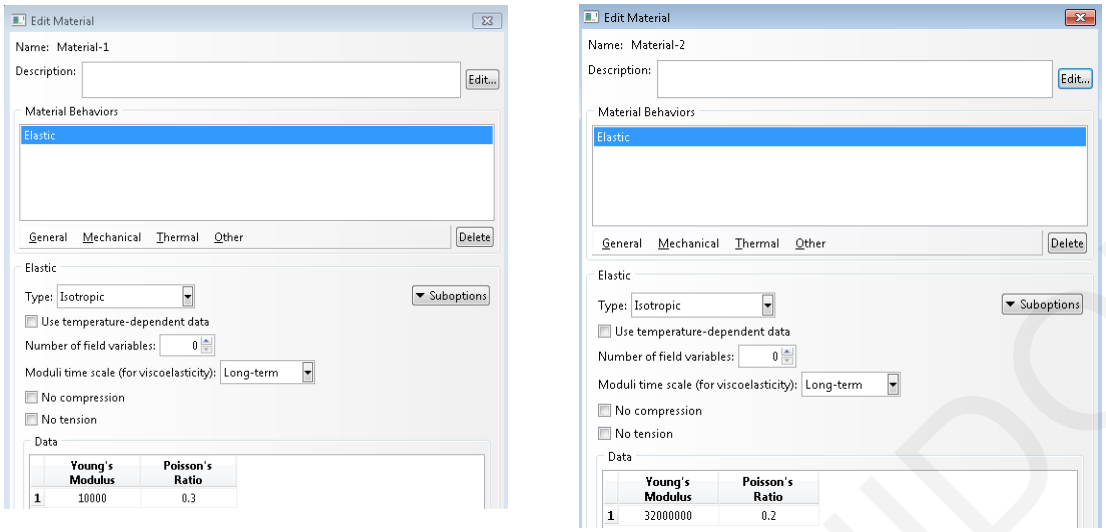

Figure 3.5: Creation of the soil and mat (concrete) materials at module Property.

6) After the material definition, the sections of the soil and the plate need to be created through the Section Manager and each material was assigned at its section, as shown in Figure 3.6:

Section soil -> solid -> homogeneous -> Material 1 -> soil

Section plate -> shell homogeneous -> Material 2 -> concrete, and shell thickness-> d=0.75m

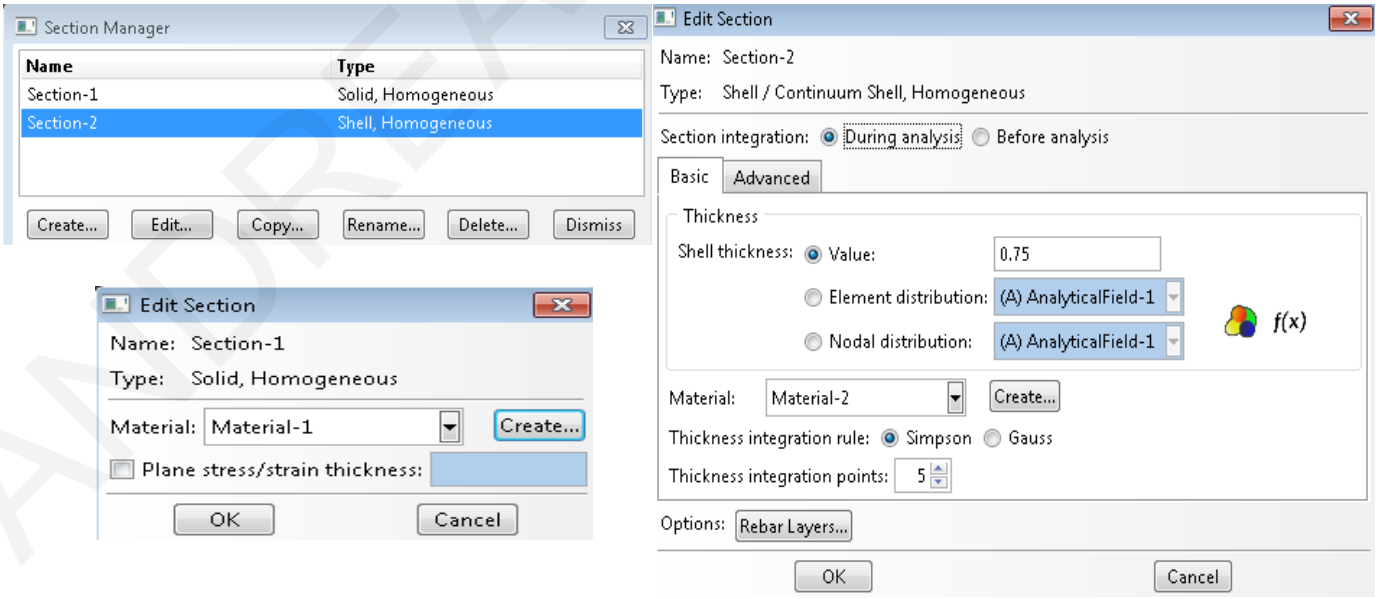

Figure 3.6: Creation of the sections and assignment of the materials to each section.

Module assembly

7) At module assembly, both parts were appointed with instance part -> dependent (mesh on part), as shown in Figure 3.7.

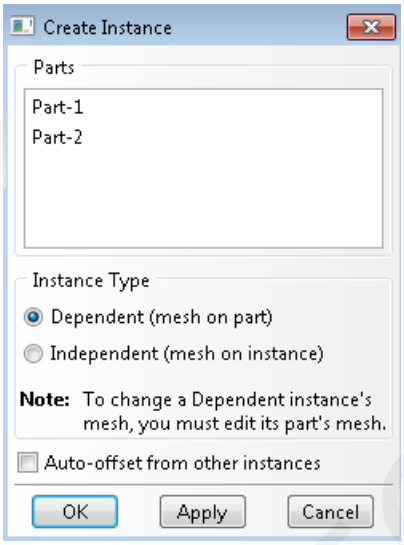

Figure 3.7: Instance creation in module Assembly.

Module step

8) Subsequently, at the module Step just one computational step was created (Step-1) as "Static, General" (Figure 3.8). This means that the problem is solved using a classical static solver. Given that the soil material is assumed to behave purely elastically and the model is weightless, there is no need for a geostatic step to precede Step-1.

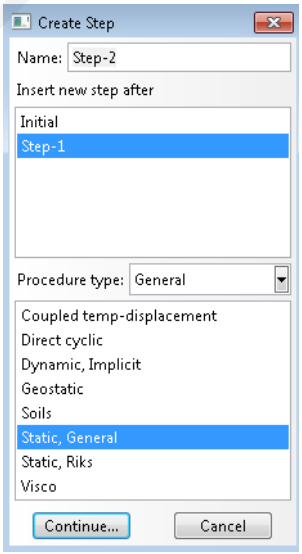

Figure 3.8: Creation of the static computational step.

Module Interaction

9) Step 9 was the creation of the interaction between the soil and the slab. As mentioned above, it was chosen to be a complete tie between coinciding soil and mat nodes (Figure 3.9).

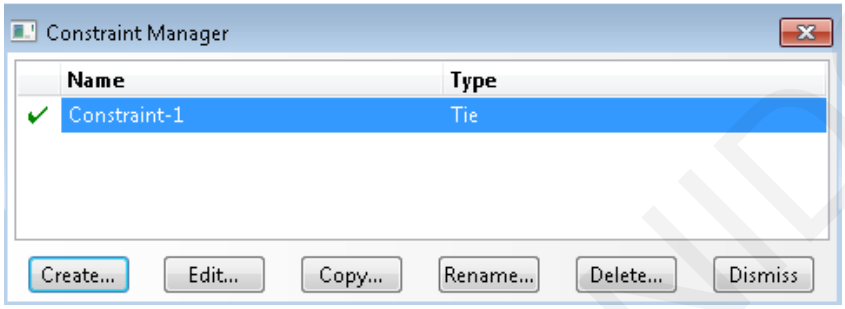

Figure 3.9: Creation of the interaction between the slab and the soil.

Module Loads

10) The mats were loaded with concentrated vertical nodal forces representing column loads. For Analysis #1, the type of the loading was that of C1, namely 100kN were applied at the corners of the mat, in the center of the mat 400 kN and at the middle of the mat edges 200kN (Figure 3.10). The loads were applied with the command Load Manager (Figure 3.11).

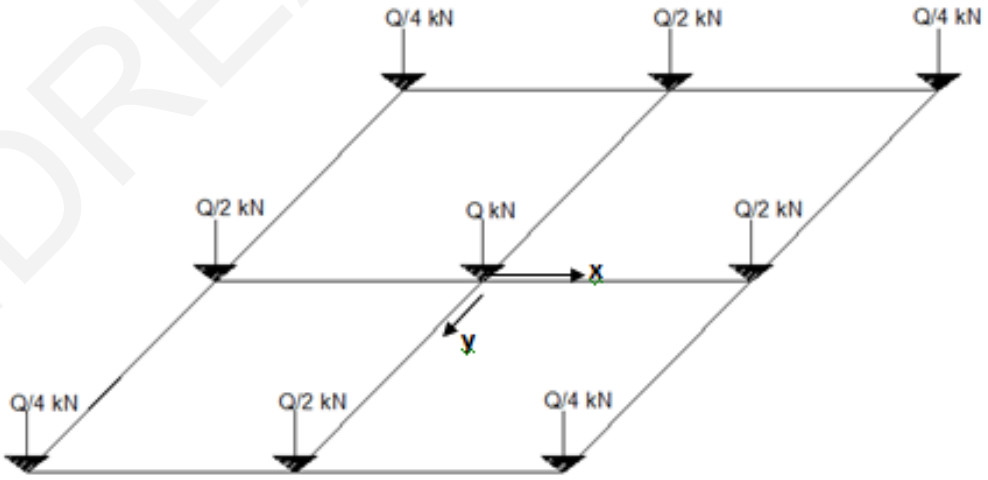

Figure 3.10: Type of loading C1.

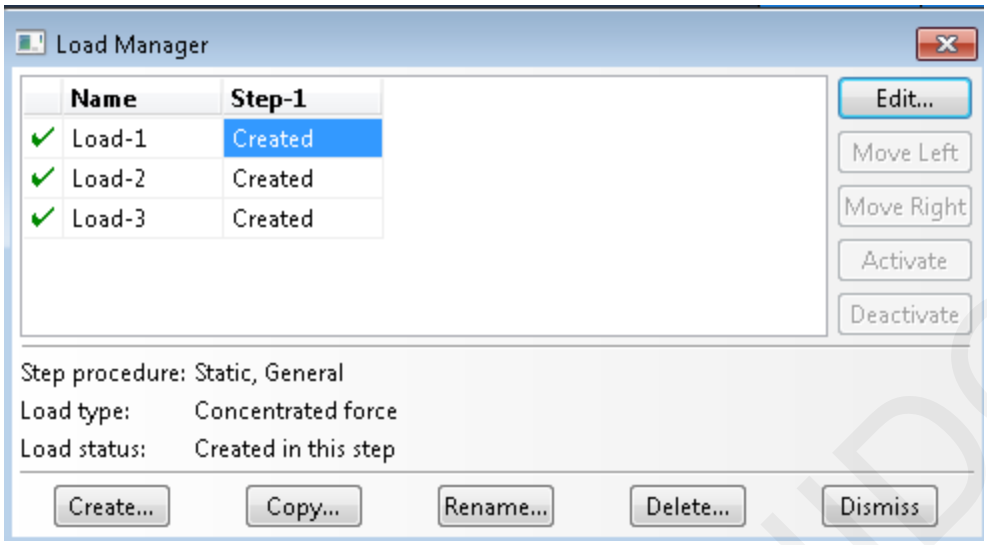

Figure 3.11: Assignment of the loads with the command Load Manager.

Module mesh

11) In module Mesh, we have first the creation of the "seeds" along edges and internal boundaries. The mat is "seeded" in such a way so that the shell elements discretizing the mat are square element 0.5m wide, which is a size often used by engineers in structural analysis programs. The soil right underneath the mat is discretized with elements that have the same dimensions in the horizontal plane (0.5m x 0.5m). This way the locations of the mat nodes coincide with those of the nodes of the soil brick elements at the foundation level. The same size of soil elements (0.5m x 0.5m) is prescribed in a region that extends twice as much as the dimensions of the mat. Beyond this central region, the element size is allowed to progressively increase as we move towards the external boundaries of the model in order to reduce the computational cost of the analysis in terms of memory requirements and runtime. More specifically, the seeds along the diagonal partitions were placed at minimum distance equal to 0.707m, progressively increasing to 5m at the corners of the model (Figure 3.12). The final mesh is shown in Figure 3.13 and it contains 697172 nodes and 680640 C3D8 solid elements. The same process was followed for the slab, discretizing it into 400 square S4R5 shell elements with 0.5m width.

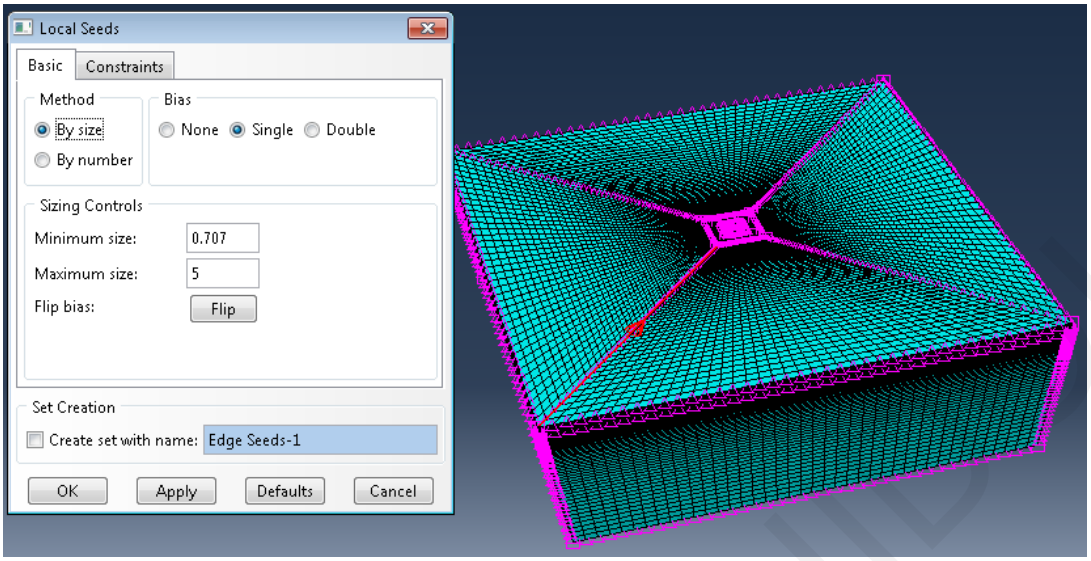

Figure 3.12: Seeding of diagonal partitions using single bias towards the model corners

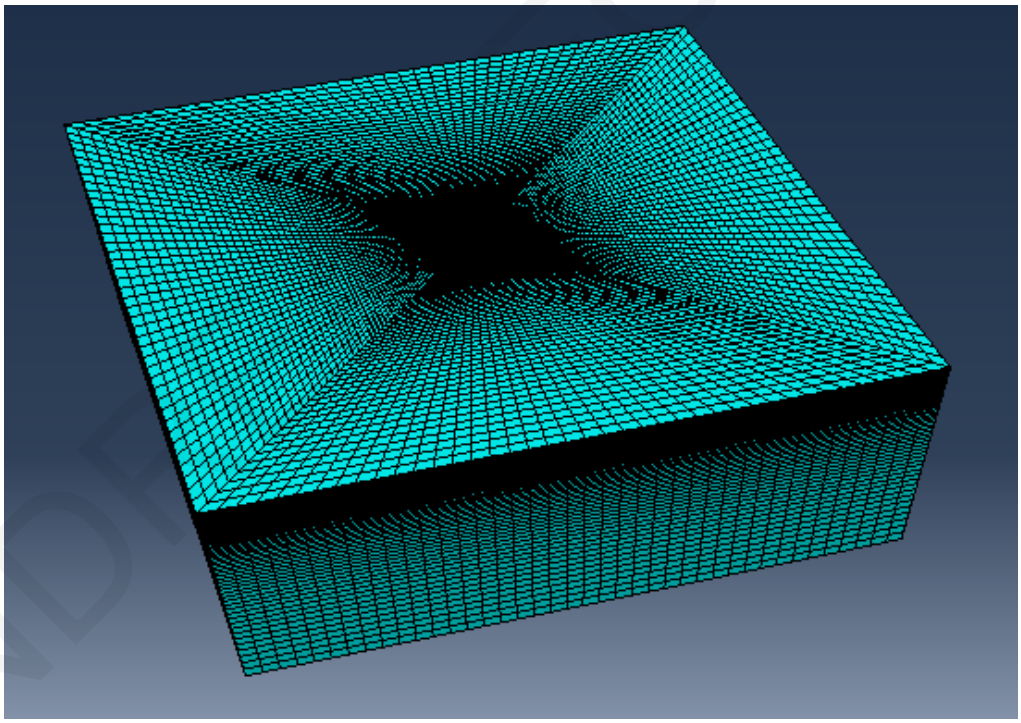

Figure 3.13: Mesh for parametric analysis #1.

Module job

12) The last step is to submit the analysis for calculation execution through the job manager. Once the analysis run finishes, the deformed shape of the model was inspected, and the settlements of the mat nodes were exported to an RPT text file.

3.2.2 Establishing linear increase of soil Young's modulus with depth

The above presented model building procedure is complete for most parametric analyses. Yet, analyses 30,31,33-40 have a linear increase of the soil Young's modulus E_1 with depth. In order to establish this increase with depth, the procedure is the following:

Step A: In Module Load, an increase of temperature with depth was prescribed as a predefined field throughout the soil part. The temperature is set to be equal to zero at the level of the foundation slab and equal to unity at the bottom of the model.

Step B: In Module Property, the Young's modulus of the soil is set to be temperature dependent. In the dialog boxes, the modulus values at zero temperature and at the maximum (=1) temperature are prescribed, effectively producing a variation in the form A+ρ*z, where z is the depth from the foundation level and A is the soil elastic modulus at that level, which in all cases is set equal to 10000kPa.

3.3 Mat loading patterns

As shown in Table 3.1, parametric analyses were performed for various patterns of loading, namely C1 through C10. These patterns are shown in Figs. 3.14-3.23, where Q=400kN. Because the problem does not include material non-linearities (all materials are linear elastic), the actual magnitude of loading does not affect the equivalent spring stiffness values sought to be established through the FEA.

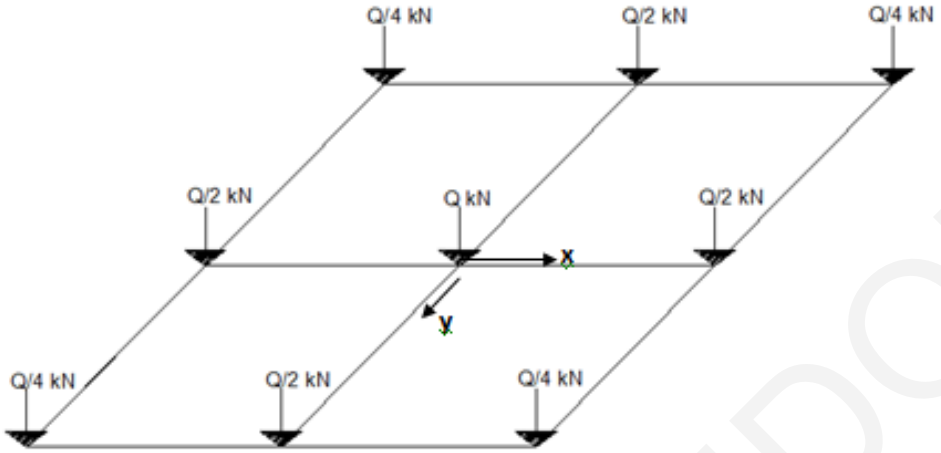

Figure 3.14: Loading pattern C1.

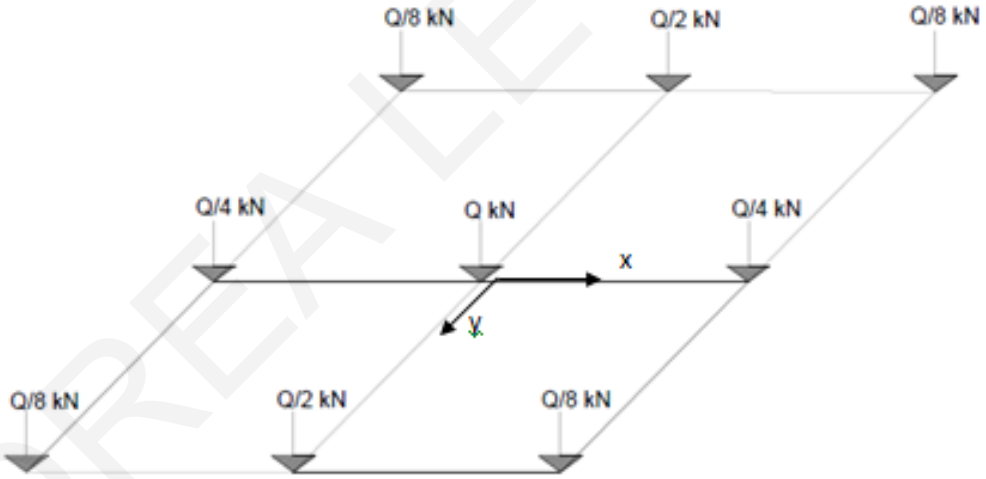

Figure 3.15: Loading pattern C2.

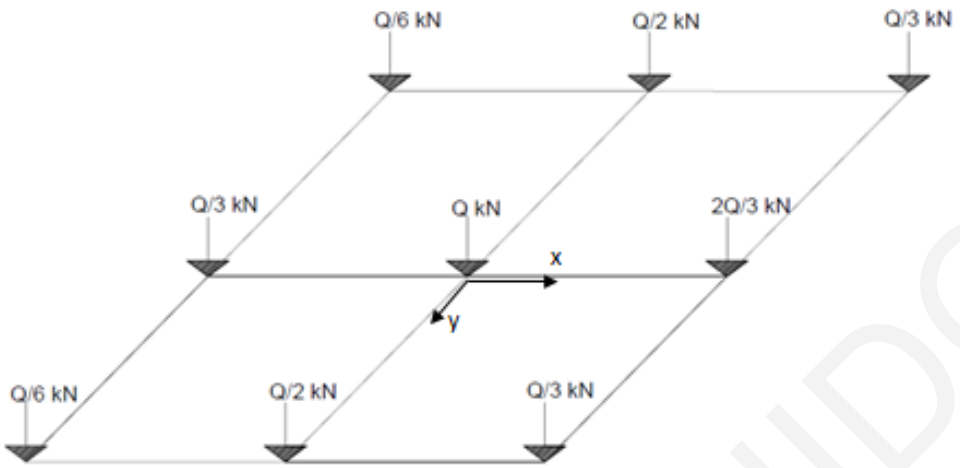

Figure 3.16: Loading pattern C3.

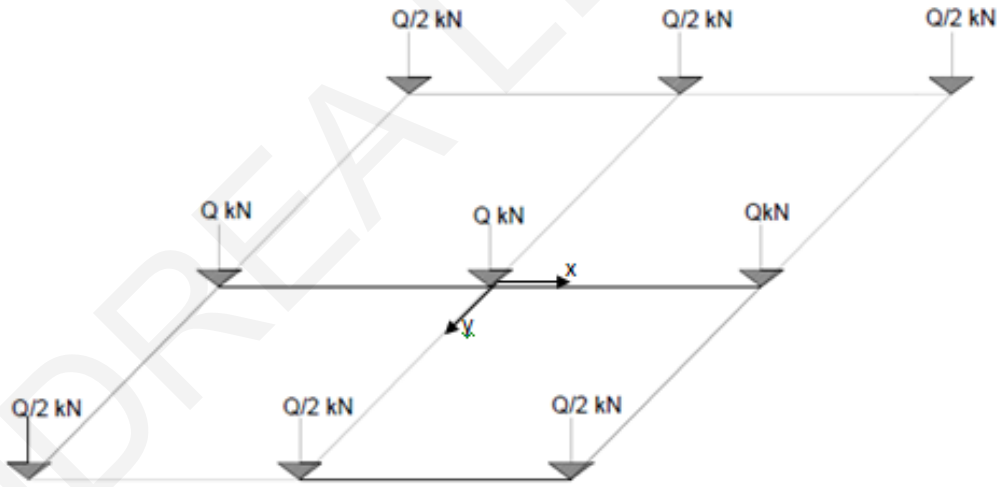

Figure 3.17: Loading pattern C4.

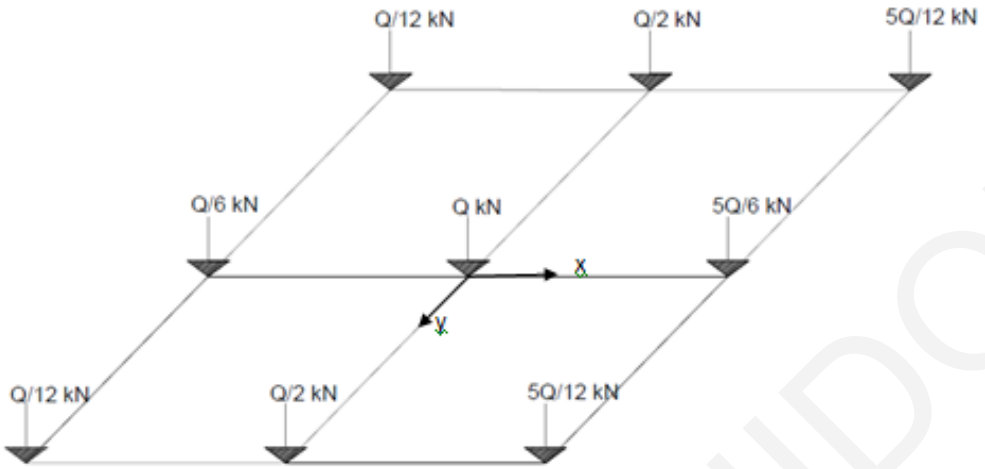

Figure 3.18: Loading pattern C5.

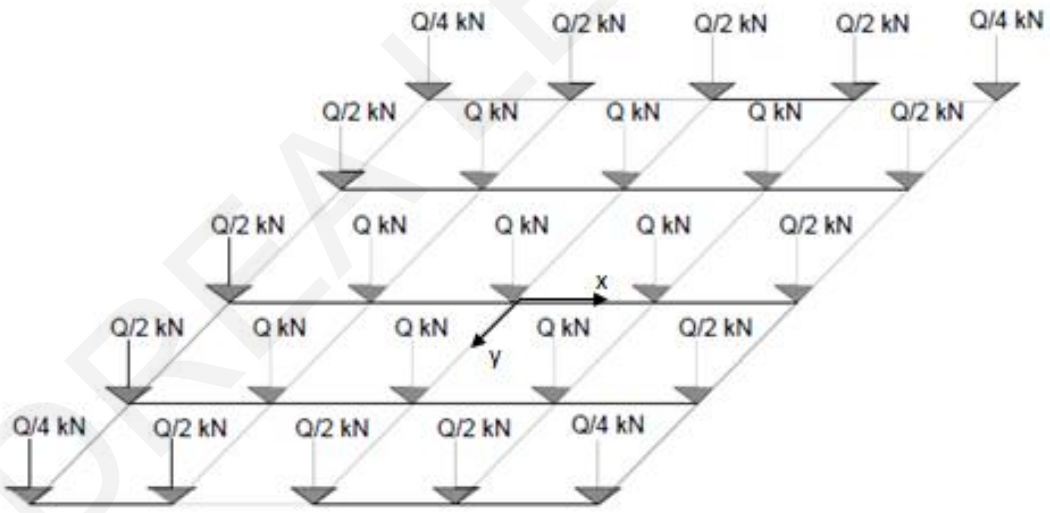

Figure 3.19: Loading pattern C6.

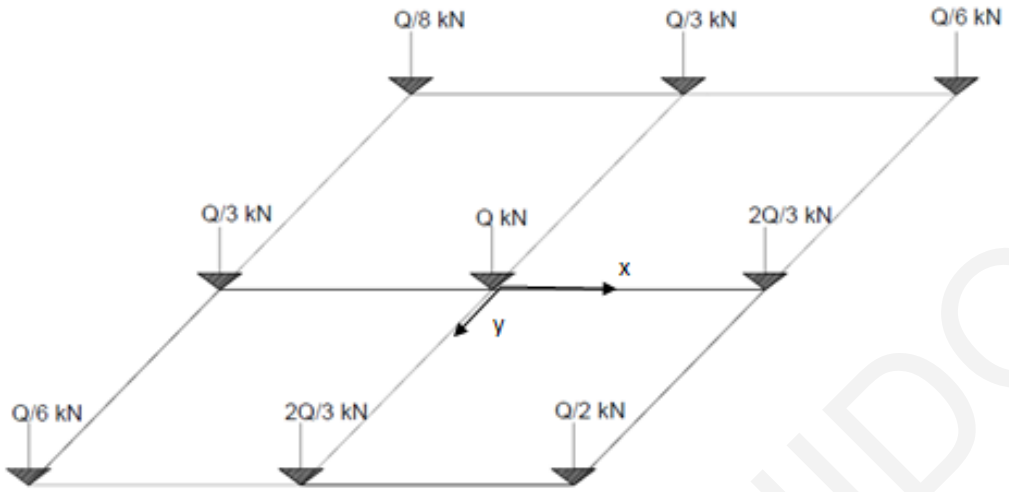

Figure 3.20: Loading pattern C7.

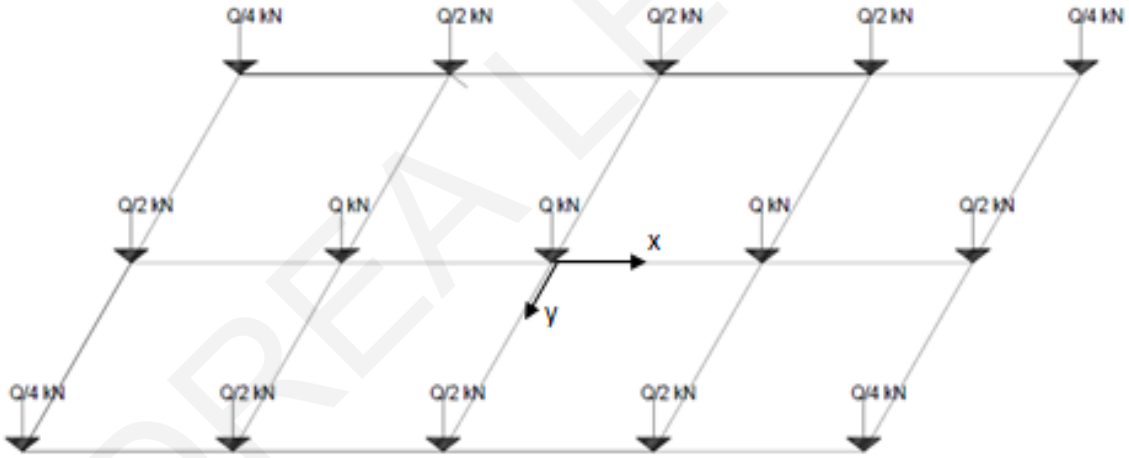

Figure 3.21: Loading pattern C8.

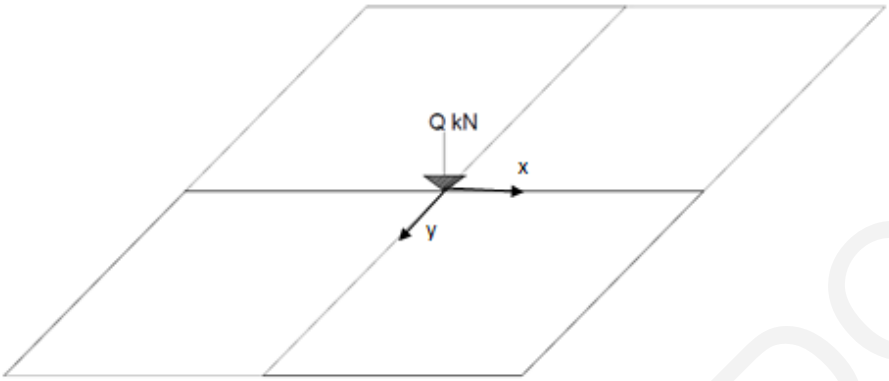

Figure 3.22: Loading pattern C9.

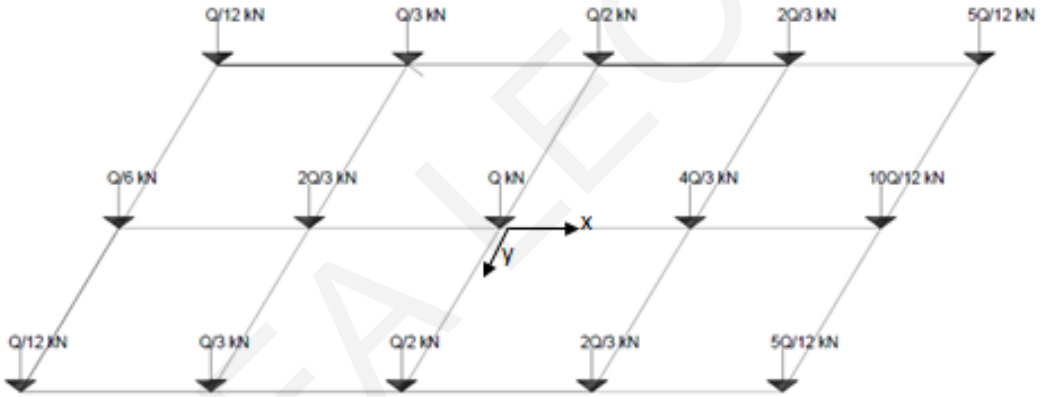

Figure 3.23: Loading pattern C10.

The distance S between the column loads in most of the analyses is 5m, which can be seen as a typical span in residential buildings. However, there are analyses in which the distances are 4m and 8m (Table 3.1). Loading C9 is not typical of a building but is reminiscent of special structures such as bridge piers, water towers, e.t.c. In most loading patterns, the loading is fully symmetric. This means that the resultant force passes from the center of the mat foundation. The load is non-symmetrical in loading patterns C3, C5 and C10, with the resultant force eccentricity being along the x-axis. In the case of C7, there is load eccentricity of the same magnitude along both x- and y-axes.

3.4 Finite element model validation

In order to check the accuracy of the results produced by the aforementioned model configuration, 9 trial analyses were performed (validation analyses), with the parameters shown in Table 3.2.

Table 3.2: Catalogue of validation analyses.

#	H/B	B(m)	L/B	D(m)	v	E(kPa)	p (kPa)	d(m)
V1	10	10	1	0	0.49	10000	100	3
V2	10	10	1	3	0.49	10000	100	3
V3	10	10	1	3	0.3	10000	100	3
V4	10	10	1	6	0.49	10000	100	3
V5	10	10	1	6	0.3	10000	100	3
V6	10	10	1	9	0.49	10000	100	3
V7	10	10	1	9	0.3	10000	100	3
V8	10	10	1	12	0.49	10000	100	3
V9	10	10	1	12	0.3	10000	100	3

These analyses had a slab thickness of 3m, rendering the mat practically perfectly rigid, and uniform pressure loading 100kPa. This was done in order to be able to compare with the predictions of well-established formulas and charts that are applicable for perfectly rigid foundations in uniform elastic soil layer, namely Steinbrenner (1934), Frazer & Wardle (1976) and Gazetas et al. (1985), which are based on semi-analytical solutions. The seminal work of Steinbrenner (1934) is the oldest one and provides the settlement of a perfectly flexible foundation on the surface of a soil layer of finite thickness H. It is combined here with the depth factor from Burland (1969) and the Chow (1987) rigidity factor in order to obtain the settlement of embedded rigid foundations. The Frazer and Wardle (1976) solutions hold also for foundations on the ground surface. To account for the presence of embedment, the settlement is multiplied also with the depth factor of Burland (1969). It should be noted that this depth factor was established by Burland (1969) using FEM and considering circular footing (axisymmetric conditions) in a circular trench with unsupported walls. The Gazetas et al. (1985) equations provide the settlement of an embedded rigid foundation at depth D inside a rectangular trench with unsupported walls. However, it should be noted that this solution holds for soil layer of infinite thickness (elastic half-space). In order to match the boundary conditions assumed by the Burland (1969) and Gazetas et al. (1985) solutions, these FE runs were performed without support on the excavation walls

(the supporting rollers were removed). The mathematical expressions and diagrams needed for the calculation of foundation settlement based on these methods are given below.

Gazetas et al. (1985)

$w = \mu_{trench} * w_{sur}$ (3.1)

where μ_{trench} the depth factor

$$\mu_{trench}=1-0.04*\frac{D}{B/2} * \left(1 + \frac{4}{3} * \frac{Ab}{L^2}\right) \quad (3.2)$$

The settlement w_{sur} if the footing was at the free surface is given by

$$w_{sur}=\frac{P}{E(\frac{L}{2})} * (1 - \nu^2) * \mu_{shape} \quad (3.3)$$

where $\mu_{shape}=0.45*(\frac{A_b}{L^2})^{-0.38}$ (3.4)

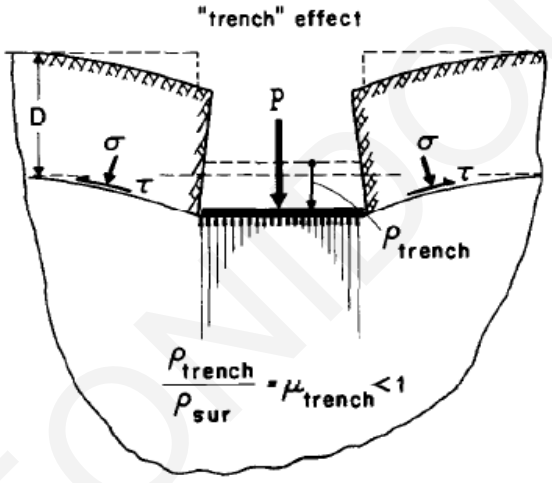

Figure 3.24: Calculation of the settlement according to Gazetas et al. (1985).

Steinbrenner (1934) with Burland depth factor

The Steinbrenner (1934) solution gives directly the settlement at the corner of a perfectly flexible foundation.

$$w_{corner} = \frac{(1-\nu^2) * q_{b*} B}{E} * I * I_F \quad (3.5)$$

$$I = F_1 + \frac{1-2\nu}{1-\nu} * F_2 \quad (3.6)$$

From Figure 3.25, we can find the depth factor I_F of Burland (1969) and from Figure 3.26, the coefficients F_1 and F_2. In order to obtain the (uniform) settlement of a perfectly rigid foundation, w_{corner} is multiplied first by 2 to obtain the settlement at the center of the flexible foundation and then by a factor of 0.77 (Chow, 1987) to obtain the settlement *w* of the rigid foundation.

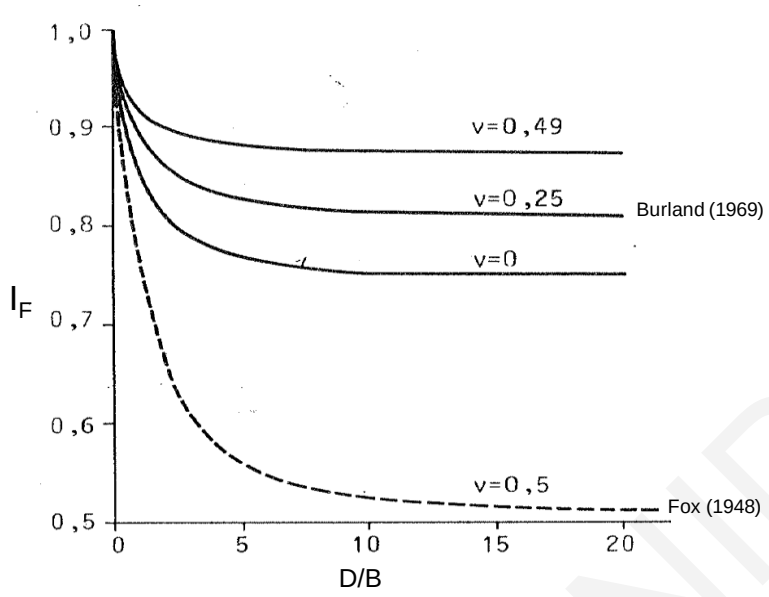

Figure 3.25: Depth factor I_F vs. embedment depth ratio D/B (after Αναγνωστόπουλος & Παπαδόπουλος, 1989).

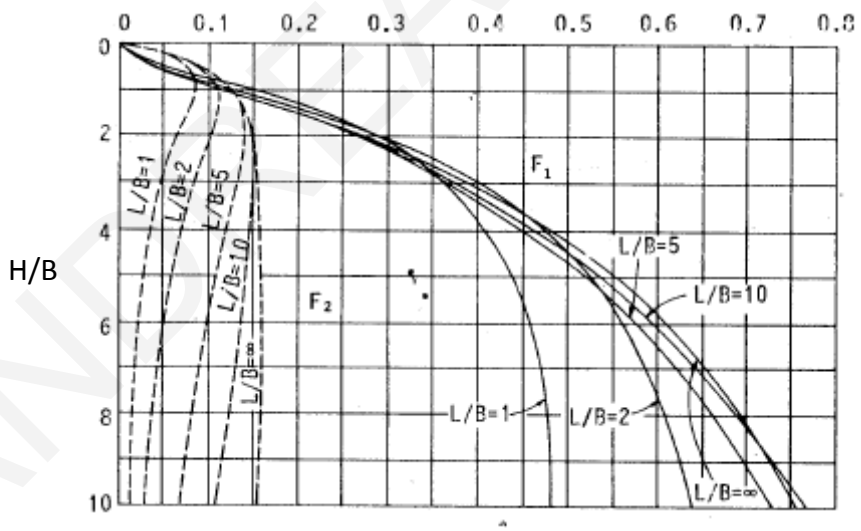

Figure 3.26: Coefficients F_1 and F_2 for uniformly loaded rectangular surface (after Αναγνωστόπουλος & Παπαδόπουλος, 1989).

Fraser & Wardle (1976) with Burland depth factor

The settlement is calculated as:

$$\boldsymbol{w = \frac{pb(1-{v_s}^2)}{E_s} I * S * I_F} \tag{3.7}$$

where *b* is the foundation width, *p* is the applied uniform pressure, *I* is the influence factor for the settlement of the raft, I_F is the depth factor from Burland (1969) and *S* is a coefficient that introduces the effect of a rigid bedrock underneath the deformable soil layer (Fig. 2.4a). The influence factor is read from the plot of Fig. 3.27, with K being the relative stiffness factor of the foundation:

$$\boldsymbol{K = \frac{4}{3}\frac{E_r(1-{v_s}^2)}{E_s(1-{v_r}^2)}\frac{t^3}{b^3}} \tag{3.8}$$

where E_r is the modulus of elasticity of the mat (concrete material) equal to 32GPa, v_r is the mat Poisson's ratio equal to 0.2, E_s is the modulus of elasticity of the soil, v_s is the soil Poisson's ratio, and t is the mat thickness. For the material properties of Table 3.2, K turns to be 91 to 109 and, thus, I=0.87. It should be noted that *d* in Fig. 3.27 denotes the thickness of the deformable soil layer, not the mat thickness as in the rest of Chapter 3 and Chapter 4.

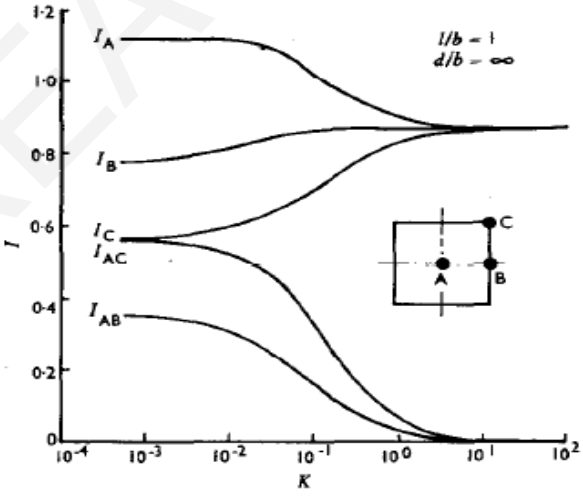

Figure 3.27: Settlement influence factor I for square foundation (l/b=1) on elastic half-space (d/b=∞) from Fraser & Wardle (1976).

Table 3.3 compares the settlements resulting from the Abaqus validation analyses with those from the above semi-analytical methods. It can be seen that the thickness of 3m

prescribed in the Abaqus analyses is capable in replicating an absolutely rigid foundation from a practical perspective, since the differences between minimum and maximum settlement are less than 0.25%. Another interesting observation is that the three semi-analytical methods do not agree with each other, most likely due to the different assumptions made in each one. The Gazetas (1985) equations predict larger settlements than the other two methods. This is understandable as this solution ignores the presence of a fixed bottom boundary at H=10B.

Table 3.3: Comparison between FEA calculated settlement of rigid foundation and the predictions of existing semi-analytical solutions.

#	w (m) from Abaqus FEA			w (m) based on Steinbrenner (1934)	w (m) based on Fraser & Wardle (1976)	w (m) based on Gazetas (1985)
	max	min	average			
V1	0.059	0.059	0.059	0.056	0.066	0.068
V2	0.055	0.055	0.055	0.052	0.056	0.061
V3	0.065	0.065	0.065	0.063	0.068	0.073
V4	0.052	0.051	0.051	0.053	0.057	0.065
V5	0.060	0.060	0.060	0.065	0.069	0.077
V6	0.049	0.049	0.049	0.052	0.056	0.057
V7	0.056	0.056	0.056	0.063	0.067	0.068
V8	0.047	0.047	0.047	0.051	0.055	0.053
V9	0.054	0.054	0.054	0.062	0.066	0.064

Table 3.4: Absolute relative error between average settlements from Abaqus FEA and the three semi-analytical methods.

#	Steinbrenner (1934)	Fraser & Wardle (1976)	Gazetas (1985)
V1	5.4%	10.4%	13.4%
V2	5.0%	2.4%	9.4%
V3	2.5%	3.7%	10.6%
V4	4.4%	11.2%	21.0%
V5	7.1%	13.3%	22.4%
V6	5.4%	12.0%	13.9%
V7	10.7%	16.6%	17.8%
V8	8.3%	14.8%	11.4%
V9	13.0%	18.8%	15.0%
average	**6.9%**	**11.5%**	**15.0%**

Table 3.4 presents the value of the corresponding relative error of the Abaqus results in relation to the semi-analytical predictions. The FEA results are closer to Steinbrenner (1934), with an average error of 6.9%, as opposed to the 11.5% average error with respect to Fraser & Wardle (1976). It should be noted that for foundation on the free surface (zero embedment) with soil Poisson's ratio v=0.3, Loukidis & Tamiolakis (2017), who also used 0.5m x 0.5m elements in the vicinity of the mat, report relative error in comparison to the Fraser & Wardle (1976) solution equal to 6.8%. Herein, for surface foundation on soil with v=0.49, the corresponding error rises to 10.4%. This relative reduction in accuracy is probably due to the near incompressibility caused by the high value of soil Poisson's ratio. In general, these values of relative error (of the order of 10%) are deemed herein acceptable given the fact that further increase in the mesh density (aiming at achieving better accuracy) would result in an increase in the RAM (computer memory) requirement above the capabilities of the available workstations.

3.5 Back-calculation of equivalent spring constants

The resulting vertical displacements (U3) of all the mat nodes from each parametric analysis were exported from Abaqus in the form of ASCII files (report files .rpt). An example of the distributions of mat vertical displacements is given in Figs. 3.28 and 3.29.

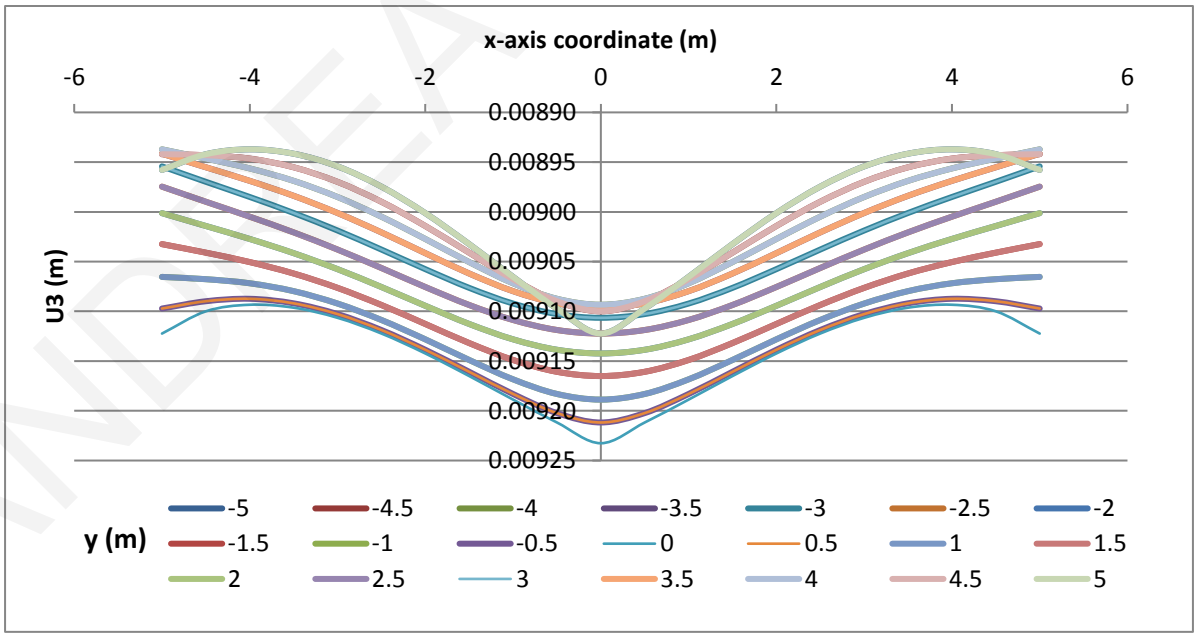

Figure 3.28: Distributions of mat vertical displacement along the x-axis direction from Analysis 1.

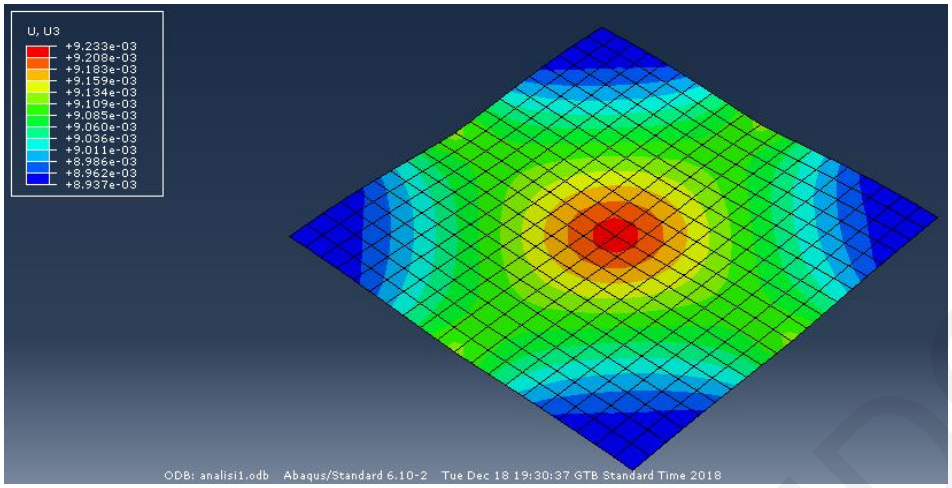

Figure 3.29: Contours of vertical displacement of the mat foundation from Analysis 1.

Subsequently, these nodal displacements were introduced as input in the Matlab script developed by Tamiolakis (2012) that solves inversely the problem of a mat foundation resting on Winkler springs (shown here in Annex D). This algorithm uses the mat nodal displacements as known values and solves the global system of nodal equilibrium equations with respect to the unknown equivalent Winkler spring constants K_{el}. The plate is modeled using exactly the same shell elements as in Abaqus. The Matlab algorithm operates according to the following flow chart (Fig. 3.30).

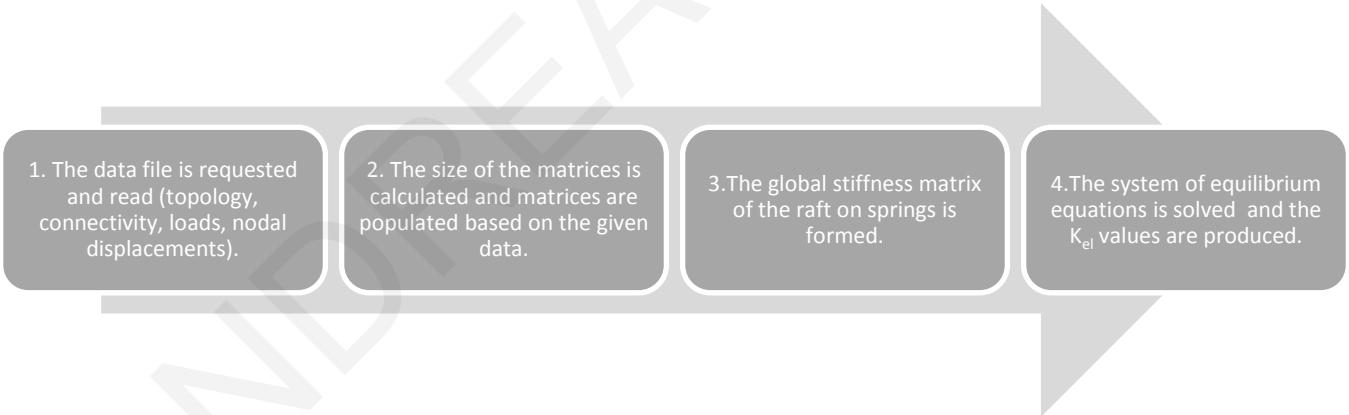

Figure 3.30: Flow chart of Matlab algorithm.

Fig. 3.31 shows an example (Analysis 1) of the K_{el} distribution produced by the back-analysis Matlab script.

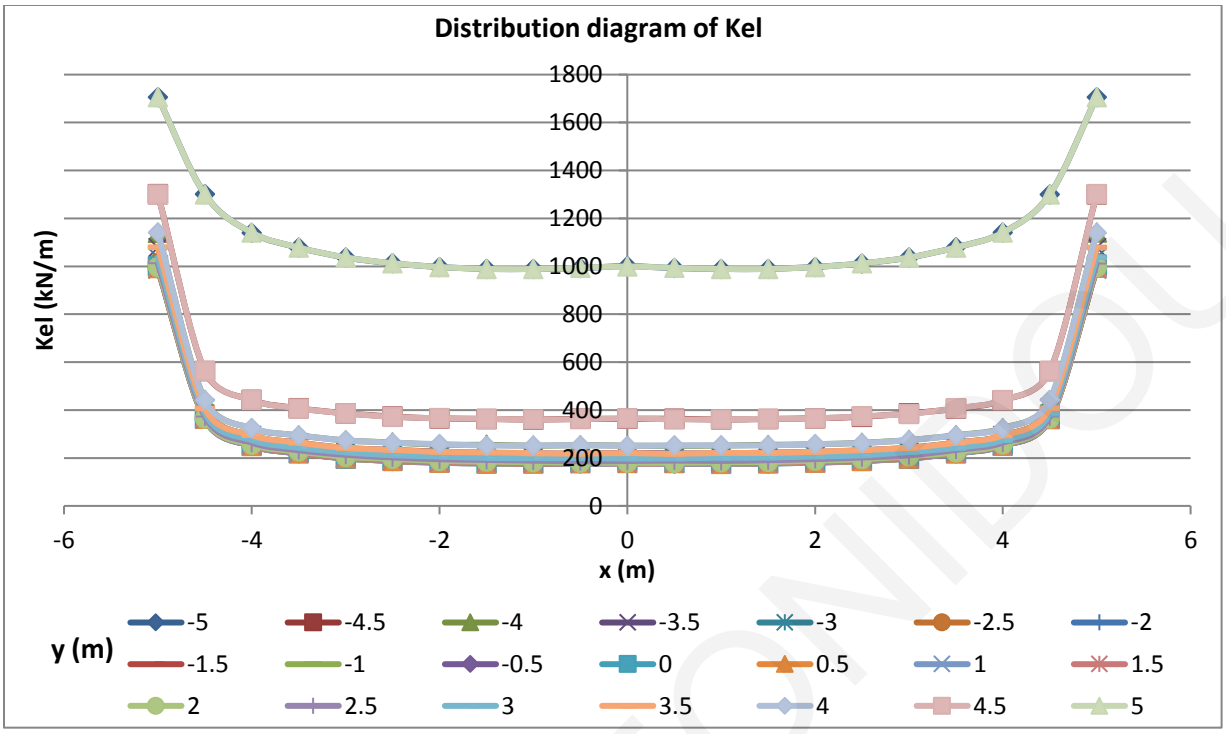

Figure 3.31: Distribution of K_{el} along the x-axis direction resulting from the Matlab algorithm for Analysis 1.

By observing the above figure, one can easily see that the K_{el} values at the edges of the mat are about five times larger than those in the middle. This rise in K_{el} towards the mat edges is rather abrupt and happens inside a narrow peripheral zone. The distributions of K_{el} from the rest of the parametric analyses are presented in Annex A.

To facilitate comparisons and interpretation of the results, the K_{el} values are normalized with respect to the spring coefficient that would be applicable if the foundation was perfectly rigid (K_r). The K_r was calculated using the following formulas:

$$K_r = \frac{E_1 * A_{inner}}{C_f * (1-\nu^2) * B * D_f} \quad (3.9)$$

where

E_1: the elastic modulus of the foundation soil

v: soil Poisson's ratio

B: width of the mat

A_{inner}: the influence area of the inner nodes of the mat (= 0.25m²)

C_f: factor introducing the effect of foundation shape and the effect of deformable soil layer thickness

$$C_f = \frac{0.85 * (\frac{L}{B})^{0.45}}{[1 + 0.1 * \left(2 + \frac{L}{B}\right) * \frac{B}{H_1}]^{1+\exp(5\nu^3)}}$$

Depth factor D_f = 1+ (0.27- 0.12ln ν)*{1-exp (-0.83$(\frac{D}{B})^{0.83}$)}

L: length of the mat

H_1: thickness of the soil model below the mat

D: foundation embedment

The factor C_f was derived by Loukidis & Tamiolakis (2017) based on the semi-analytical solutions of Fraser & Wardle (1976) and Chow (1987) for a rigid rectangular plate on the free surface of a uniform elastic layer. The depth factor D_f was derived by Loukidis et al. (2008) from numerical analyses (finite difference program FLAC) of circular rigid plate at the bottom of cylindrical open hole. The walls of the hole were supported by rollers, as done in the present analyses. The K_r values for all the parametric analyses calculated using the above formulas are shown in Table B1 in Annex B.

Furthermore, the analyses were grouped together (Fig. 3.32) based on their input characteristics for comparison purposes and to be able to derive conclusions about the effects on the shape of the equivalent Winkler spring coefficients distribution of the various parameters controlling the problem at hand, such as:

- the soil Young's modulus
- the foundation embedment
- the mat thickness
- the mat size and aspect ratio
- the column loading pattern
- the rate of increase of soil Young's modulus with depth
- having the foundation soil being underlain by a softer of stiffer soil layer

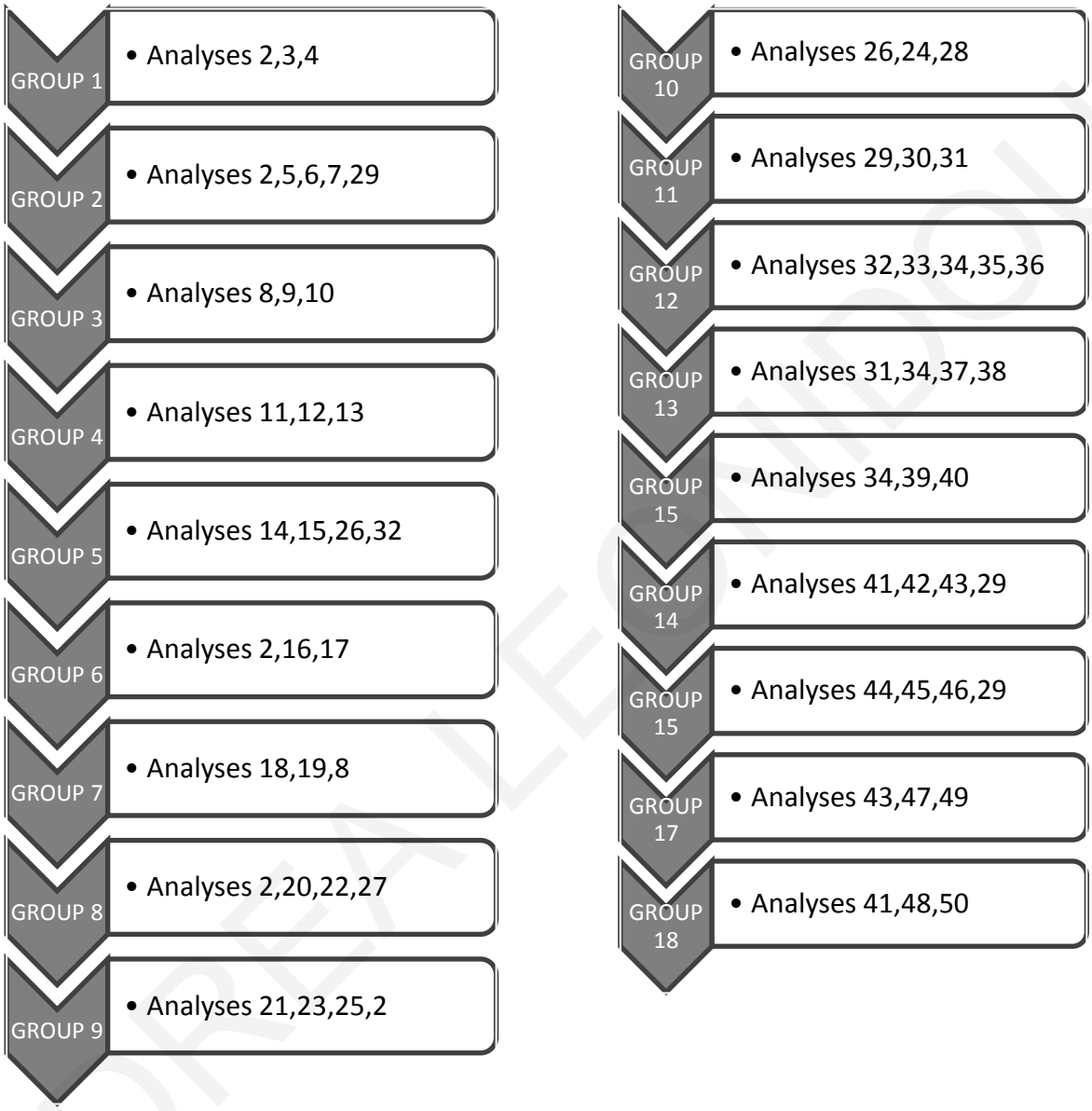

Figure 3.32: Grouping of parametric analyses for comparison purposes.

CHAPTER 4: NUMERICAL RESULTS

This chapter presents the results extracted from the finite element parametric analyses in Abaqus and Matlab. Comparison charts of the distribution of the equivalent K_{el} stiffness coefficient are presented at two different cross-sections of the mat, i.e. along the centerline and along the edge. The comparison plots were made in order to understand how the problem parameters affect the shape of the distribution of the K_{el} stiffness coefficient. Understanding the dependence of the K_{el} on these parameters is instrumental for the derivation of an equation that would describe mathematically the K_{el} distribution under the mat and allow the engineer to prescribe appropriately the Winkler springs in structural analyses of mat supported buildings.

The figures also plot with dotted curves the spring stiffness distributions predicted by the proposed equation, derived based on least squares fitting of the back-calculated distributions. The proposed equation will be presented in detail in Section 4.2.

4.1 Comparison graphs of equivalent spring stiffness coefficients

Effect of the soil Young's modulus

In Group 1, we can see the effect of the Young's modulus of the soil E_1, which for analysis 2 is equal to 10000kPa, 1000kPa for analysis 3 and 100000kPa for analysis 4. Fig. 4.1 plots the values of K_{el} along the centerline and along the edge of the mat.

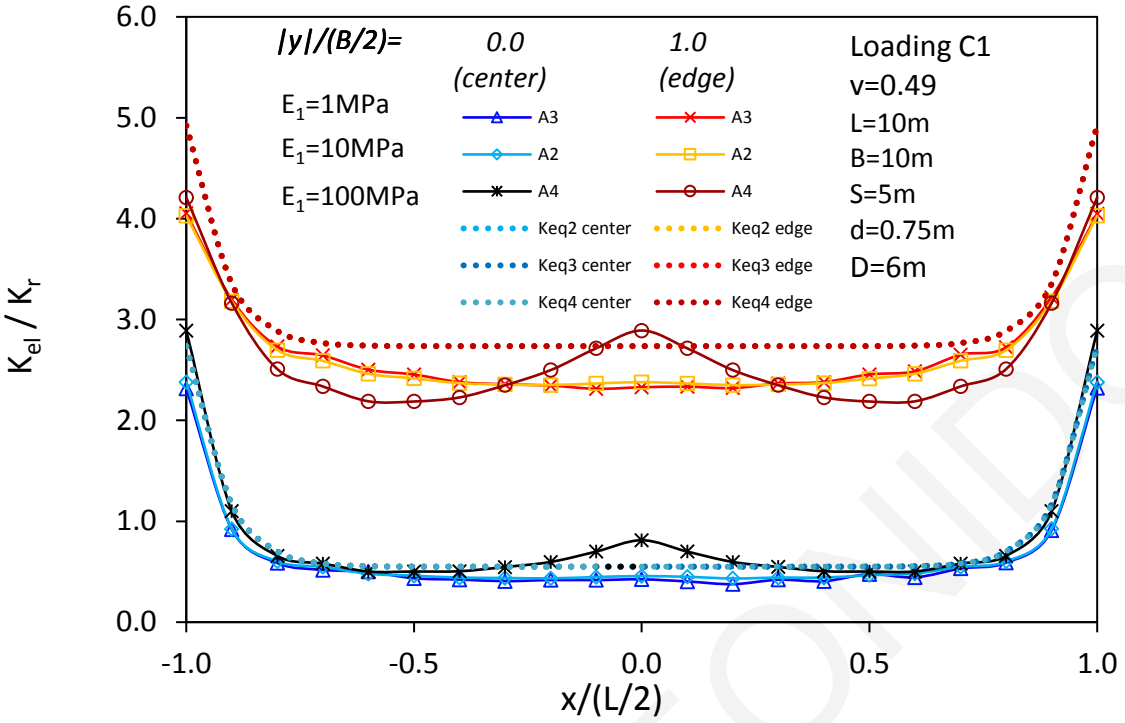

Figure 4.1: Effect of soil Young's modulus on the spring stiffness distribution.

It can be seen that the distribution of K_{el} at the edges is well above that at the centerline of the slab. In Analysis 4 (stiff soil) there is an increase in the value of K_{el} at the location of the application of the central load. Apart from that, the value of E_1 appears to not affect the normalized distribution K_{el}/K_r. In other, words the normalization with K_r works well and K_{el} is essentially directly proportional E_1.

Effect of embedment D for mat on uniform soil

Group 2 examines the effect of the embedment D in the case of uniform soil. Analysis 29 has zero embedment, analysis 5 has D=3m, analysis 2 has D=6m, analysis 6 has D=9m and analysis 7 has D=12m.

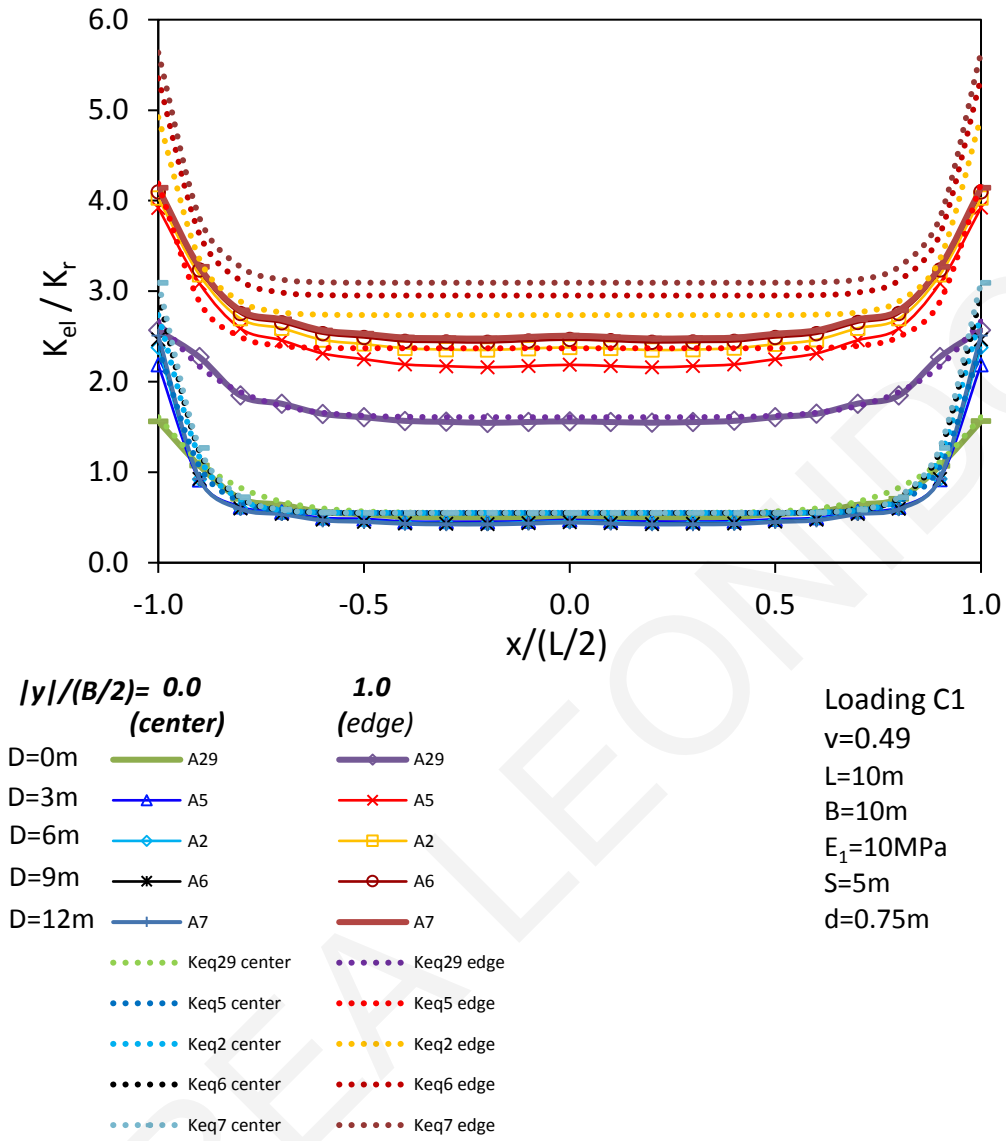

Figure 4.2: Effect of embedment on the spring stiffness distribution of mat on uniform soil (B=L=10m).

At the edge, analysis 29 (D=0) exhibits the smallest values of K_{el}. The opposite happens at the centerline where the values of K_{el} are slightly larger when embedment D=0. When D=12m, the values at the mat edges are clearly higher. Therefore, it can be stated that the higher the embedment D is, the higher the values of K_{el}/K_r at the edges.

In group 3 there are the analyses 8, 9 and 10, in which the width of the slab is larger (B=16m) than in group 2. This group also examines the effect of the embedment D. Analysis 8 has an embedment D=6m, analysis 9 has D=9m and analysis 10 has D=12m.

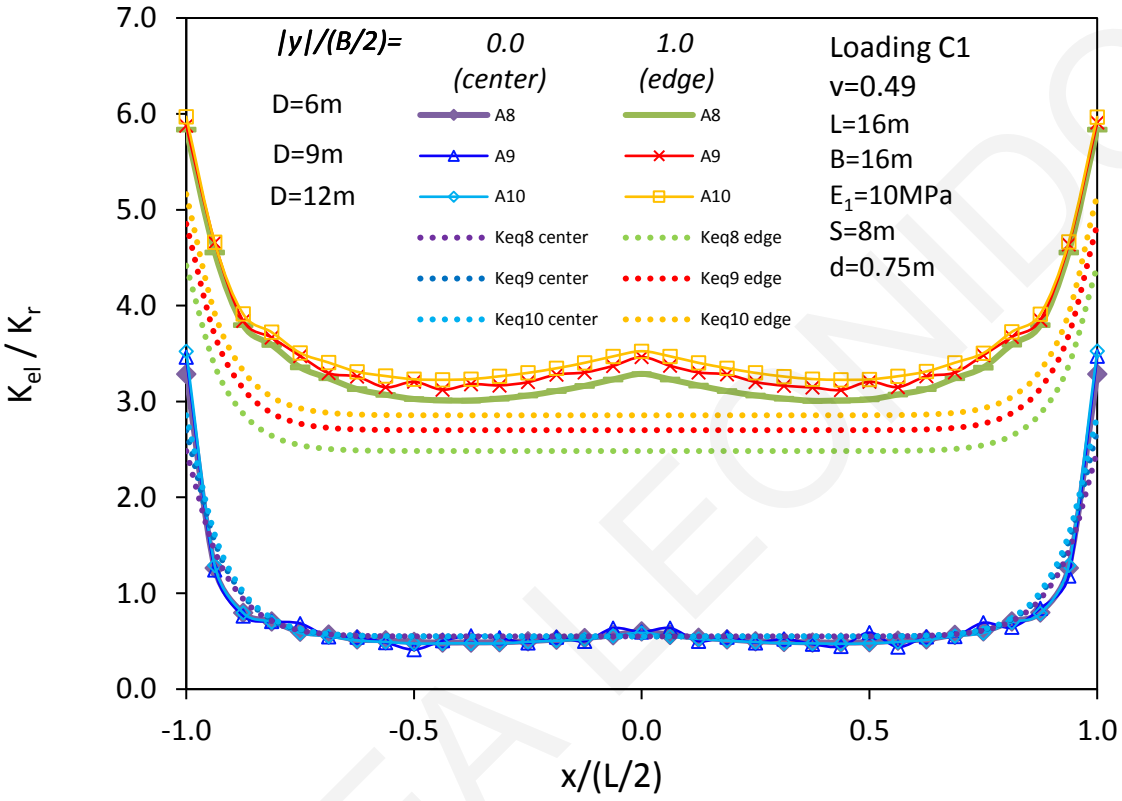

Figure 4.3: Effect of embedment on the spring stiffness distribution of mat on uniform soil (B=L=16m, v=0.49, loading C1).

As before we observe that at the edges when the embedment is large, the values of K_{el}/ K_r are amplified. Therefore, the higher the embedment D is, the higher the values of K_{el}/K_r at the edges are. Moreover, the larger the dimensions of the slab become, the effect of the embedment is less noticeable.

In group 4, we have analyses 11, 12 and 13, with the width of the slab being B=16m. Again the effect of the embedment D is examined, but this time with Poisson's ratio v=0.3 instead of 0.49. Analysis 11 has an embedment D=3m, analysis 12 has D=9m and analysis 13 has D=12m. Comparing Figs. 4.3 and 4.4, we notice that the Poisson's ratio doesn't seem to affect the shape of the K_{el} distribution.

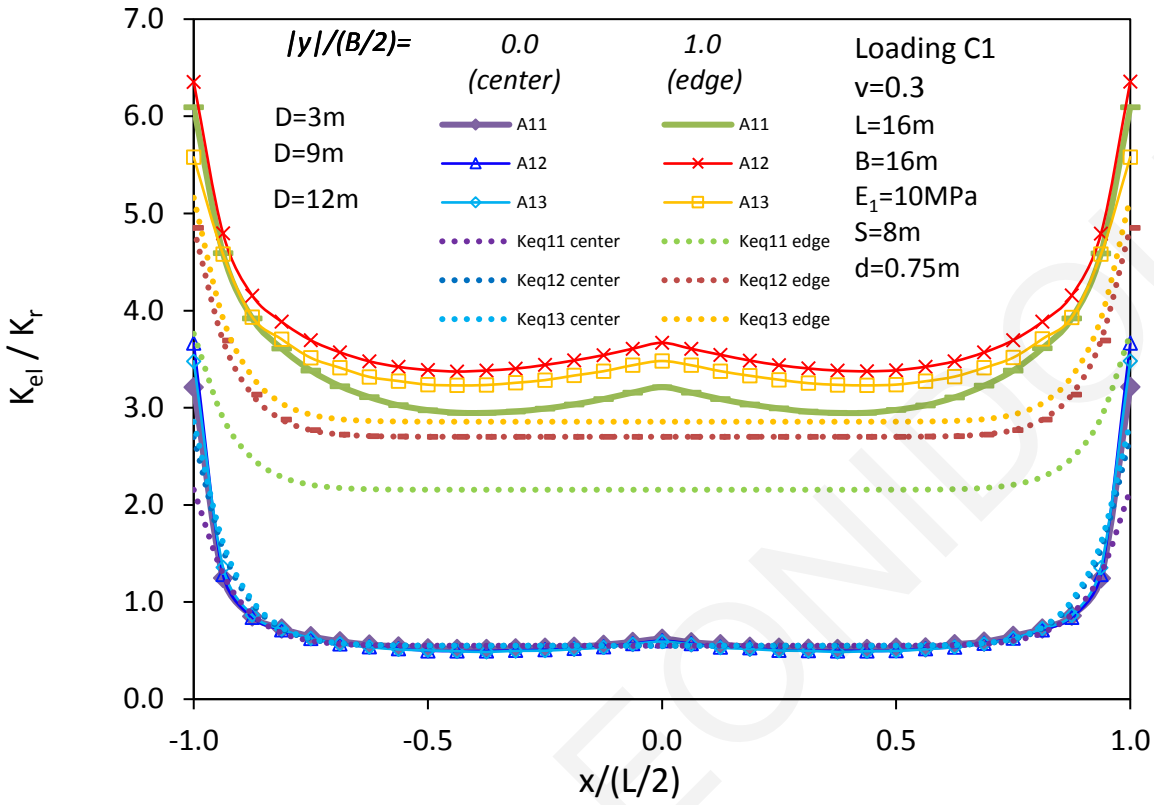

Figure 4.4: Effect of embedment on the spring stiffness distribution of mat on uniform soil (B=L=16m, v=0.3).

Group 5 comprises the analyses 14, 15, 26 and 32, which have mats that are not squared-shaped but have L/B ratio equal to 2.

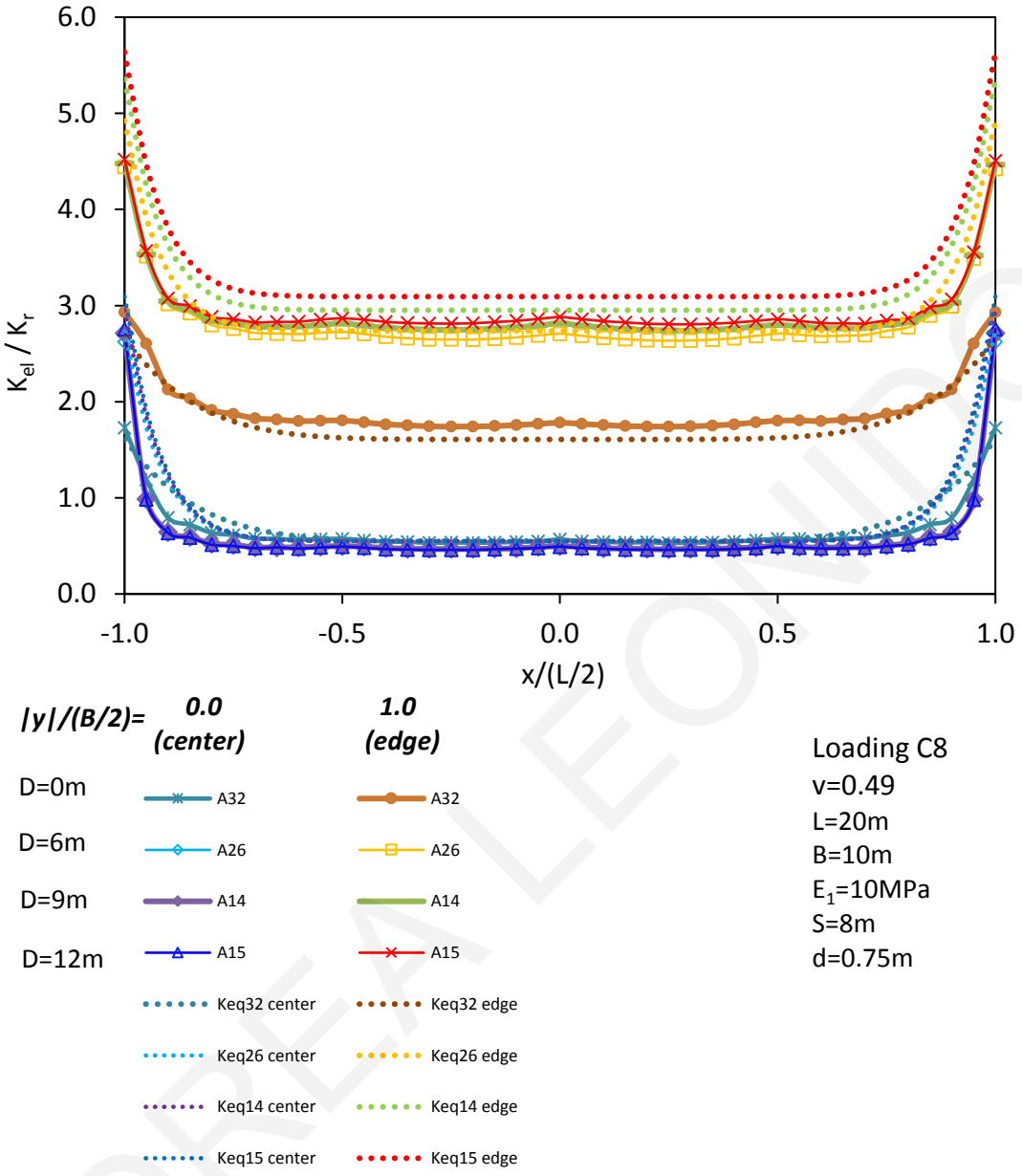

Figure 4.5: Effect of embedment on the spring stiffness distribution of mat on uniform soil (B=L=16m, v=0.49, loading C8)

It can be observed that the values of K_{el} converge to each other when there is an embedment. Hence, it can be concluded that the effect of embedment on the edge distribution is more prominent in the case of square foundation than in that of elongated foundations.

Effect of the thickness of the slab

In group 6, there is a comparison of the analyses 2, 16 and 17. The parameter that changes in this case is the thickness of the slab d. For analysis 16, 2 and 17, the value of d is 0.5m, 0.75m and 1m, respectively. In the following graph, we see that there is practically no effect of the thickness of the slab on the shape of the spring stiffness distribution.

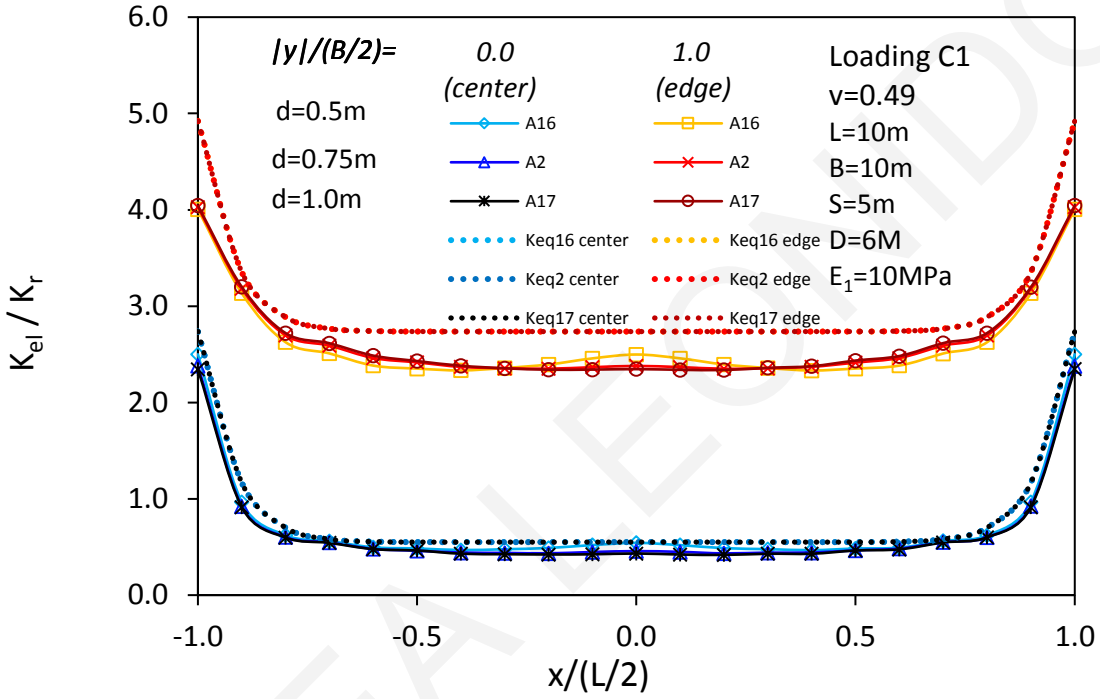

Figure 4.6: Effect of mat thickness on the spring stiffness distribution.

Effect of the thickness of deformable soil layer

In group 7, there is a comparison of the analyses 8, 18 and 19, where the mat is square with width B=16m and the Poisson's ratio is v=0.49. The parameter that is examined is the thickness of the model, i.e. the thickness of the deformable soil H_1 below the slab. In Fig. 4.7, it appears that the values of K_{el}/K_r at the center and at the edge converge as the thickness of the model below the slab is getting smaller. Nonetheless, this effect is not as strong as the one observed by Loukidis & Tamiolakis (2017) for mat foundations resting on the free ground surface. So, the presence of embedment reduces the influence of the presence of bedrock.

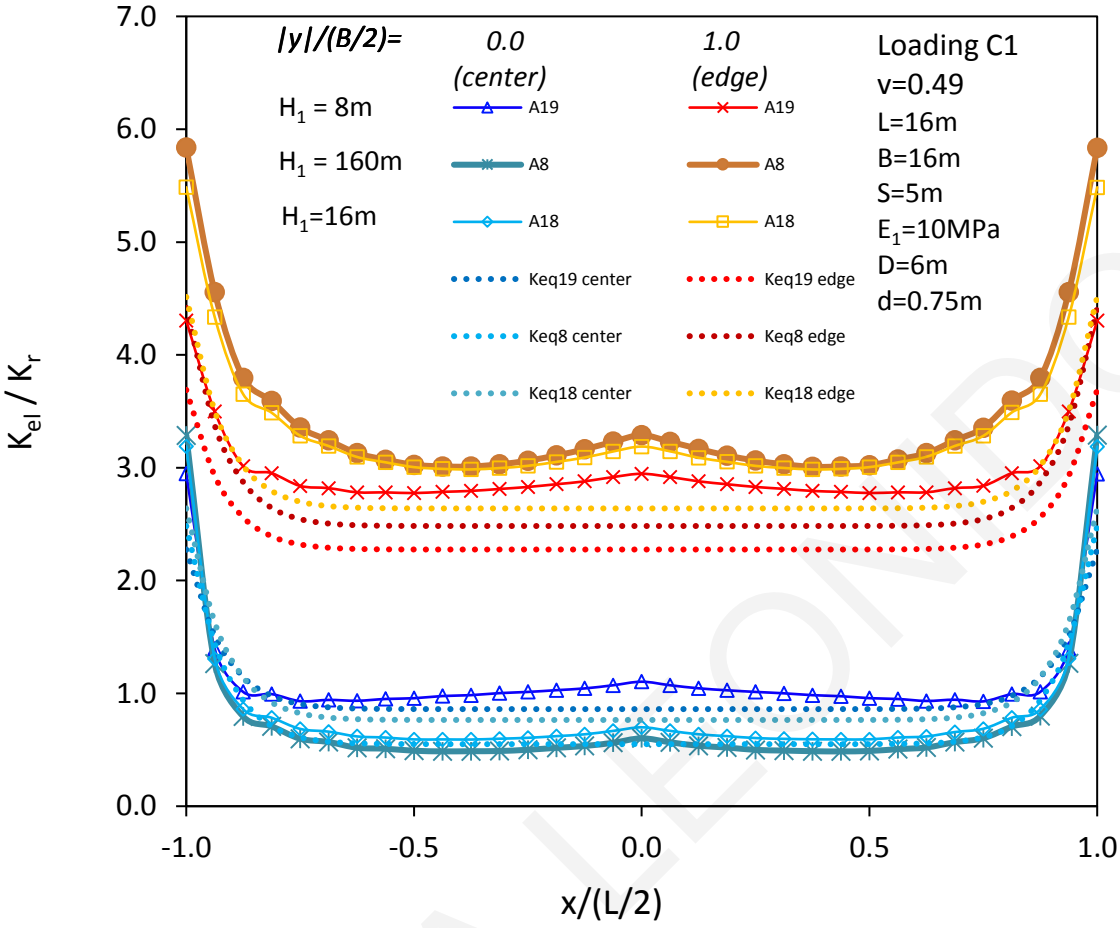

Figure 4.7: Effect of deformable soil layer thickness on the spring stiffness distribution.

Effect of the type of loading

In group 8, we have analyses 2, 20, 22 and 27, with width of mat B=10m and length L=10m, Poisson's ratio v=0.49 and the embedment D=6m. The comparison of the K_{el} this time is on the loading applied to the slab. It is important to note that all the loadings in this group (C1, C2, C4, C9) are perfectly symmetric in both axes (no load eccentricity). The loading that gives the highest values of K_{el} at the centerline is C9 (analysis 27), but at the same time gives the lowest K_{el} along the edge. This happens because loading C9 has only one load which is applied at the center of the mat and none at the mat edges or corners. Nonetheless, the differences between in the spring stiffness distributions are quite small for all cases. Therefore, it can be said that the column loading pattern has no effect on the spring stiffness distribution, as along as the loading is symmetric in both directions.

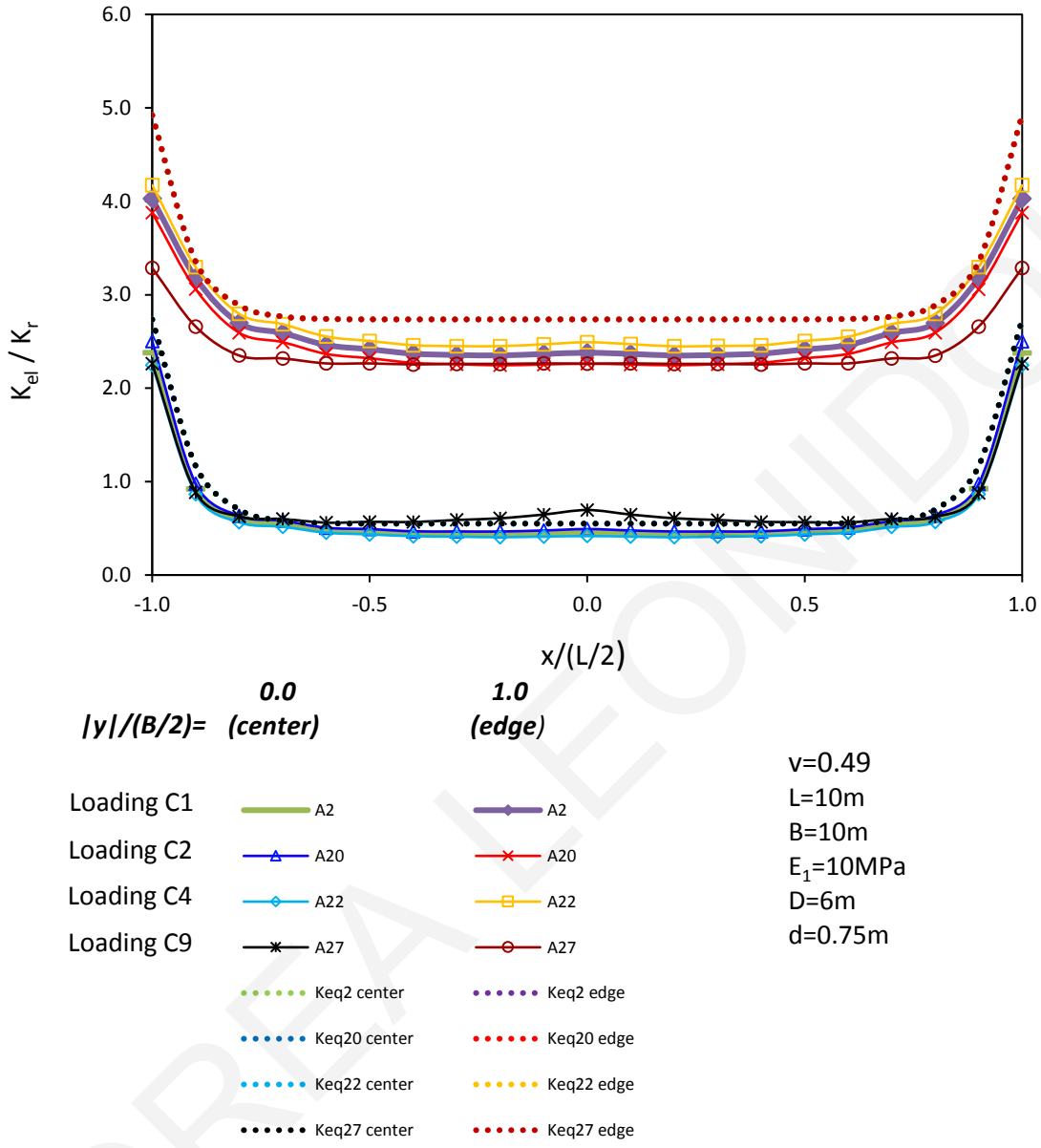

Figure 4.8: Effect of column loading pattern on the spring stiffness distribution (symmetric loading) of mat on uniform soil.

Group 9 contains analyses 2, 21, 23 and 25, having a mat with width B=10m and length L=10m, and soil Poisson's ratio v=0.49. The embedment is D=6m, the elastic modulus of the soil E=10MPa and the thickness of the slab is equal to 0.75m. What changes from analysis to analysis is again the loading type, but this time the loading has eccentricity. In the following figure, we can easily discern that in the case of eccentric loading the spring stiffness

distribution appears rotated towards the side that the eccentricity vector points to. Moreover, the larger the eccentricity value is, the more rotated appears the K_{el} distribution.

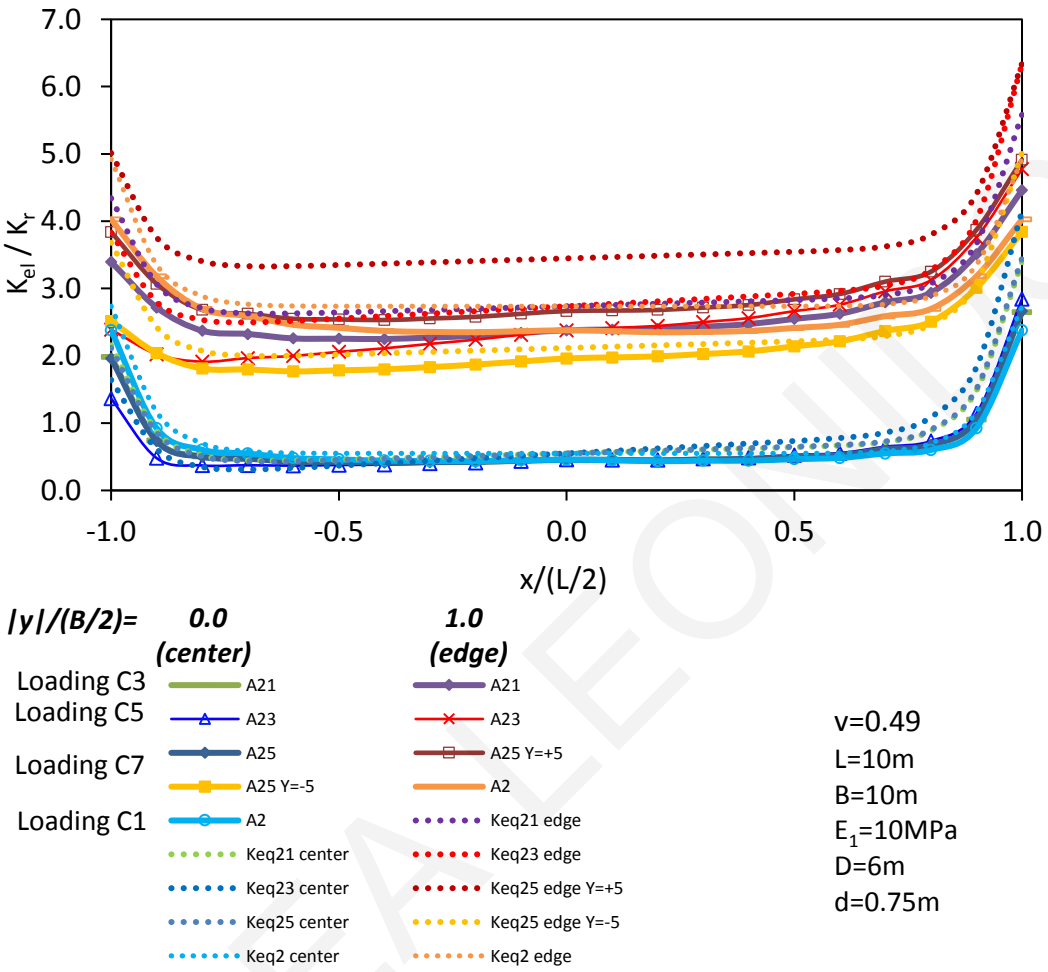

Figure 4.9: Effect of loading eccentricity on the spring stiffness distribution of mat on uniform soil.

In group 10, there are analyses 26, 24 and 28, having a mat with width B=10m, length L=20m, elastic modulus of the soil E=10MPa, soil Poisson's ratio v=0.49, embedment D=6m, and thickness of the slab 0.75m. In this comparison, it is again examined what is the effect of the loading pattern on the spring stiffness distribution. In this case, loading C8 of analysis 26 is symmetric (no eccentricity) and that of analysis 28 (loading C10) is non-symmetric. As a consequence, the distribution of K_{el} from analysis 28 appears rotated. The shape and size of the slab appears to not have an effect on the distribution of the K_{el}.

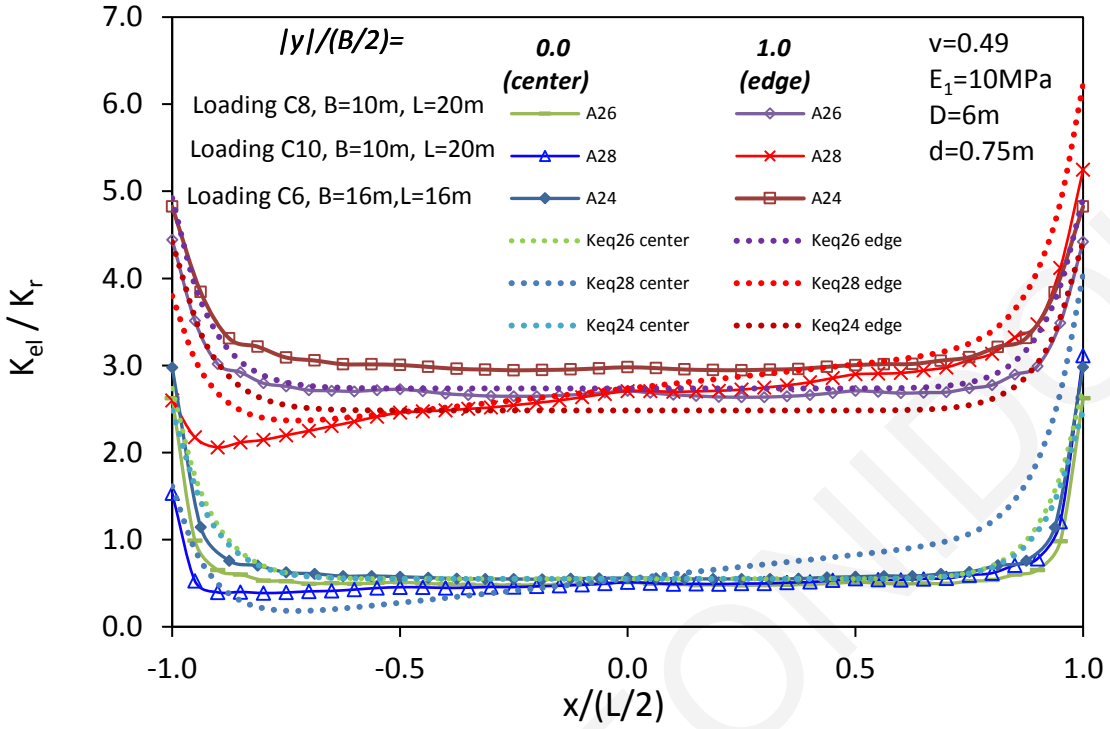

Figure 4.10: Effect of mat size and shape on the spring stiffness distribution of mat on uniform soil.

Linearly increasing elastic modulus with depth

Group 11 comprises analyses 29, 30 and 31, which have mats with width B=10m and length L=10m, soil Poisson's ratio ν=0.49, no embedment (D=0m), and elastic modulus of the soil that increases linearly with depth z in the form of E=10000+ρ*z (kPa). This group examines the effect of the rate of increase ρ of elastic modulus with depth. From the following graph (Fig. 4.11), as the growth rate with depth ρ increases, the distributions of the K_{el} at the center and at the edges rise substantially. Nonetheless, the shape of the spring stiffness distribution along the centerline, as well as along the edge, is practically independent of the value of ρ.

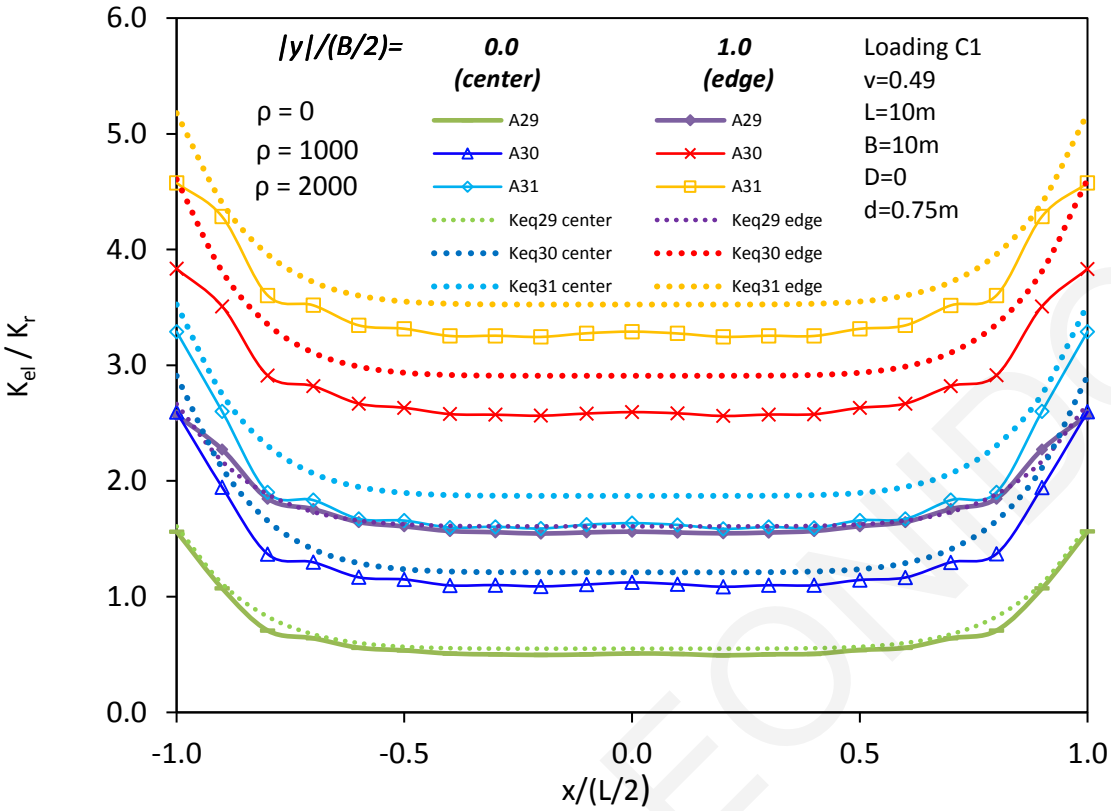

Figure 4.11: Effect of increase of soil elastic modulus with depth on the spring stiffness distribution.

Group 12 contains the analyses 32,33,34,35 and 36, which have mats with length 20m and width 10m on soil with increasing Young's modulus with depth. As shown in Fig. 4.12, as the ρ coefficient increases, the values of the K_{el} at the center and at the edge become larger. This is also true when there is embedment D.

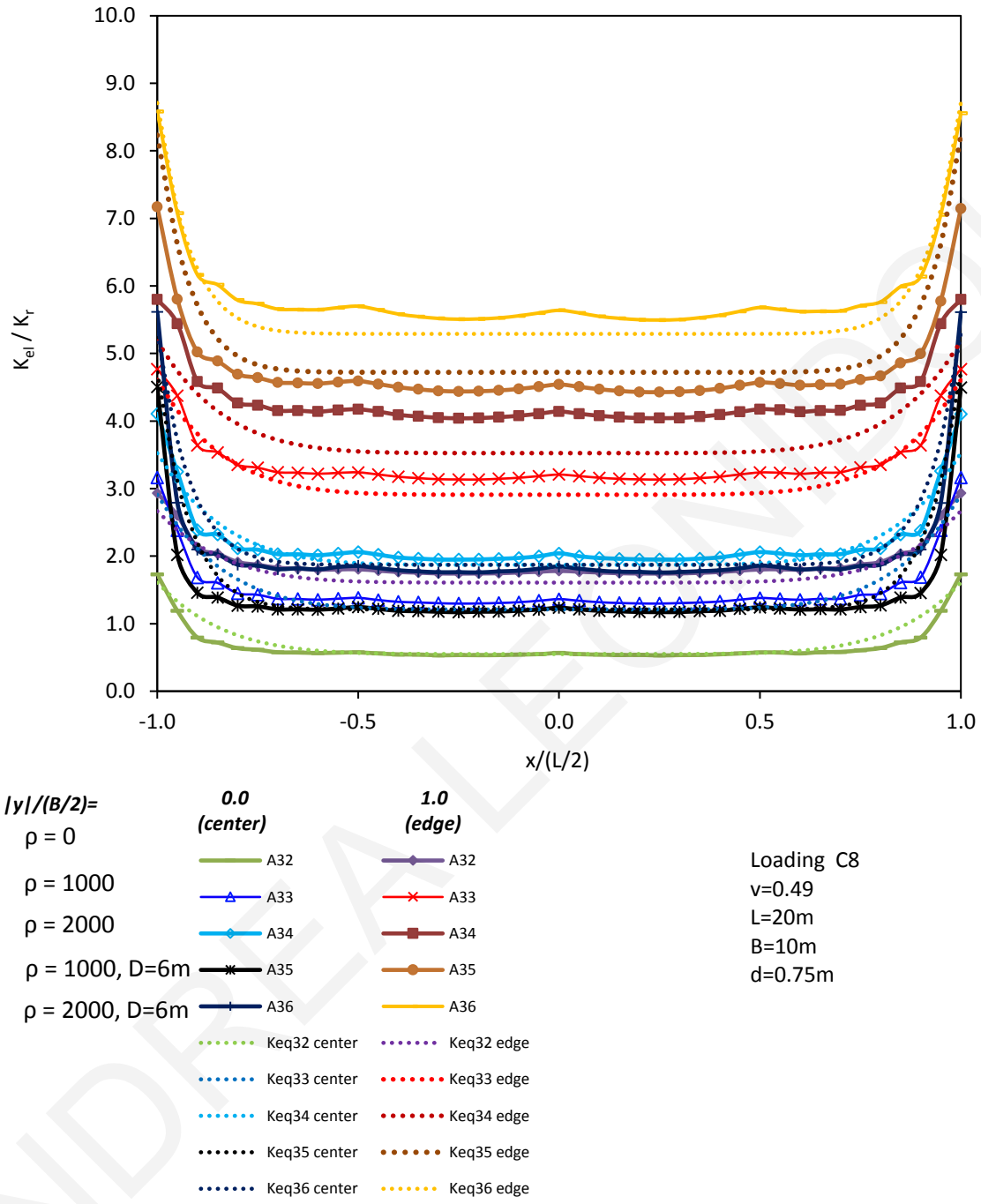

Figure 4.12: Effect of embedment on the spring stiffness distribution in the case of soil with increasing elastic modulus with depth.

In group 13, analyses 31, 38, 34, 37 and 38 are about mats loaded eccentrically. In this case too, we see that when the loading is non-symmetric spring stiffness distributions exhibit a rotation. However, this rotation is smaller in this case in which ρ=2000 than in the case of

uniform soil (Fig. 4.5). Loading C7 has eccentricity in both axes and that is why there are two different edge distributions, one at y=+5m (dark blue) that is higher than the red one the opposite edge y=-5m.

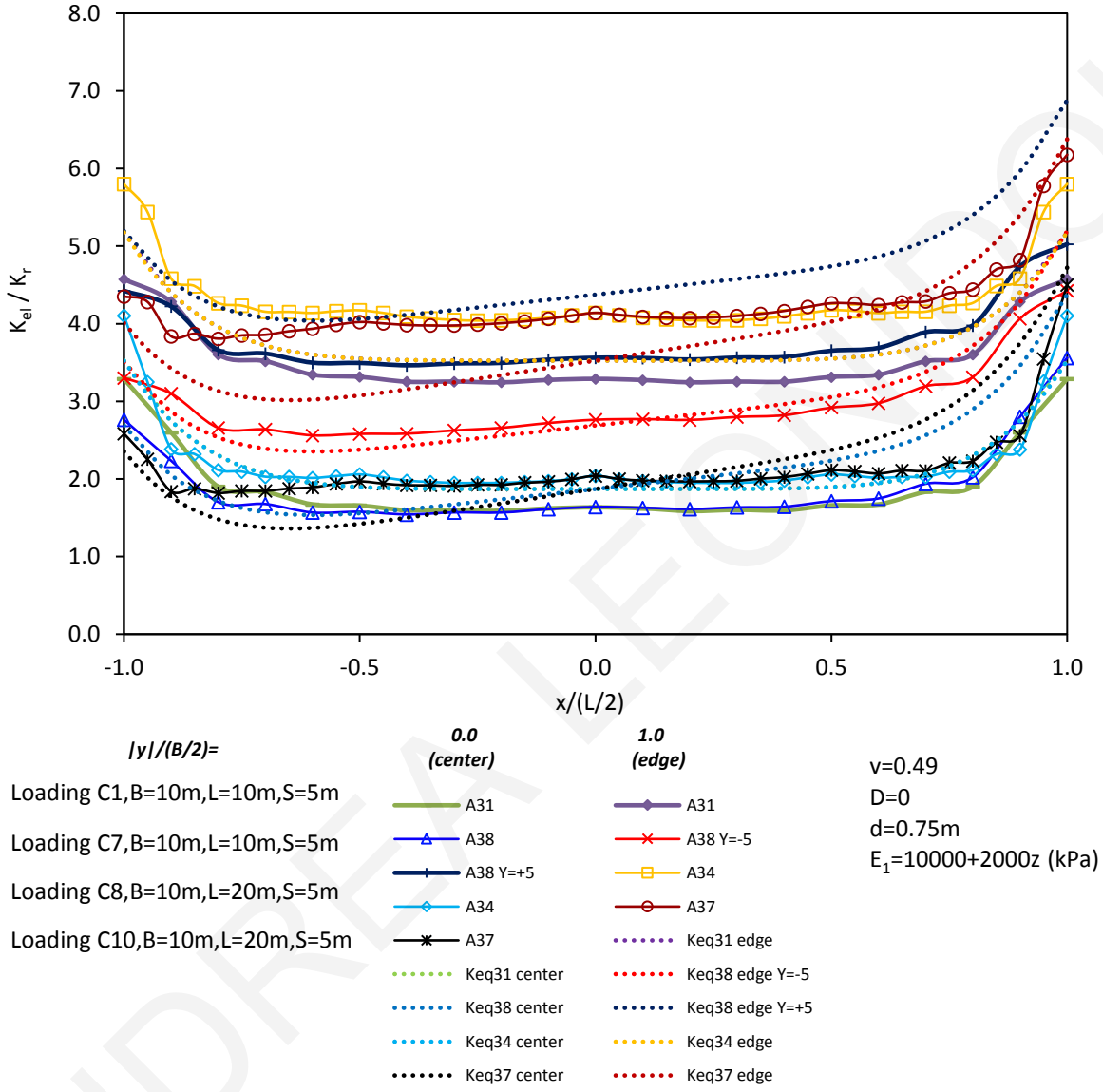

Figure 4.13: Effect of column loading pattern on the spring stiffness distribution in the case of soil with increasing elastic modulus with depth.

Group 15 contains analyses 39, 34 and 40, with the mat dimensions being L=20m and B=10m, in absence of embedment and with the soil elastic modulus increasing linearly with depth. In this case, it is examined whether the thickness of the slab has an effect on the distribution of the K_{el}. Again, as in the case of uniform soil, the effect of the thickness of the

slab is negligible. There is only a small effect which is the presence local of local peaks at the points we have load application when the thickness of the slab is small (0.5m). In other words, for relatively flexible mats, larger values of K_{el} are needed at the locations of the columns.

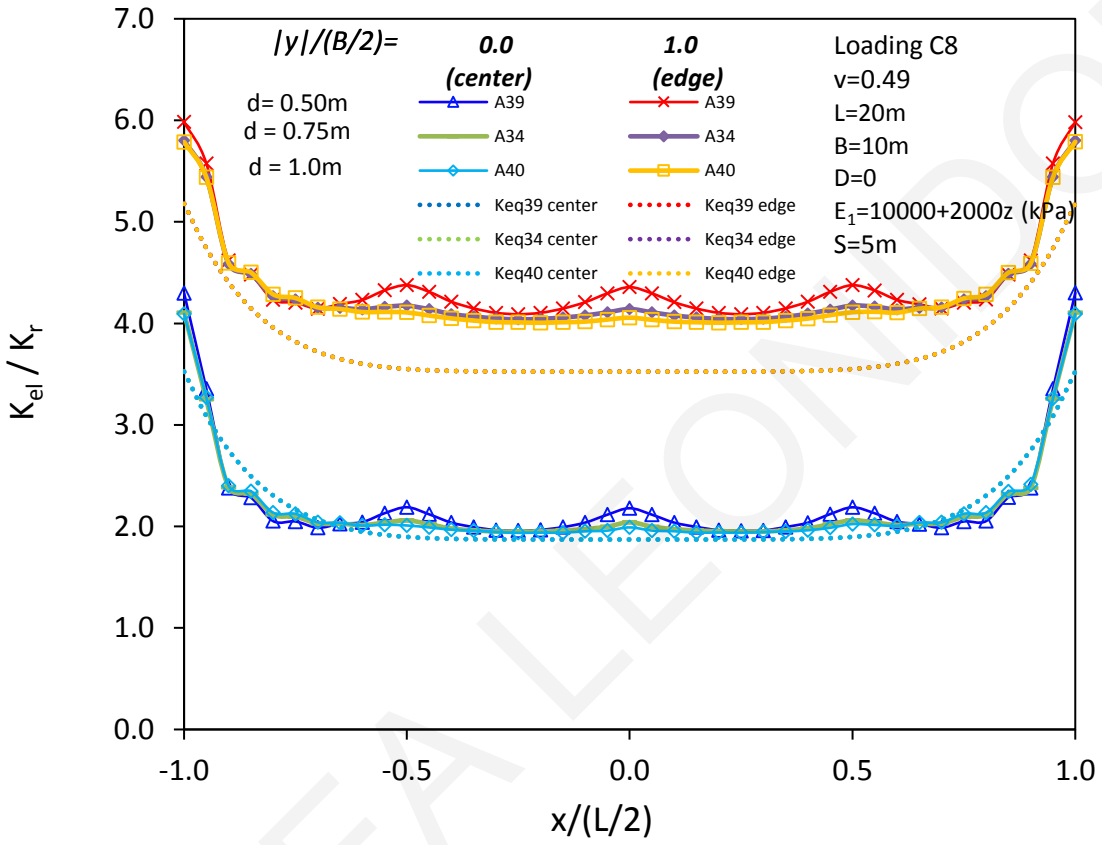

Figure 4.14: Effect of mat thickness on the spring stiffness distribution in the case of soil with increasing elastic modulus with depth.

Two-layered soil profile

Fig. 4.15 compares analyses 29, 43, 42 and 41, in which the mat has length L=10m and width B=10m, and rests on a two-layered soil profile. These cases examine the effect of the ratio E_1/E_2, where E_2 is the elastic modulus of the lower layer of soil and E_1 is the elastic modulus of the upper soil layer (foundation soil). It can be seen that as the ratio E_1/E_2 gets smaller (E_2 is increased), the distribution of the K_{el} at the edge and at the center gets raised.

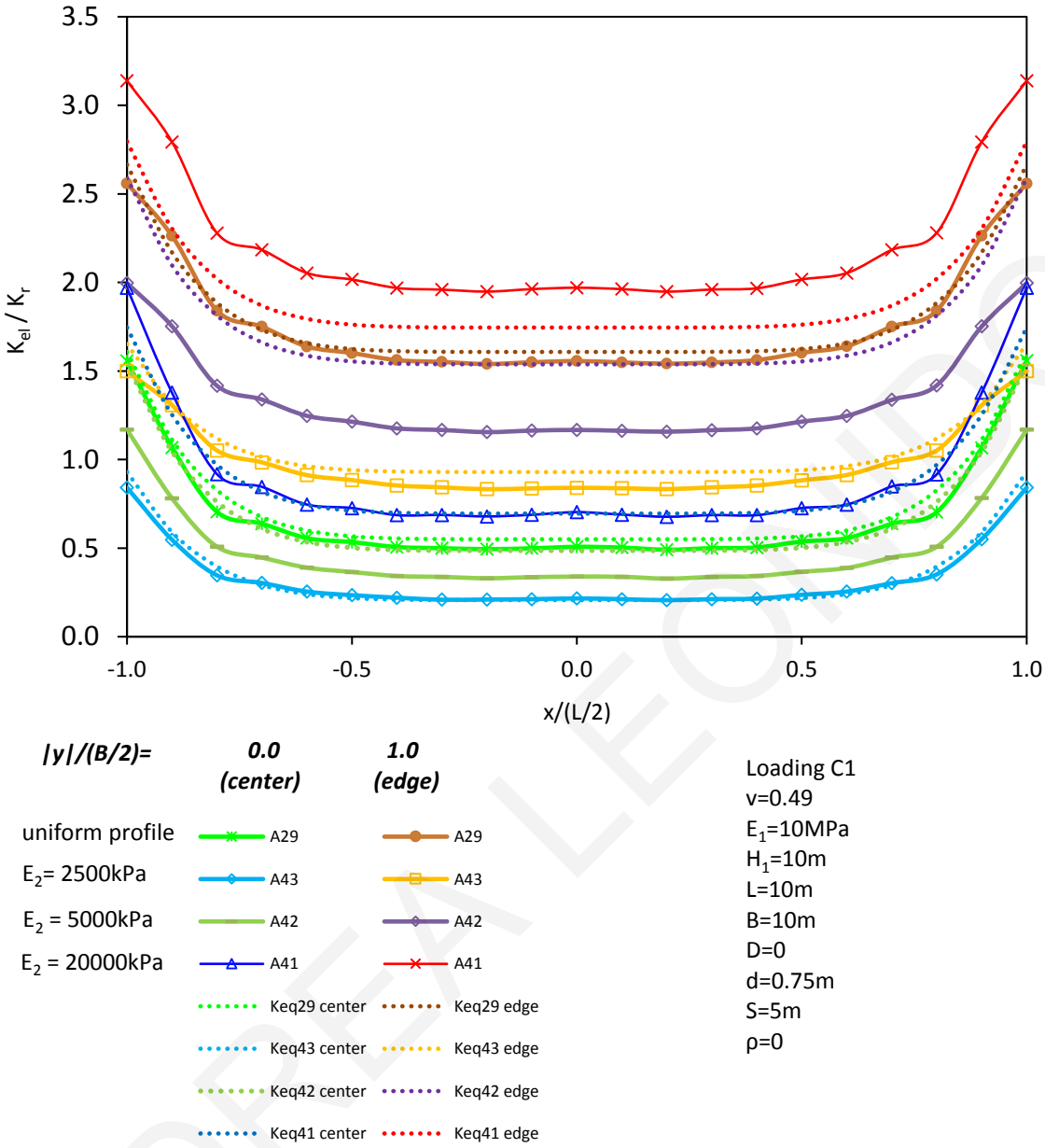

Figure 4.15: Effect of the presence of a second layer below the foundation soil on the spring stiffness distribution.

Fig 4.16 compares the analyses 29, 44, 45 and 46, which have different shape of the mat, as well as different loading pattern. The non-symmetric loading C7 in analysis 46 causes a rotation in the distribution of the K_{el}. But most importantly, the shape of the slab does not affect substantially the K_{el} distribution, since the results of the square mats (10mx10m and 16mx16m) are relatively close to those of the rectangular slab 10mx20m.

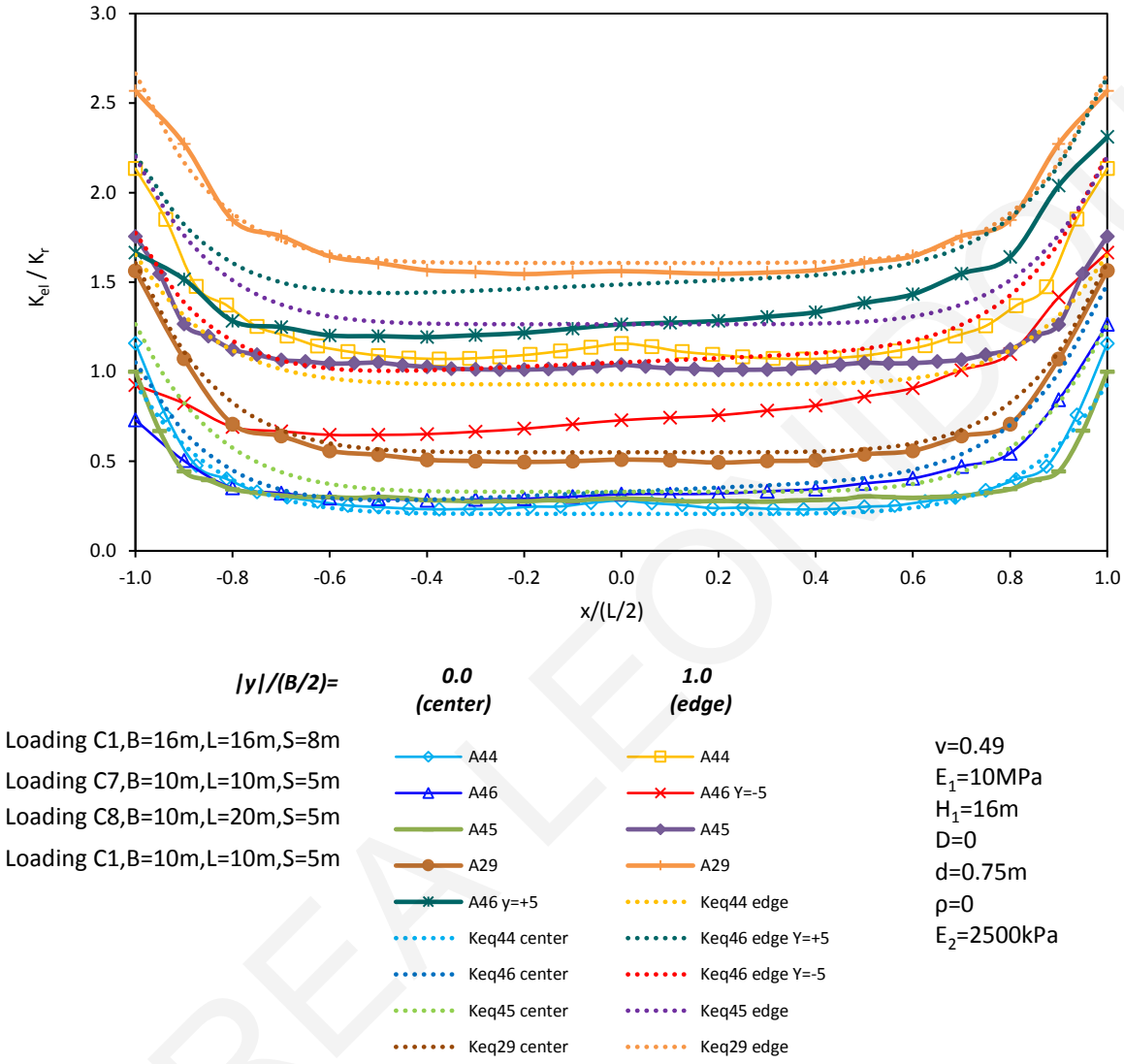

Figure 4.16: Effect of column loading pattern on the spring stiffness distribution in the case of a two-layered profile.

Fig. 4.17 shows the results of analyses 43, 47 and 49 examining the effect of the thickness of the upper soil layer H_1, when E_1=10000kPa (hard upper soil layer) and E2=2500KPa (soft lower soil layer). As H_1 increases, the distribution of the K_{el} at the centerline and at the edge rises substantially.

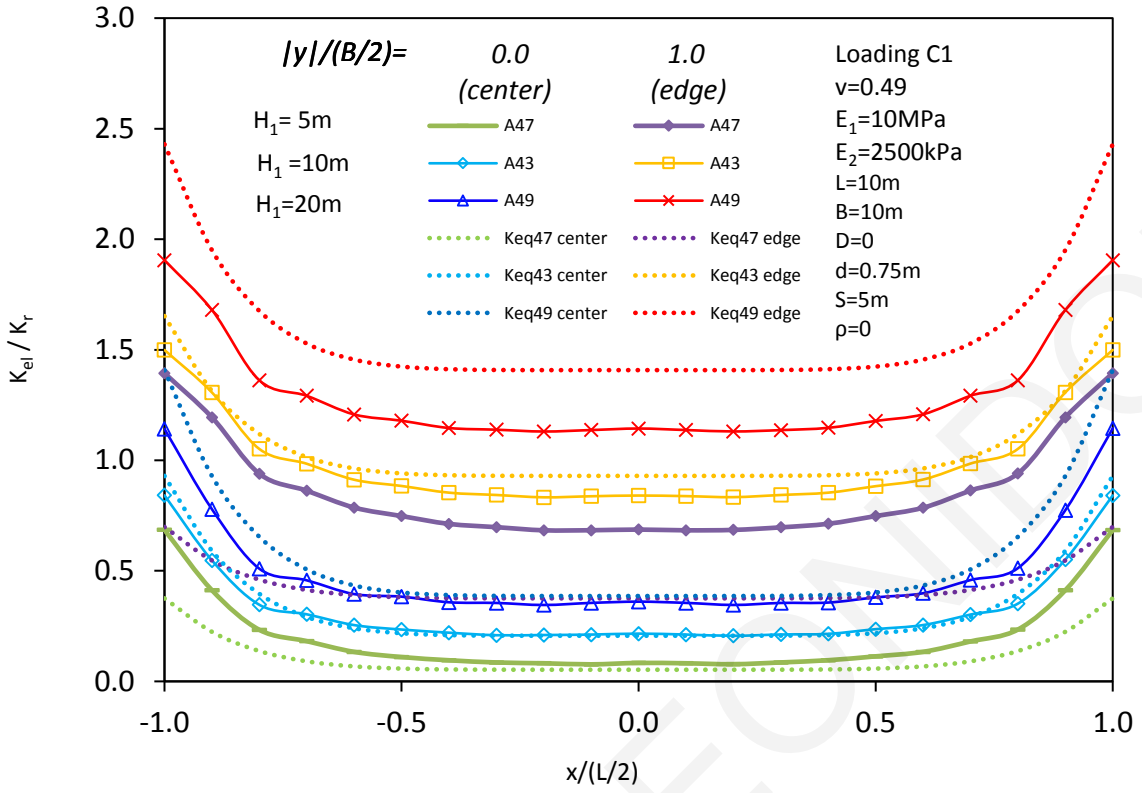

Figure 4.17: Effect of thickness of overlying layer on the spring stiffness distribution in the case of a two-layered soil profile (stiff soil overlying soft soil).

Finally, Fig. 4.18 presents results from analyses 41, 48 and 50, where the effect of the thickness of the upper soil layer H_1 is examined when E_1=10000kPa (soft upper soil layer) and E_2=20000kPa (harder lower soil layer). As H_1 gets larger, the distributions of K_{el} at the mat centerline and at the edge are lowered, i.e. the opposite of what happens in the previous case (Fig. 4.17).

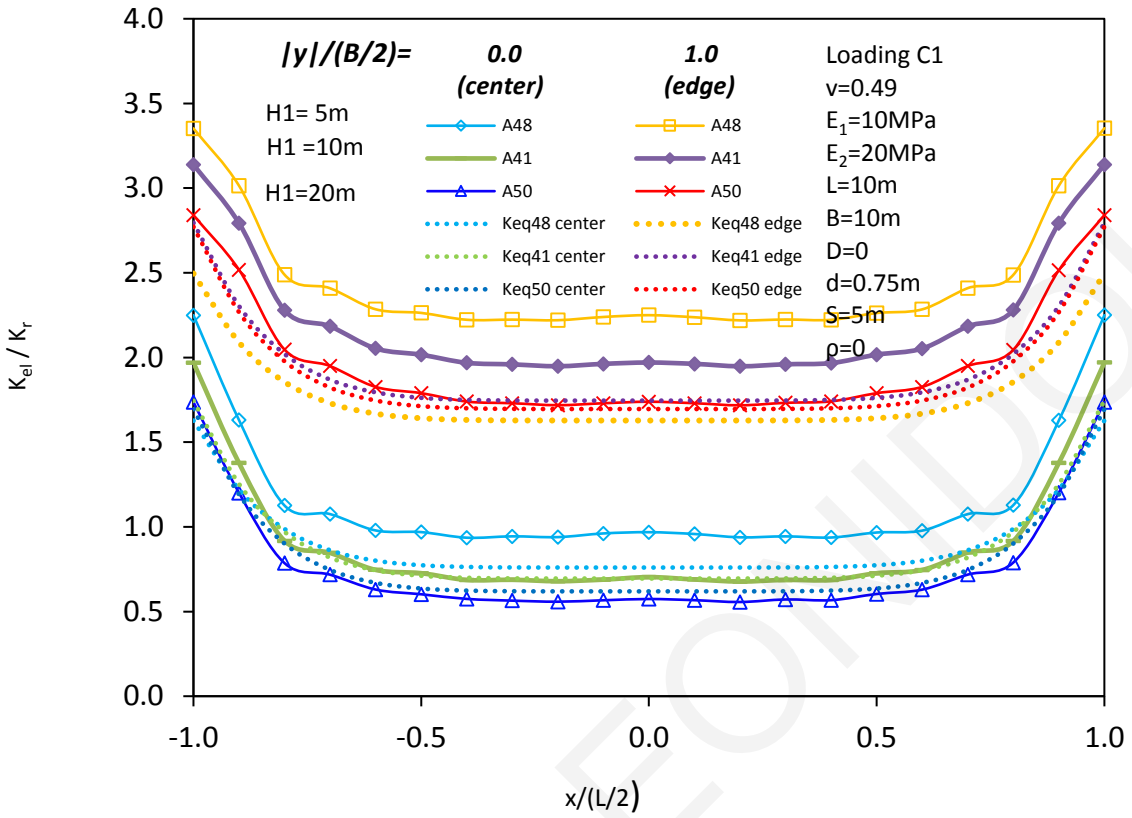

Figure 4.18: Effect of thickness of overlying layer on the spring stiffness distribution in the case of a two-layered soil profile (stiff soil underlying soft soil).

4.2 Least squares method in excel

In order to establish an equation for the determination of K_{el} to be used in practice, the K_{el} distributions back-calculated from the Abaqus results were fitted by a polynomial function of the form $K_{el}=a*x^n+b*y^n+c+(d_1x+d_2y)$. This was done by applying least squares regression with the help of the Excel Solver tool. With the use of the list squares method, the best fit coefficients a, b, c, d_1, d_2 of the polynomial equation were determined initially for each parametric analysis separately. The optimal exponent *n* value was not produced automatically by the Excel Solver, as it had to be an even integer number (4, 6, 8, e.t.c.). Hence, the optimal *n* was established by trying consecutively several scenarios of even integer values and observing the trend in the value of the sum of squared errors after least squares fitting the rest of the parameters.

The best fit parameter values of a, b, c, d_1, d_2 and *n* are shown in Table 4.1. The graphs comparing the best fit K_{el} distribution with the original, Abaqus-derived distribution for all parametric analyses are shown in Annex C.

Table 4.1: Best fit parameters for polynomial equation for the distribution of K_{el}.

Analysis	**Parameters of the polynomial equation of the form** $K_{el}=ax^n+bx^n+c+(d_1x+d_2y)$					
#	**a**	**b**	**c**	**d_1**	**d_2**	**n**
1	812.6	812.6	190.4	-	-	12
2	908.7	908.7	224.1	-	-	10
3	91.7	91.7	22.2	-	-	10
4	8958.5	8958.5	2244.7	-	-	12
5	800.1	800.1	222.6	-	-	12
6	908.7	908.7	224.1	-	-	12
7	978.3	978.3	227.8	-	-	12
8	1028.0	1028.0	231.7	-	-	18
9	716.1	716.1	125.3	-	-	20
10	767.1	767.1	125.4	-	-	20
11	805.9	805.9	126.2	-	-	18
12	560.8	560.8	108.0	-	-	20
13	681.2	681.2	106.8	-	-	18
14	666.0	666.0	115.1	-	-	20
15	773.8	773.8	168.9	-	-	20
16	814.8	814.8	170.8	-	-	12
17	895.9	895.9	226.9	-	-	12
18	913.6	913.6	222.8	-	-	20
19	1286.2	1286.2	295.8	-	-	24
20	1675.7	1675.7	832.7	-	-	12
21	883.0	883.0	230.2	93.7	0	12
22	889.6	889.6	222.7	-	-	12
23	969.8	895.4	217.6	204.6	0	12
24	824.0	824.0	218.6	-	-	22
25	630.0	630.0	142.6	102.1	102.1	12
26	862.2	862.2	221.5	-	-	18
27	719.8	719.8	167.6	-	-	12
28	762.4	762.4	257.2	113.3	0	20
29	662.7	662.7	166.2	-	-	6

Table 4.1 (continued)

#	a	b	c	d_1	d_2	n
30	451.4	451.4	212.8	-	-	6
31	622.5	622.5	465.7	-	-	6
32	695.2	695.2	680.7	-	-	8
33	358.0	358.0	162.3	-	-	8
34	540.7	540.7	403.9	-	-	8
35	618.6	618.6	610.7	-	-	18
36	1097.0	1097.0	415.7	-	-	16
37	1260.7	1260.7	627.3	128.2	0	10
38	546.5	546.5	610.6	232.3	232.3	10
39	634.2	634.2	676.8	-	-	8
40	635.2	635.2	603.6	-	-	8
41	620.2	620.2	610.6	-	-	6
42	541.7	541.6	287.9	-	-	6
43	358.0	358.0	144.7	-	-	6
44	274.1	274.2	93.1	-	-	8
45	219.0	219.0	51.9	-	-	8
46	218.5	218.5	84.5	76.6	76.6	6
47	290.6	290.6	131.7	-	-	6
48	271.9	271.9	42.7	-	-	6
49	541.8	541.8	384.1	-	-	6
50	336.9	336.9	150.4	-	-	6

By using the above parameters, the Loukidis & Tamiolakis (2017) equation for the estimation of K_{el} was modified to account for the effects of embedment D, the rate (ρ) of increase of the elastic modulus of the foundation soil with depth, and the presence of a second soil layer with different Young modulus (E_2) below the foundation soil layer. The final form of the proposed equation is the following:

$$K_{el} = K_r\left(0.55 + C_{H1}\right)\left(1 + 1.2\frac{\rho B}{E_1}\right)\left\{1 + 2C_{H2}\left[\left(\frac{x + 0.1e_x}{L/2}\right)^n + \left(\frac{y + 0.1e_y}{B/2}\right)^n\right] + 4\left[\frac{e_x}{L}\left(\frac{x}{L/2}\right) + \frac{e_y}{B}\left(\frac{y}{B/2}\right)\right]\right\} \quad (4.1)$$

where

$$C_{H1} = 0.45\left(1 - 0.65\frac{E_1}{E_2}\right)\exp\left(-0.74\frac{H_1}{B}\right) \quad (4.2)$$

$$C_{H2} = \left[\frac{1+5.5\frac{D}{B}}{1+1.8\frac{D}{B}}\right]\left(1-0.27\frac{\rho B}{E_1}\right)\exp\left[-0.4\frac{B}{H_1}\left(1-0.6\frac{E_1}{E_2}\right)\right] \quad (4.3)$$

$$n = \begin{cases} 6 & \text{for D=0} \\ 12 & \text{for D>0} \end{cases} \quad (4.4)$$

According to eq. (4.4), if a mat is embedded in the ground, the exponent is raised from the original value of 6 to 12. As seen in Table 4.1, there are several parametric runs the results of which are best fitted using *n* values much larger than 12 (up to 20). Nonetheless, as shown in the following section, the use of a flat (independent of embedment) value for *n* and the consequent discrepancy in the K_{el} distribution result in negligible errors in the predicted moment diagrams.

The effect of embedment D enters also C_{H2} (eq. 4.3) which is the factor controlling how much larger will be the spring coefficients at the edges compared to those in near the center of the mat. The expression in the first brackets in eq. 4.3 reaches an asymptotic value of 3.05 for very large values of foundation embedment.

The effect of the rate *ρ* of increase of the soil elastic modulus with depth affects mainly the baseline K_{el} (i.e. the K_{el} values at the central region of the mat) through the parentheses in the form of $(1+A*\rho B/E_1)$ in eqs. (4.1) and (4.3). On the other hand, the presence of a second, underlying layer enter the expressions of both C_{H1} and C_{H2}.

From Figs. 4.1-4.18, it can be seen that although eq. (4.1) produces spring stiffness distributions that match adequately the Abaqus-derived distributions, the fit deteriorates along the edges of the mat. This has to do mainly with the factor C_{H2} and to a lesser extent with the exponent *n*.

4.3 Bending moment diagrams

In this section, the bending moments diagrams from a selection of 16 analyses of mat foundation on springs with coefficients estimated using the proposed equation are compared with those using directly the Abaqus derived springs. These analyses are 2, 5, 6, 7, 8, 10, 24, 26, 28, 29, 30, 31, 41, 43, 47 and 48 and the diagrams of bending moment m_x, i.e. along the centerline aligned with the x-axis, are plotted in Figs. 4.19-4.34. This is done to

assess the loss of accuracy due to the inherent fitting error of the K_{el} equation (eq. 4.1). The codes in Matlab used for the extraction of the moment diagrams were originally developed by Tamiolakis (2012) and were modified herein according to the new equation for K_{el}. The corresponding Matlab codes and examples of input files are shown in Annex D.

In the case of plates, the bending moments have units of kNm/m, i.e. kNm per meter of width or length of the slab. Furthermore, the moments in the plots below are normalized with respect to the sum of the column loads ΣQ multiplied by the column spacing S. It can be seen that despite the discrepancies observed in many of the K_{el} comparison plots (most notably in Figs. 4.2, 4.7, 4.11, 4.14, 4.17) along the mat edge, the moments obtained using the spring coefficients determined using the proposed equation (eq. 4.1) are practically identical to those corresponding to the back-calculated springs from the Abaqus FEA results. Hence, it can be stated that the proposed equation performs very well and can be adopted for use in the engineering practice.

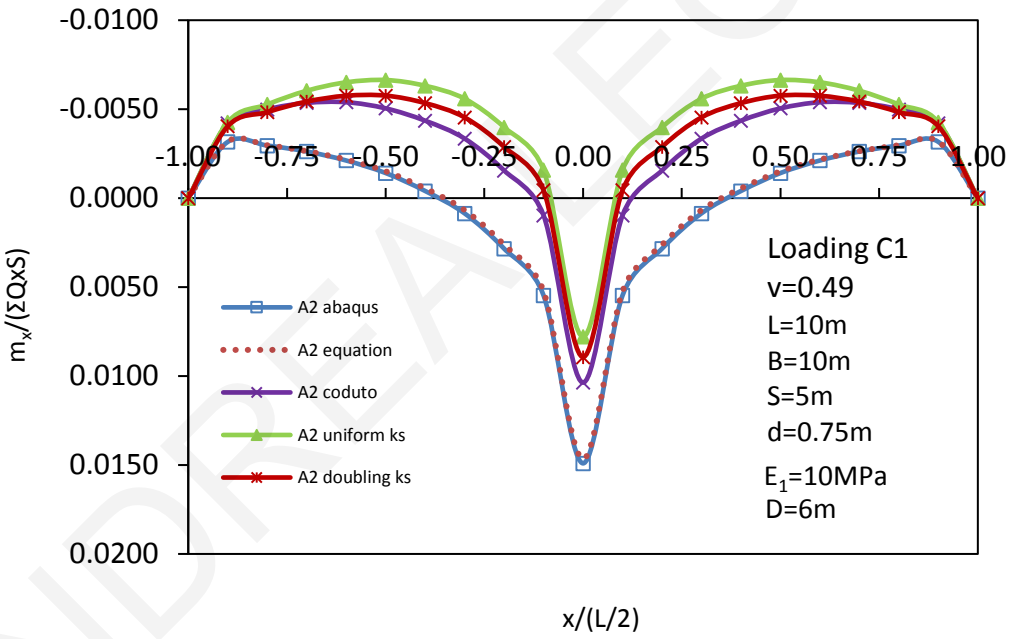

Figure 4.19: Moment diagram for Analysis 2.

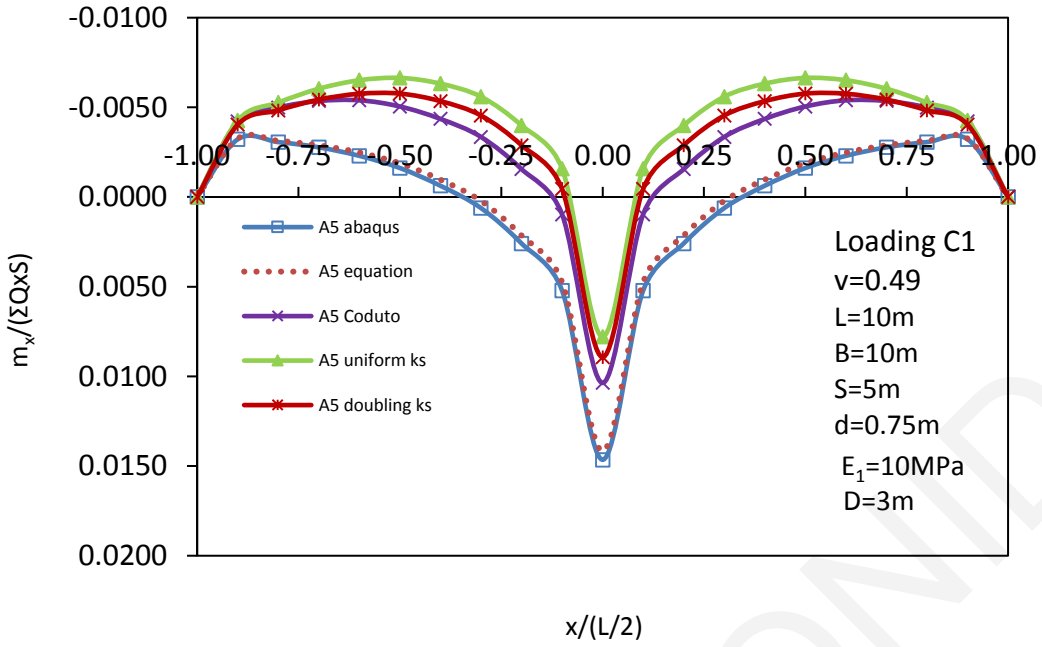

Figure 4.20: Moment diagram for Analysis 5.

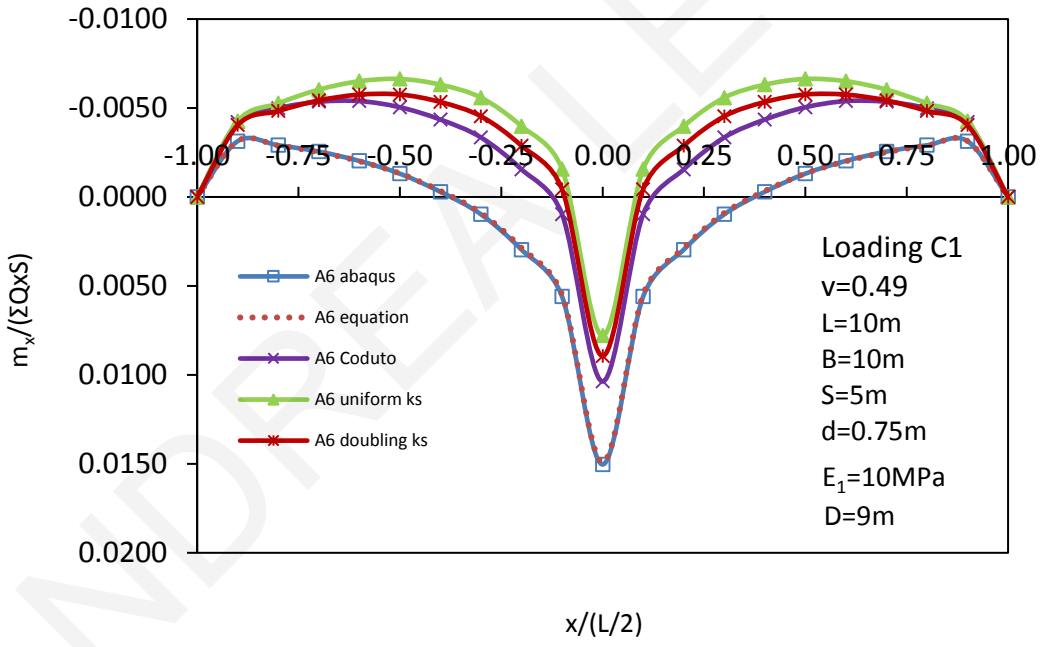

Figure 4.21: Moment diagram for Analysis 6.

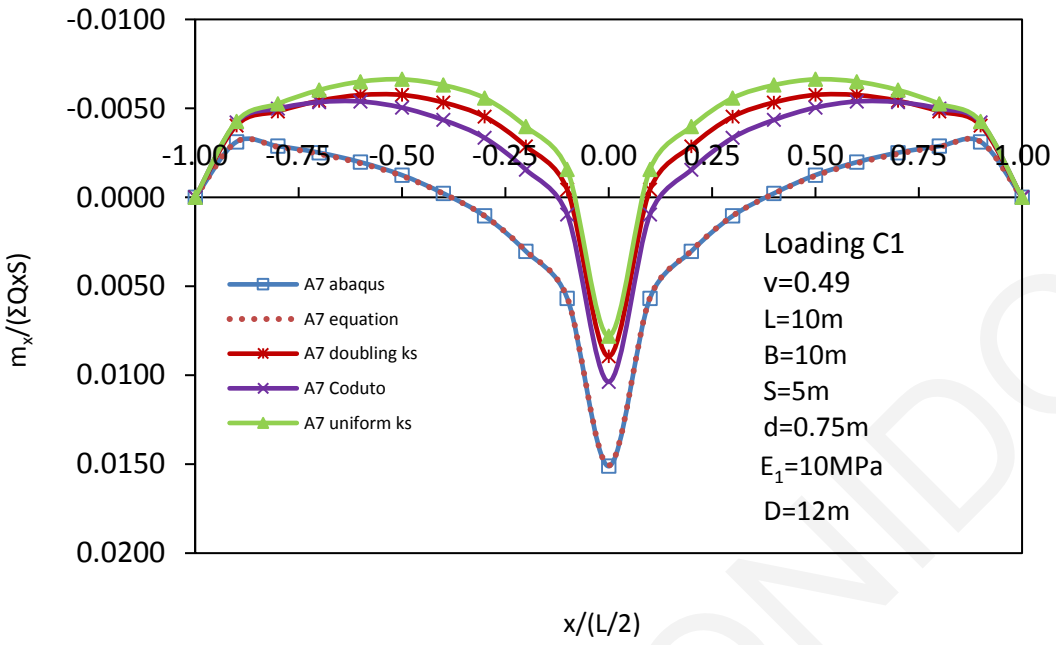

Figure 4.22: Moment diagram for Analysis 7.

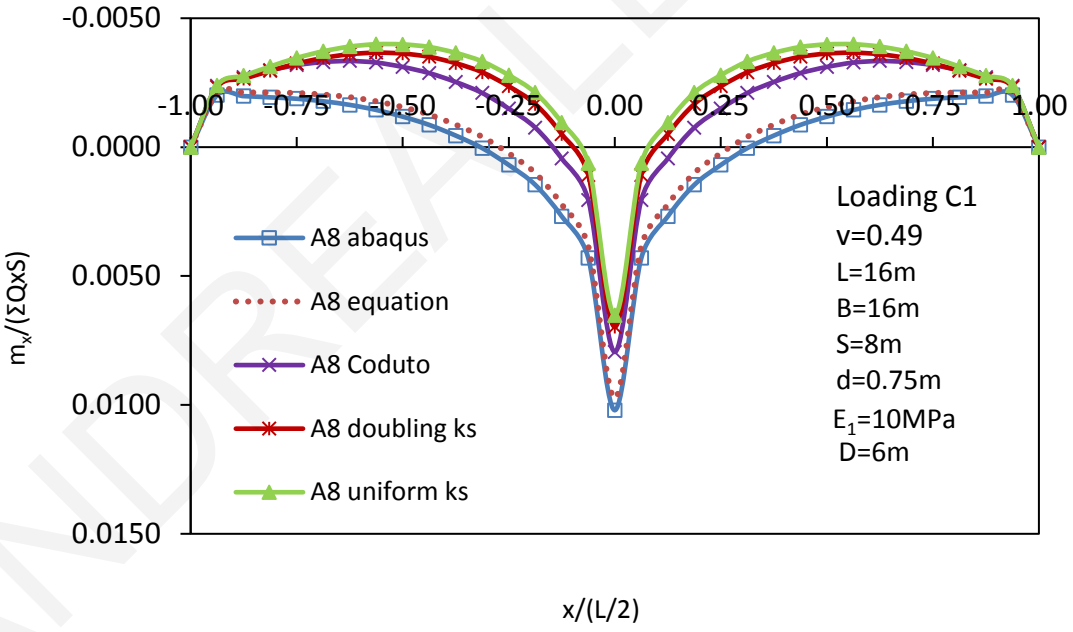

Figure 4.23: Moment diagram for Analysis 8.

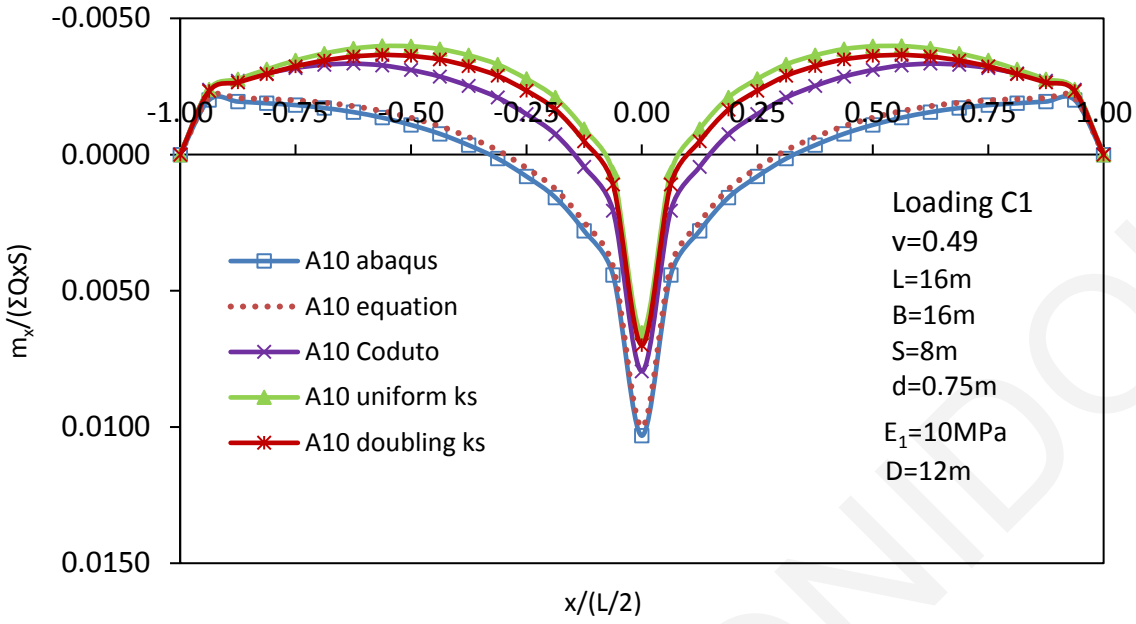

Figure 4.24: Moment diagram for Analysis 10.

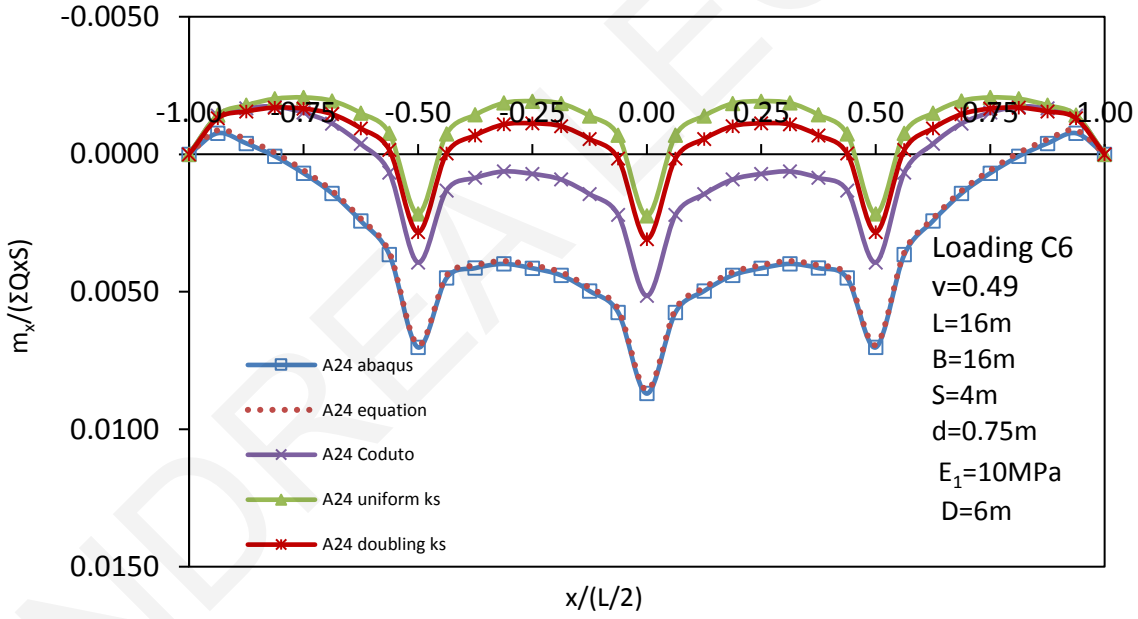

Figure 4.25: Moment diagram for Analysis 24.

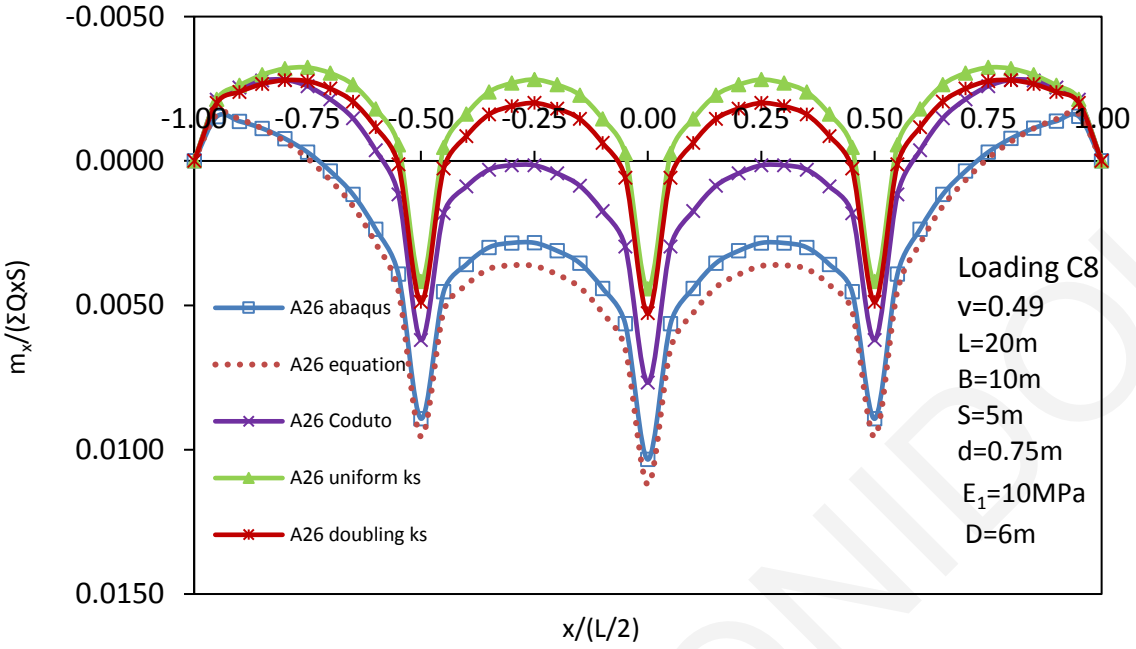

Figure 4.26: Moment diagram for Analysis 26.

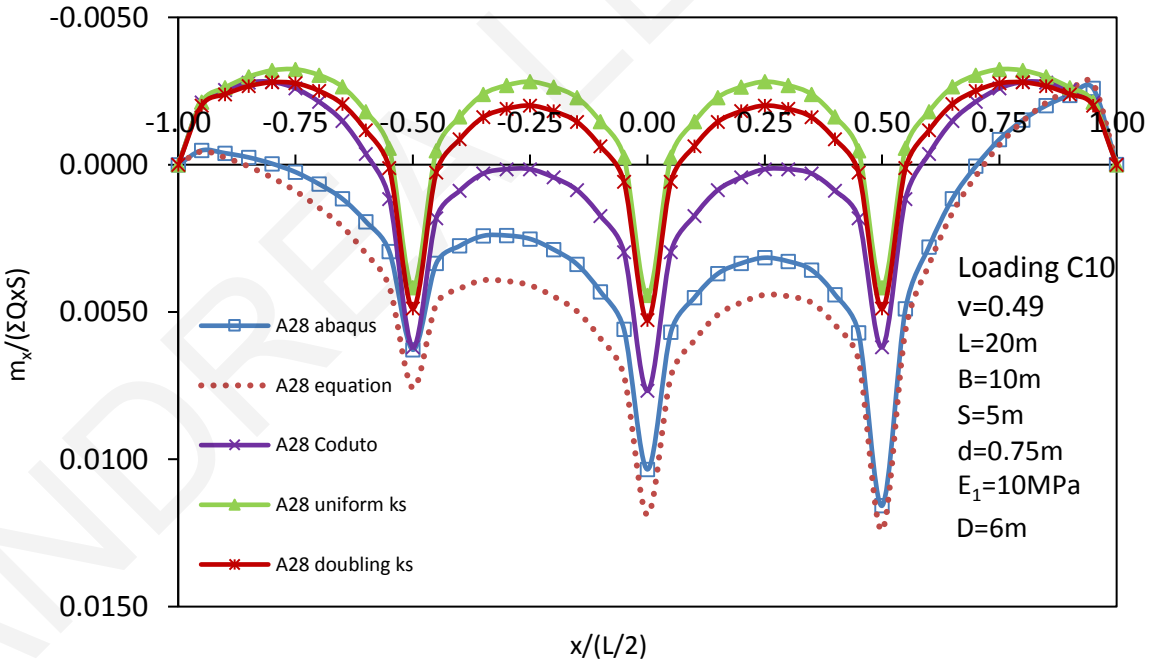

Figure 4.27: Moment diagram for Analysis 28.

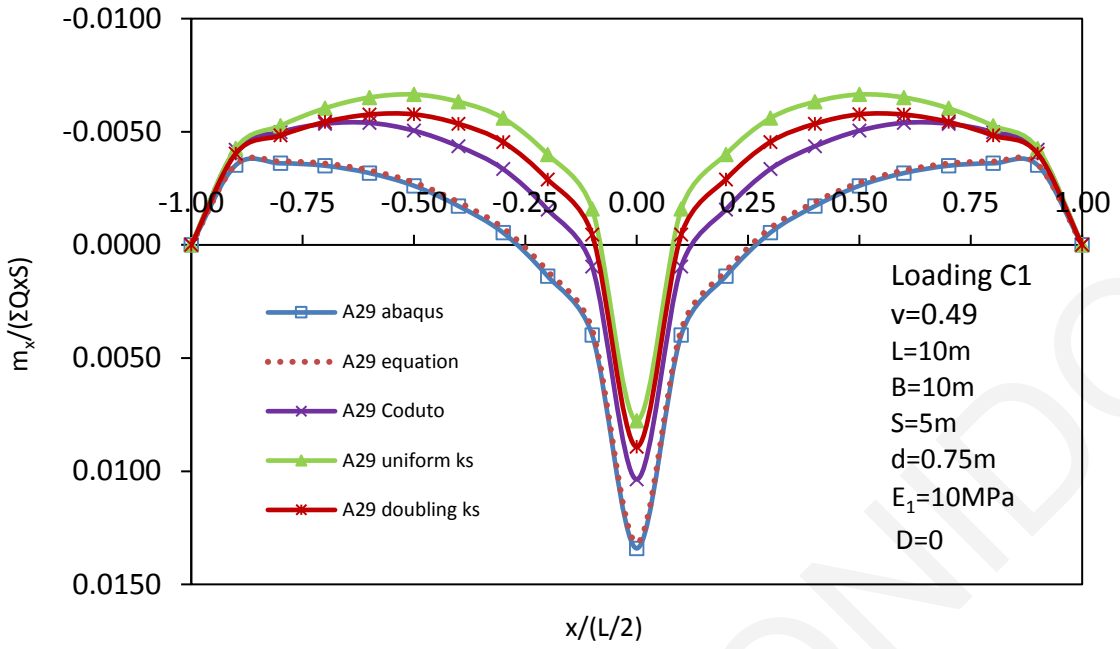

Figure 4.28: Moment diagram for Analysis 29.

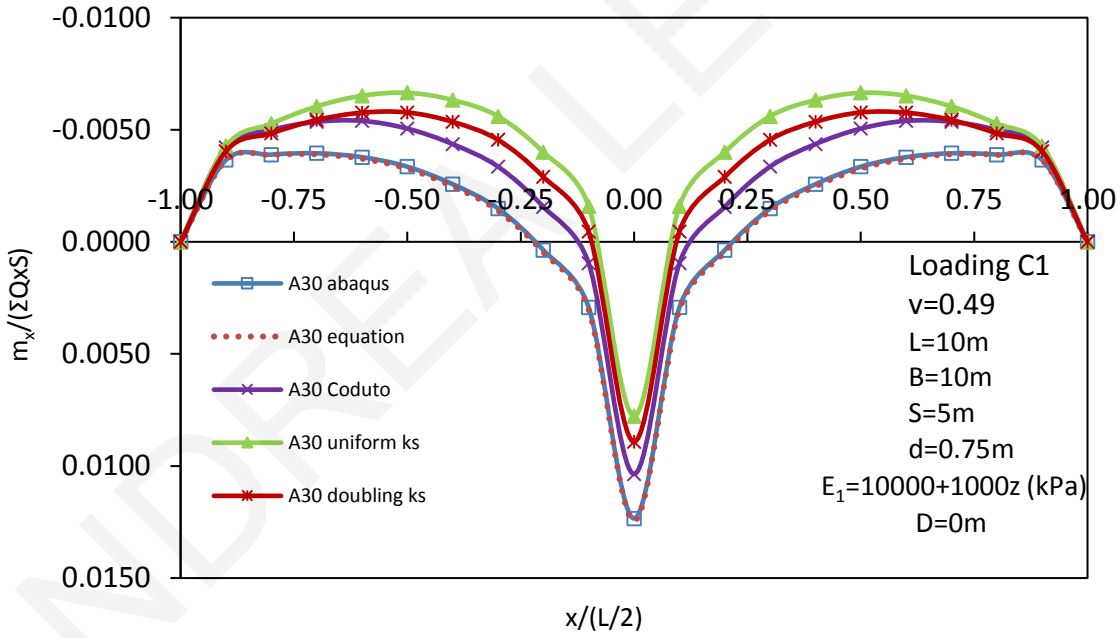

Figure 4.29: Moment diagram for Analysis 30.

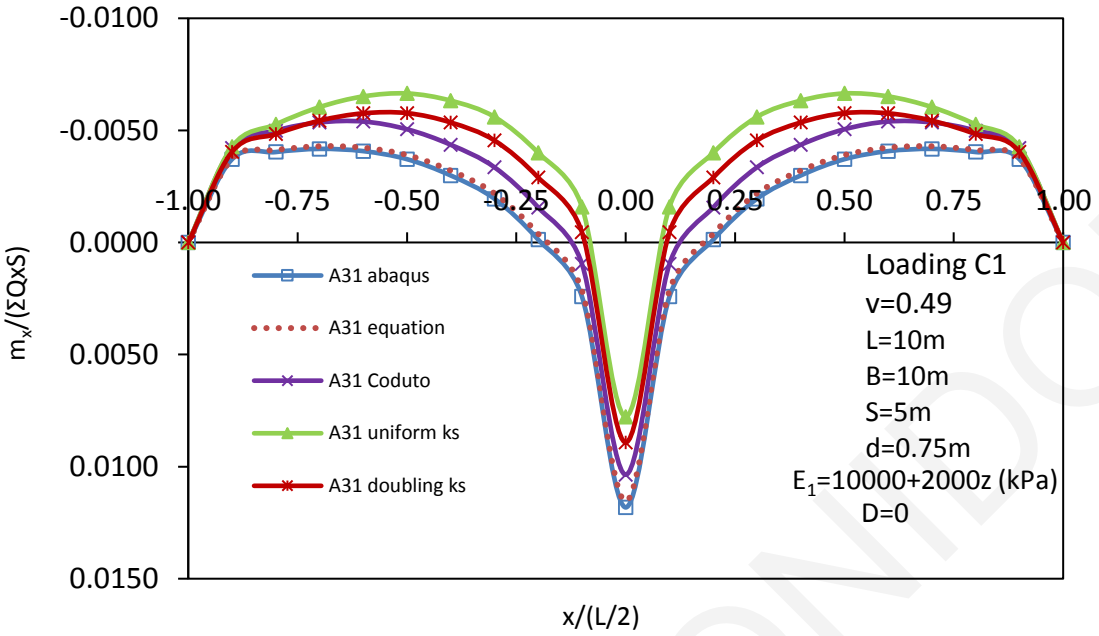

Figure 4.30: Moment diagram for Analysis 31

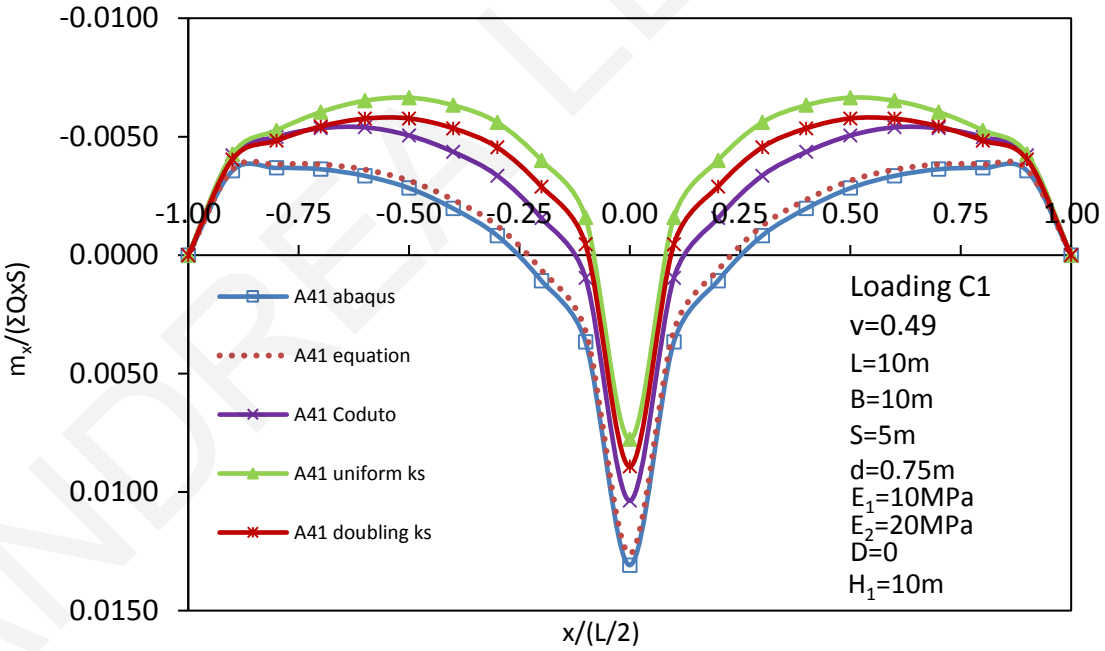

Figure 4.31: Moment diagram for Analysis 41.

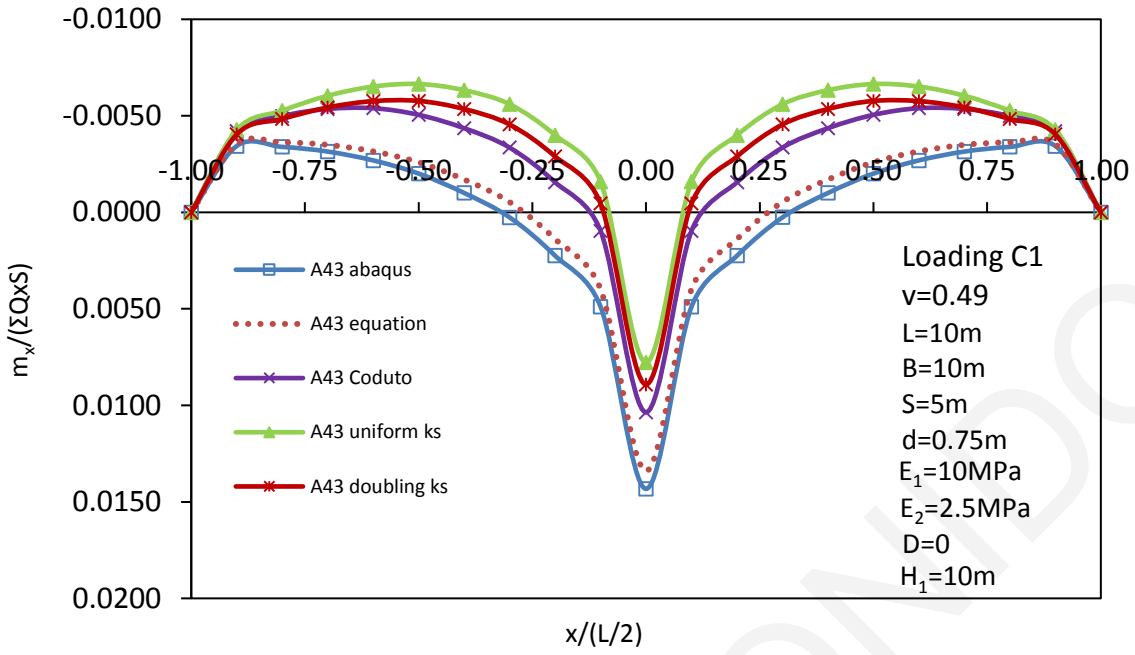

Figure 4.32: Moments diagrams for Analysis 43.

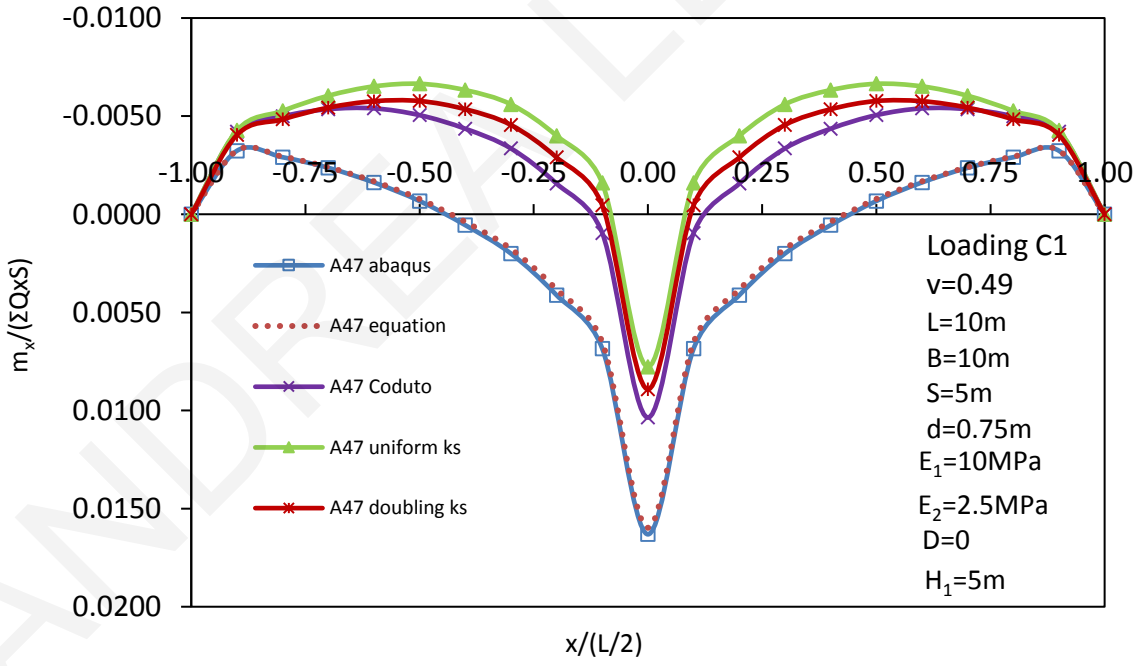

Figure 4.33: Moment diagram for Analysis 47.

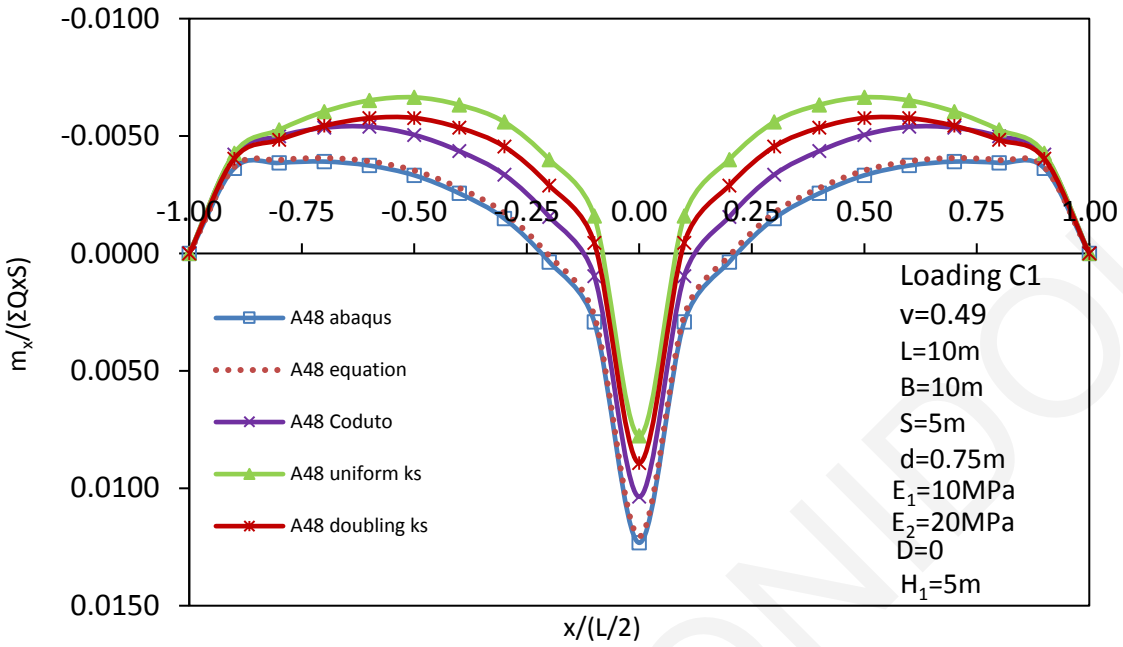

Figure 4.34: Moment diagram for Analysis 48.

Table 4.2: Absolute relative error in the maximum positive moment.

Analysis #	$m_{equation}$ (kNm/m)	m_{abaqus} (kNm/m)	abs. rel. error (%)
2	0.0147	0.0149	1.59
5	0.0142	0.0146	3.27
6	0.0149	0.0150	0.75
7	0.0151	0.0151	0.24
8	0.0097	0.0102	4.51
10	0.0100	0.0103	2.98
24	0.0086	0.0087	1.35
26	0.0112	0.0103	8.36
28	0.0119	0.0103	14.93
29	0.0132	0.0134	1.77
30	0.0124	0.0123	0.84
31	0.0115	0.0118	2.30
41	0.0126	0.0131	3.61
43	0.0134	0.0143	6.43
47	0.0160	0.0163	2.06
48	0.0121	0.0123	2.16

The errors in the peak positive moments (which are the most important ones for the design of mat foundations) resulting from the use of the fitted equation are smaller than 10%, as shown in Table 4.2, with an average value of 3.6%.

Finally, Figures 4.19-4.34 plot also the moments produced using three well-known existing distributions of modulus of subgrade reaction k_s for the analysis of mat foundations. The first one, which is still used in practice frequently, is the uniform distribution of k_s. A variation of that method is to double the k_s value at the edges of the slab. The third distribution is the one found in Coduto (2001), which divides the slab in zones with different subgrade reaction coefficients k_s (Fig. 2.7). It can be seen from the moment diagrams produced by these methods that they lead to severe underestimation of the positive bending moments. The Coduto (2001) distribution exhibits a relatively better performance, while, as expected, the assumption of a uniform k_s distribution results in the worst accuracy, with the peak positive bending moment being up to 74% (for analysis 24) smaller than that based on Abaqus FEA. Among the cases examined, the uniform distribution underestimates the peak positive bending moments by 46% on average (peak moment values are almost half of what they should be), while the approach of doubling k_s at the edges and the Coduto (2001) distribution produce an average underestimation of 38% and 27%, respectively. Hence, it can be concluded that the use of these existing k_s distributions in practice leads to unsafe designs. It is worth to point out that similar (albeit slightly smaller) relative error values were observed by Loukidis & Tamiolakis (2017) for the case of surface mat foundations (no embedment) and uniform soil layer.

CHAPTER 5: CONCLUSIONS

In this chapter, the main points of the present study are highlighted and conclusions are derived regarding the methodology used and the results of the analyses that were carried out and presented in the previous chapters. The purpose of this work was to estimate the appropriate distribution of the stiffness coefficient of Winkler springs for use in the pseudo-coupled method of mat foundation static analysis, focusing particularly on embedded foundations. This was achieved through a methodology that includes finite element analysis in the software Abaqus of the problem of a foundation plate in a 3-dimensional continuous medium representing the soil, and reverse analysis to extract the spring stiffness coefficients using a Matlab script (Tamiolakis, 2012). Based on the results obtained from the application of this methodology, an equation was constructed, which approximates the actual distribution of the stiffness coefficients of the Winkler springs and constitutes the final product of the study. The equation can be used directly and without difficulty to perform analyses of mat foundations in existing structural analysis programs that are widely used in practice.

From the numerical results, the following main conclusions are derived:

- When there is embedment D, the values of the K_{el} coefficient at the mat edges are significantly larger than in the case of absence of embedment.

- The form of the proper distribution of the K_{el} coefficient resembles a “cup” in most cases.

- The values of K_{el} at the center and at the edge converge to each other as the thickness of the deformable soil under the slab is getting smaller.

- The presence of eccentricity in the resultant of column loads leads to a rotation in the K_{el} distribution .

- The effect of the slab thickness on the K_{el} distribution is generally small. Nonetheless, in the case of thin mat foundations, local peak values appear at the points we have application of column loads.

- In the case of a two-layered soil, as the ratio of E_1/E_2 gets smaller (elastic modulus of bottom layer E_2 is increased), the distribution of the K_{el} at the edge and at the center of the mat is increased.

- The shape of the slab does not affect significantly the shape of the distribution of the K_{el}, given that the normalized results for the 10mx10m and 16mx16m slabs are comparable to those of the rectangular slab 10mx20m.

- The equation that was established herein for the estimation of the K_{el} coefficients seems to function very well as it allows accurate prediction of the mat bending moments.

- Existing distributions of the modulus of subgrade reaction that are widely used in practice lead to significant underestimation of the peak positive bending moments and, thus, to unsafe mat designs.

The present research could be extended in the future by considering soil material non-linearity. Analyses could be performed with the mat resting on elasto-plastic soil in order to investigate the effect of potential plastic yielding of the soil near the mat edges on the shape of the Winkler spring distribution.

REFERENCES

1. ABAQUS, (2010), ‘’Analysis User’s Manual’’, V. II, Simulia, Dassault Systems.
2. ACI Committee 336, (2002), ‘’Suggested Analysis and Design Procedures for Combined Footings and Mats (ACI 336.2R-88)’’, American Concrete Institute, p. 336.2R-1-336.2R-21.
3. Bowles J. E., (1996), ‘’FOUNDATION ANALYSIS AND DESIGN’’, McGraw - Hill, 5th Edition.
4. Burland, J. B. (1969). Discussion on Session A, Proc. Conf. In-situ Investigations in Soils and Rocks, British Geotechnical Society, London, p. 62.
5. Chow, Y. K. (1987). Vertical deformation of rigid foundations of arbitrary shape on layered soil media. International journal for numerical and analytical methods in geomechanics, 11(1), 1-15.
6. Coduto D. P., (2001), ‘’FOUNDATION DESIGN – Principles and Practices’’, Prentice Hall, 2nd Edition.
7. Colasanti R. J., Horvath J.S., (2010), ‘’Practical Subgrade Model for Improved Soil-Structure Interaction Analysis: Software Implementation’’, Practise periodical on structural design and construction, ASCE.
8. Fraser, R.A. & Wardle, L.J (1976), “Numerical analysis of rectangular rafts on layered foundations”, Geotechnique 26, No.4,613-630.
9. Gazetas, G., Tassoulas, J. L., Dobry, R., & O'Rourke, M. J. (1985). Elastic settlement of arbitrarily shaped foundations embedded in half-space. Geotechnique, 35(3), 339-346.
10. Gazetas, G. (1991). Foundation vibrations. In Foundation engineering handbook (pp. 553-593). Springer, Boston, MA.
11. Gerrard, C. M., & Harrison, W. J. (1971). The analysis of a loaded half-space comprised of anisotropic layers (No. Tech Pap).

12. Horvath J. S., (2002), ''Soil-Structure Interaction Research Project – Basic SSI Concepts and applications Overview'', Center for Geotechnology, Manhattan College, No. CGT-2002-2.
13. Horvilleur J. F., Patel V. B., (1995), '' Mat Foundation Design-A Soil-Structure Interaction Problem'', ACI, V.152, p. 51-94.
14. Matlab, (2012), ''User's Guide'', Mathworks
15. Liao S.S.C., (1995), ''Estimating the coefficient of subgrade reaction for plain strain condition'', Proceedings of the institution of civil engineers: geotechnical engineering, p. 166-81.
16. Loukidis, D., Salgado, R. & Abou-Jaoude, G. (2008). Assessment of axially-loaded pile dynamic design methods and review of INDOT axially-loaded pile dynamic design methods. Final Report. Purdue University, FHWA/IN/JTRP-2008/6, SPR-2856.
17. Loukidis, D. and Tamiolakis, G-P (2017). "Spatial distribution of Winkler spring stiffness for rectangular mat foundation analysis." Engineering Structures, 153, 443-459.
18. Salgado R., (2008), ''The Engineering of Foundations'', McGraw – Hill, International Edition.
19. Steinbrenner W., (1934), ''Tafeln zur Setzungberechnung'', Die Strasse, V. 1, p. 121
20. Svec, O. J., & Gladwell, G. M. L. (1973). A triangular plate bending element for contact problems. International Journal of Solids and Structures, 9(3), 435-446.
21. Tamiolakis (2012). Investigation of the spatial distribution of Winkler springs for the static analysis of mat foundations. MSc Thesis, University of Cyprus, Nicosia, Cyprus.
22. Timoshenko, S., & Goodier, J. N. (1951). Theory of Elasticity. McGraw-Hill Book Company. Inc. New York.
23. Ulrich Jr E. J., (1991), '' Subgrade Reaction in Mat Foundation Design'', Concrete International, V. 13, No. 4, p. 41-50.
24. Winkler E., (1867), ''Die Lehre von Elastizität und Festigkeit (On Elasticity and Fixity), H. Dominicus, Prague

25. Zienkiewicz, O. C., & Cheung, Y. K. (1965). Finite elements in the solution of field problems. The Engineer, 220(5722), 507-510.
26. Αναγνωστόπουλος, Α. Γ. & Παπαδόπουλος, Β. Π. (1989). Επιφανειακές Θεμελιώσεις. Εκδόσεις Συμεών, Αθήνα.

ANNEX A

PLOTS OF DISTRIBUTION OF K_{el} COEFFICIENTS FROM ABAQUS ANALYSES

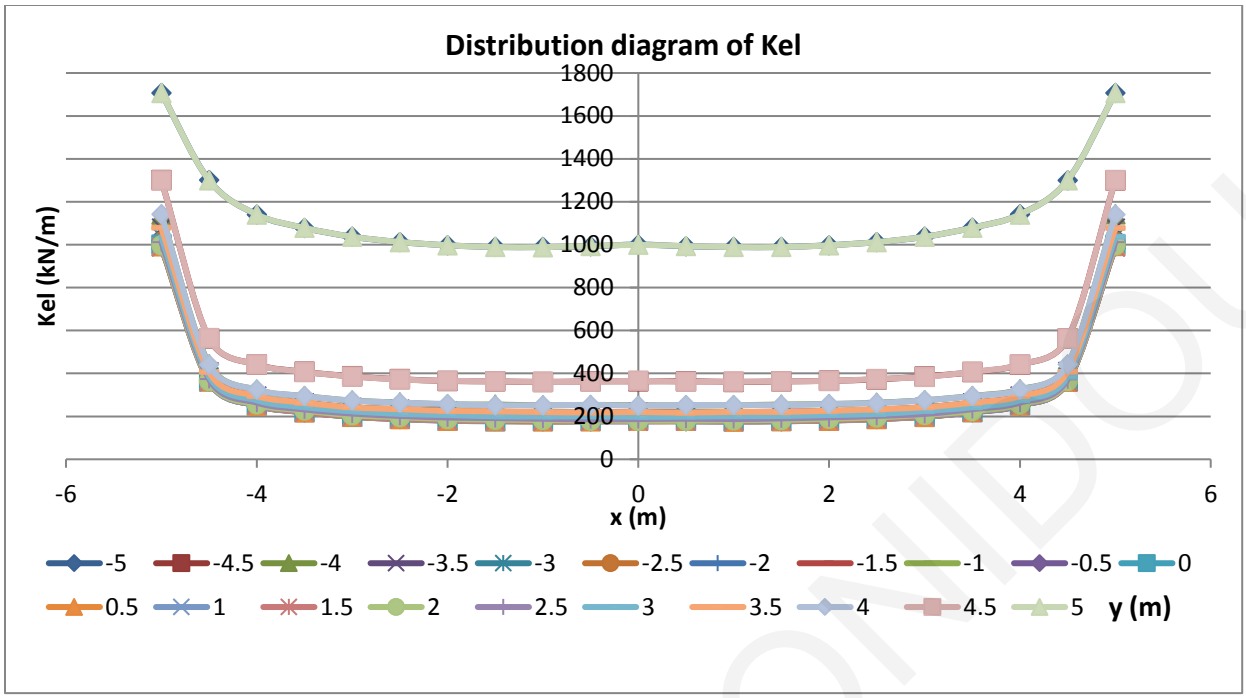

Figure A1: Distribution of K_{el} along the x-axis from analysis 1

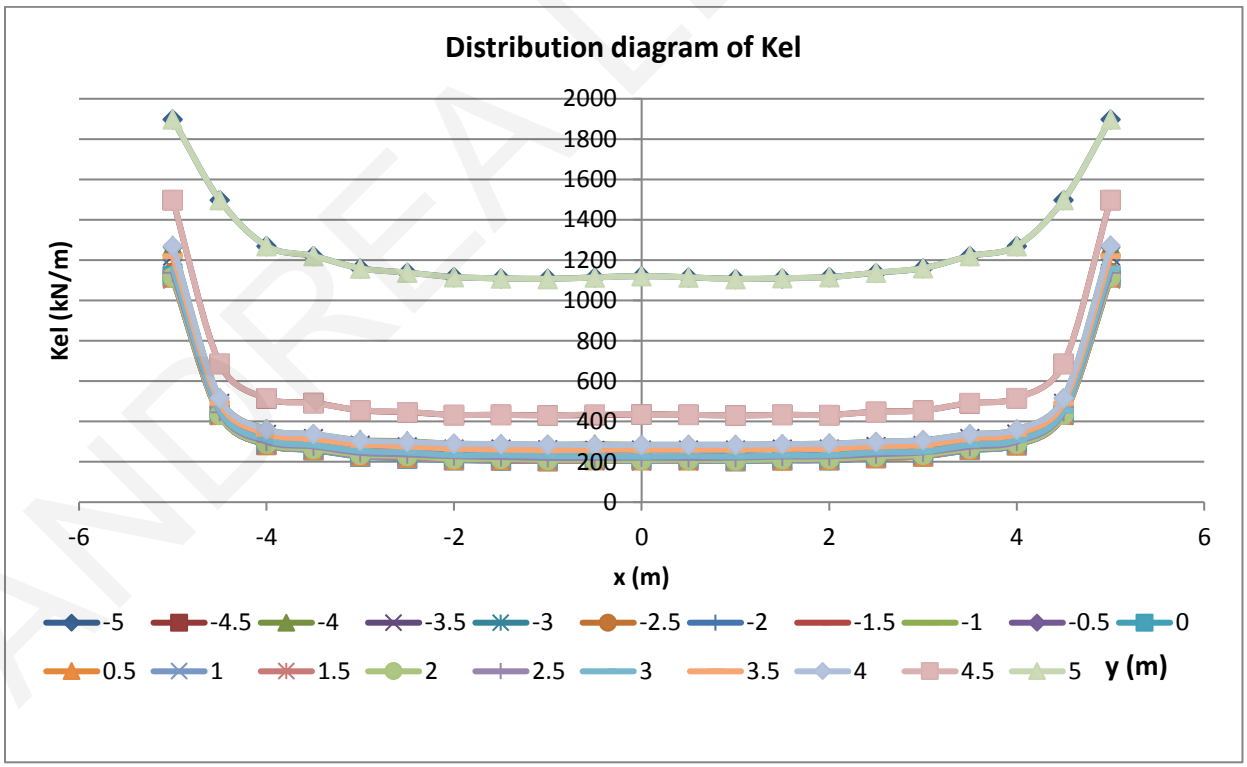

Figure A2: Distribution of K_{el} along the x-axis from analysis 2.

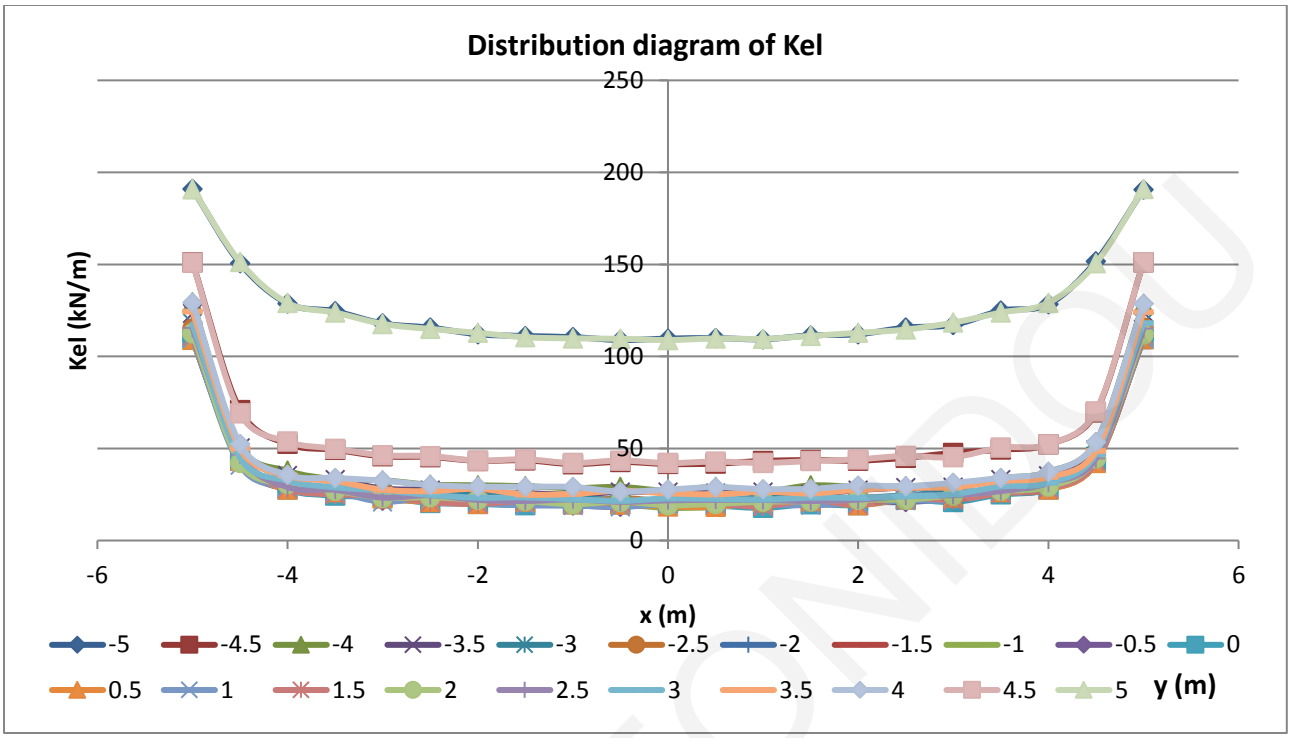

Figure A3: Distribution of K_{el} along the x-axis from analysis 3.

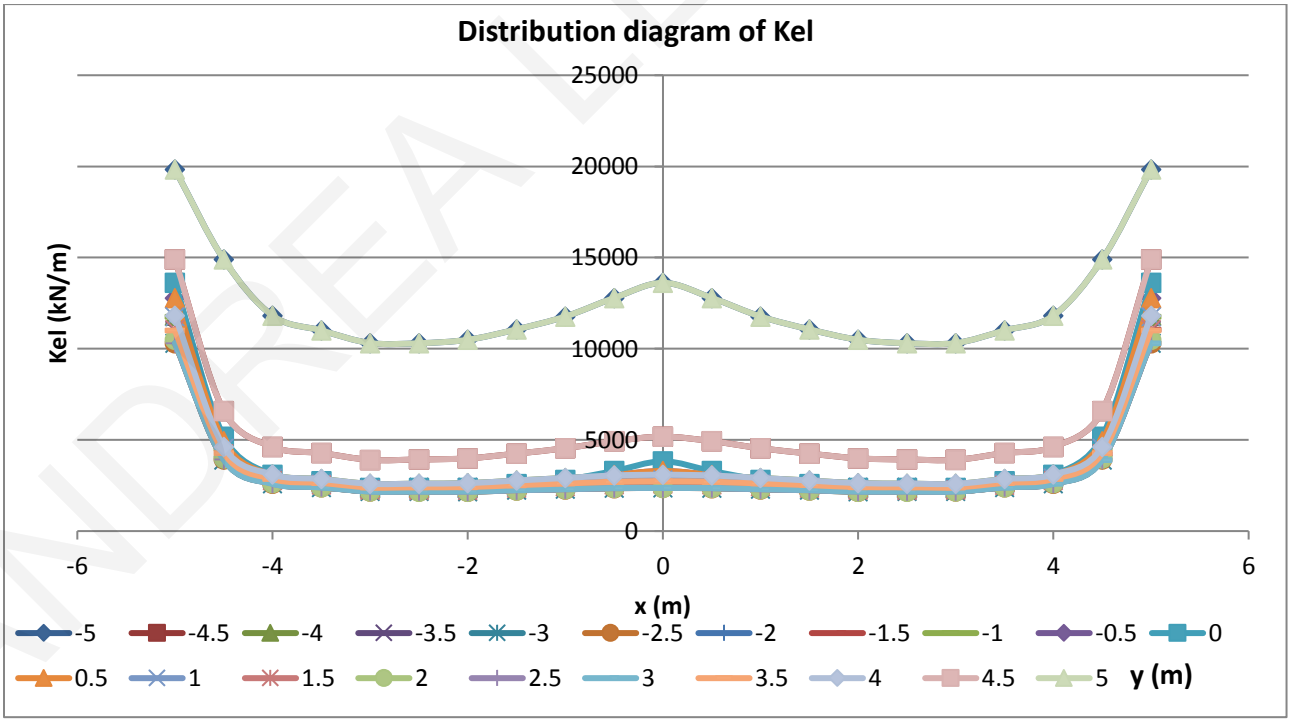

Figure A4: Distribution of K_{el} along the x-axis from analysis 4.

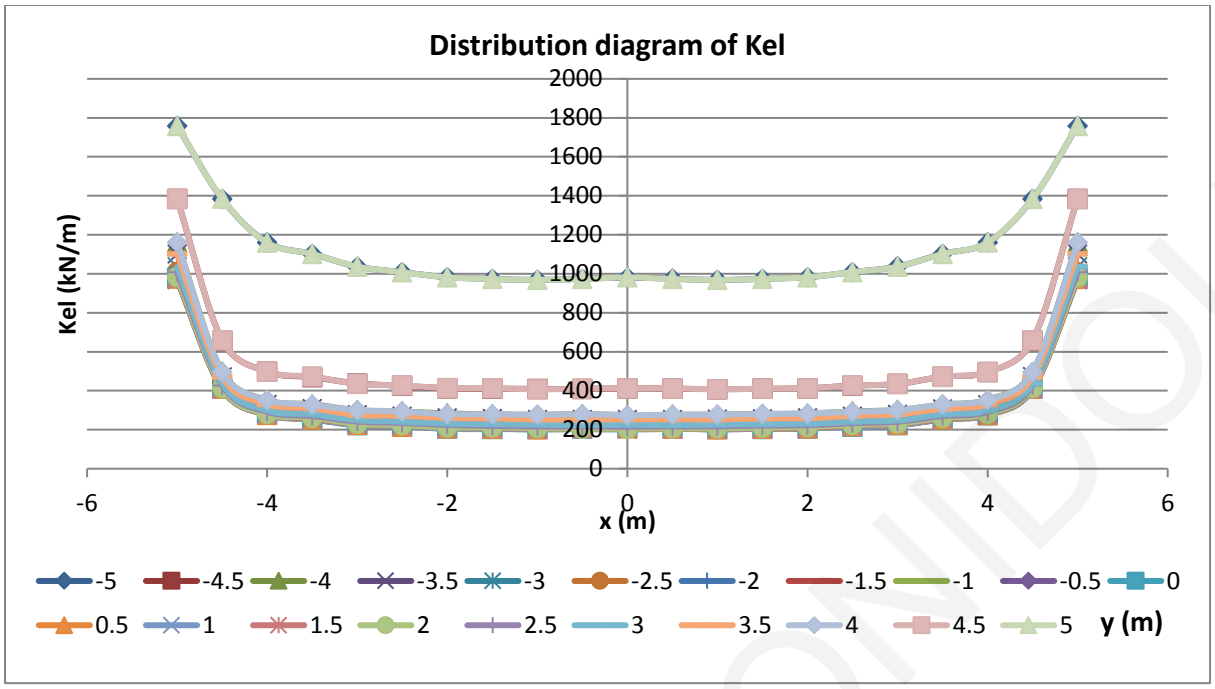

Figure A5: Distribution of K_{el} along the x-axis from analysis 5.

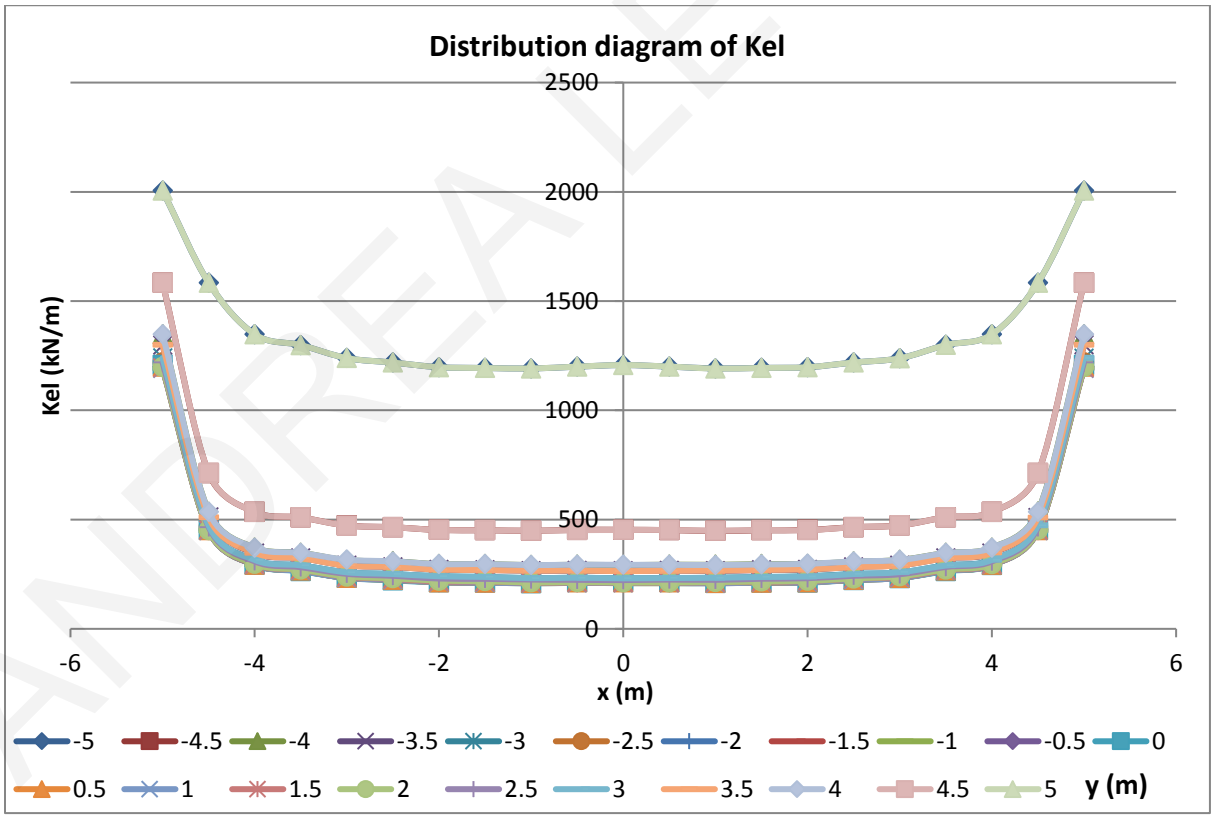

Figure A6: Distribution of K_{el} along the x-axis from analysis 6.

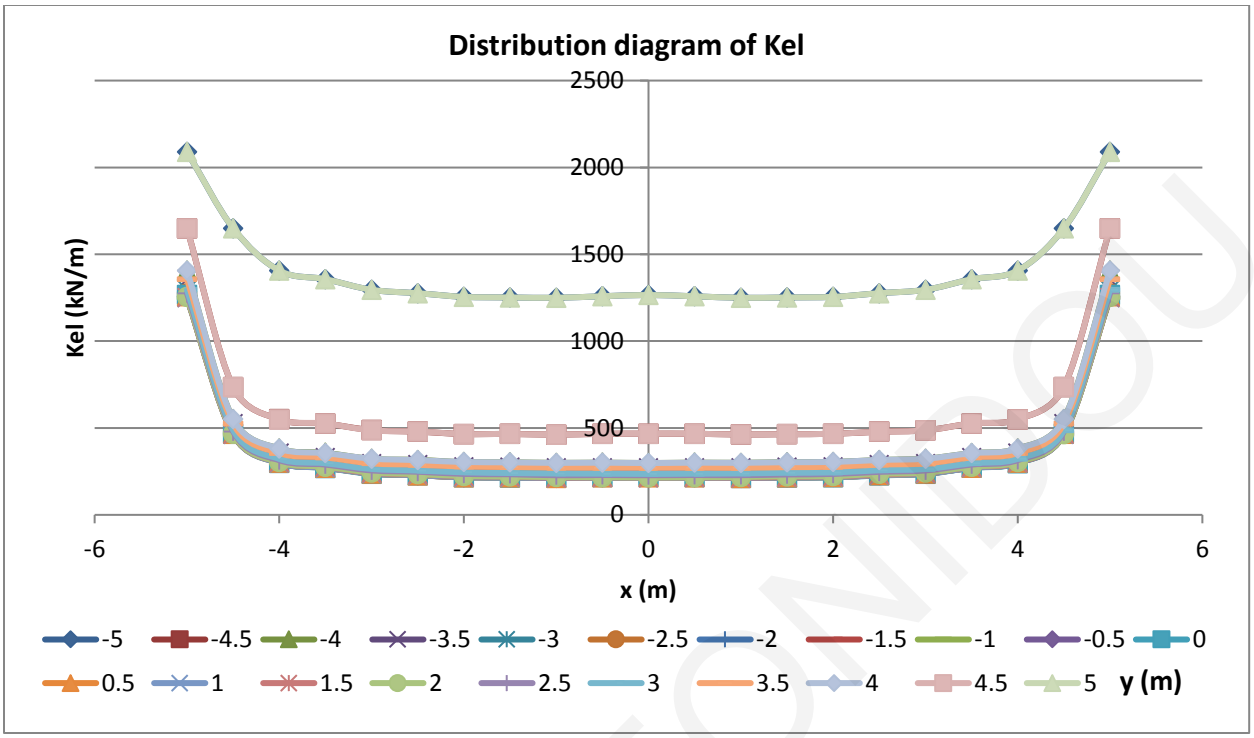

Figure A7: Distribution of K_{el} along the x-axis from analysis 7.

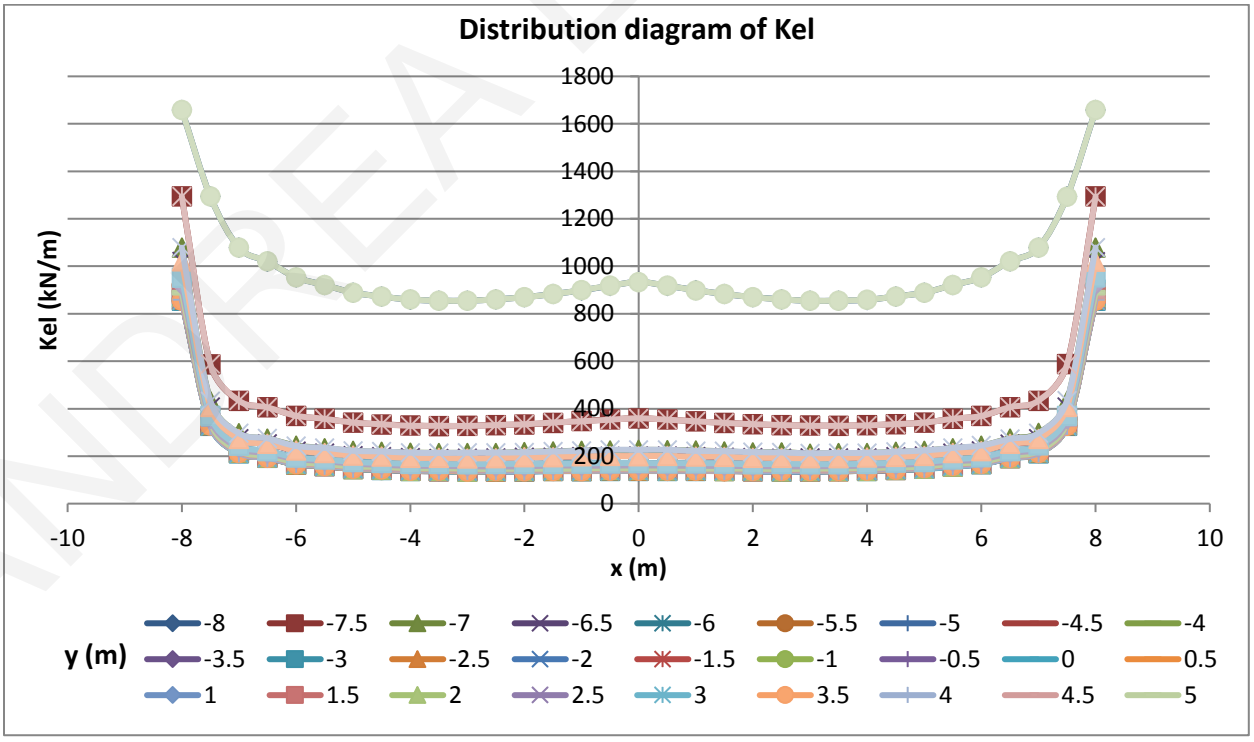

Figure A8: Distribution of K_{el} along the x-axis from analysis 8.

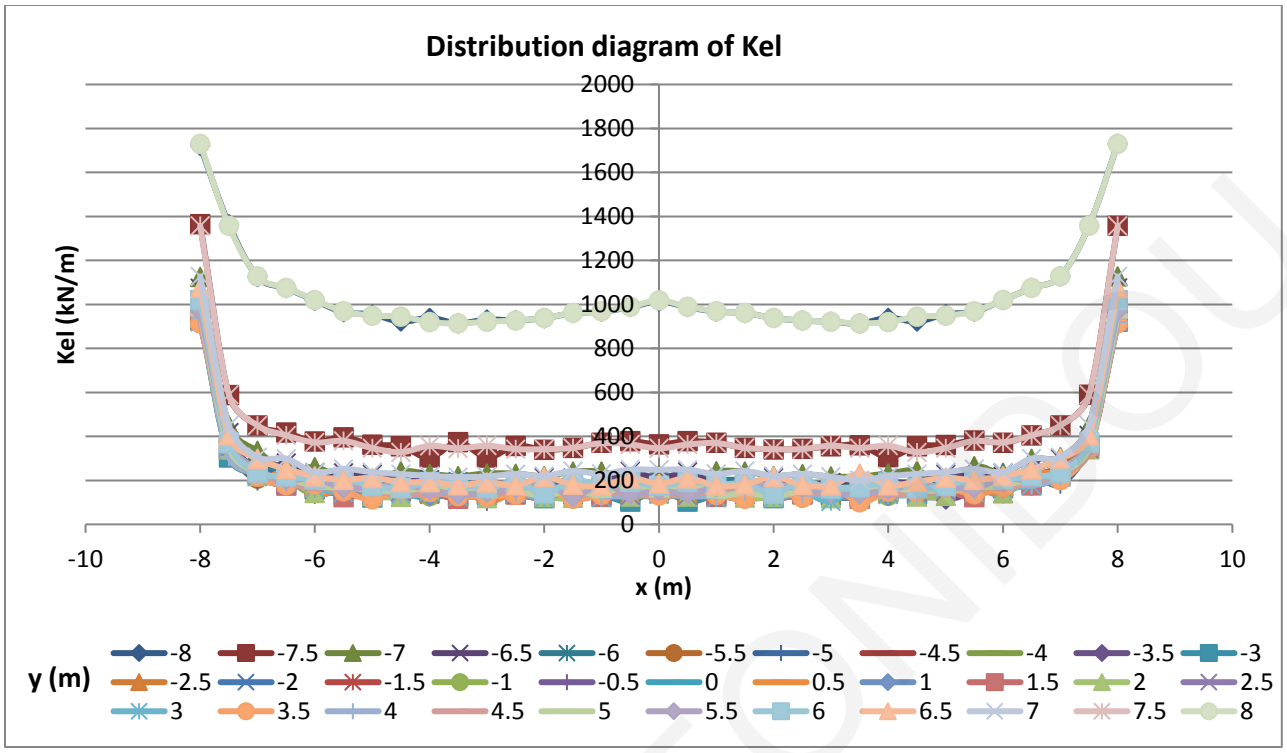

Figure A9: Distribution of K_{el} along the x-axis from analysis 9.

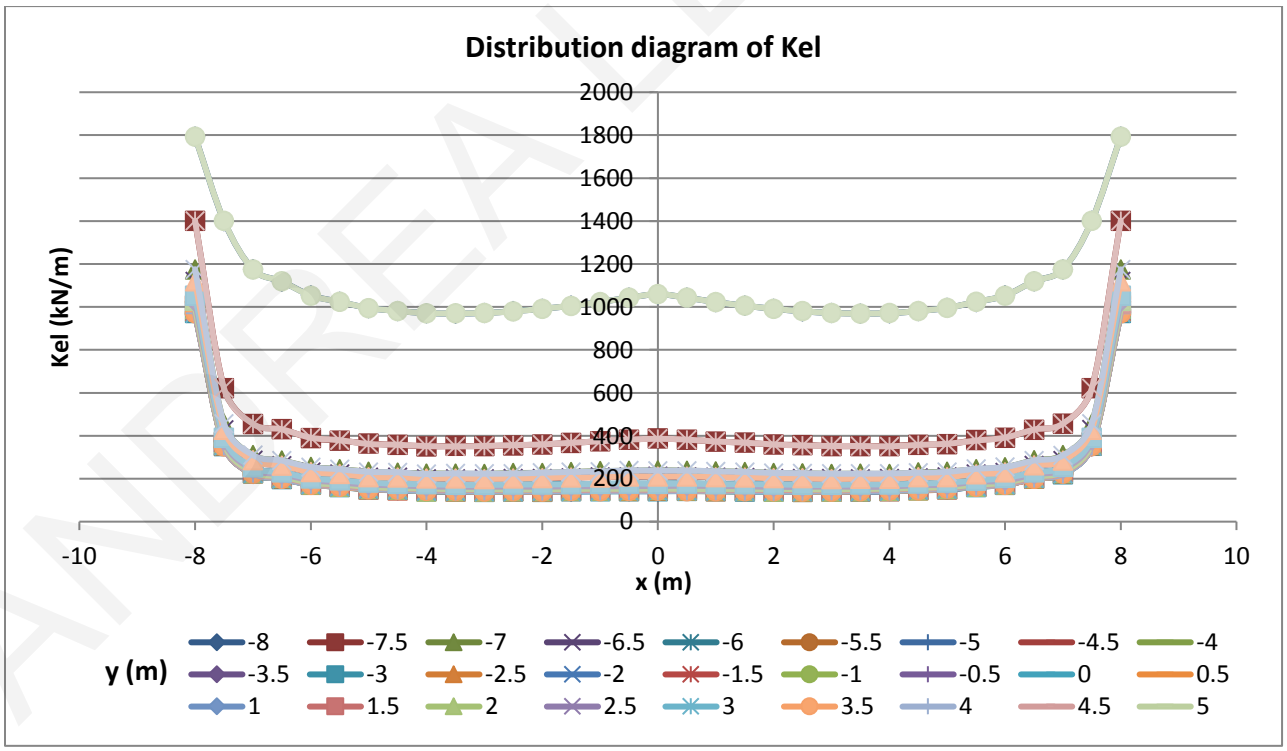

Figure A10: Distribution of K_{el} along the x-axis from analysis 10.

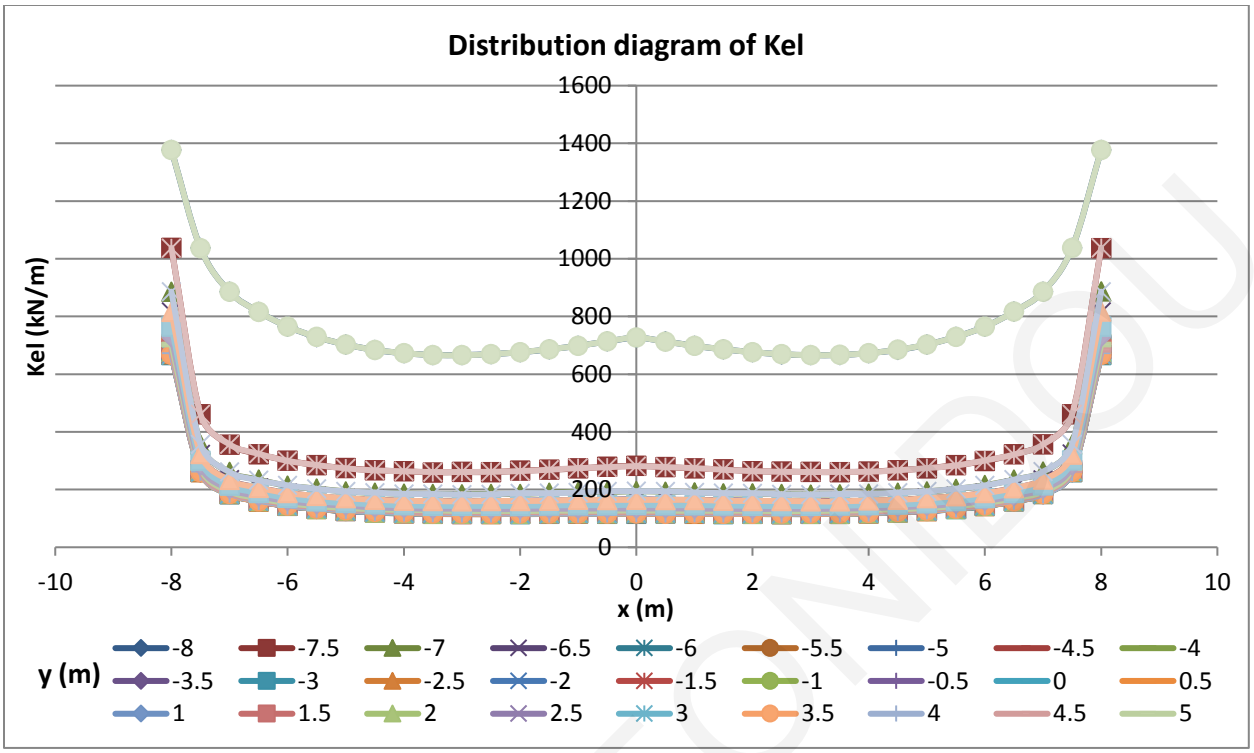

Figure A11: Distribution of K_{el} along the x-axis from analysis 11.

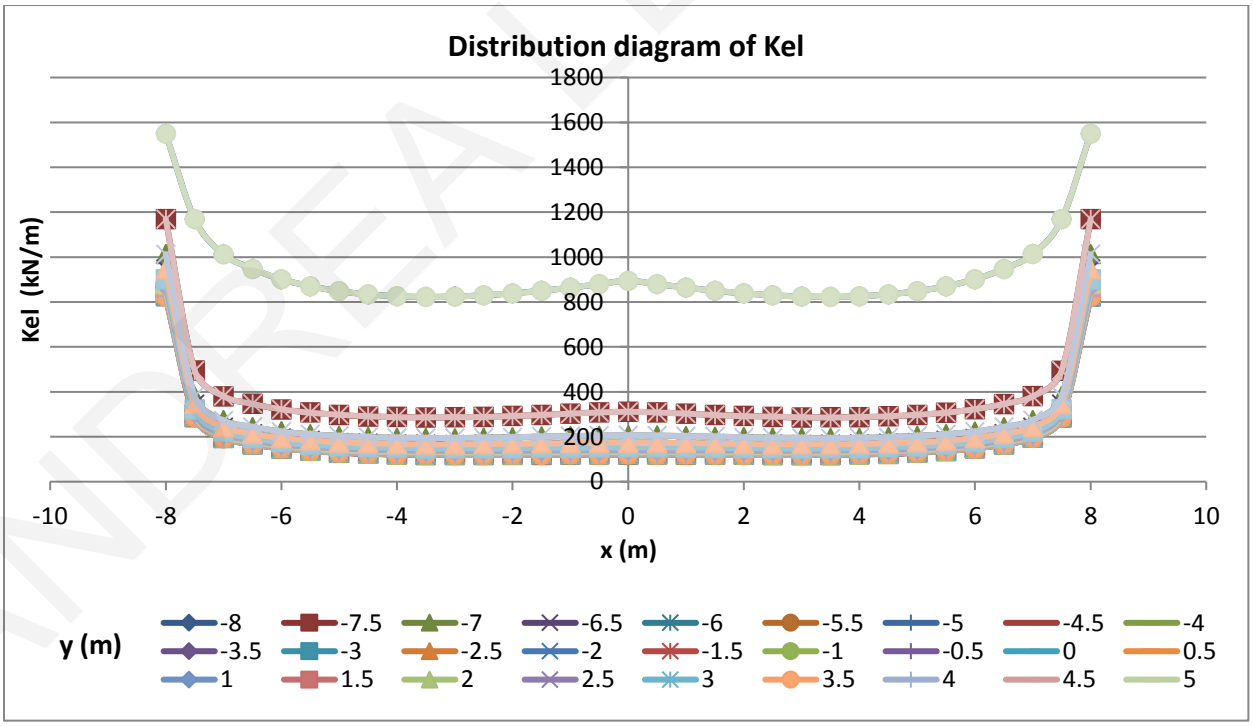

Figure A12: Distribution of K_{el} along the x-axis from analysis 12.

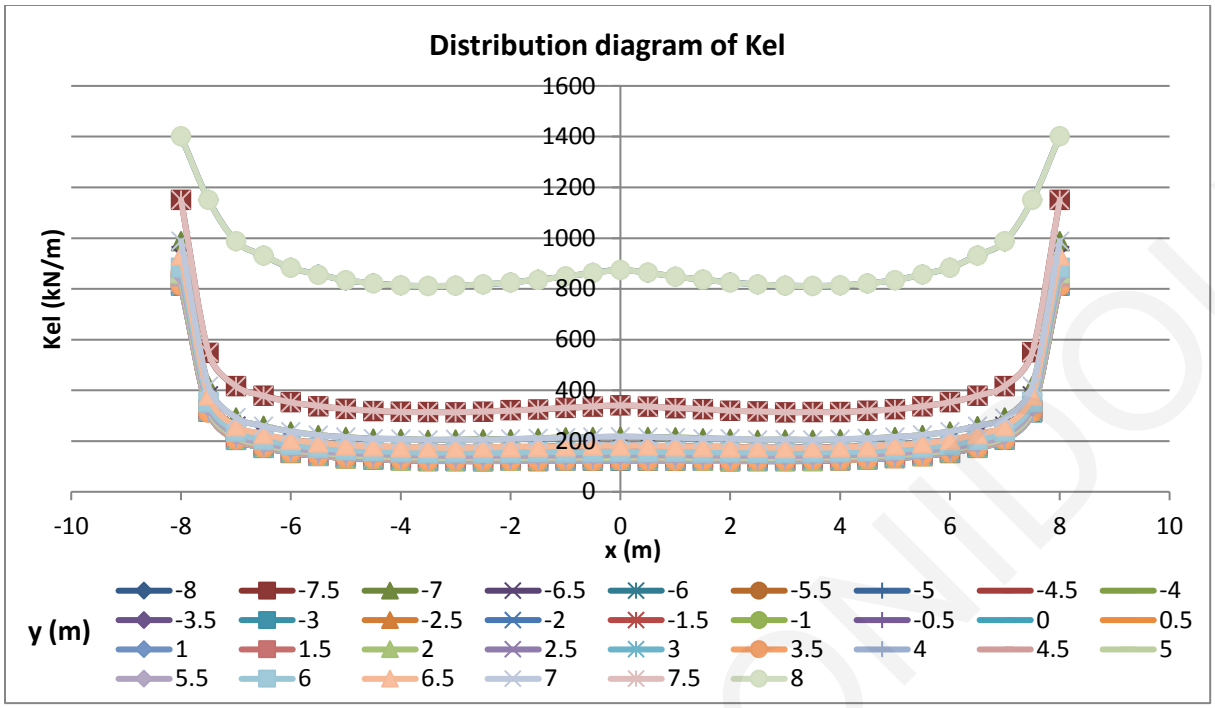

Figure A13: Distribution of K_{el} along the x-axis from analysis 13.

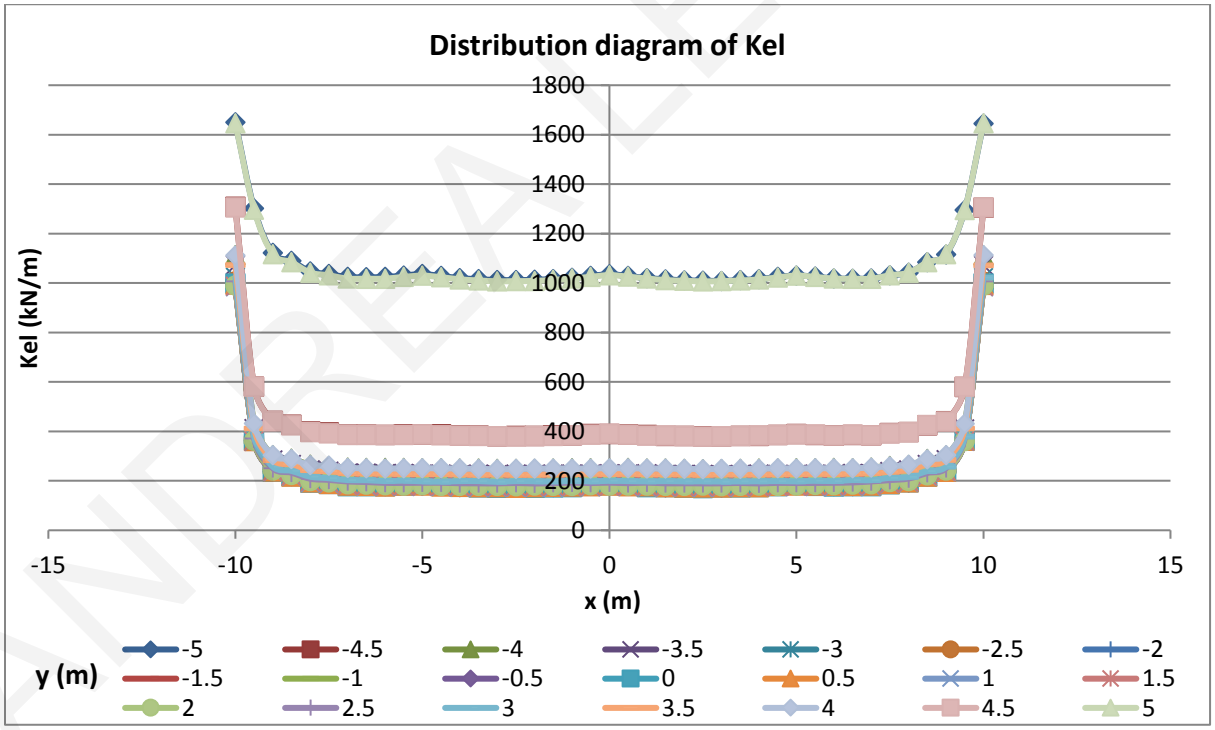

Figure A14: Distribution of K_{el} along the x-axis from analysis 14.

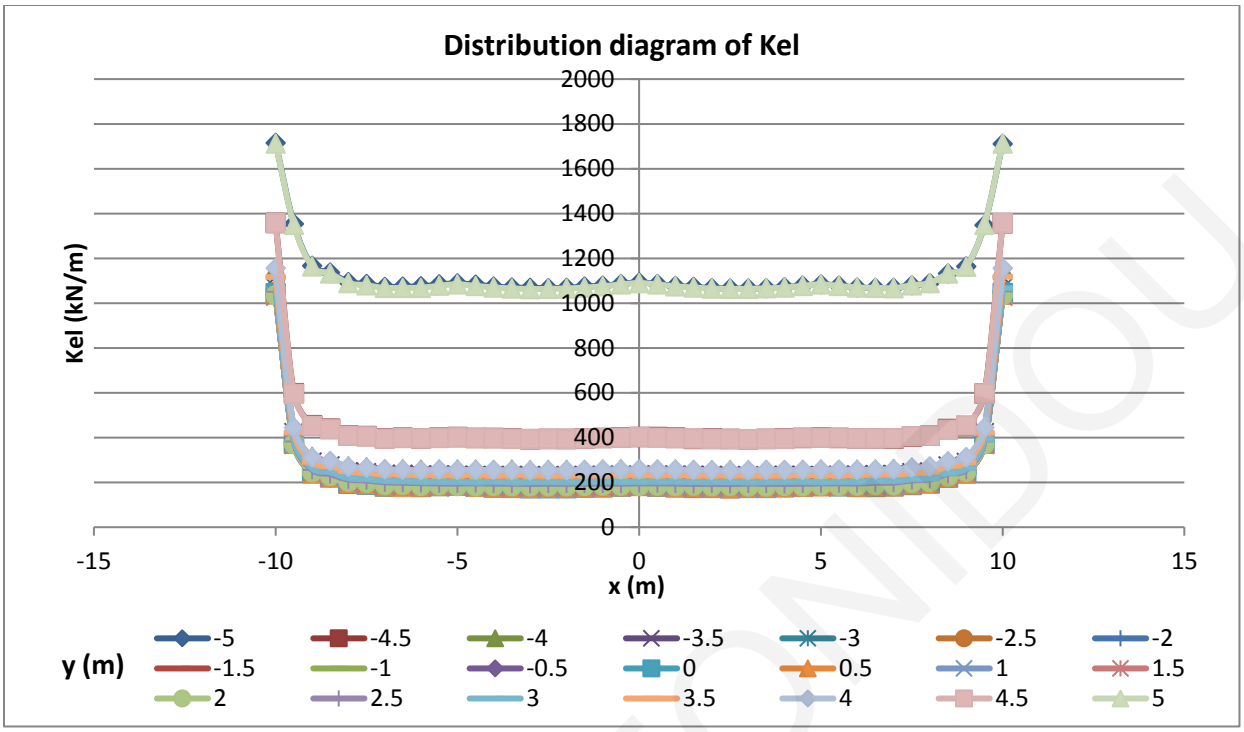

Figure A15: Distribution of K_{el} along the x-axis from analysis 15.

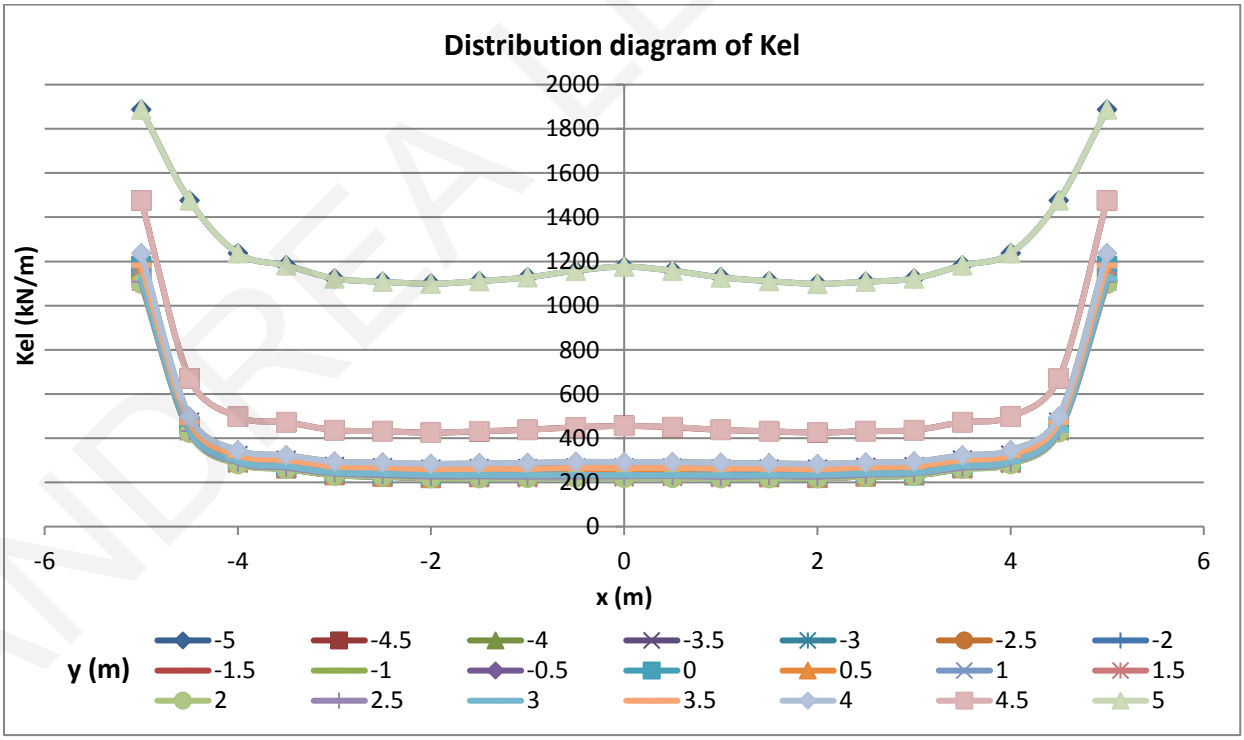

Figure A16: Distribution of K_{el} along the x-axis from analysis 16.

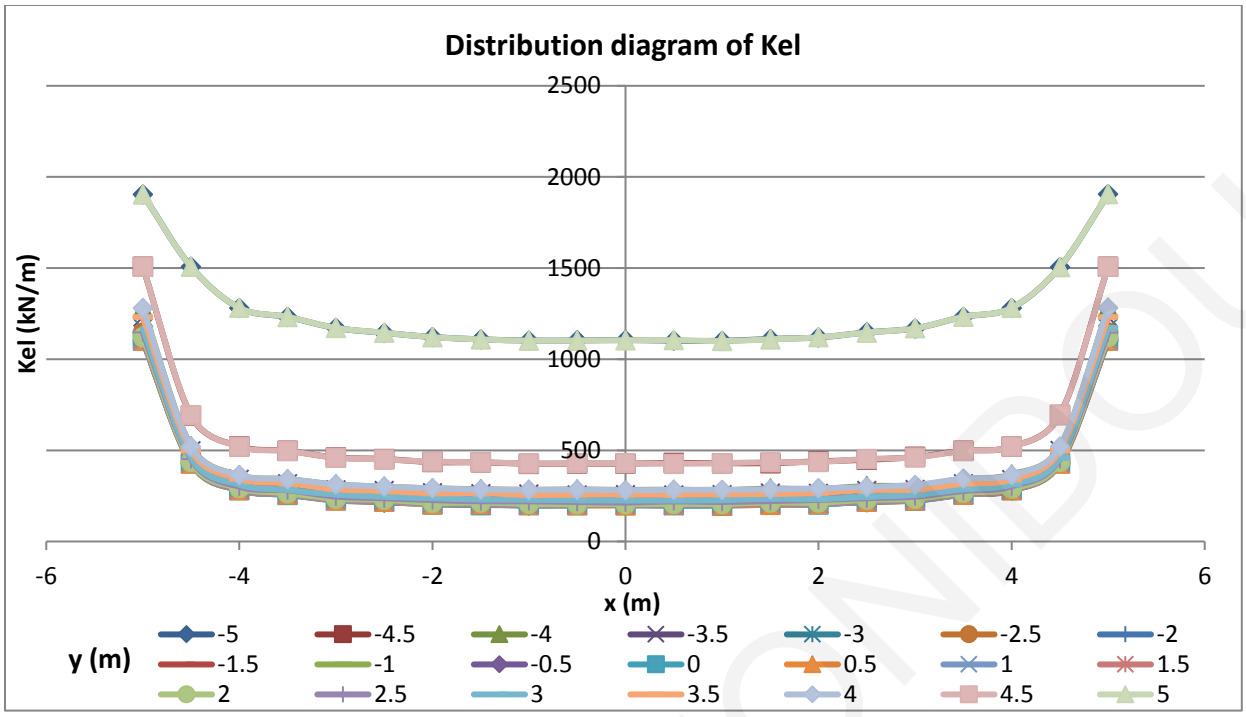

Figure A17: Distribution of K_{el} along the x-axis from analysis 17.

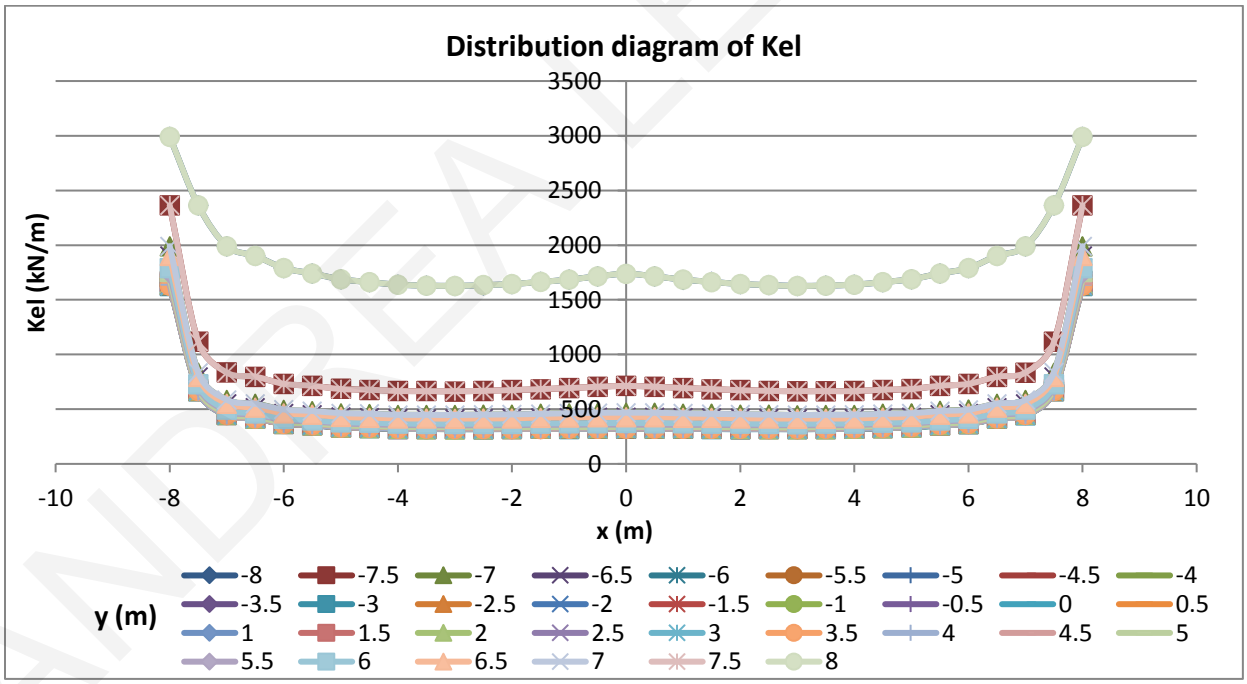

Figure A18: Distribution of K_{el} along the x-axis from analysis 18.

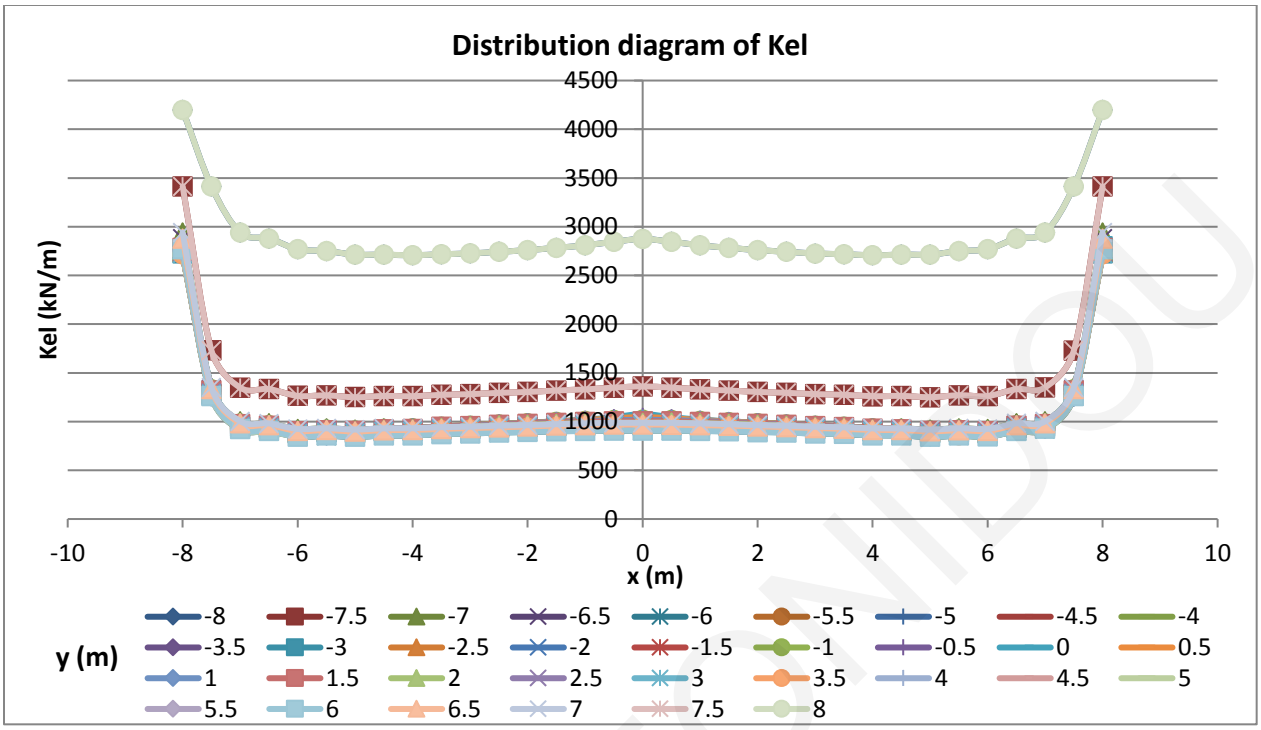

Figure A19: Distribution of K_{el} along the x-axis from analysis 19.

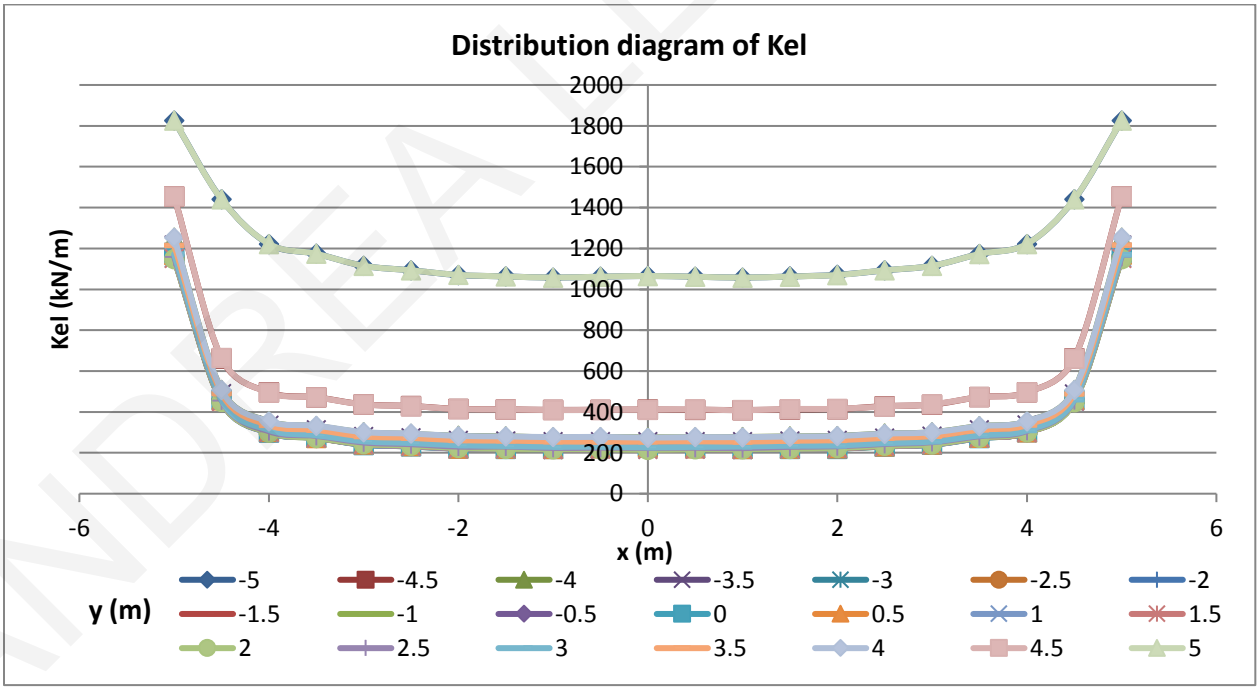

Figure A20: Distribution of K_{el} along the x-axis from analysis 20.

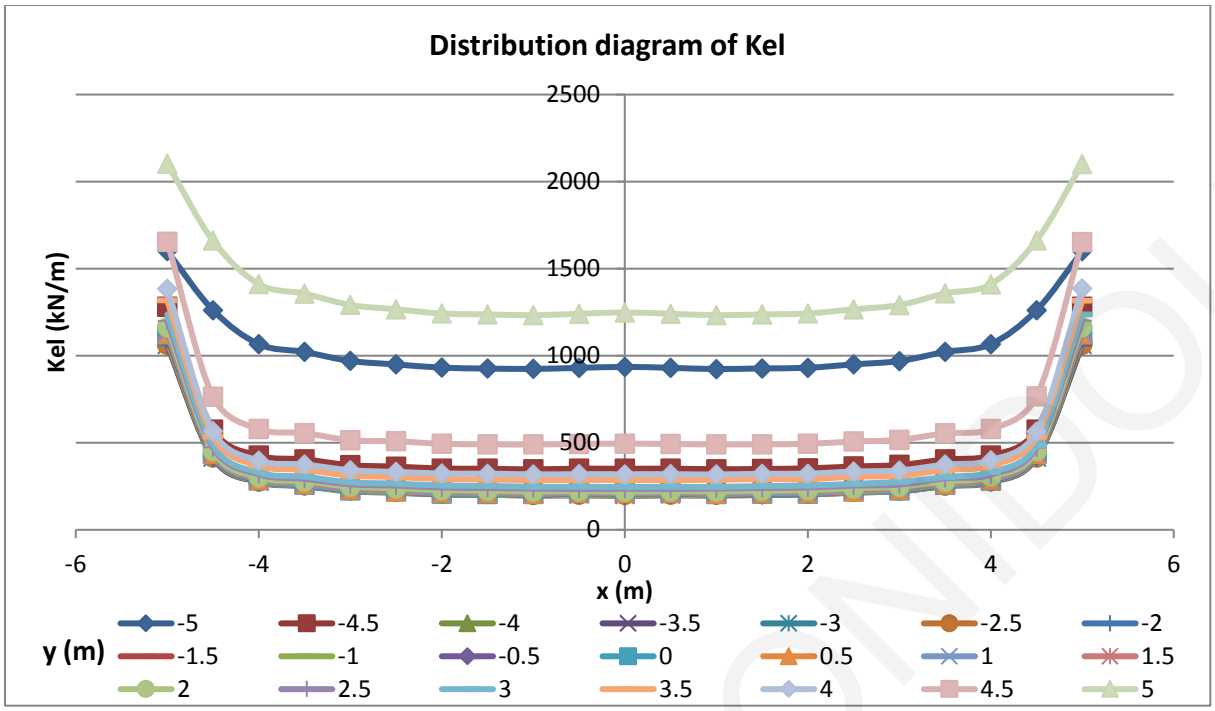

Figure A21: Distribution of K_{el} along the x-axis from analysis 21.

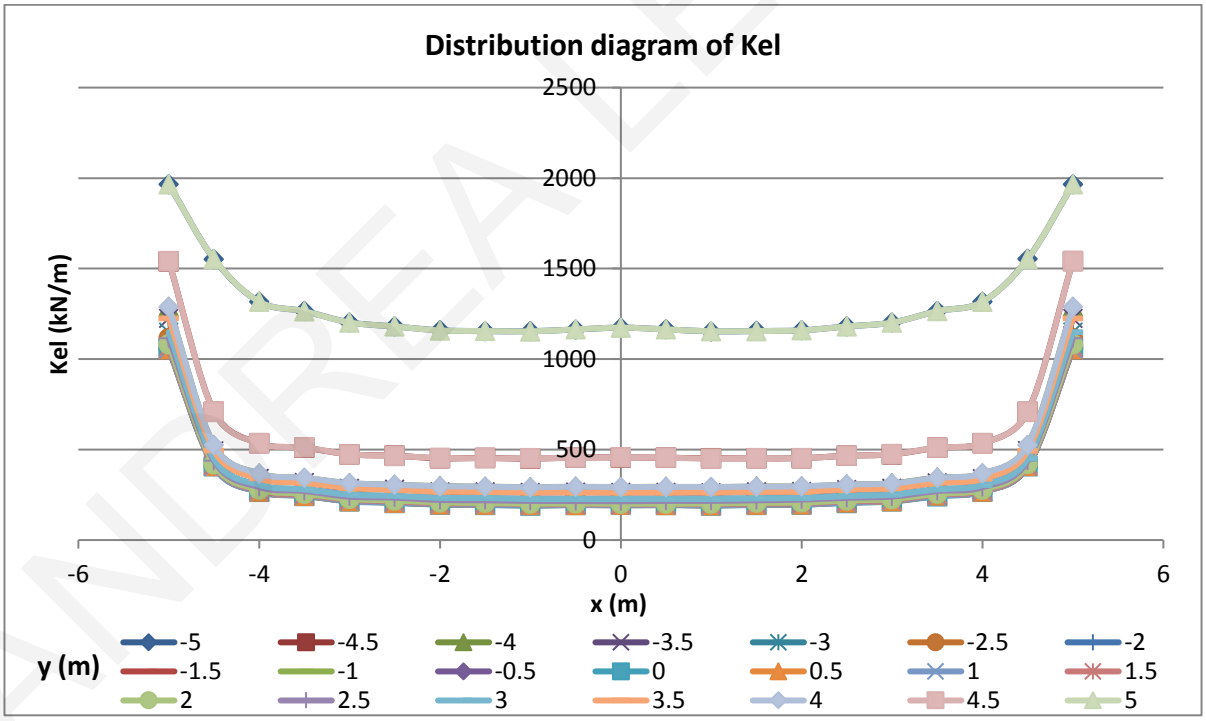

Figure A22: Distribution of K_{el} along the x-axis from analysis 22.

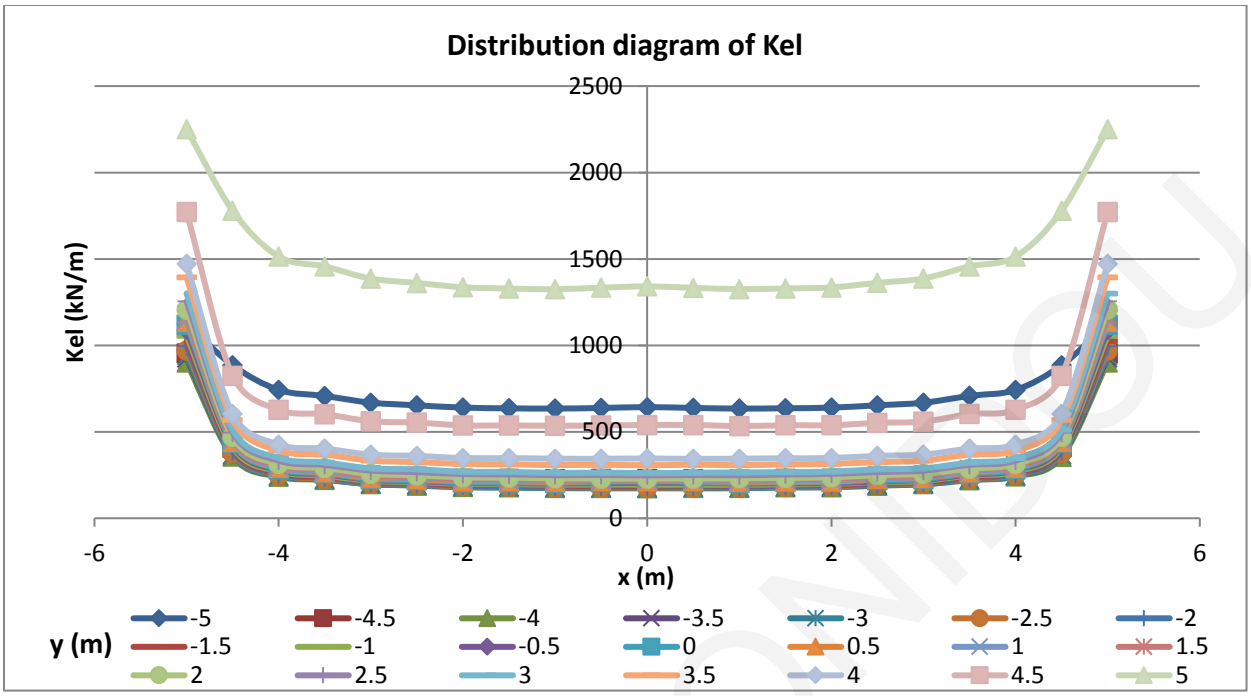

Figure A23: Distribution of K_{el} along the x-axis from analysis 23.

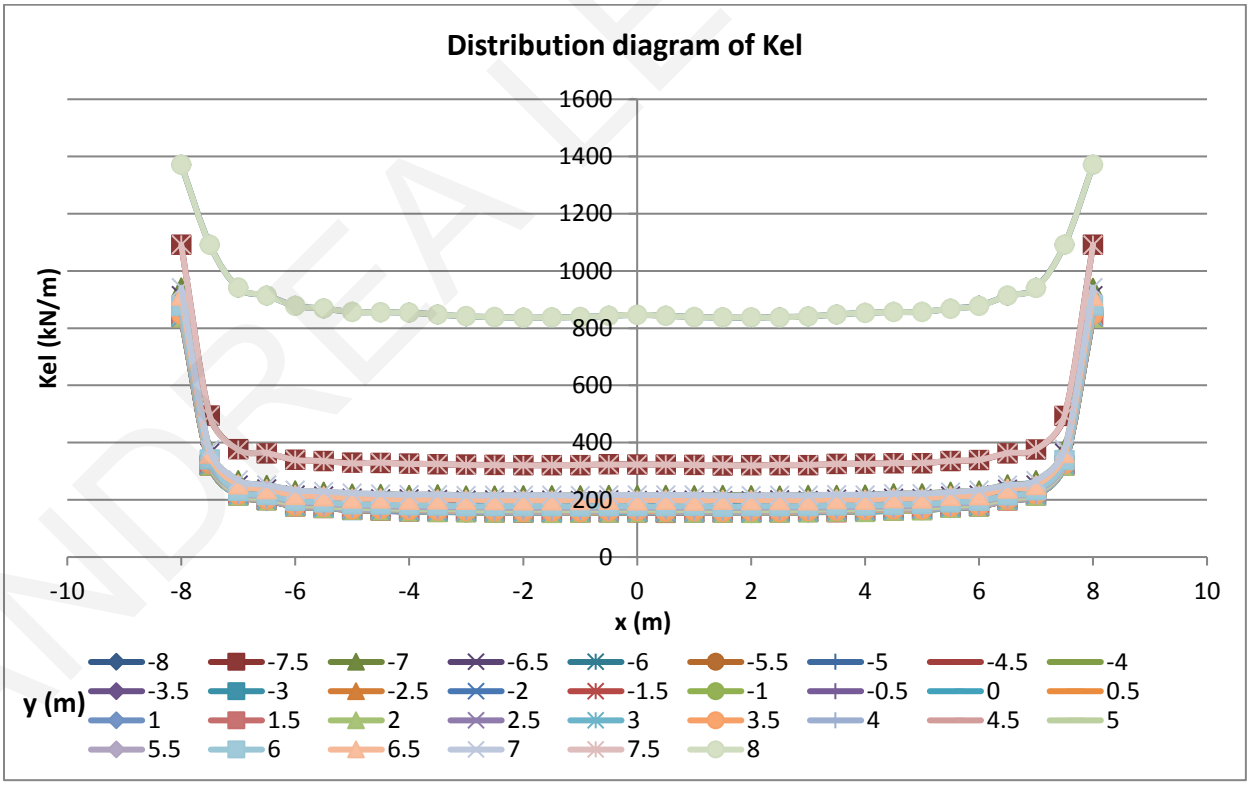

Figure A24: Distribution of K_{el} along the x-axis from analysis 24.

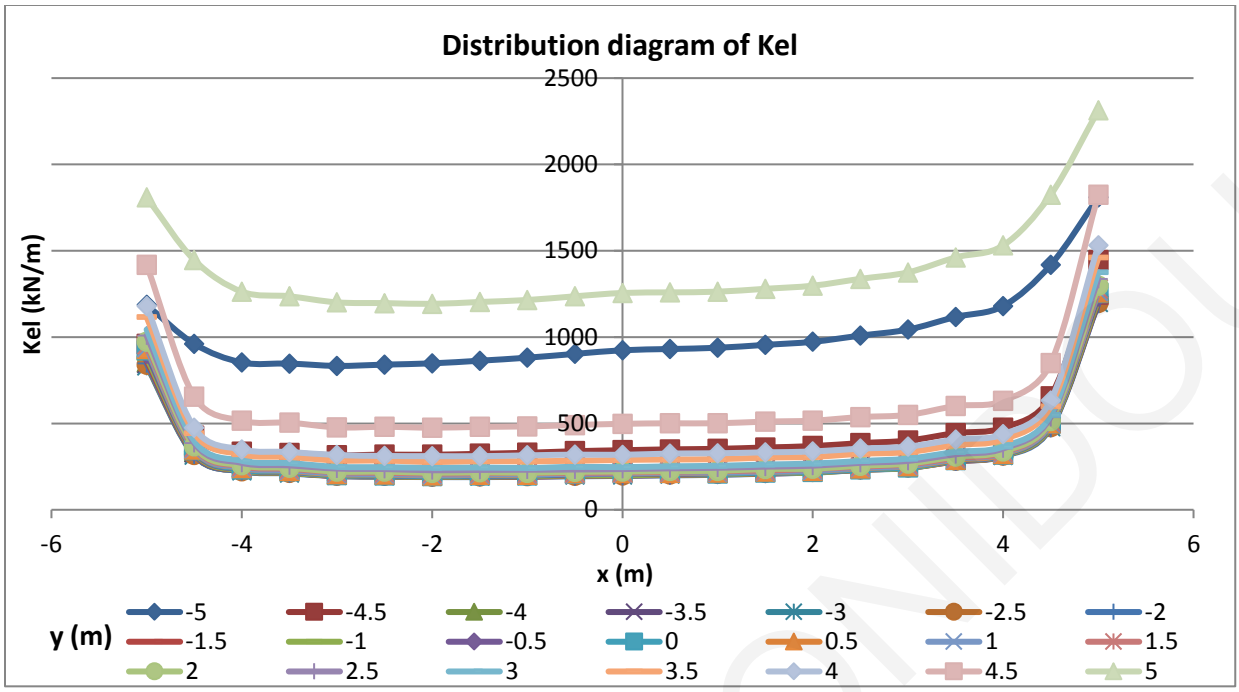

Figure A25: Distribution of K_{el} along the x-axis from analysis 25.

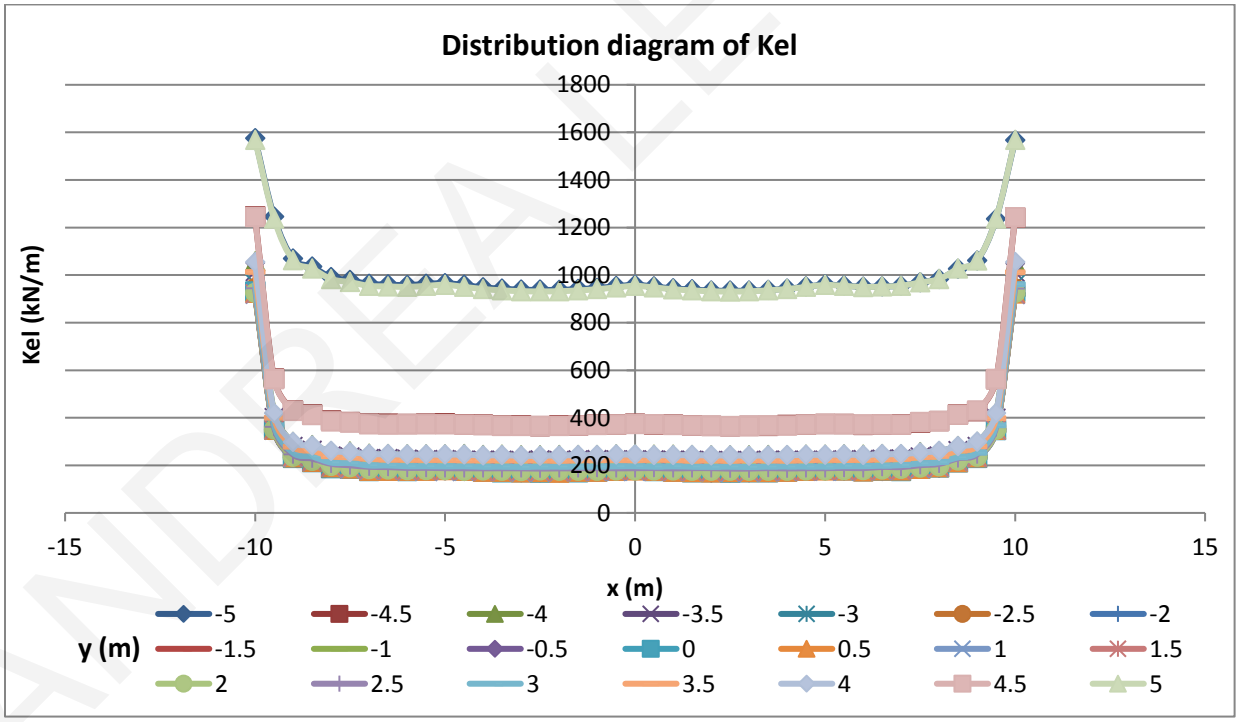

Figure A26: Distribution of K_{el} along the x-axis from analysis 26.

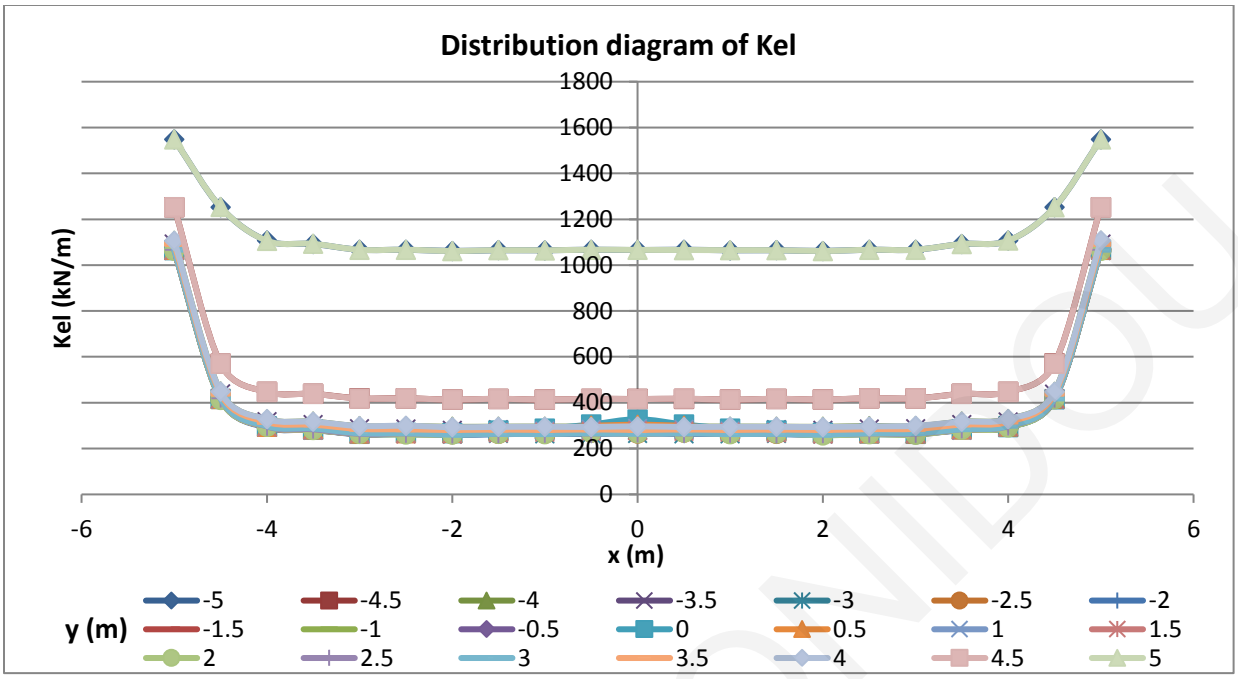

Figure A27: Distribution of K_{el} along the x-axis from analysis 27.

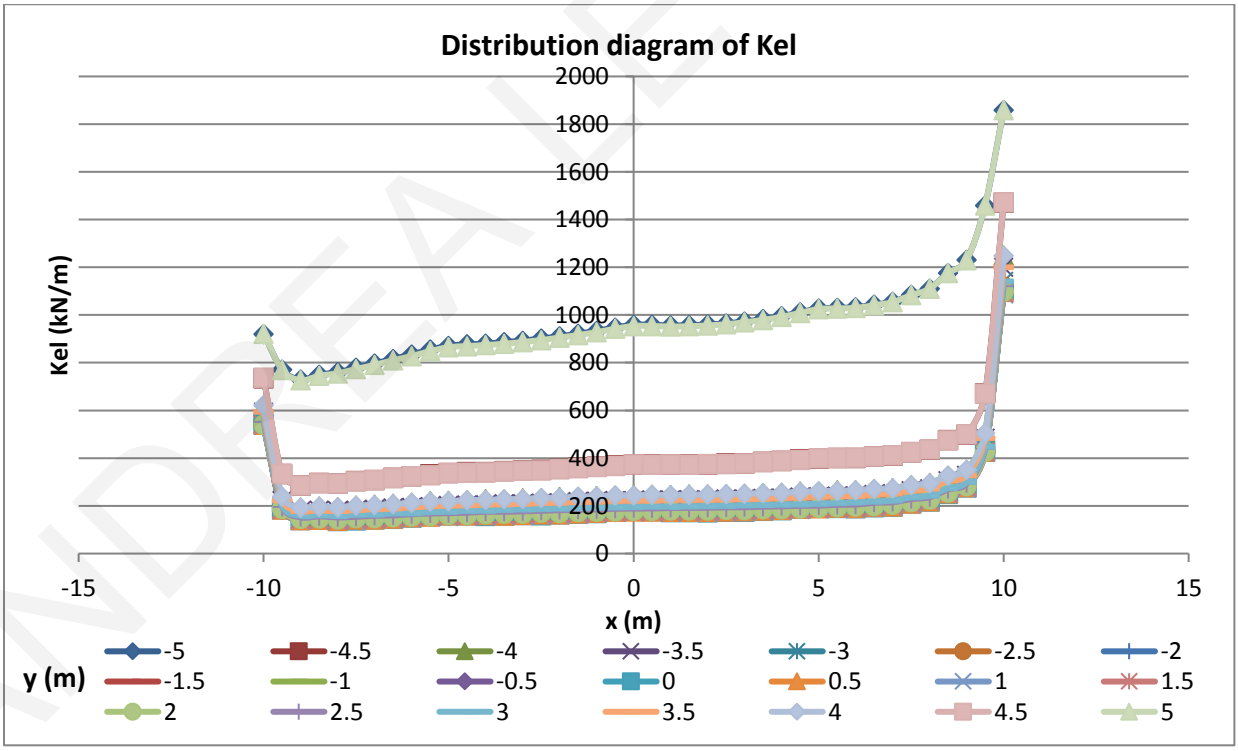

Figure A28: Distribution of K_{el} along the x-axis from analysis 28.

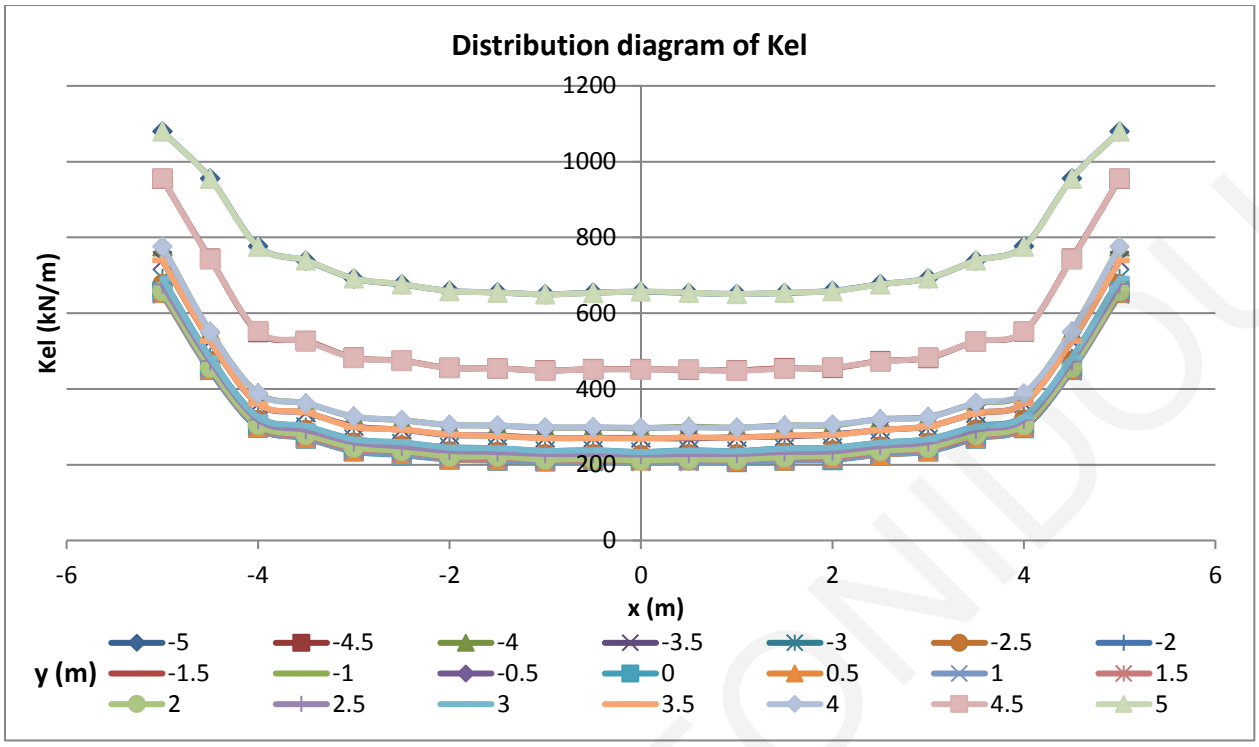

Figure A29: Distribution of K_{el} along the x-axis from analysis 29.

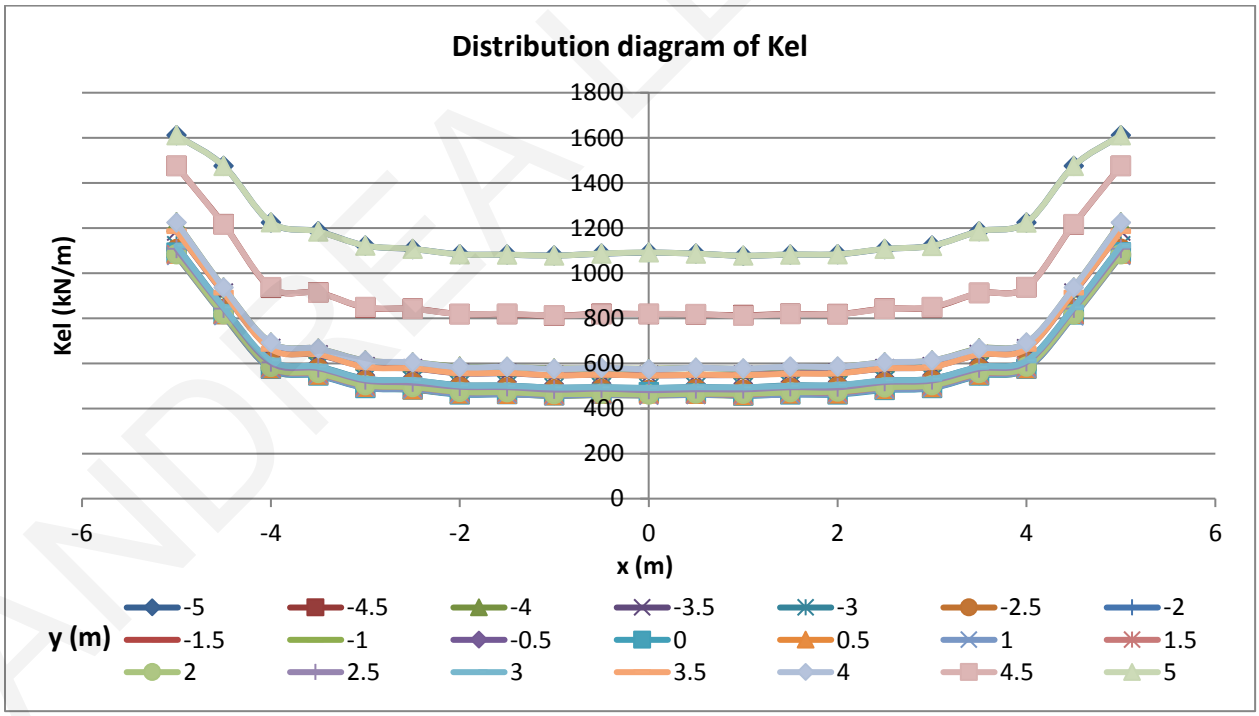

Figure A30: Distribution of K_{el} along the x-axis from analysis 30.

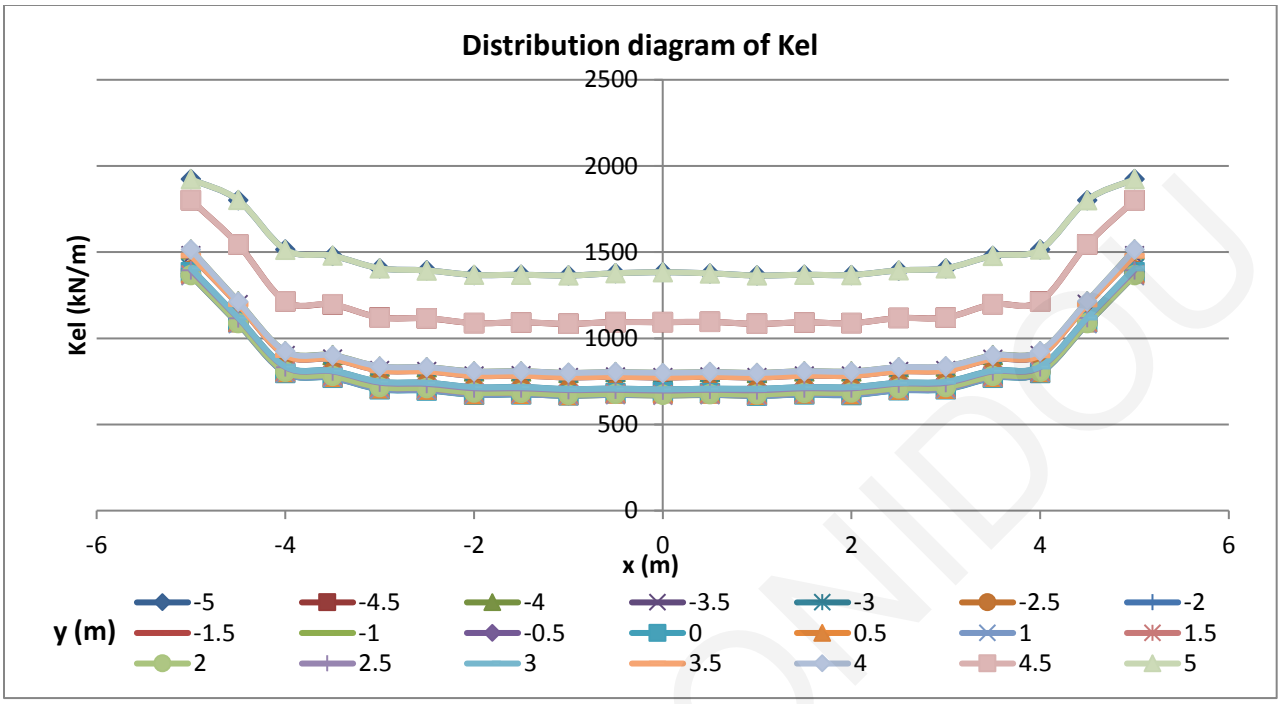

Figure A31: Distribution of K_{el} along the x-axis from analysis 31.

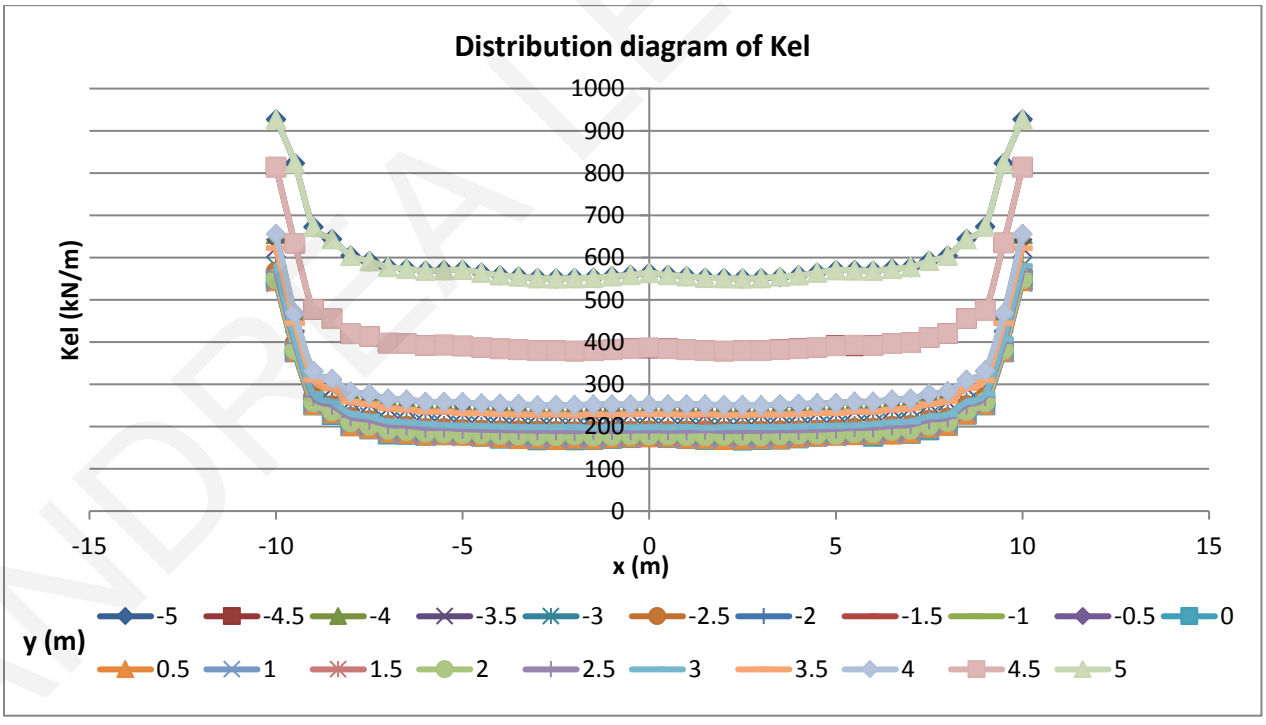

Figure A32: Distribution of K_{el} along the x-axis from analysis 32.

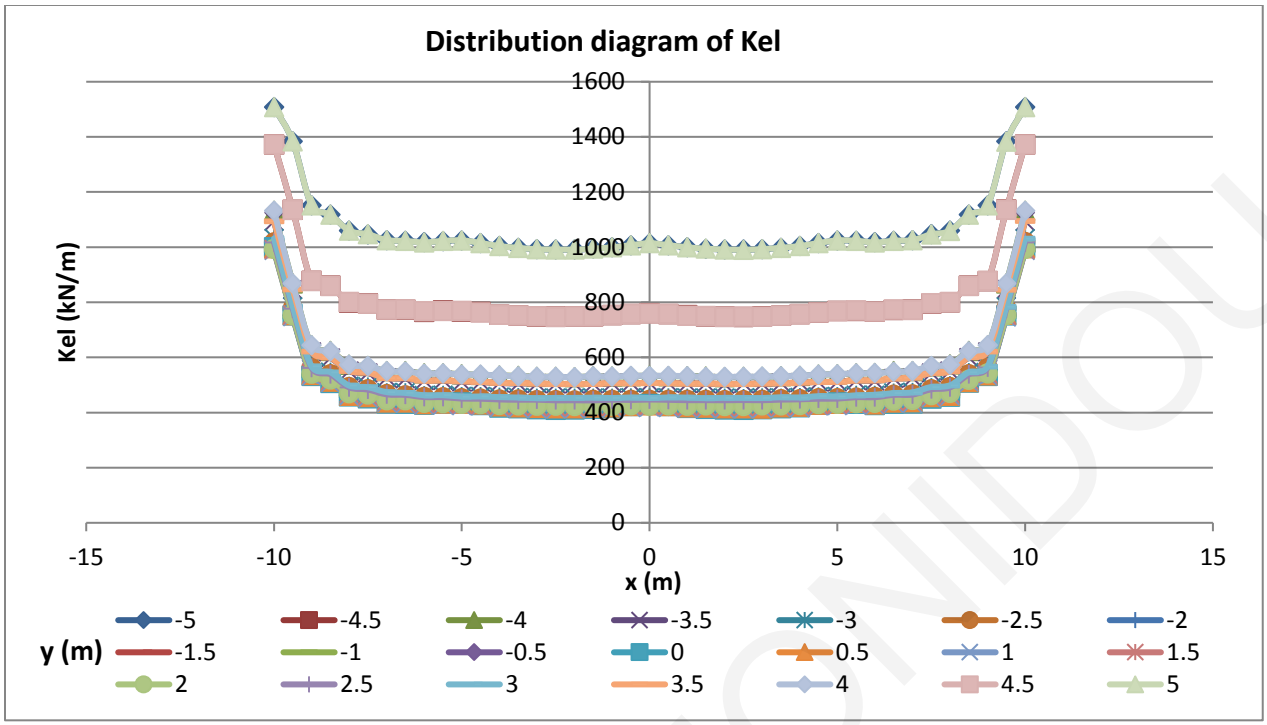

Figure A33: Distribution of K_{el} along the x-axis from analysis 33.

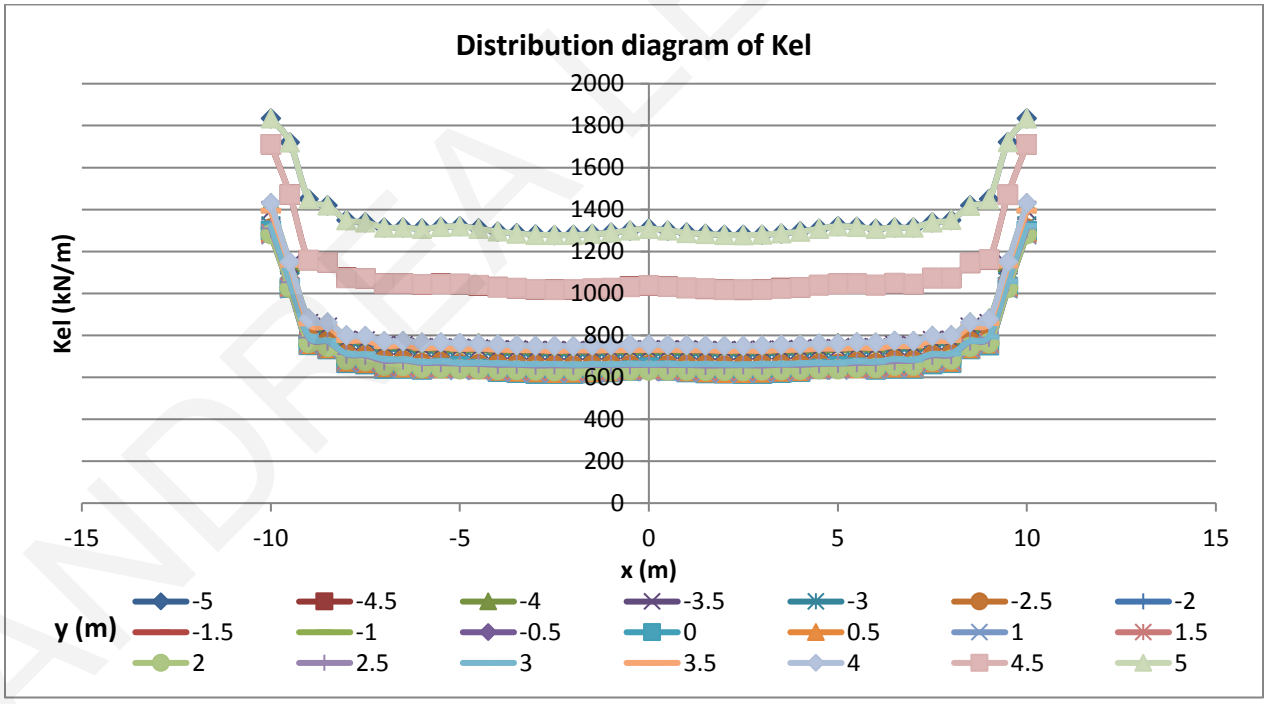

Figure A34: Distribution of K_{el} along the x-axis from analysis 34.

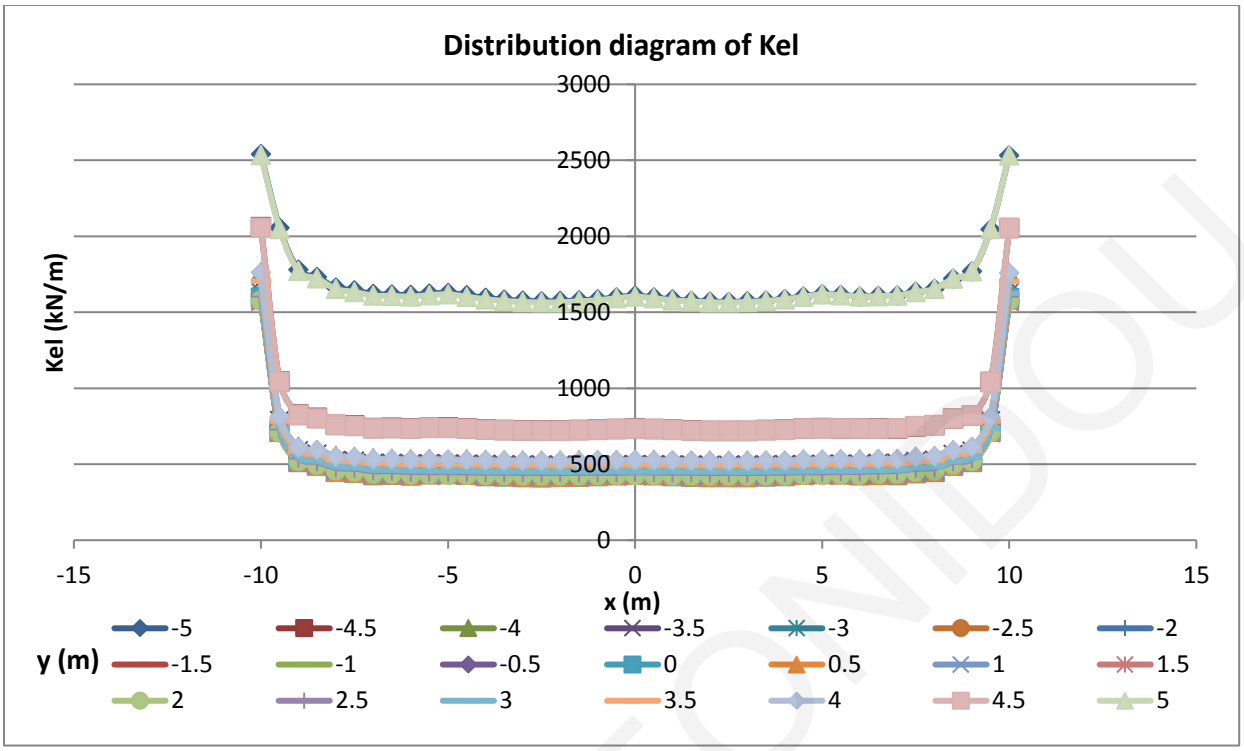

Figure A35: Distribution of K_{el} along the x-axis from analysis 35.

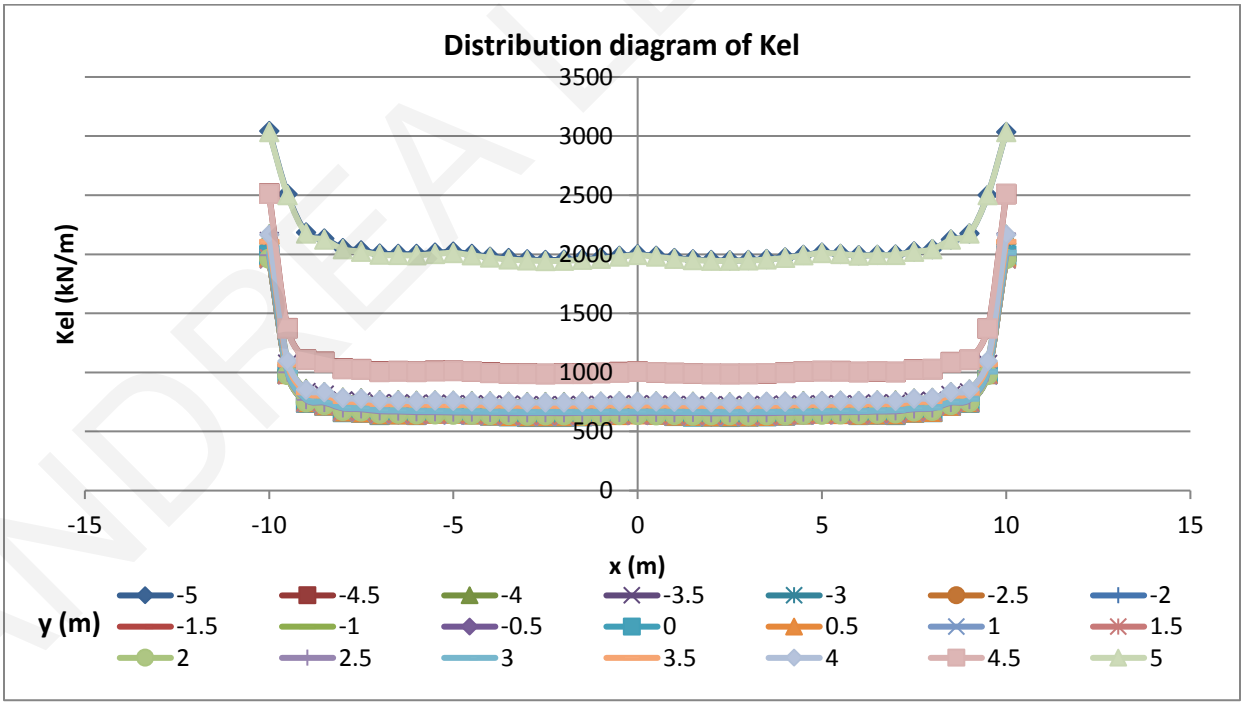

Figure A36: Distribution of K_{el} along the x-axis from analysis 36.

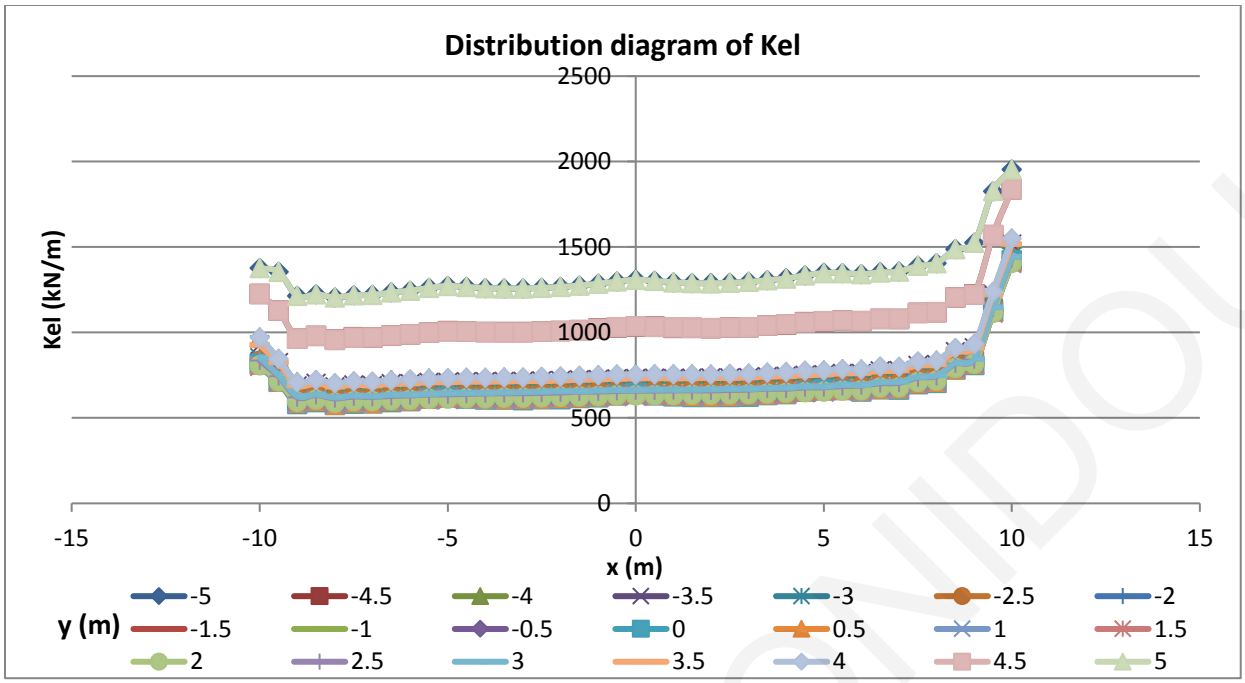

Figure A37: Distribution of K_{el} along the x-axis from analysis 37.

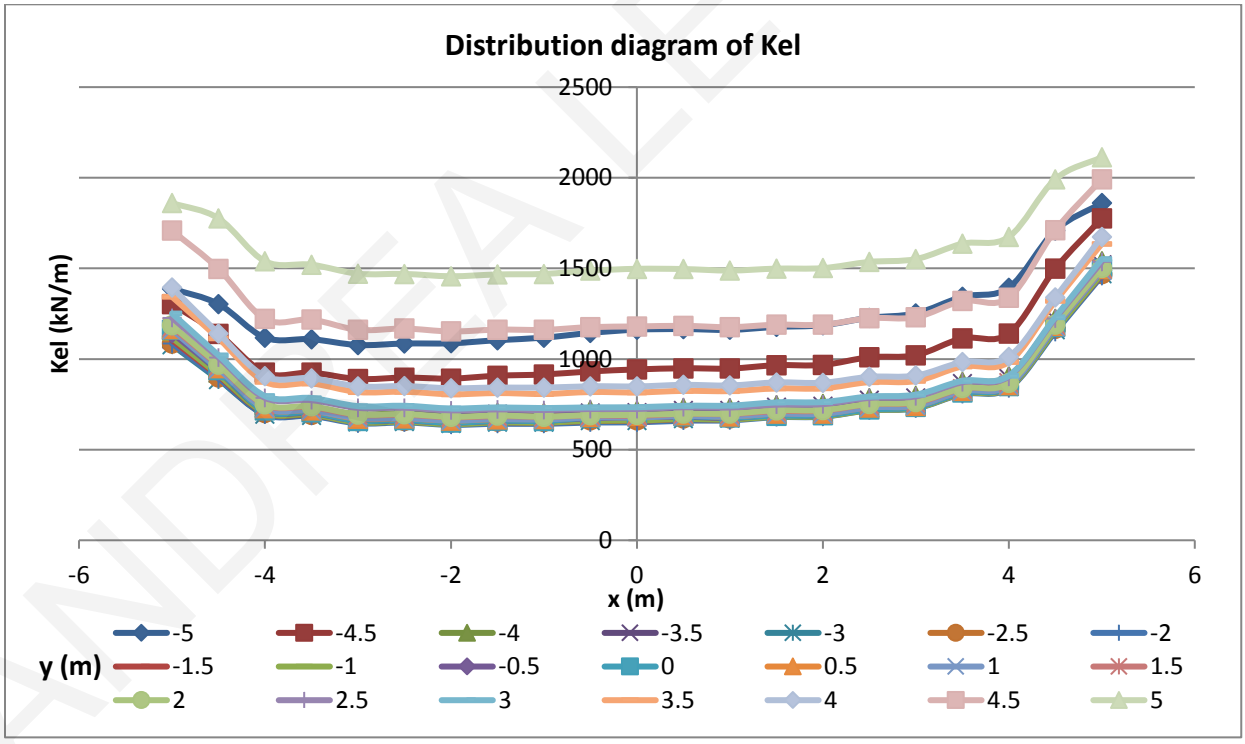

Figure A38: Distribution of K_{el} along the x-axis from analysis 38.

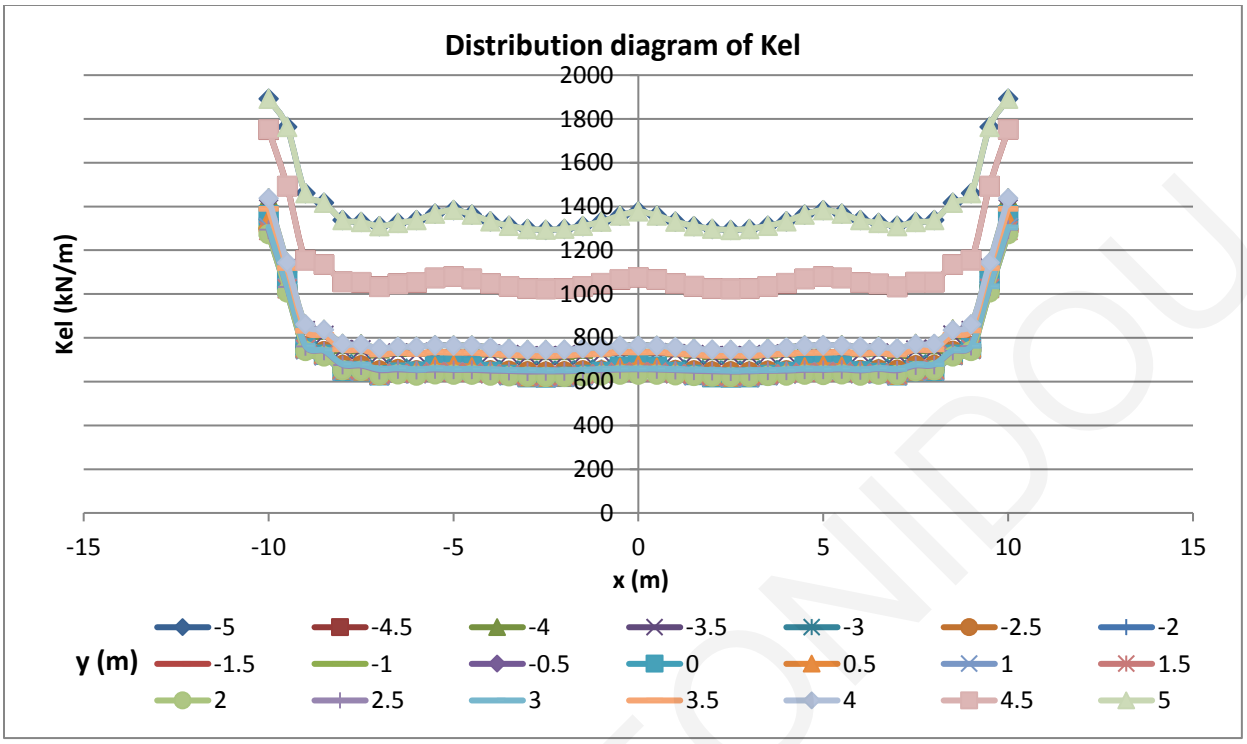

Figure A39: Distribution of K_{el} along the x-axis from analysis 39.

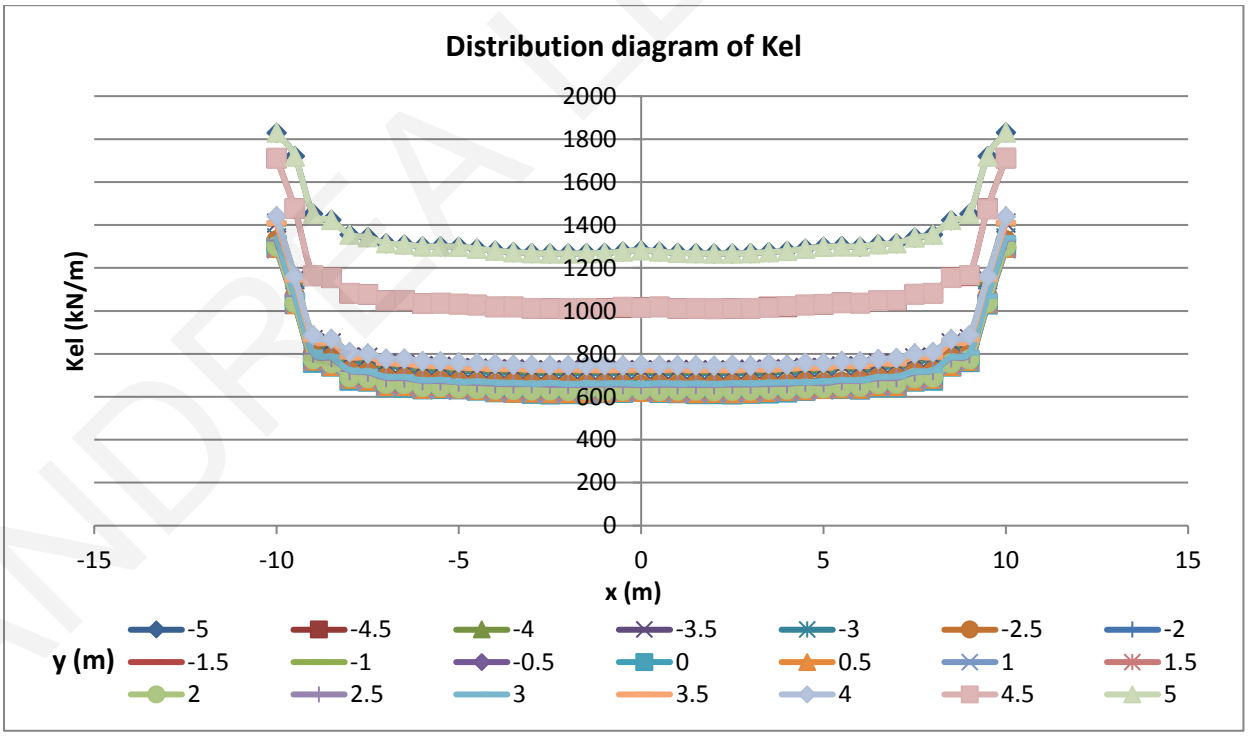

Figure A40: Distribution of K_{el} along the x-axis from analysis 40.

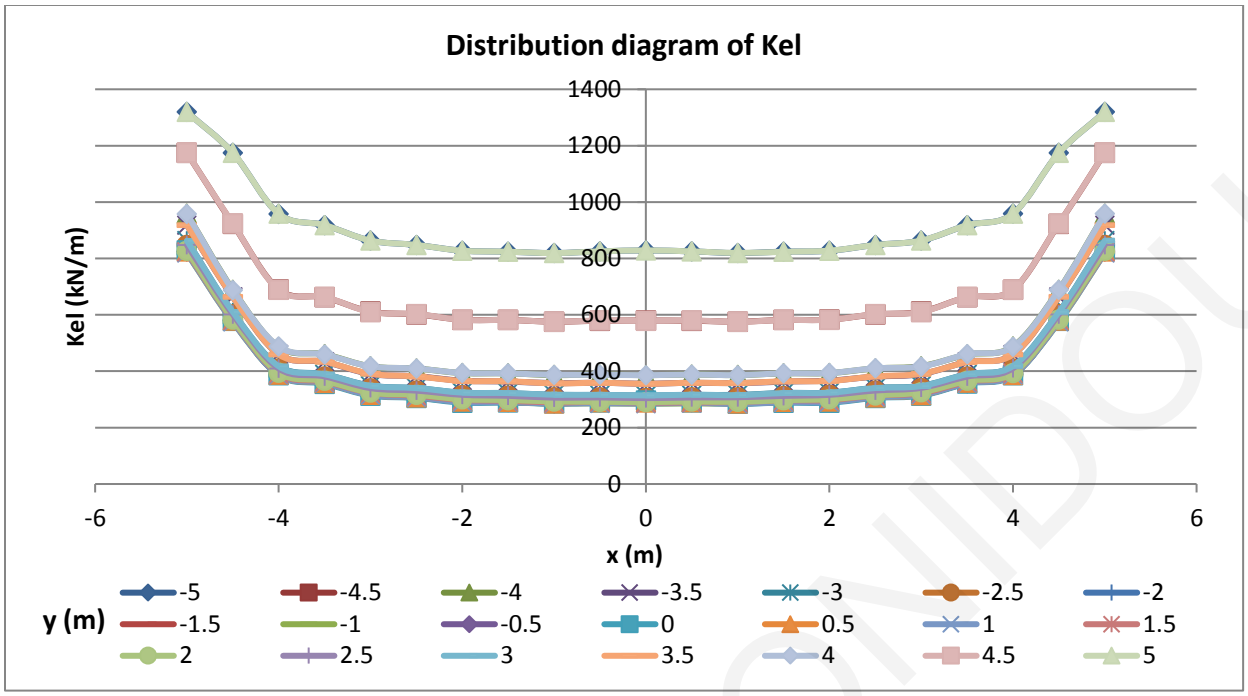

Figure A41: Distribution of K_{el} along the x-axis from analysis 41.

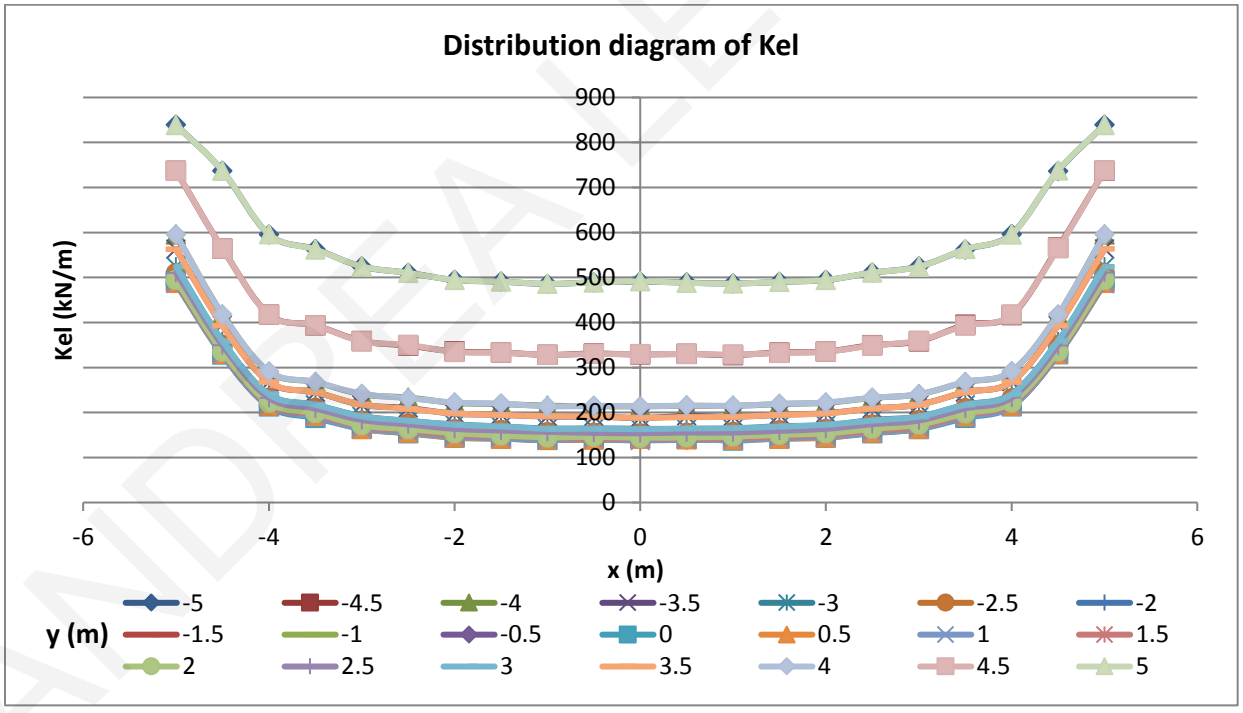

Figure A42: Distribution of K_{el} along the x-axis from analysis 42.

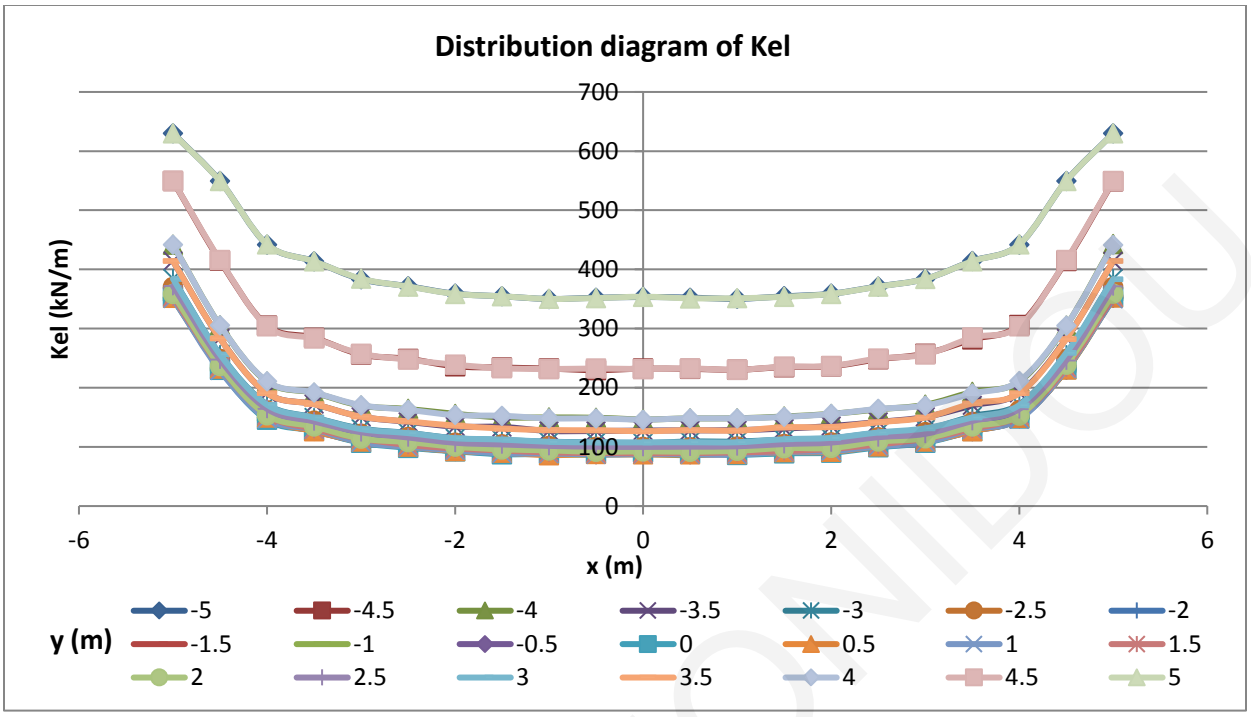

Figure A43: Distribution of K_{el} along the x-axis from analysis 43.

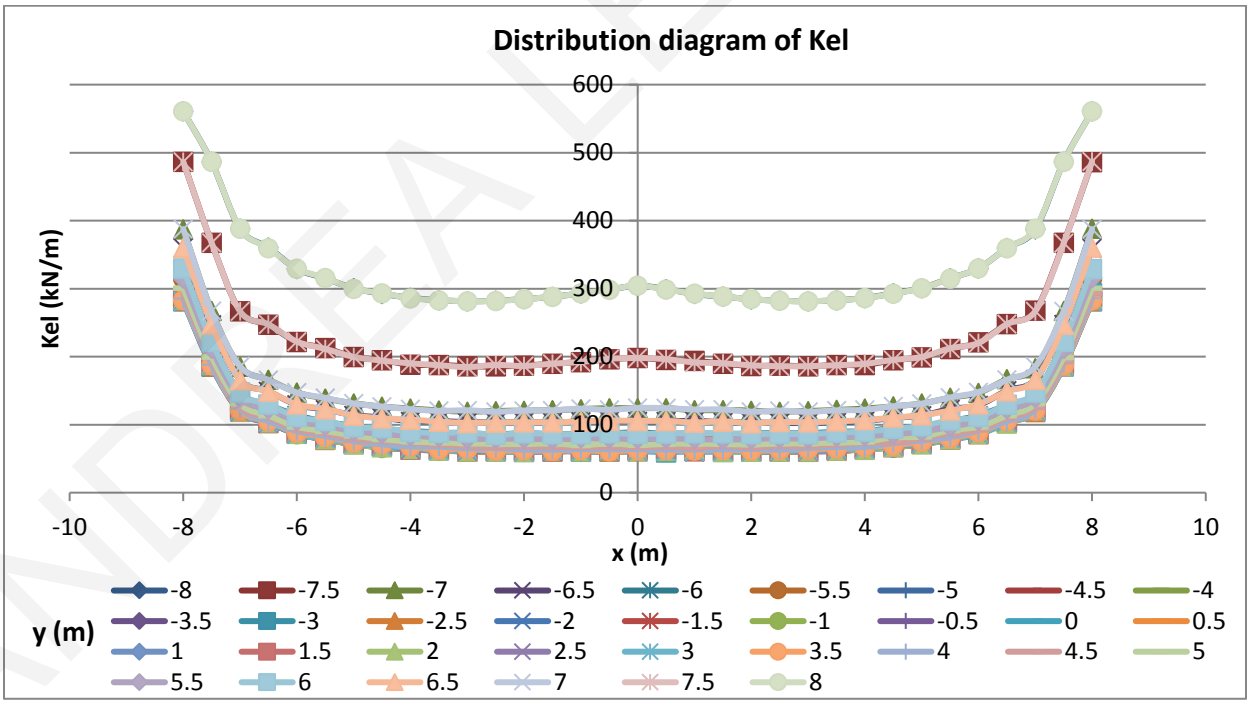

Figure A44: Distribution of K_{el} along the x-axis from analysis 44.

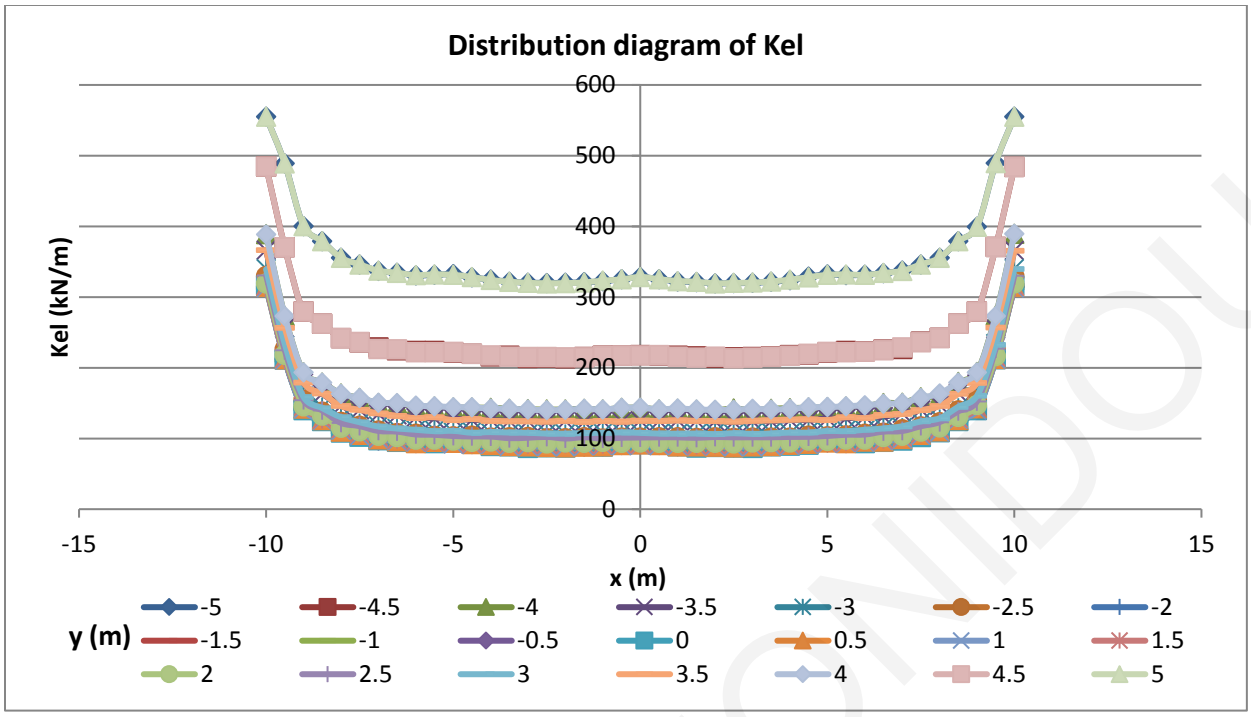

Figure A45: Distribution of K_{el} along the x-axis from analysis 45.

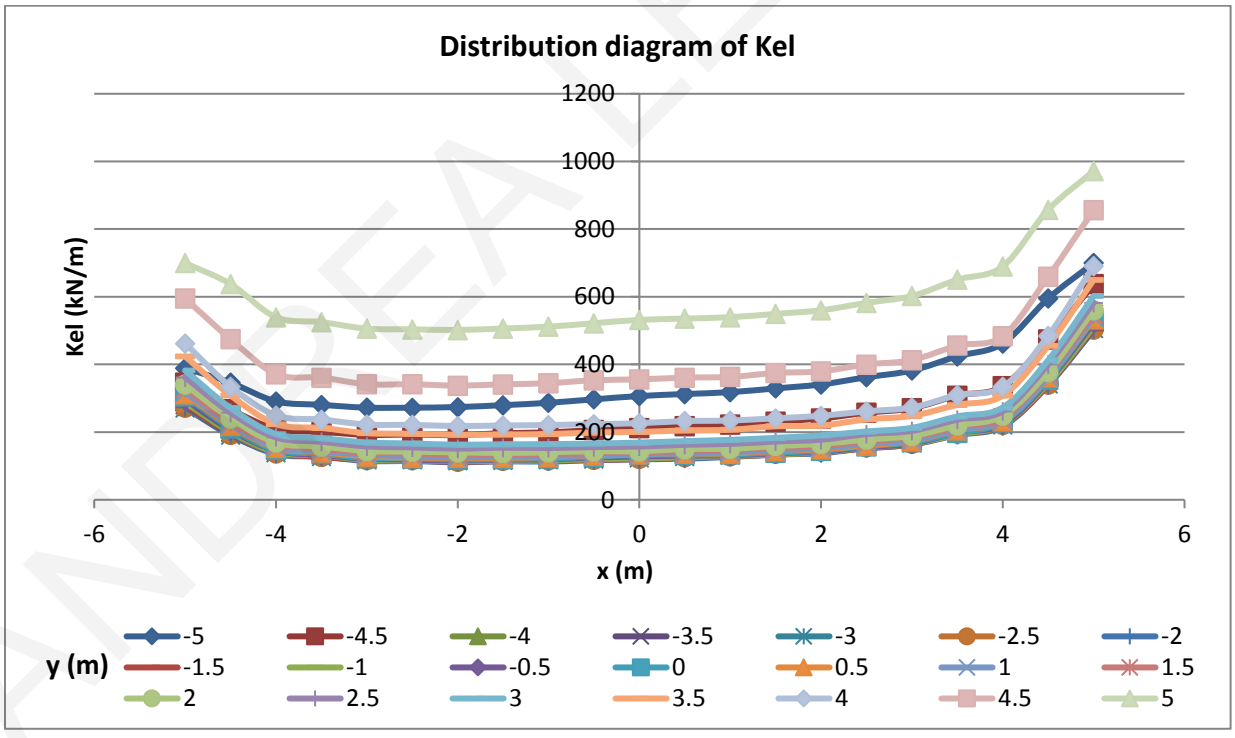

Figure A46: Distribution of K_{el} along the x-axis from analysis 46.

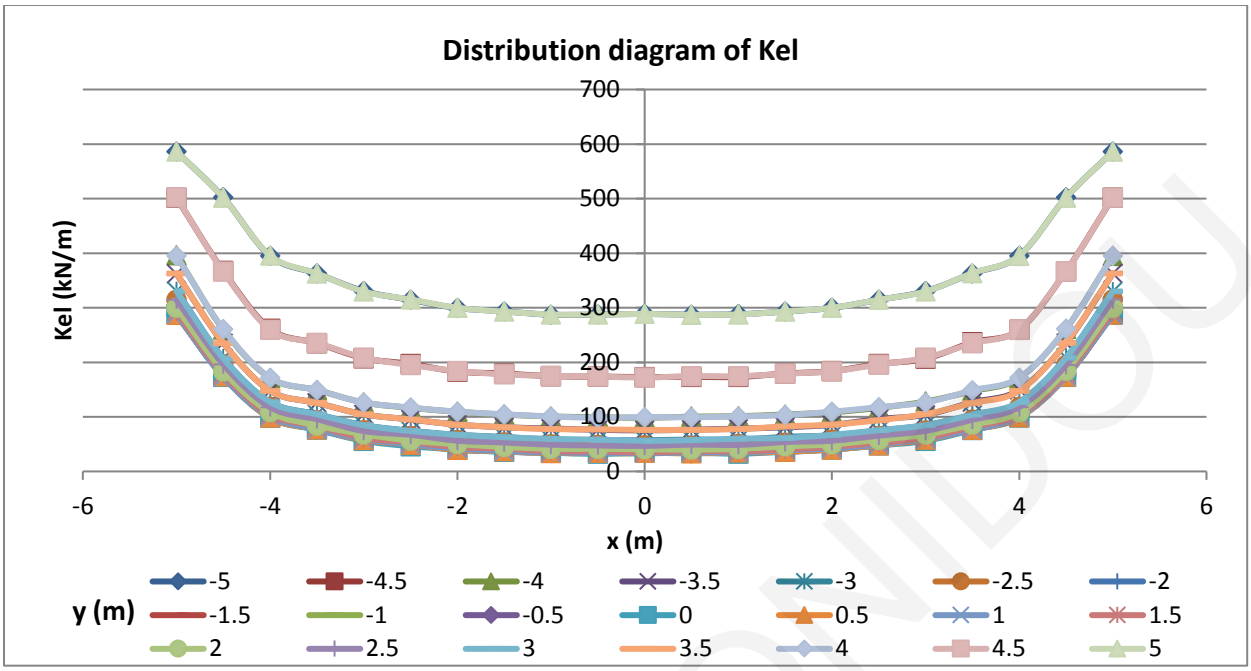

Figure A47: Distribution of K_{el} along the x-axis from analysis 47.

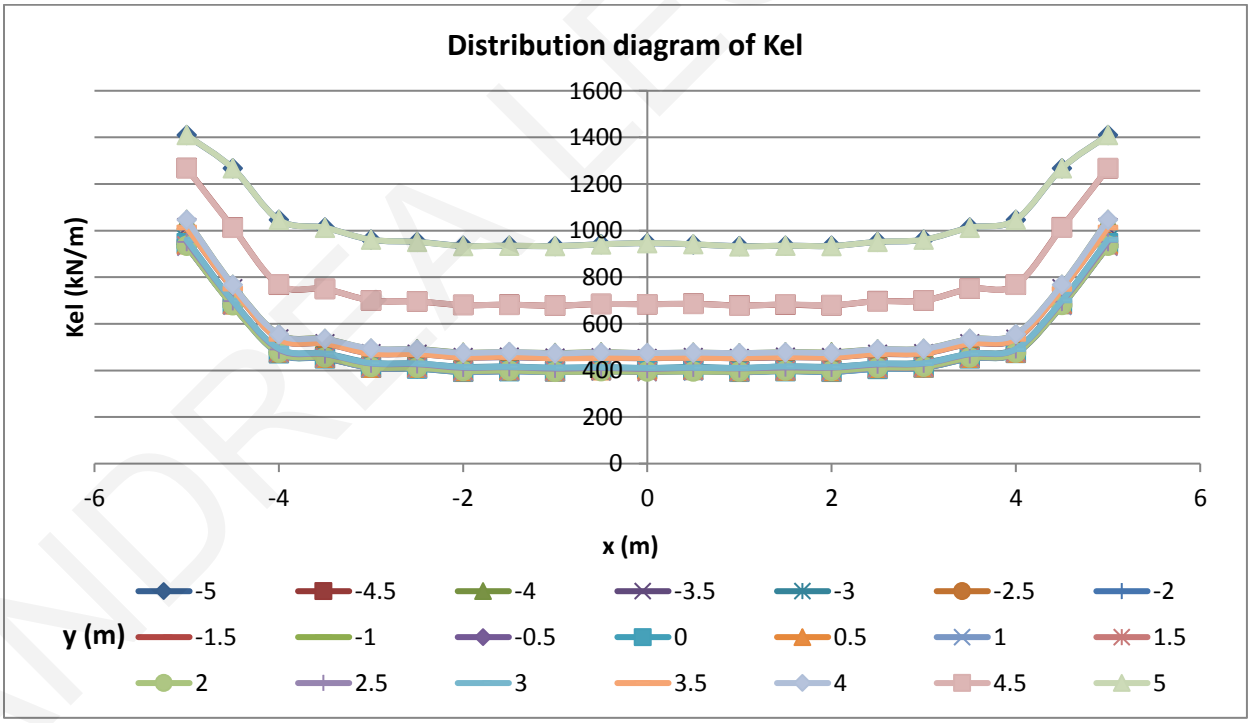

Figure A48: Distribution of K_{el} along the x-axis from analysis 48.

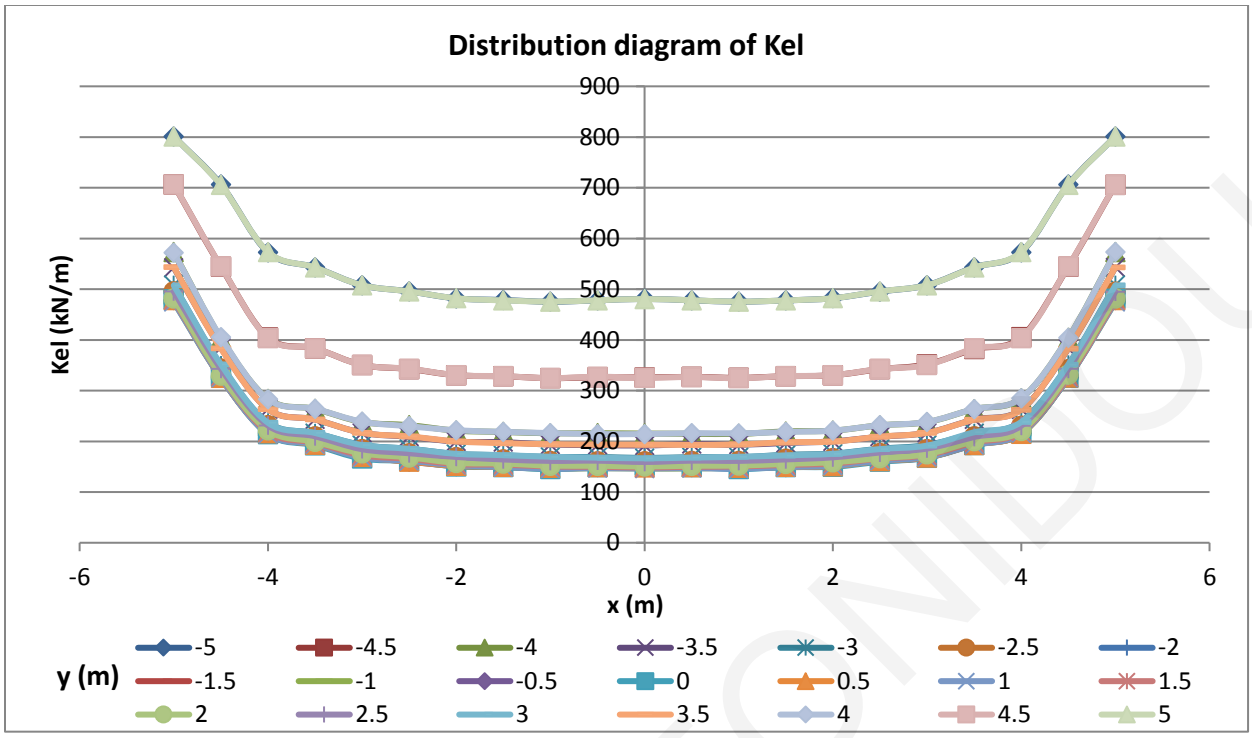

Figure A49: Distribution of K_{el} along the x-axis from analysis 49.

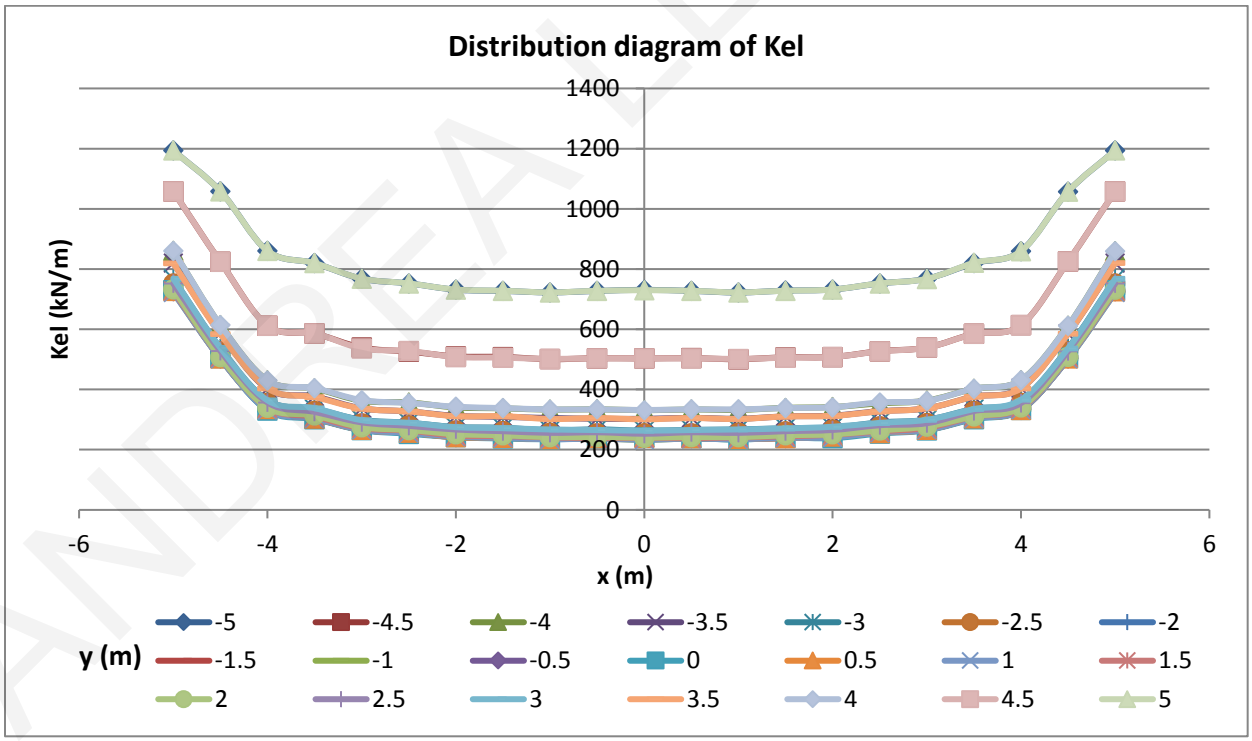

Figure A50: Distribution of K_{el} along the x-axis from analysis 50.

ANNEX B

TABLE OF K_r VALUES FOR THE PARAMETRIC ANALYSES

Table B1: Values of K_r for all parametric analyses performed.

ANALYSES												
#	H/B	B(m)	L/B	D(m)	ρ	E_2 (kPa)	H_1(m)	ν	E_1 (kPa)	Loading	d(m)	K_r (kN/m)
1	10	10	1	6	0	-	-	0.3	10000	C1	0.75	392.7
2	10	10	1	6	0	-	-	0.49	10000	C1	0.75	471.1
3	10	10	1	6	0	-	-	0.49	1000	C1	0.75	47.1
4	10	10	1	6	0	-	-	0.49	100000	C1	0.75	4710.8
5	10	10	1	3	0	-	-	0.49	10000	C1	0.75	448.4
6	10	10	1	9	0	-	-	0.49	10000	C1	0.75	489.5
7	10	10	1	12	0	-	-	0.49	10000	C1	0.75	504.6
8	10	16	1	6	0	-	-	0.49	10000	C1	0.75	284.1
9	10	16	1	9	0	-	-	0.49	10000	C1	0.75	292.8
10	10	16	1	12	0	-	-	0.49	10000	C1	0.75	300.5
11	10	16	1	3	0	-	-	0.3	10000	C1	0.75	226.0
12	10	16	1	9	0	-	-	0.3	10000	C1	0.75	243.9
13	10	16	1	12	0	-	-	0.3	10000	C1	0.75	251.2
14	10	10	2	9	0	-	-	0.49	10000	C8	0.75	368.2
15	10	10	2	12	0	-	-	0.49	10000	C8	0.75	379.5
16	10	10	1	6	0	-	-	0.49	10000	C1	0.5	471.1
17	10	10	1	6	0	-	-	0.49	10000	C1	1.0	471.1
18	1	16	1	6	0	-	-	0.49	10000	C1	0.75	545.2
19	0.5	16	1	6	0	-	-	0.49	10000	C1	0.75	975.3
20	10	10	1	6	0	-	-	0.49	10000	C2	0.75	471.1
21	10	10	1	6	0	-	-	0.49	10000	C3	0.75	471.1
22	10	10	1	6	0	-	-	0.49	10000	C4	0.75	471.1
23	10	10	1	6	0	-	-	0.49	10000	C5	0.75	471.1
24	10	16	1	6	0	-	-	0.49	10000	C6	0.75	284.1
25	10	10	1	6	0	-	-	0.49	10000	C7	0.75	471.1
26	10	10	2	6	0	-	-	0.49	10000	C8	0.75	354.3
27	10	10	1	6	0	-	-	0.49	10000	C9	0.75	471.1
28	10	10	2	6	0	-	-	0.49	10000	C10	0.75	354.3
29	10	10	1	0	0	-	-	0.49	10000	C1	0.75	420.5
30	10	10	1	0	1000	-	-	0.49	10000+1000z	C1	0.75	420.5
31	10	10	1	0	2000	-	-	0.49	10000+2000z	C1	0.75	420.5
32	10	10	2	0	0	-	-	0.49	10000	C8	0.75	316.2
33	10	10	2	0	1000	-	-	0.49	10000+1000z	C8	0.75	316.2
34	10	10	2	0	2000	-	-	0.49	10000+2000z	C8	0.75	316.2
35	10	10	2	6	1000	-	-	0.49	10000+1000z	C8	0.75	354.3
36	10	10	2	6	2000	-	-	0.49	10000+2000z	C8	0.75	354.3
37	10	10	2	0	2000	-	-	0.49	10000+2000z	C10	0.75	316.2
38	10	10	1	0	2000	-	-	0.49	10000+2000z	C7	0.75	420.5
39	10	10	2	0	2000	-	-	0.49	10000+2000z	C8	0.5	316.2
40	10	10	2	0	2000	-	-	0.49	10000+2000z	C8	1.0	316.2
41	10	10	1	0	0	20000	10	0.49	10000	C1	0.75	420.5
42	10	10	1	0	0	5000	10	0.49	10000	C1	0.75	420.5
43	10	10	1	0	0	2500	10	0.49	10000	C1	0.75	420.5
44	10	16	1	0	0	2500	16	0.49	10000	C1	0.75	262.8
45	10	10	2	0	0	2500	16	0.49	10000	C8	0.75	316.2
46	10	10	1	0	0	2500	16	0.49	10000	C7	0.75	420.5
47	10	10	1	0	0	2500	5	0.49	10000	C1	0.75	420.5
48	10	10	1	0	0	20000	5	0.49	10000	C1	0.75	420.5
49	10	10	1	0	0	2500	20	0.49	10000	C1	0.75	420.5
50	10	10	1	0	0	20000	20	0.49	10000	C1	0.75	420.5

ANNEX C

COMPARISON PLOTS OF K_{el} BACK-CALCULATED FROM ABAQUS FEA AND PREDICTED BY PROPOSED EQUATION

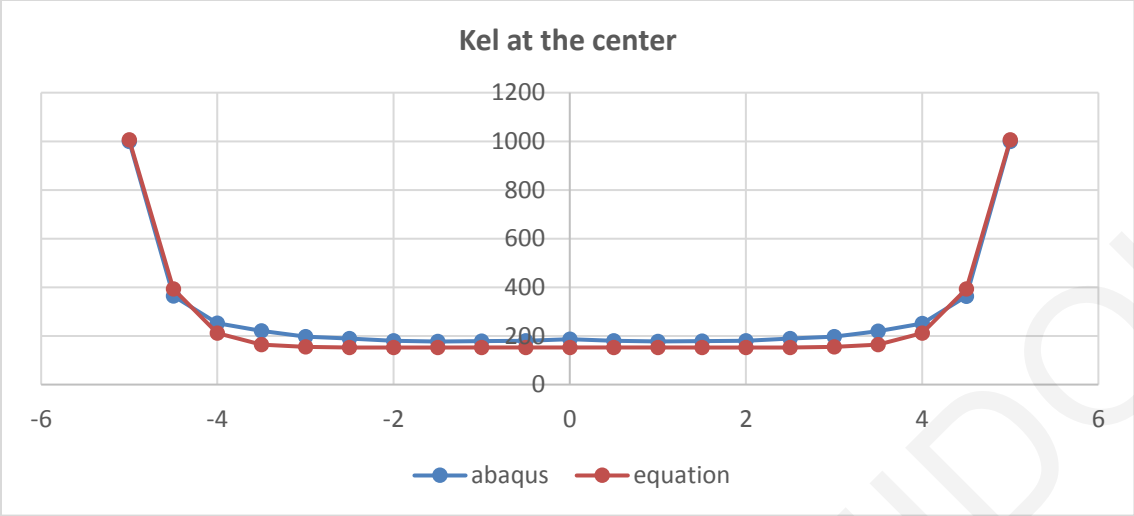

(a)

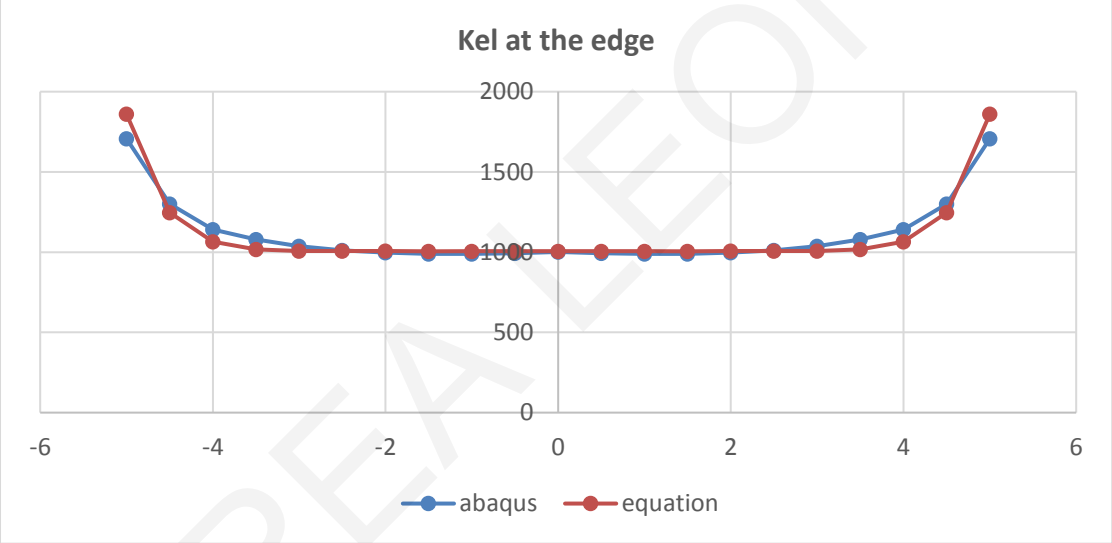

(b)

Figure C1: Comparison of K_{el} from Abaqus and the proposed equation for analysis 1 at (a) the centerline and (b) the edge of the mat.

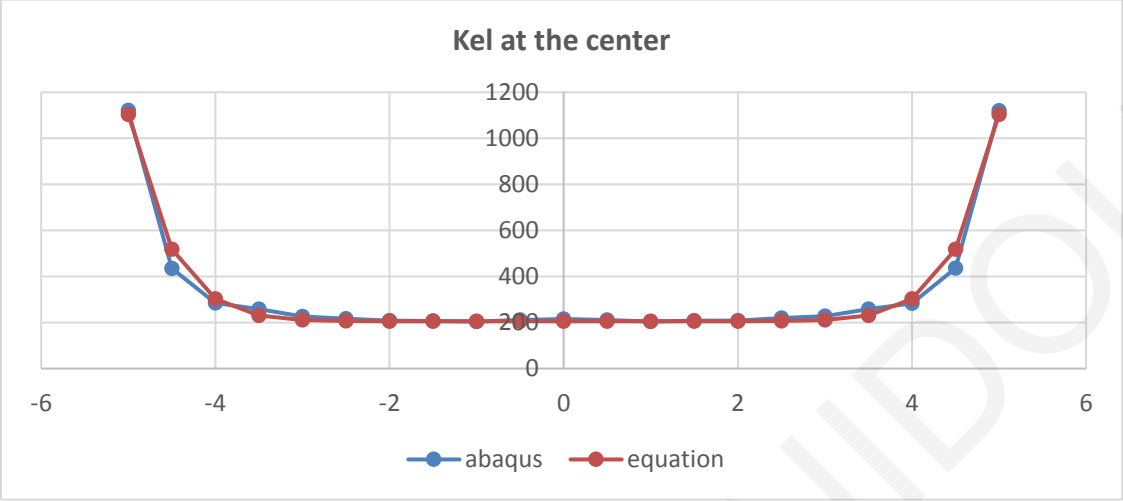

(a)

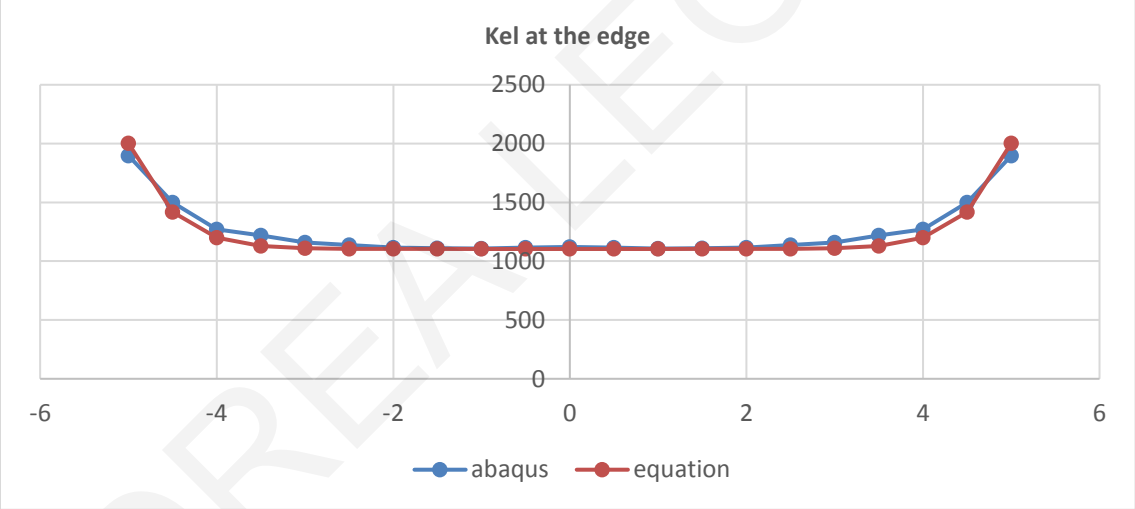

(b)

Figure C2: Comparison of K_{el} from Abaqus and the proposed equation for analysis 2 at (a) the centerline and (b) the edge of the mat.

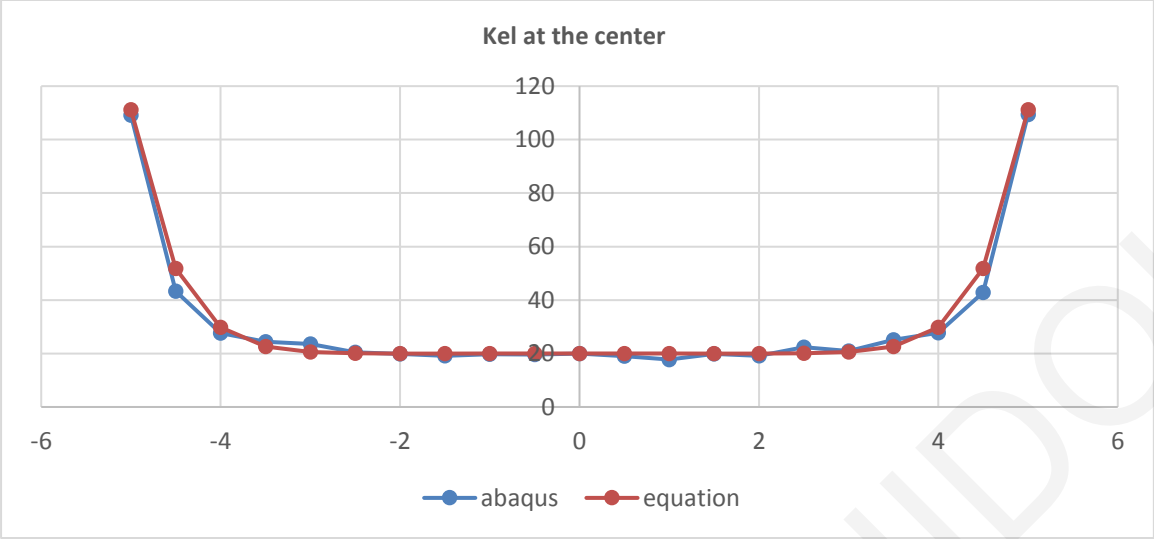

(a)

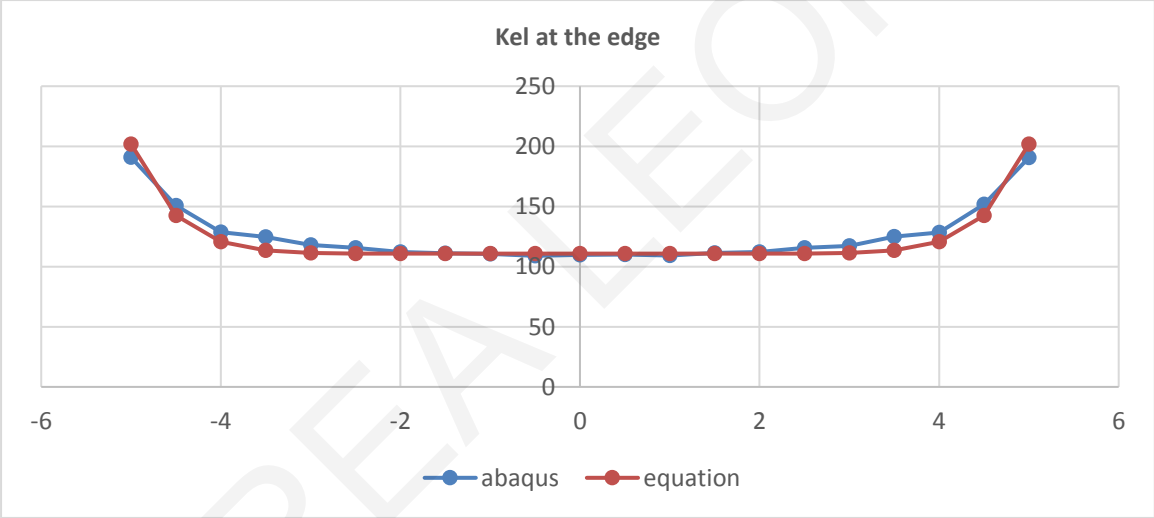

(b)

Figure C3: Comparison of K_{el} from Abaqus and the proposed equation for analysis 3 at (a) the centerline and (b) the edge of the mat.

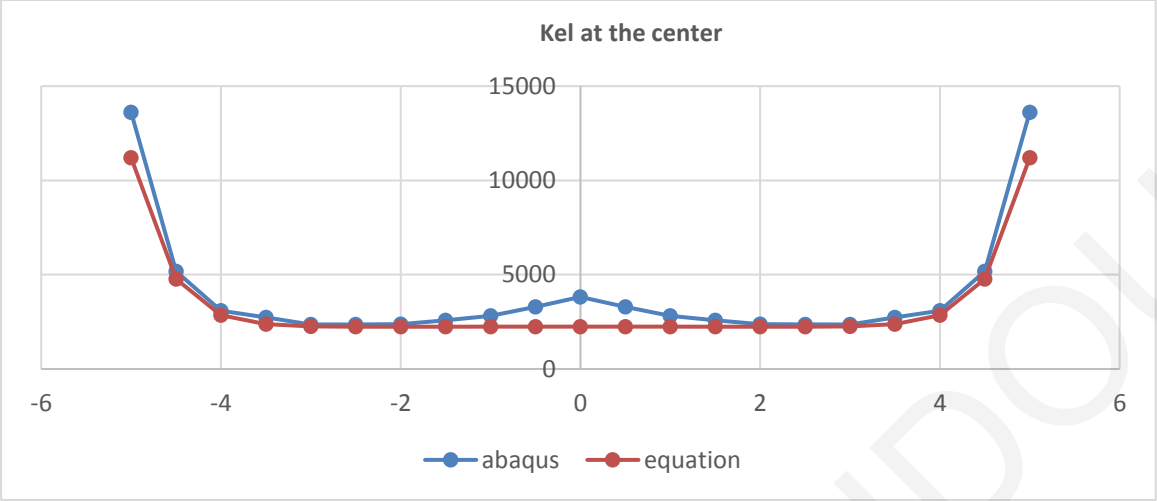

(a)

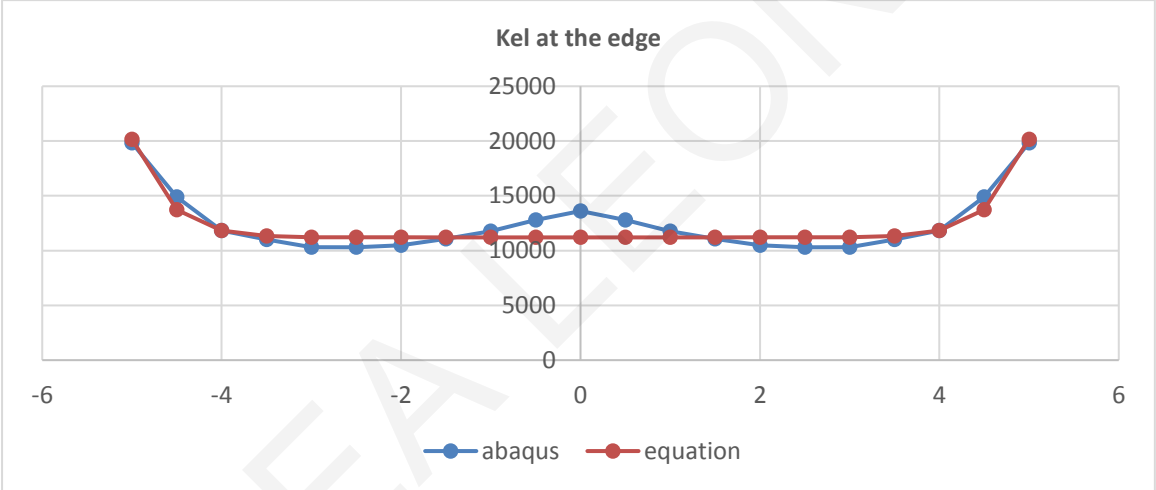

(b)

Figure C4: Comparison of K_{el} from Abaqus and the proposed equation for analysis 4 at (a) the centerline and (b) the edge of the mat.

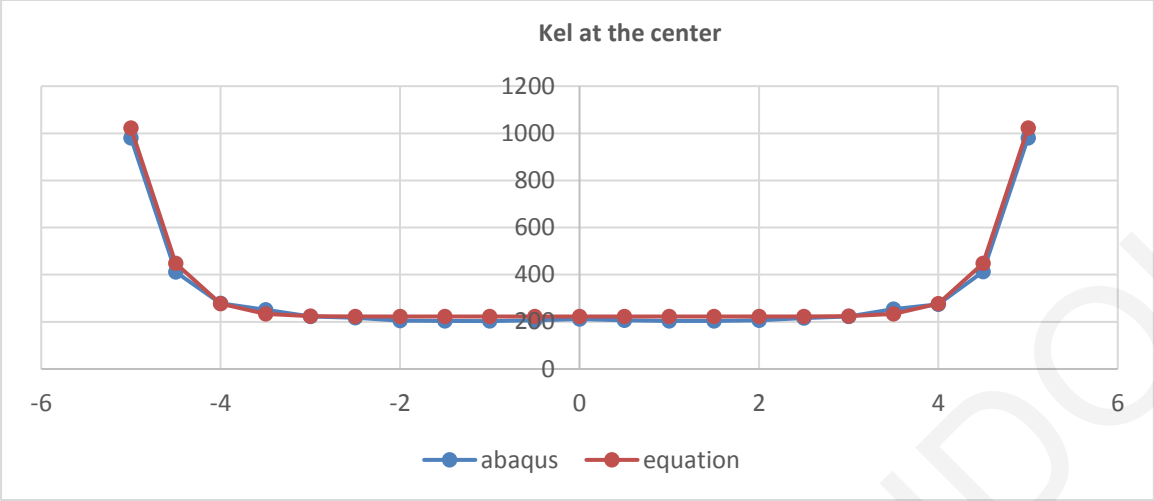

(a)

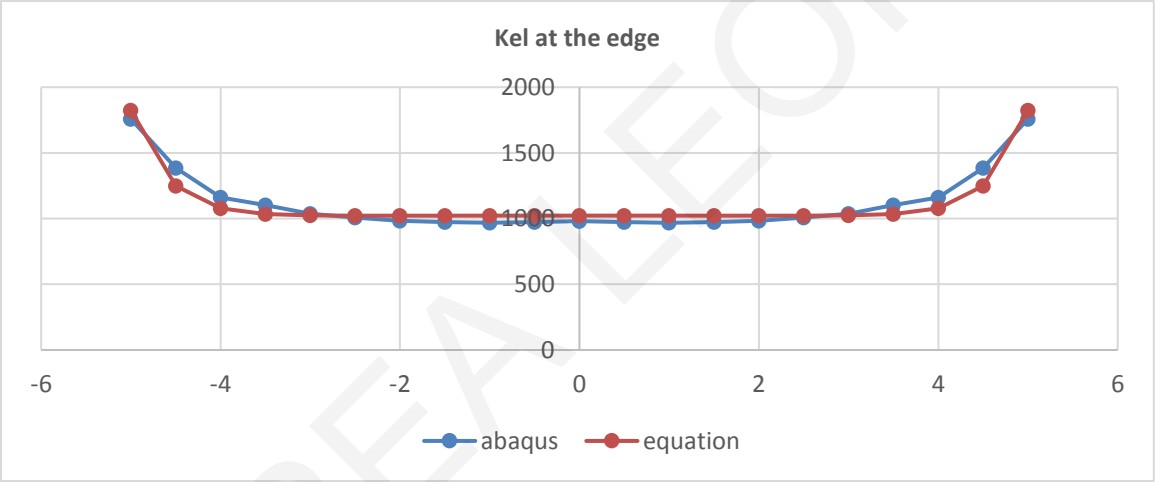

(b)

Figure C5: Comparison of K_{el} from Abaqus and the proposed equation for analysis 5 at (a) the centerline and (b) the edge of the mat.

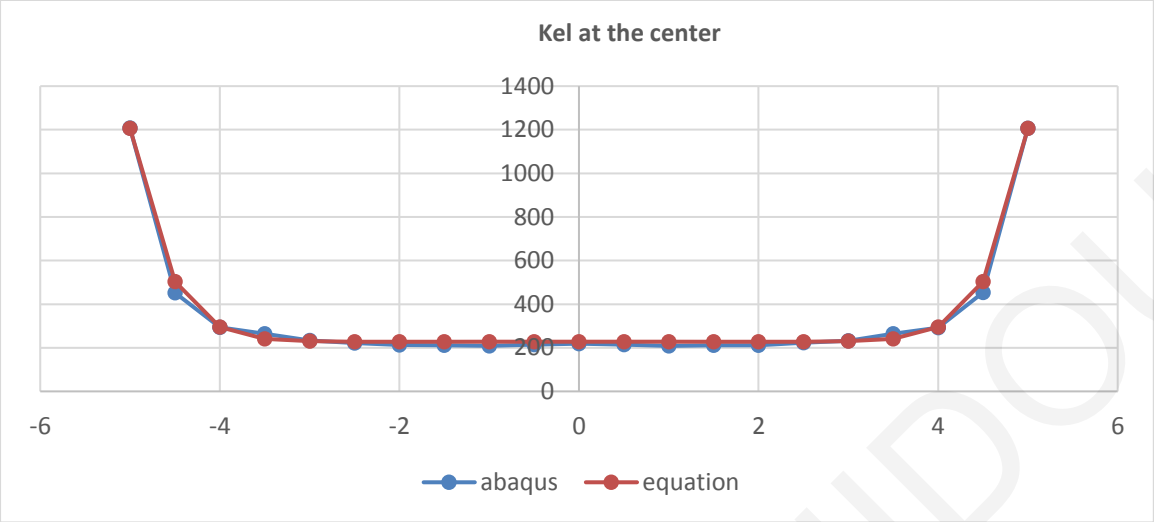

(a)

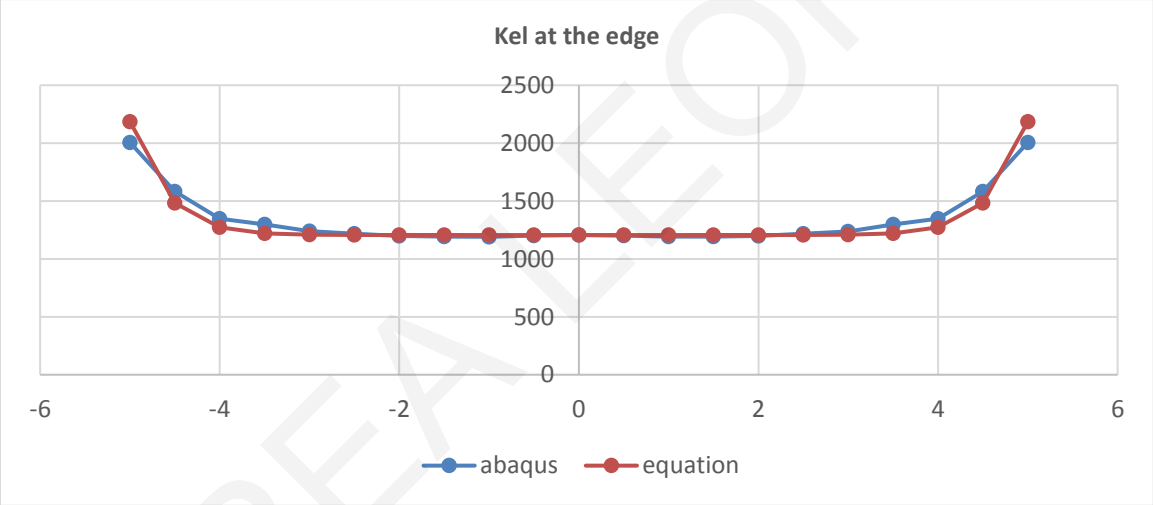

(b)

Figure C6: Comparison of K_{el} from Abaqus and the proposed equation for analysis 6 at (a) the centerline and (b) the edge of the mat.

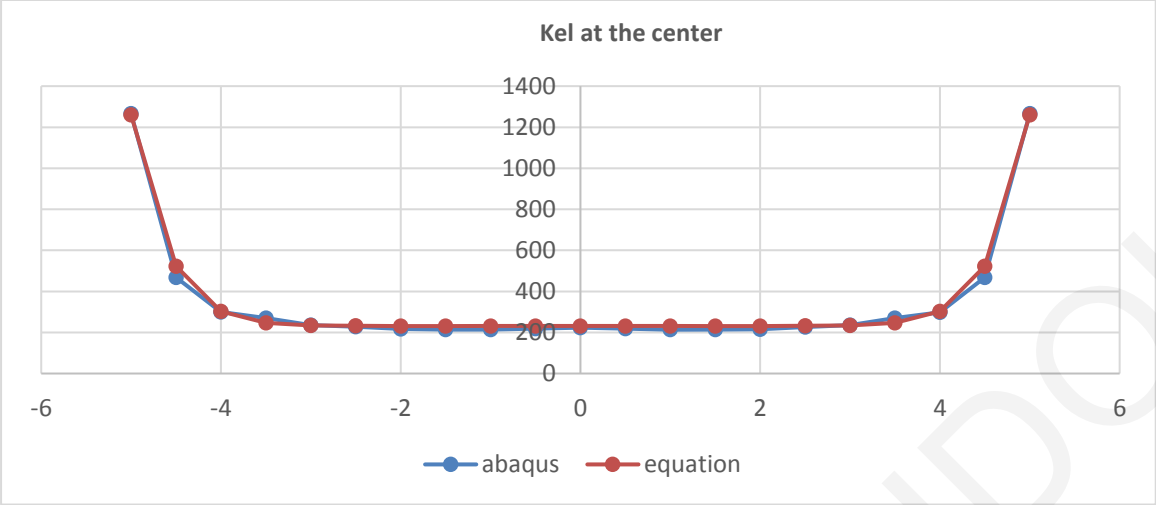

(a)

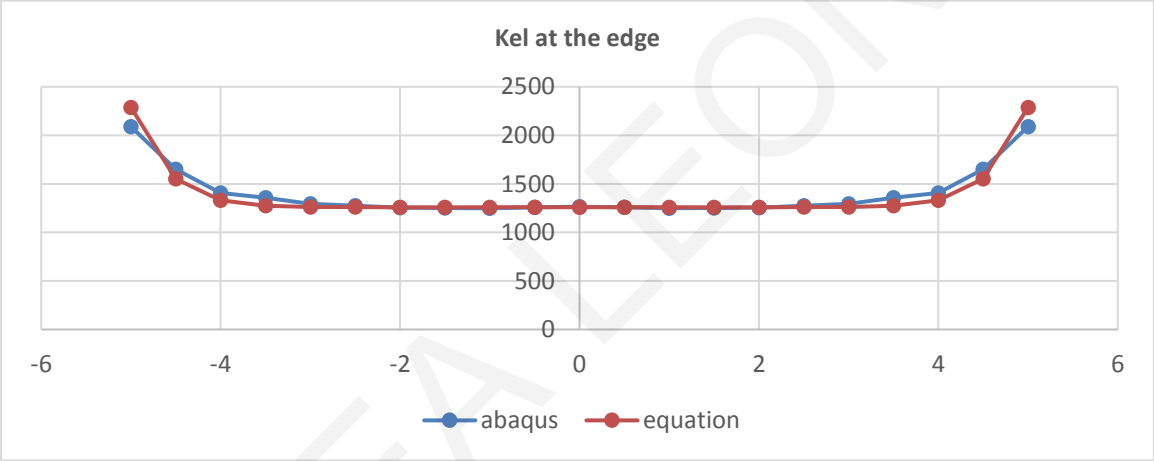

(b)

Figure C7: Comparison of K_{el} from Abaqus and the proposed equation for analysis 7 at (a) the centerline and (b) the edge of the mat.

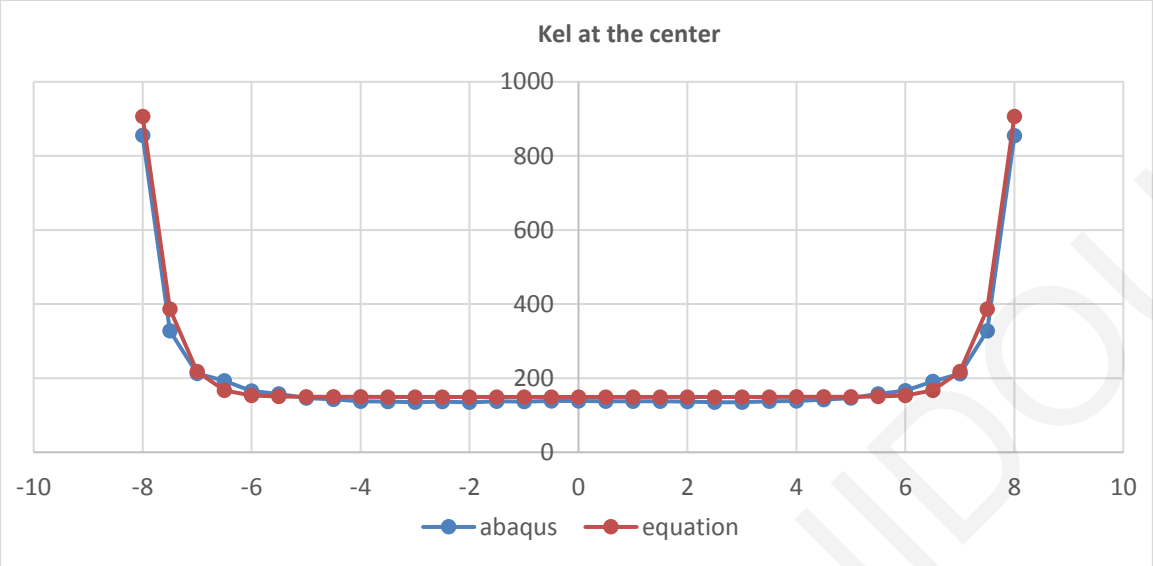

(a)

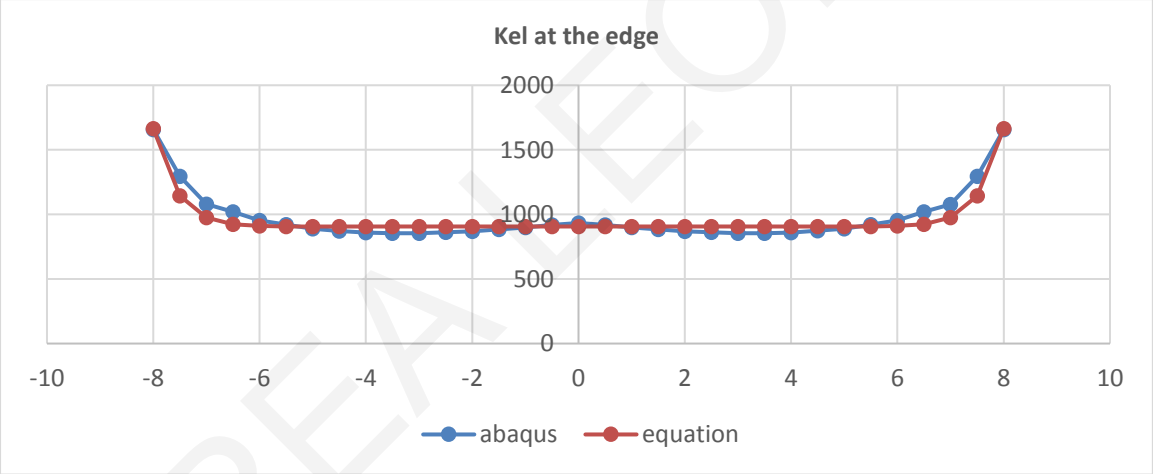

(b)

Figure C8: Comparison of K_{el} from Abaqus and the proposed equation for analysis 8 at (a) the centerline and (b) the edge of the mat.

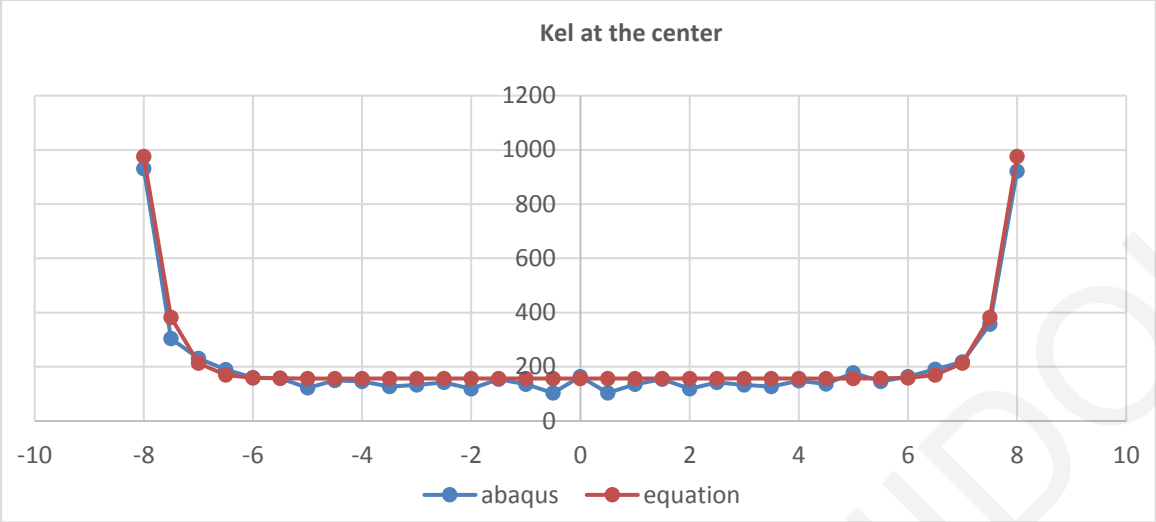

(a)

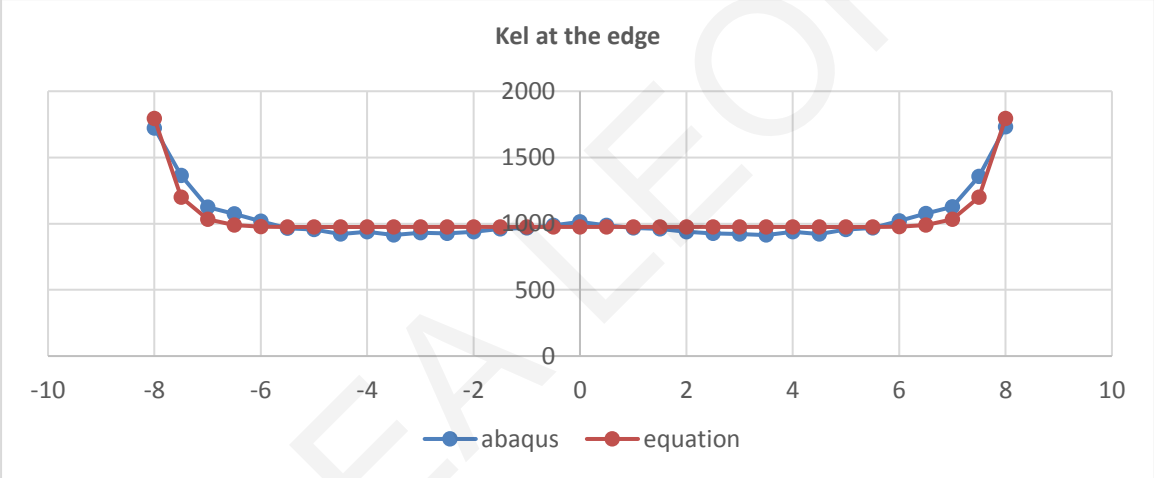

(b)

Figure C9: Comparison of K_{el} from Abaqus and the proposed equation for analysis 9 at (a) the centerline and (b) the edge of the mat

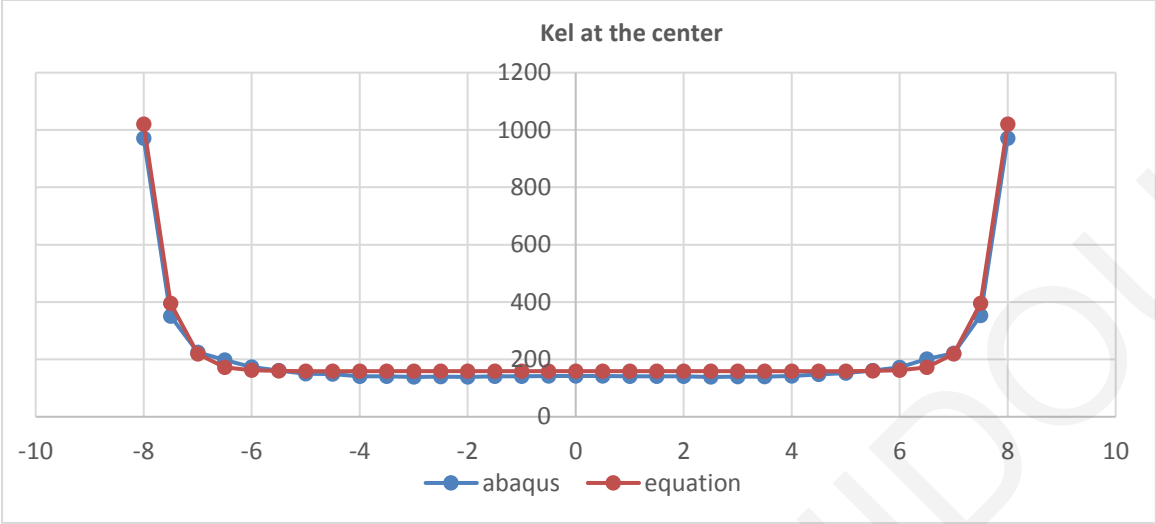

(a)

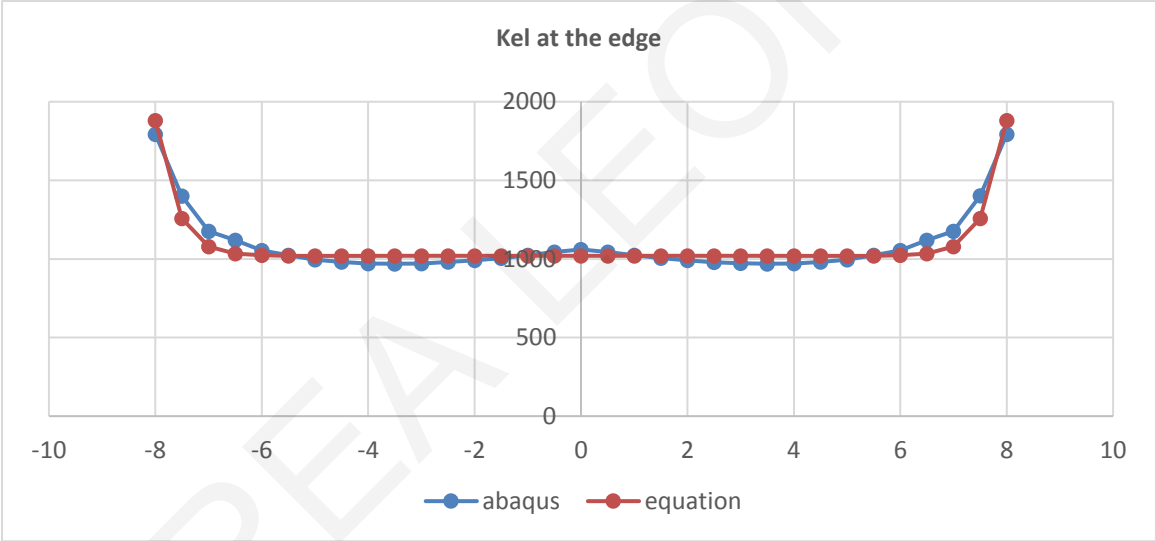

(b)

Figure C10: Comparison of K_{el} from Abaqus and the proposed equation for analysis 10 at (a) the centerline and (b) the edge of the mat.

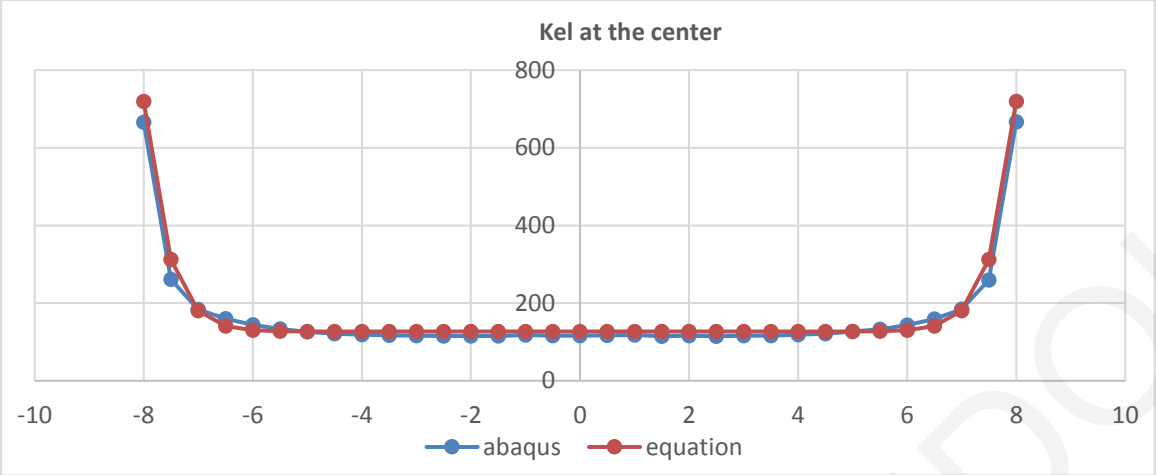

(a)

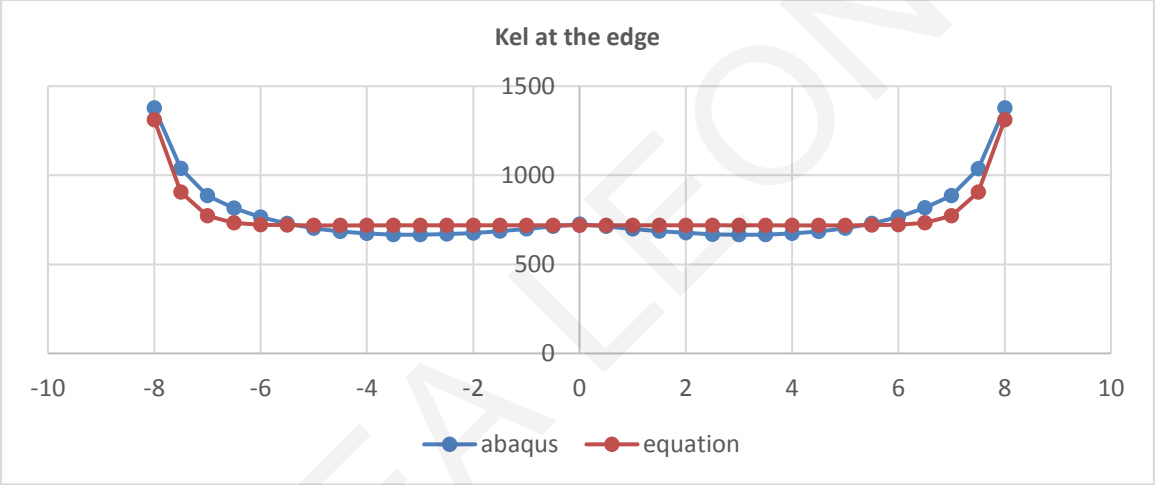

(b)

Figure C11: Comparison of K_{el} from Abaqus and the proposed equation for analysis 11 at (a) the centerline and (b) the edge of the mat.

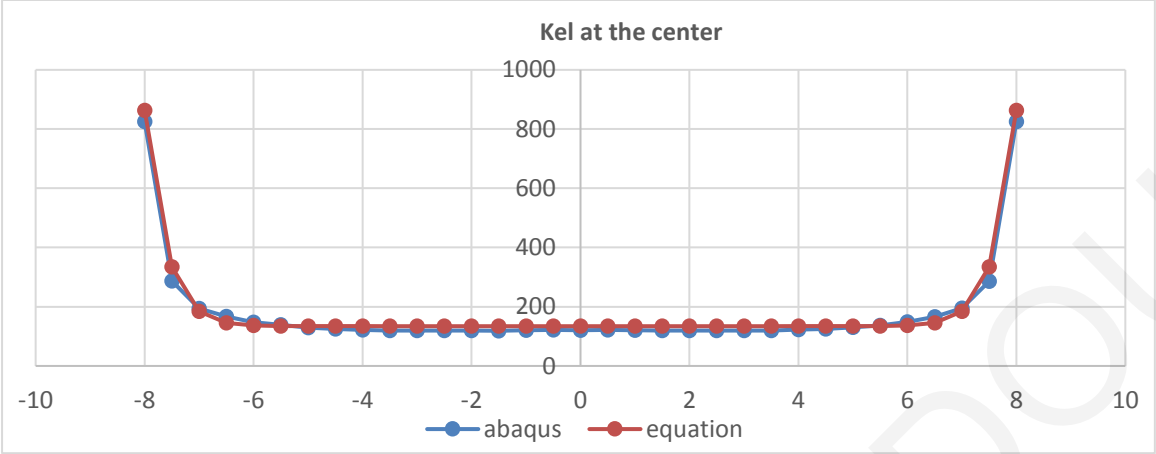

(a)

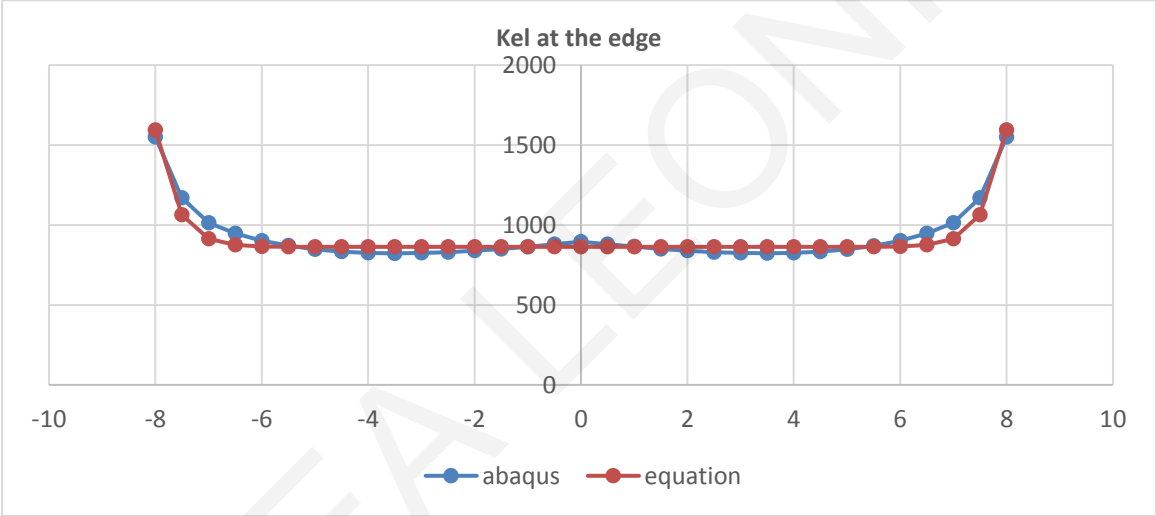

(b)

Figure C12: Comparison of K_{el} from Abaqus and the proposed equation for analysis 12 at (a) the centerline and (b) the edge of the mat.

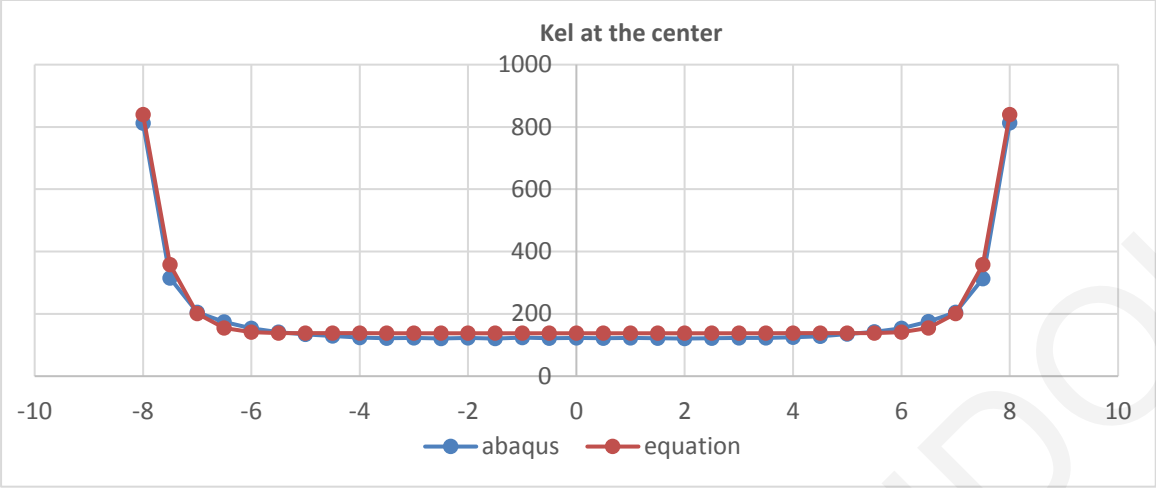

(a)

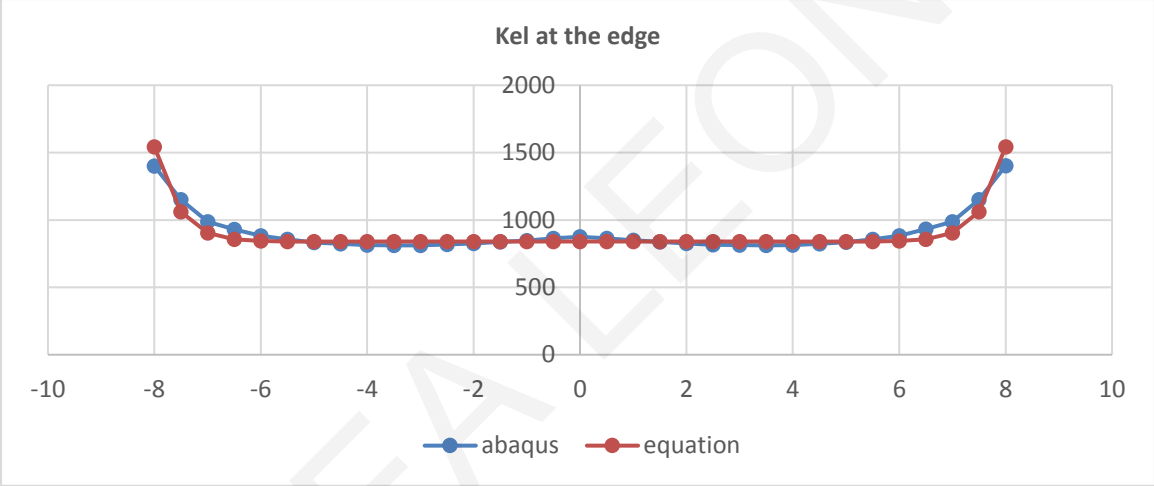

(b)

Figure C13: Comparison of K_{el} from Abaqus and the proposed equation for analysis 13 at (a) the centerline and (b) the edge of the mat.

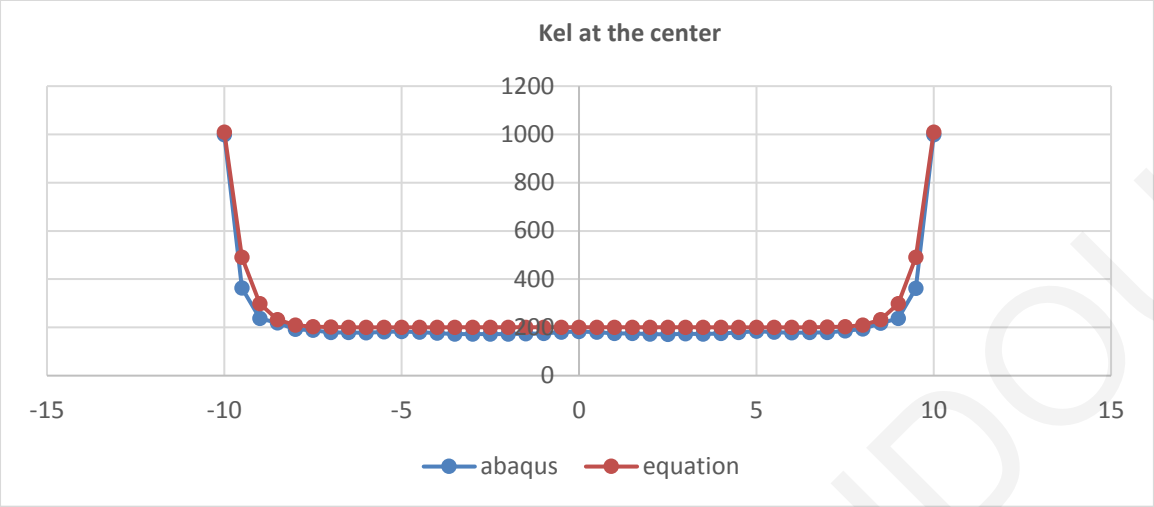

(a)

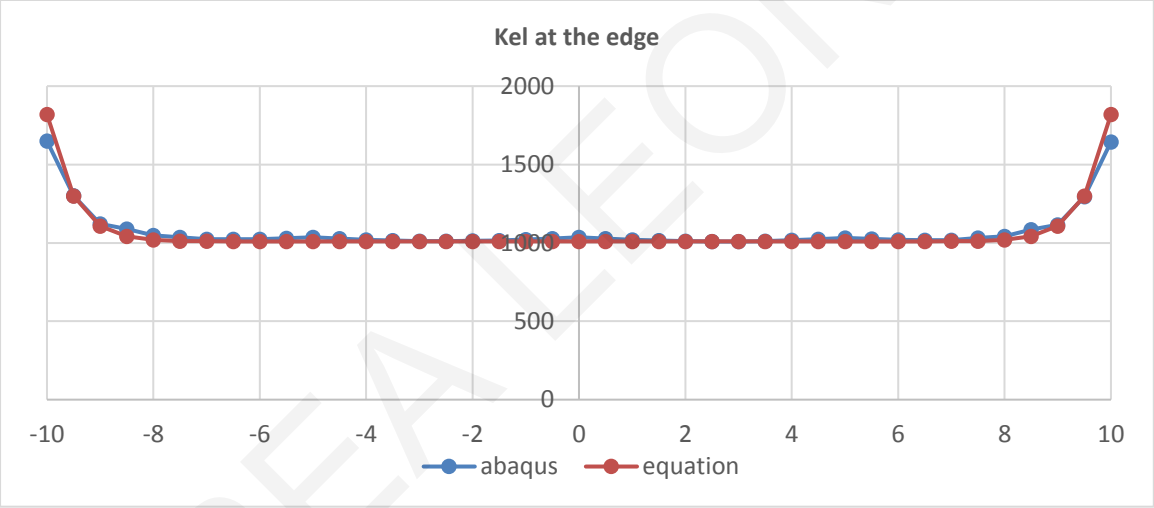

(b)

Figure C14: Comparison of K_{el} from Abaqus and the proposed equation for analysis 14 at (a) the centerline and (b) the edge of the mat.

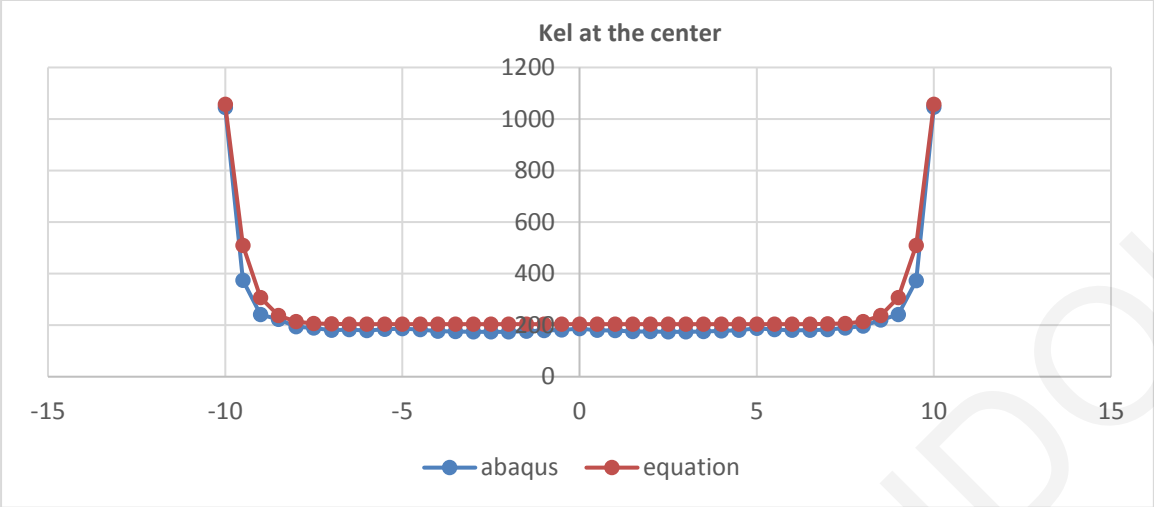

(a)

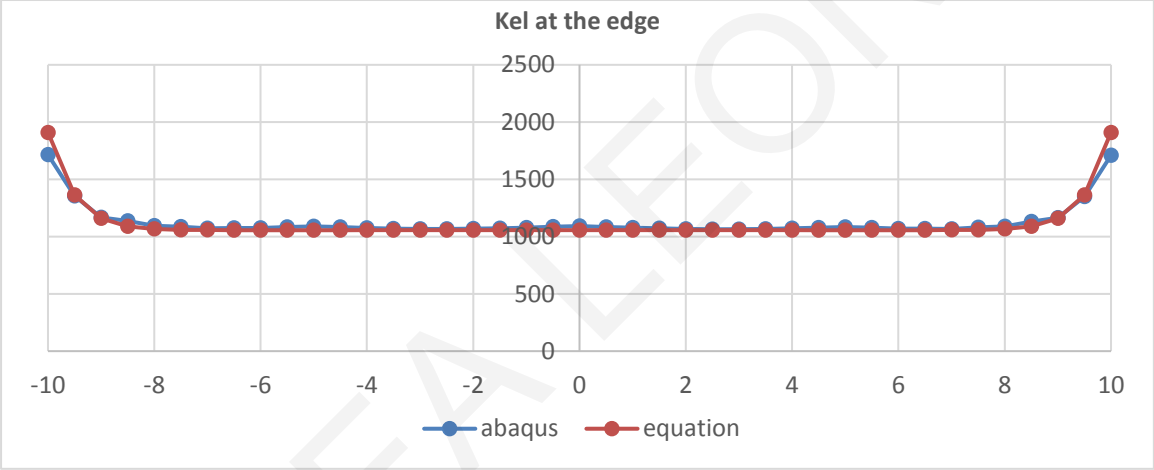

(b)

Figure C15: Comparison of K_{el} from Abaqus and the proposed equation for analysis 15 at (a) the centerline and (b) the edge of the mat.

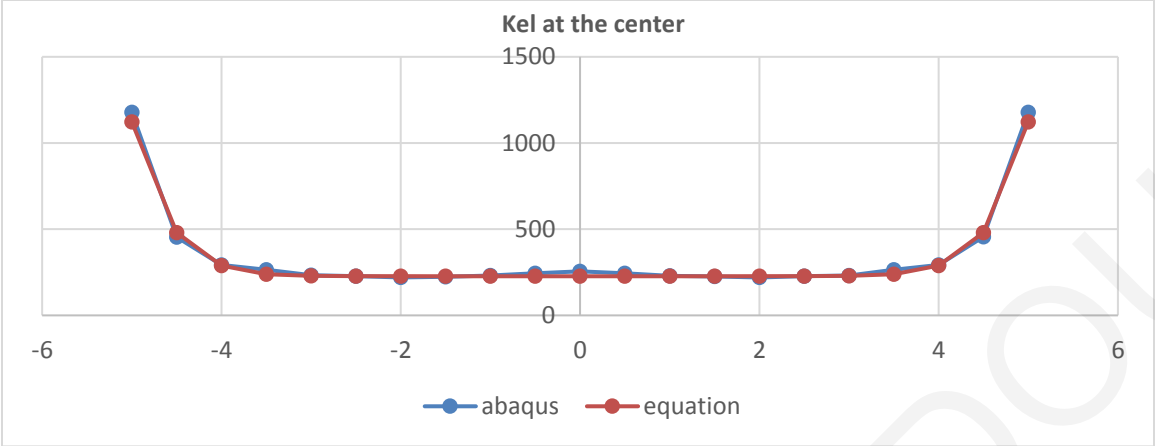

(a)

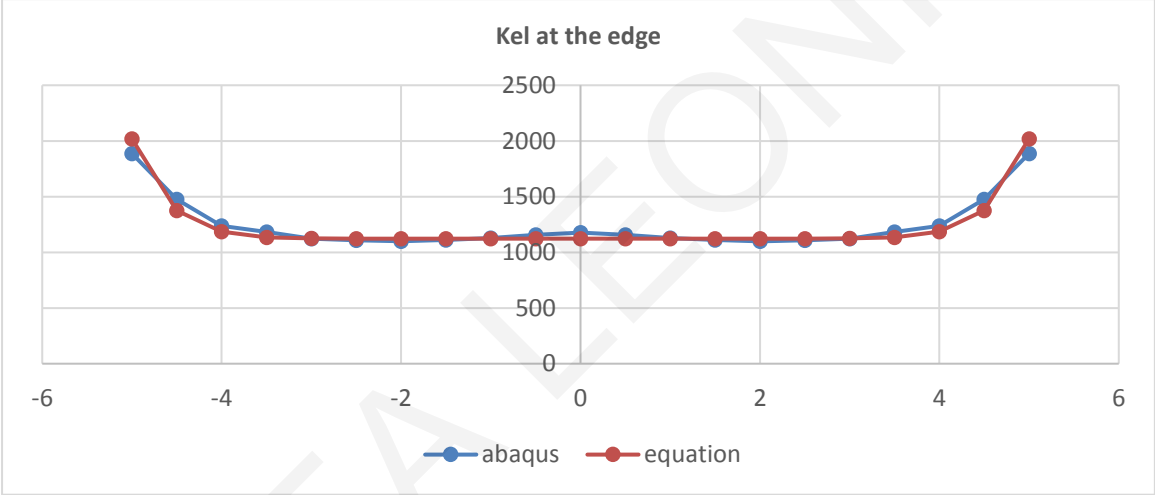

(b)

Figure C16: Comparison of K_{el} from Abaqus and the proposed equation for analysis 16 at (a) the centerline and (b) the edge of the mat.

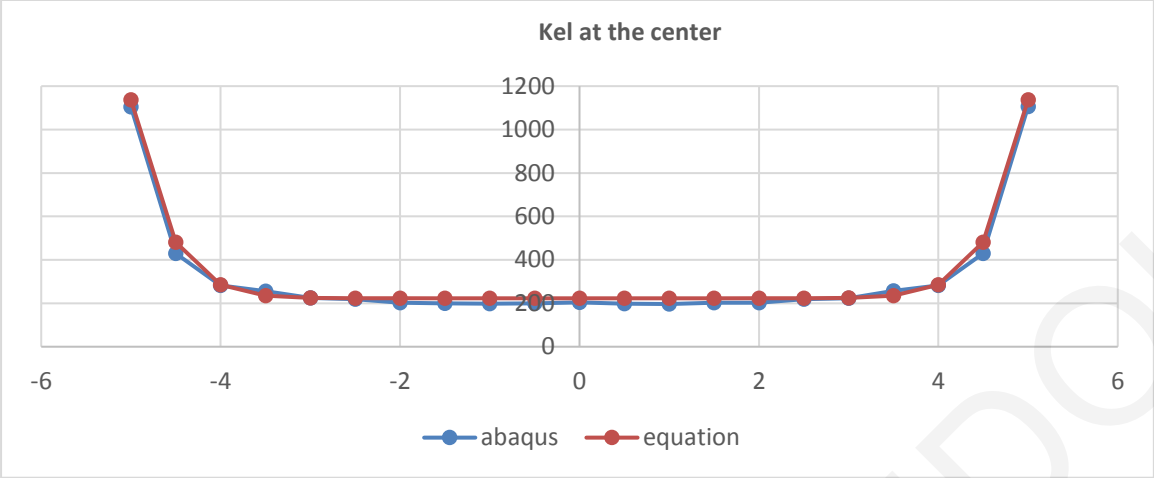

(a)

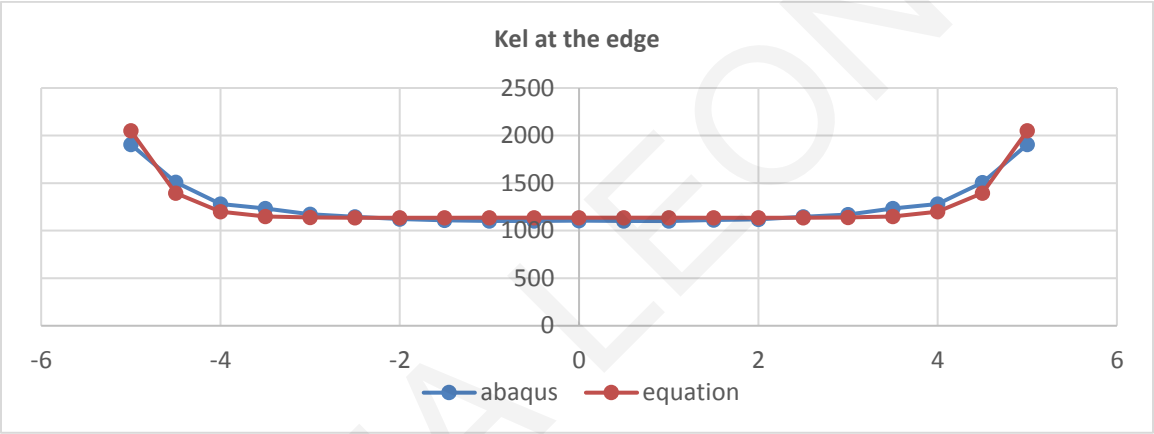

(b)

Figure C17: Comparison of K_{el} from Abaqus and the proposed equation for analysis 17 at (a) the centerline and (b) the edge of the mat.

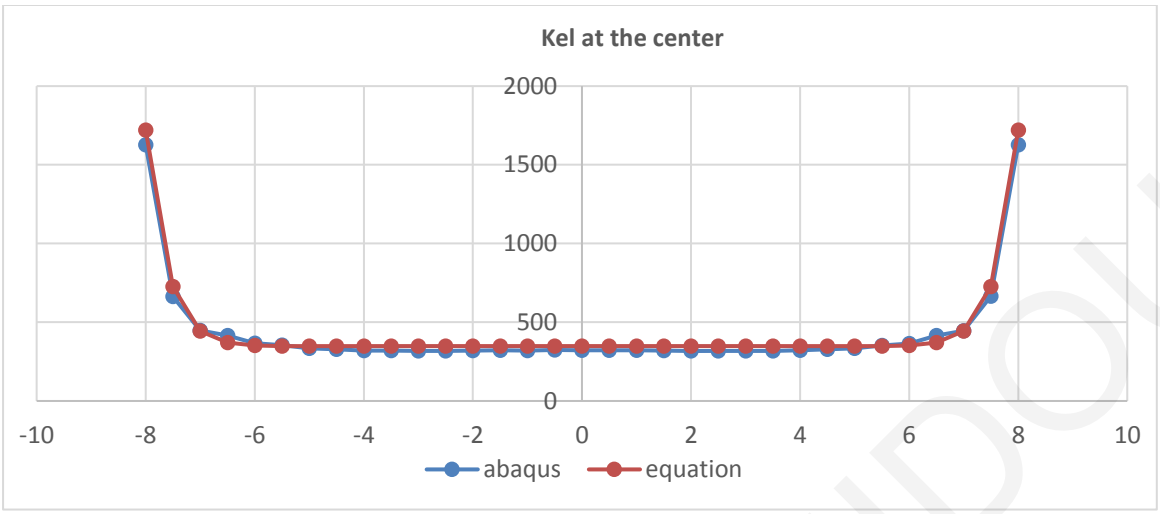

(a)

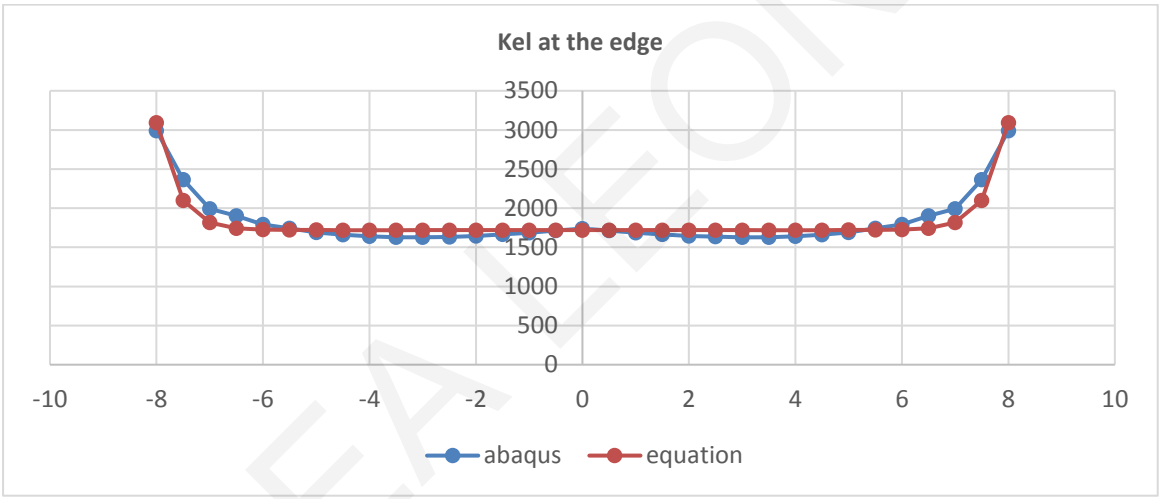

(b)

Figure C18: Comparison of K_{el} from Abaqus and the proposed equation for analysis 18 at (a) the centerline and (b) the edge of the mat.

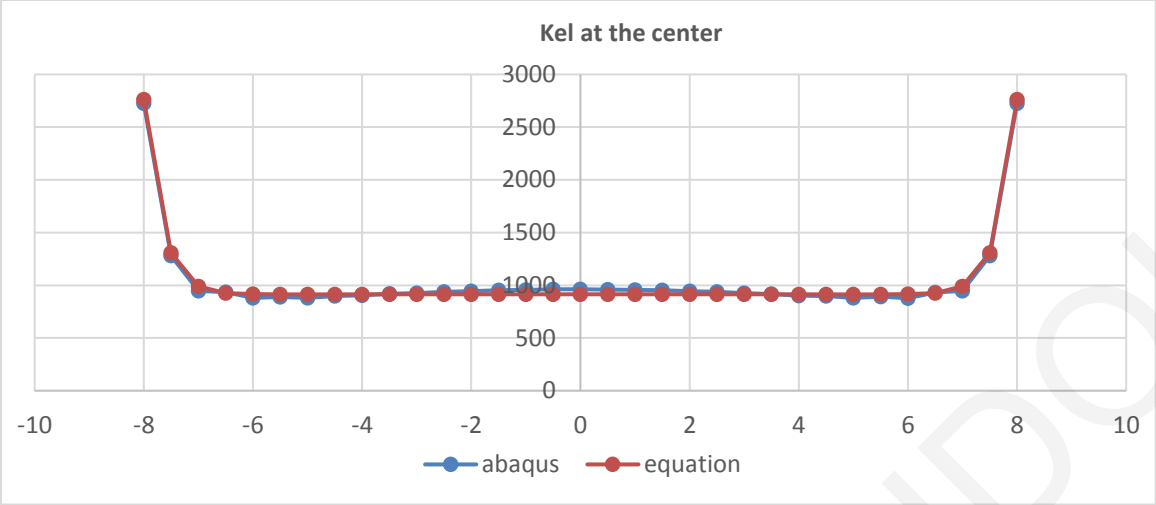

(a)

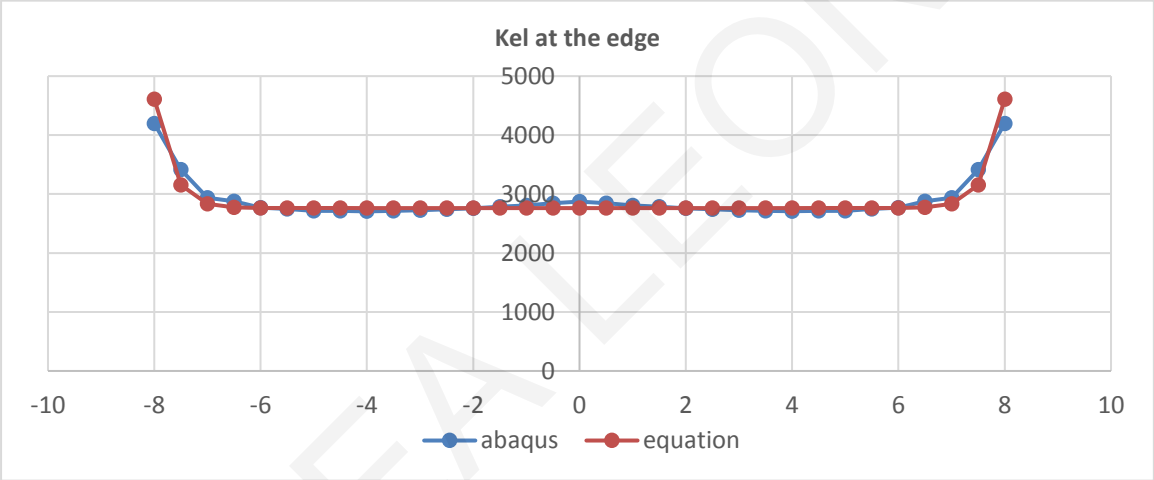

(b)

Figure C19: Comparison of K_{el} from Abaqus and the proposed equation for analysis 19 at (a) the centerline and (b) the edge of the mat.

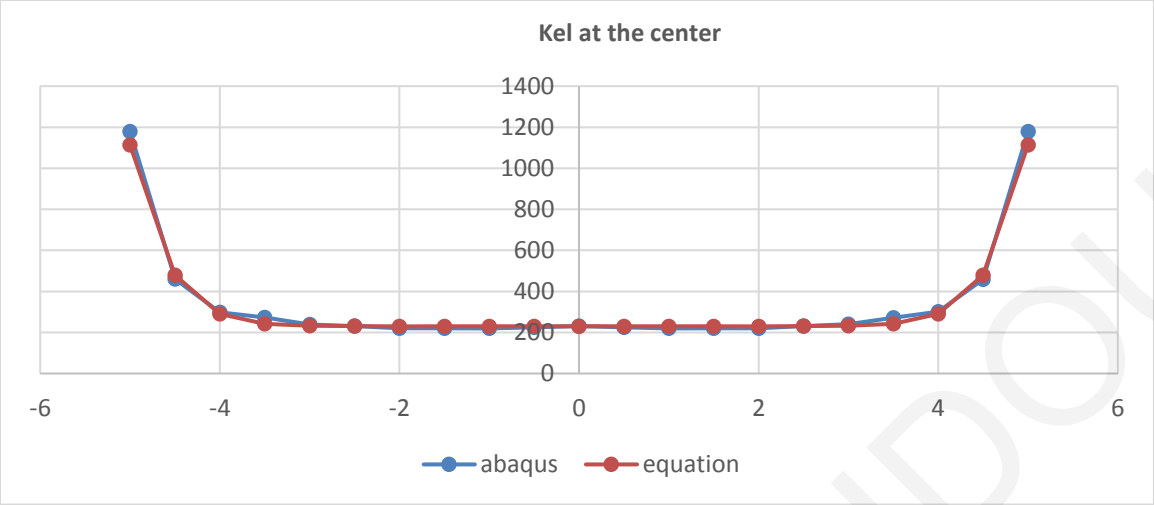

(a)

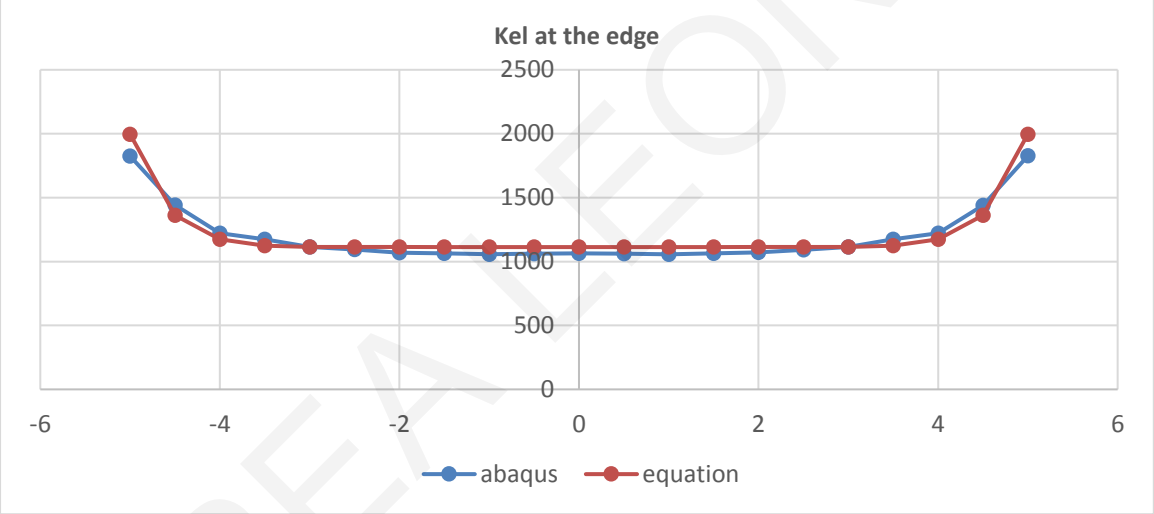

(b)

Figure C20: Comparison of K_{el} from Abaqus and the proposed equation for analysis 20 at (a) the centerline and (b) the edge of the mat.

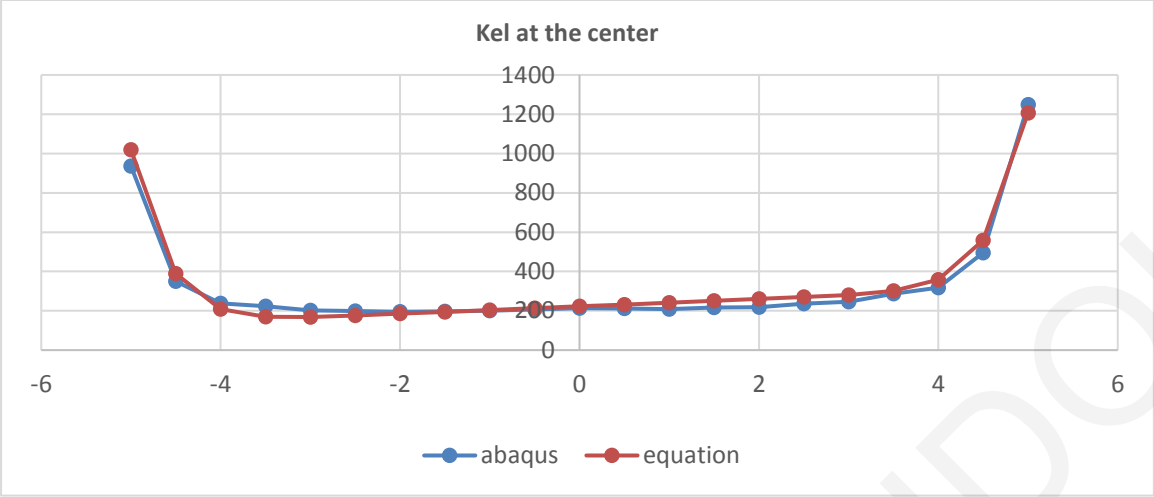

(a)

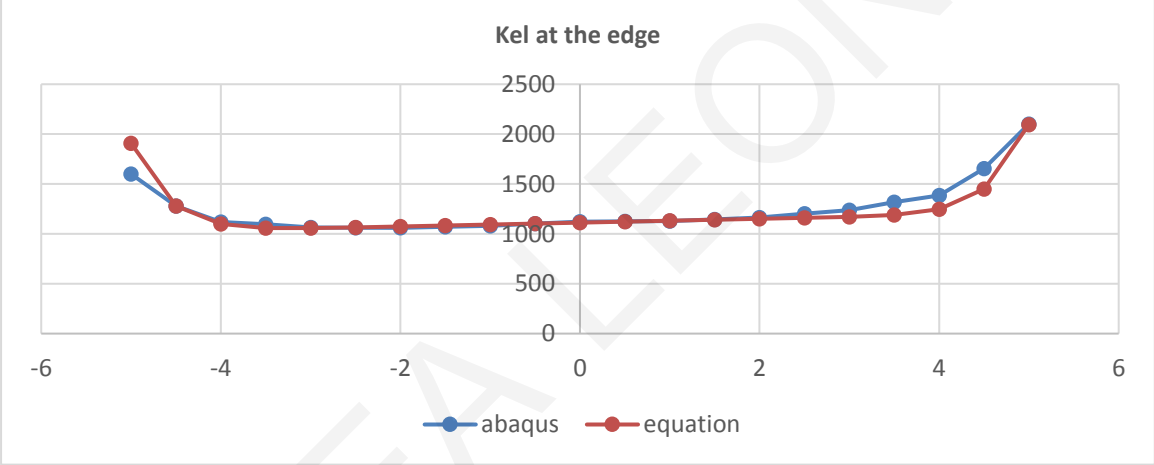

(b)

Figure C21: Comparison of K_{el} from Abaqus and the proposed equation for analysis 21 at (a) the centerline and (b) the edge of the mat.

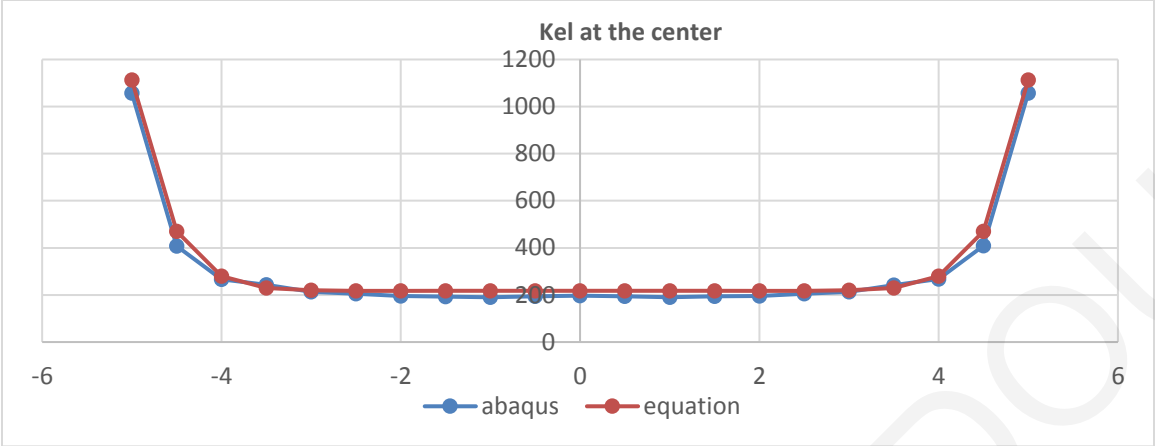

(a)

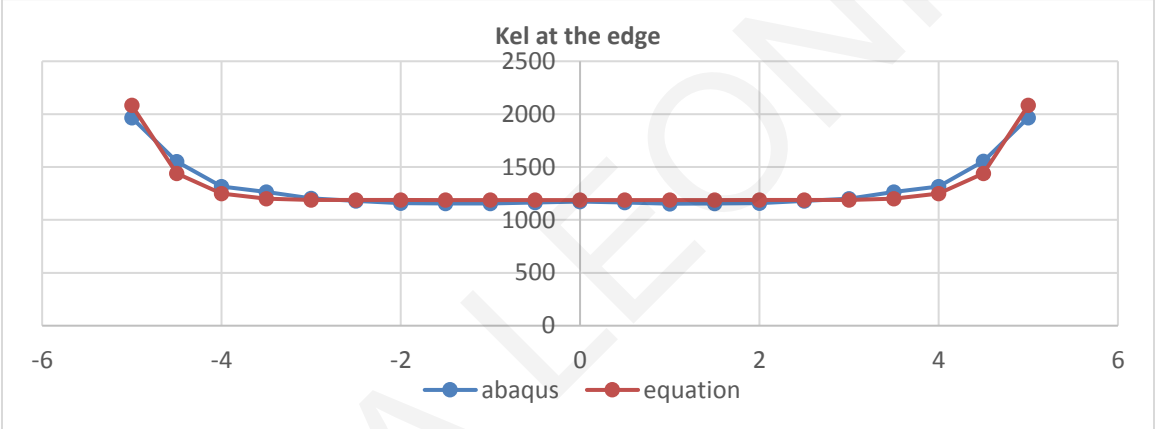

(b)

Figure C22: Comparison of K_{el} from Abaqus and the proposed equation for analysis 22 at (a) the centerline and (b) the edge of the mat.

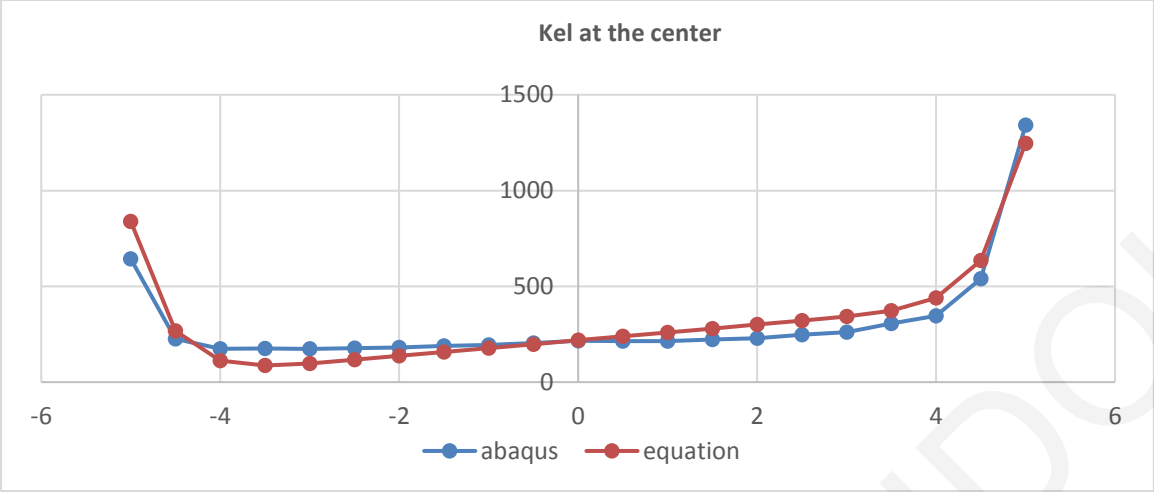

(a)

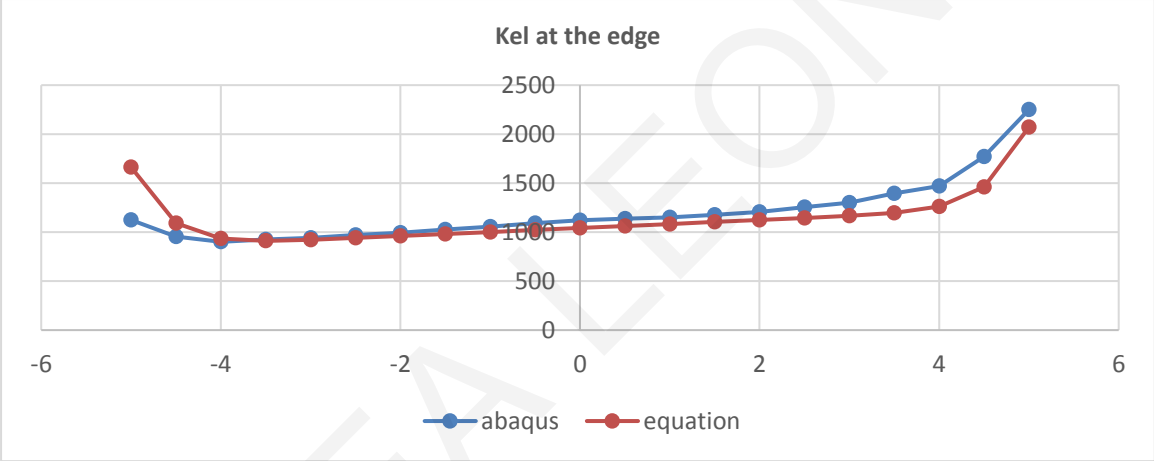

(b)

Figure C23: Comparison of K_{el} from Abaqus and the proposed equation for analysis 23 at (a) the centerline and (b) the edge of the mat.

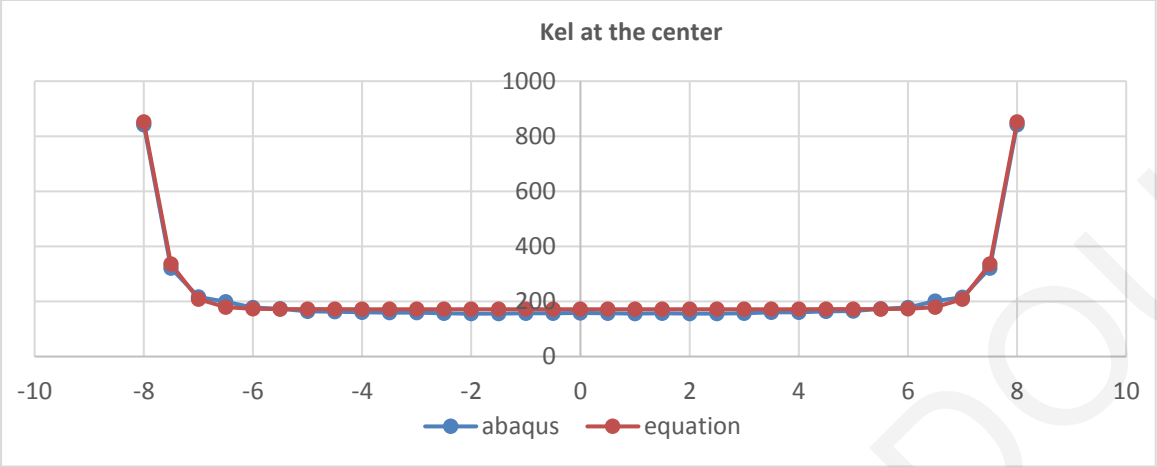

(a)

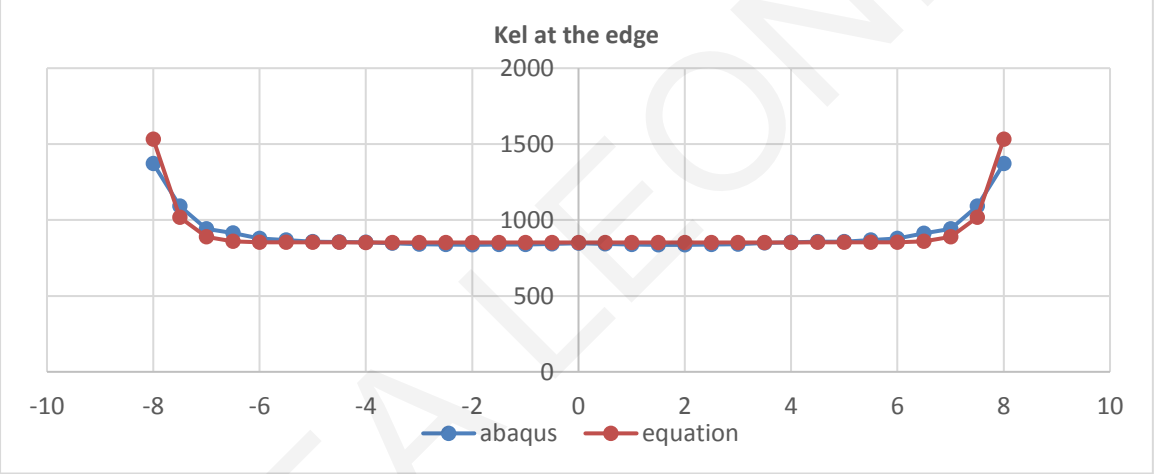

(b)

Figure C24: Comparison of K_{el} from Abaqus and the proposed equation for analysis 24 at (a) the centerline and (b) the edge of the mat.

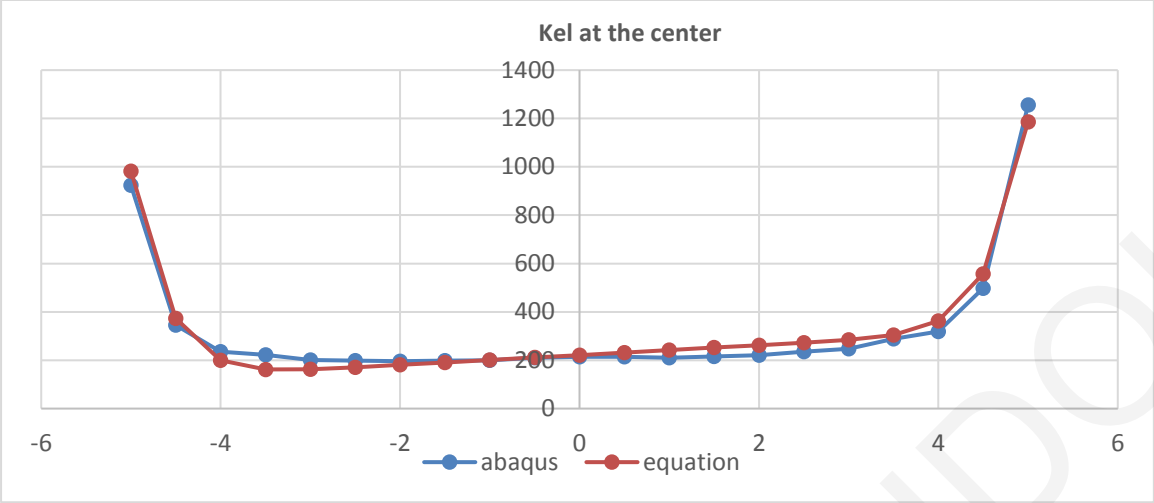

(a)

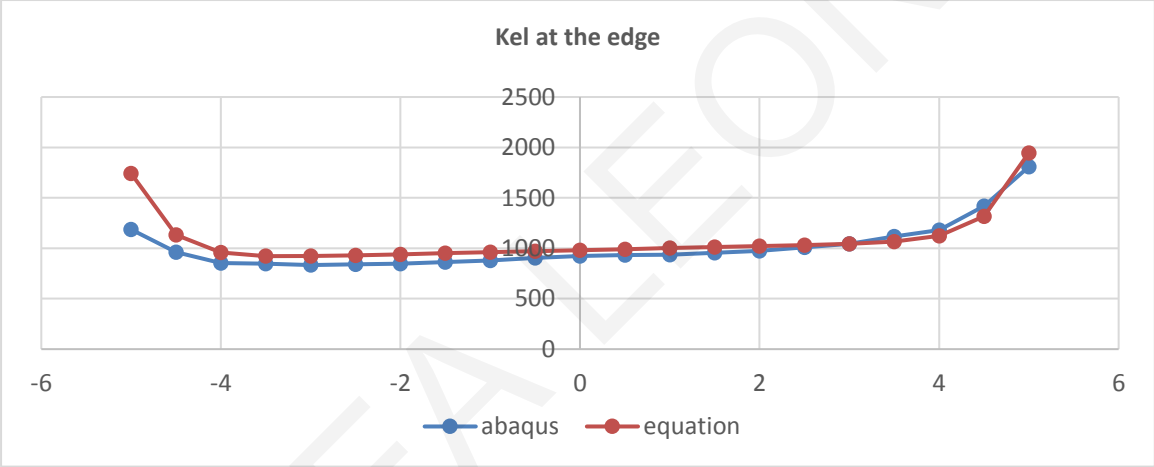

(b)

Figure C25: Comparison of K_{el} from Abaqus and the proposed equation for analysis 25 at (a) the centerline and (b) the edge of the mat.

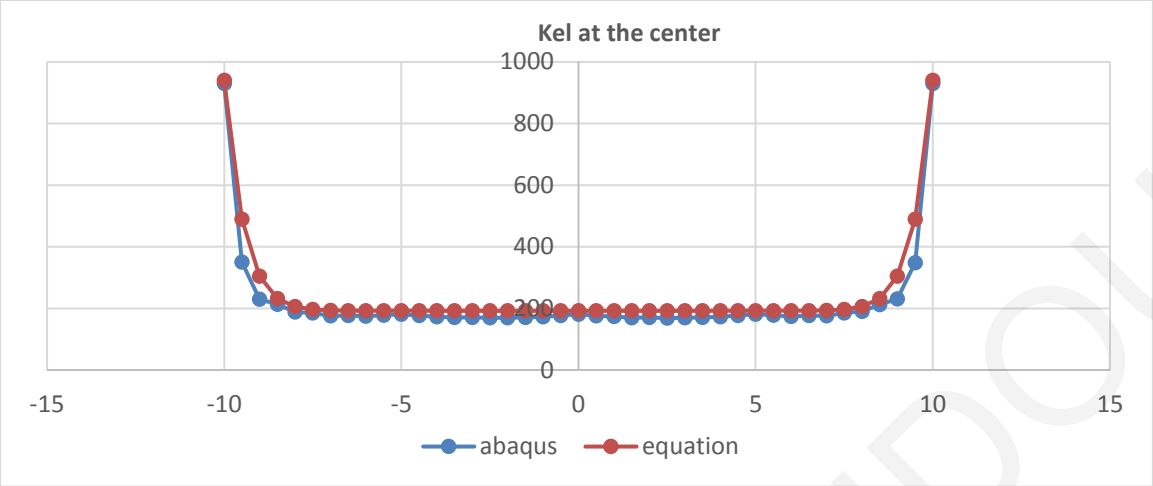

(a)

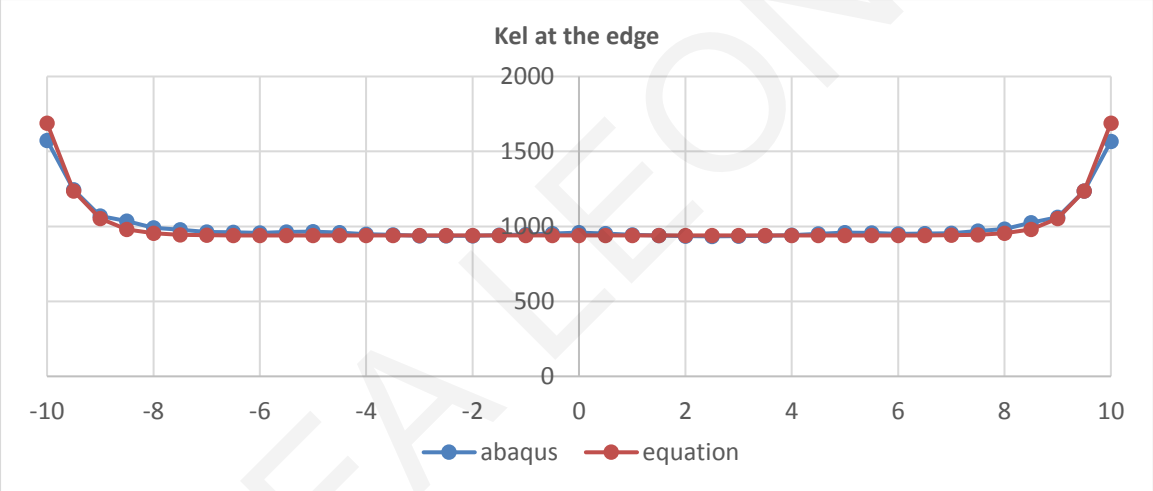

(b)

Figure C26: Comparison of K_{el} from Abaqus and the proposed equation for analysis 26 at (a) the centerline and (b) the edge of the mat.

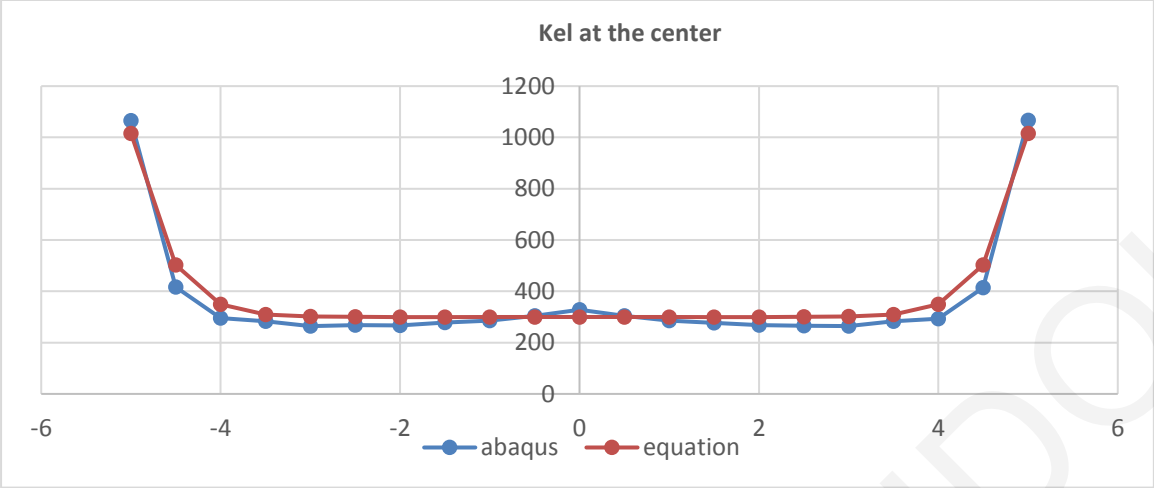

(a)

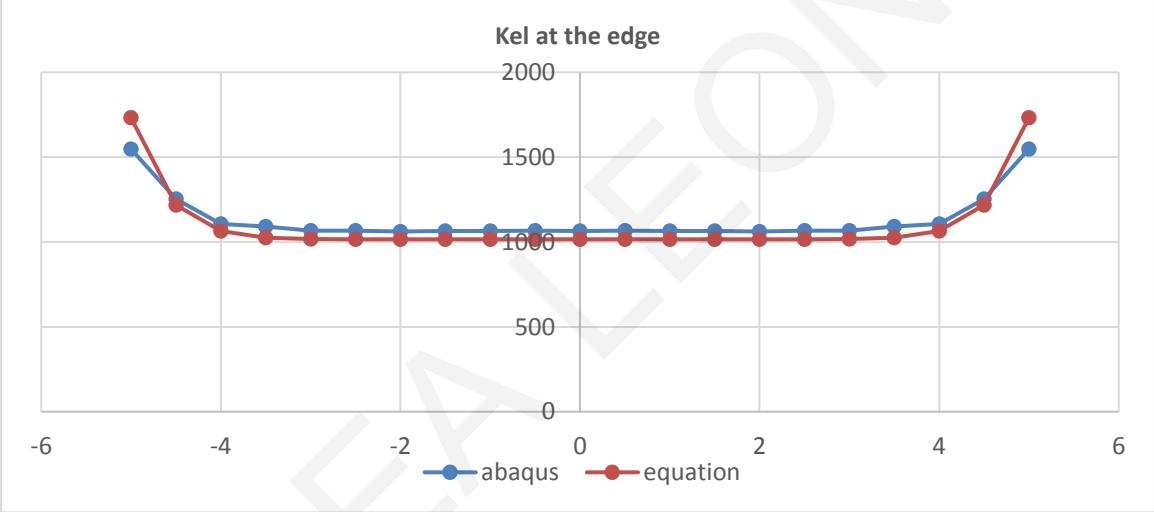

(b)

Figure C27: Comparison of K_{el} from Abaqus and the proposed equation for analysis 27 at (a) the centerline and (b) the edge of the mat.

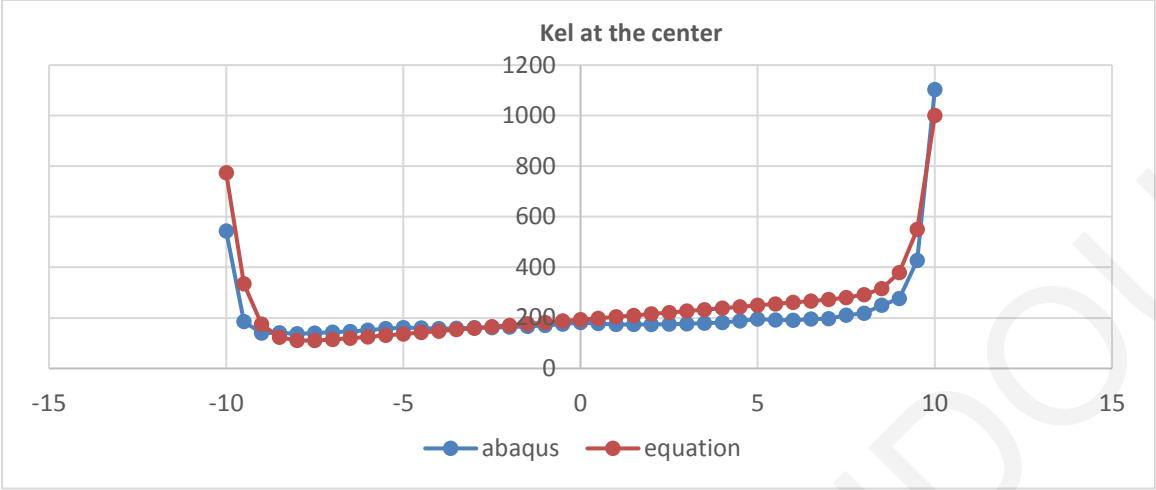

(a)

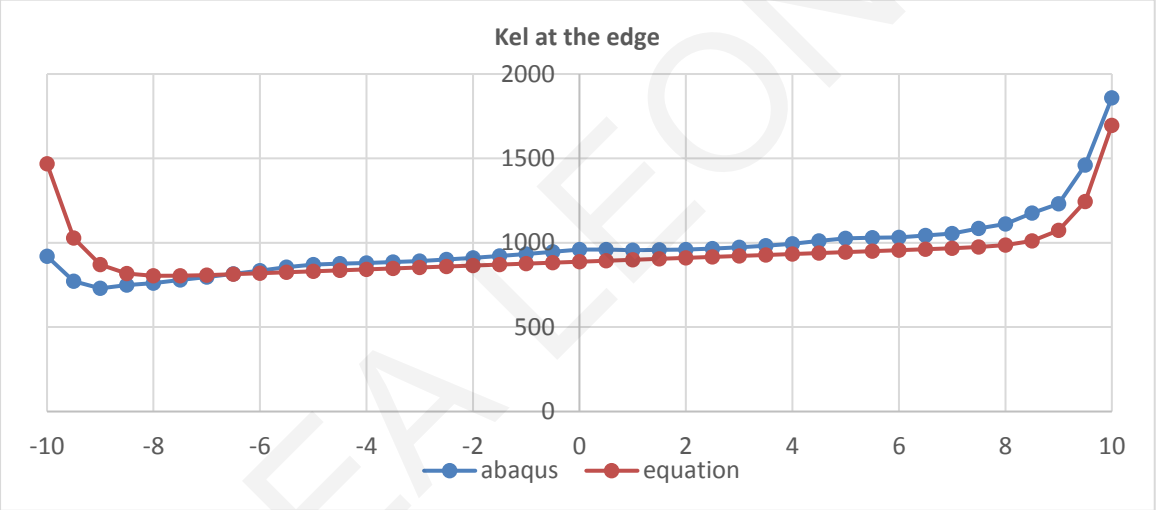

(b)

Figure C28: Comparison of K_{el} from Abaqus and the proposed equation for analysis 28 at (a) the centerline and (b) the edge of the mat.

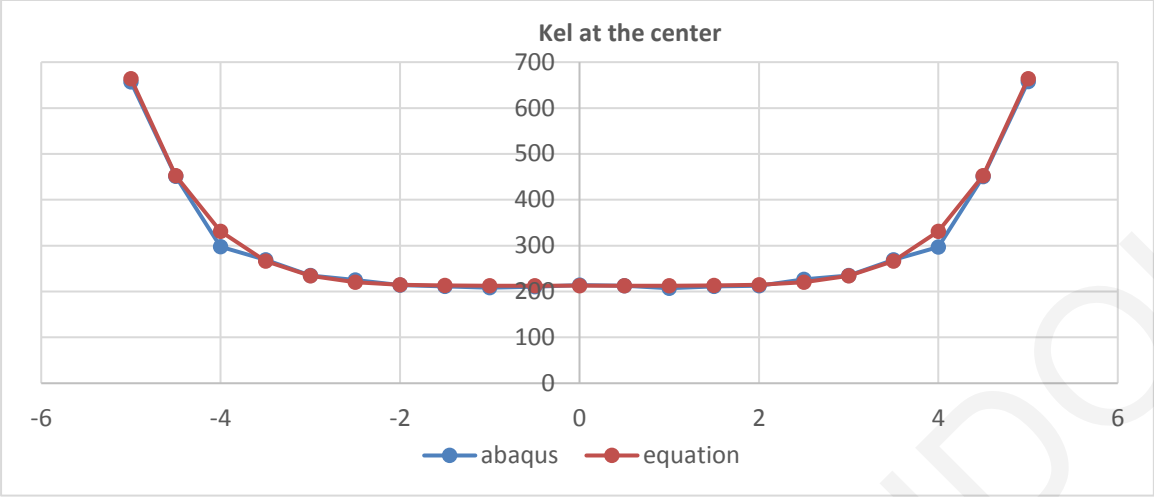

(a)

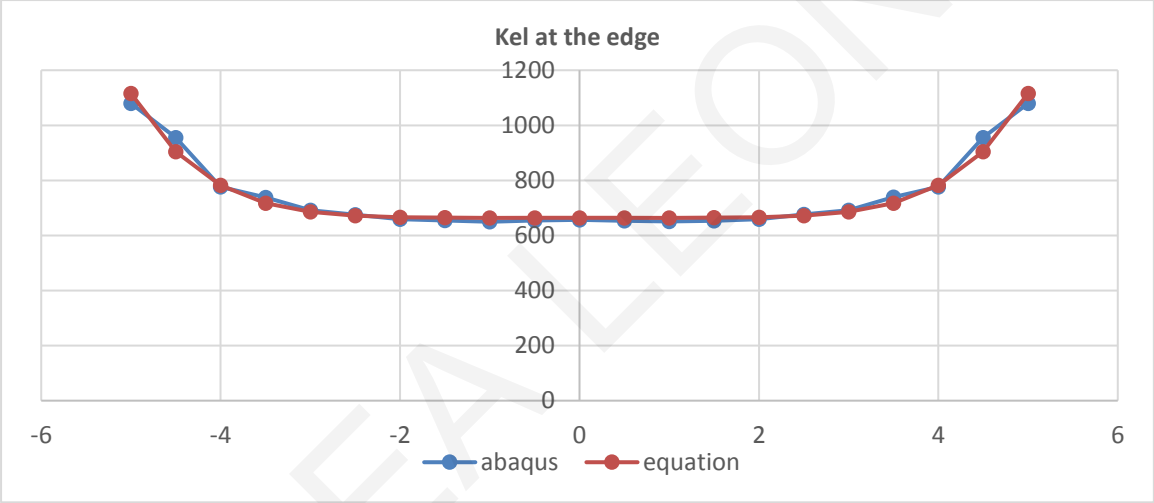

(b)

Figure C29: Comparison of K_{el} from Abaqus and the proposed equation for analysis 29 at (a) the centerline and (b) the edge of the mat.

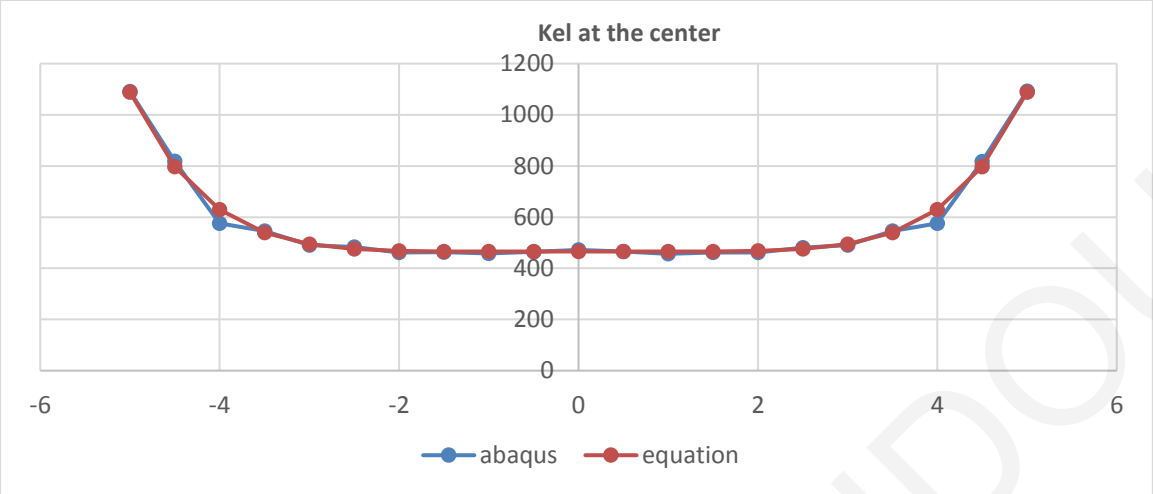

(a)

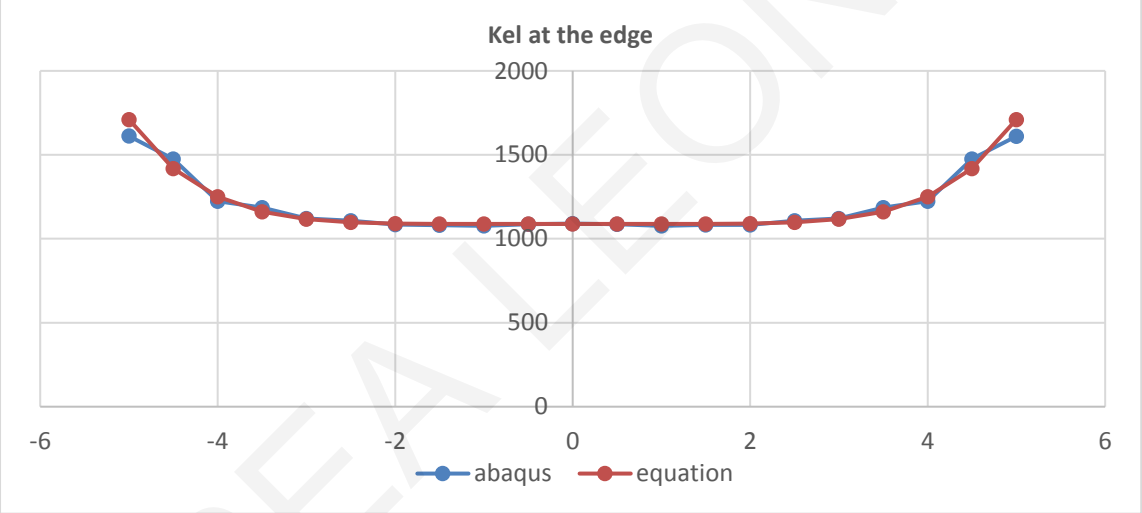

(b)

Figure C30: Comparison of K_{el} from Abaqus and the proposed equation for analysis 30 at (a) the centerline and (b) the edge of the mat.

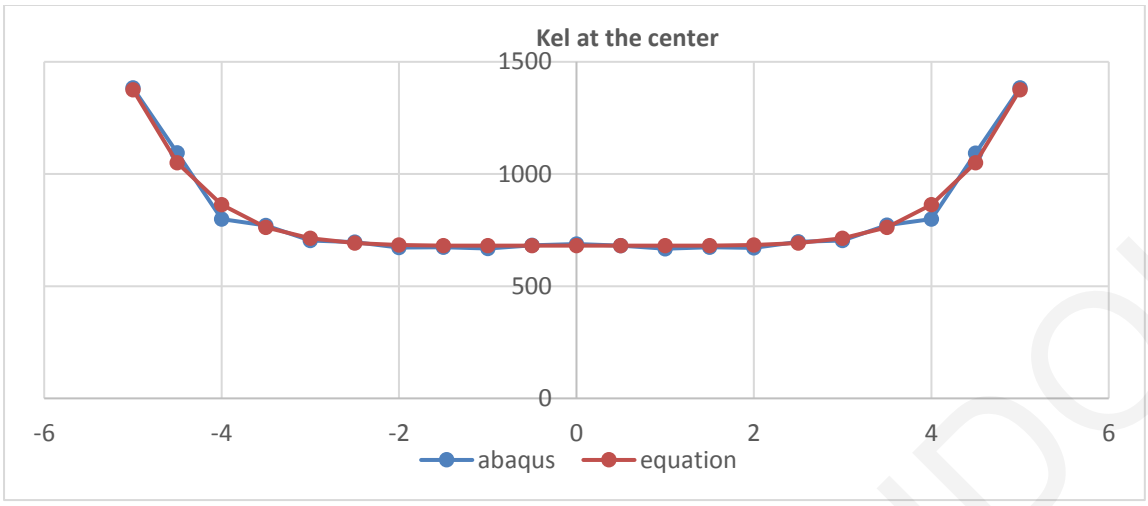

(a)

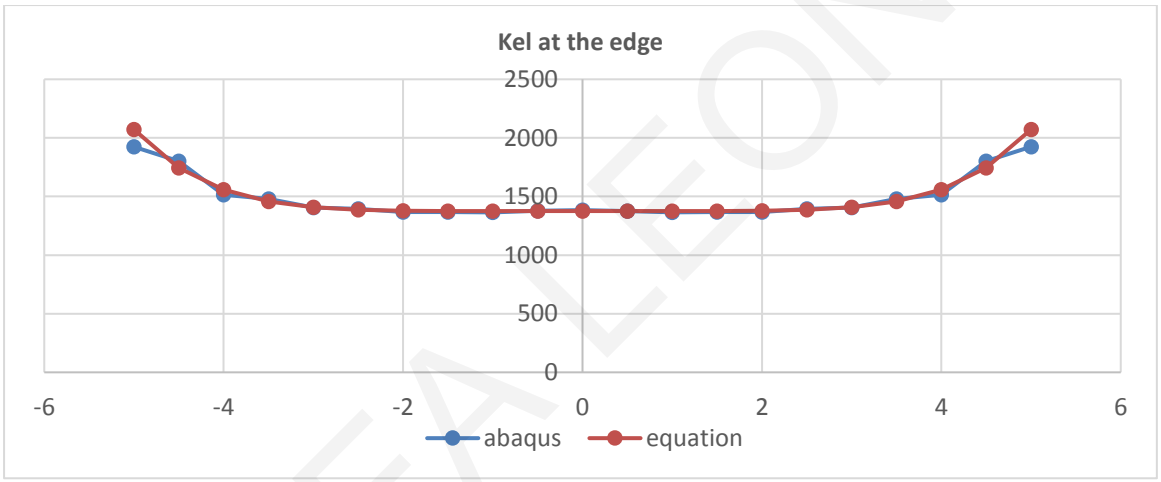

(b)

Figure C31: Comparison of K_{el} from Abaqus and the proposed equation for analysis 31 at (a) the centerline and (b) the edge of the mat.

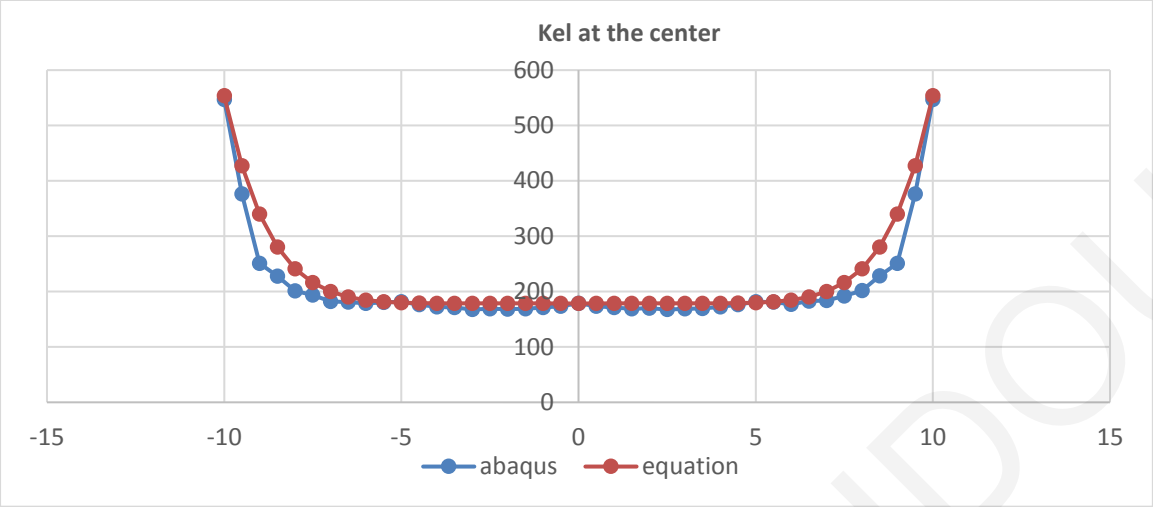

(a)

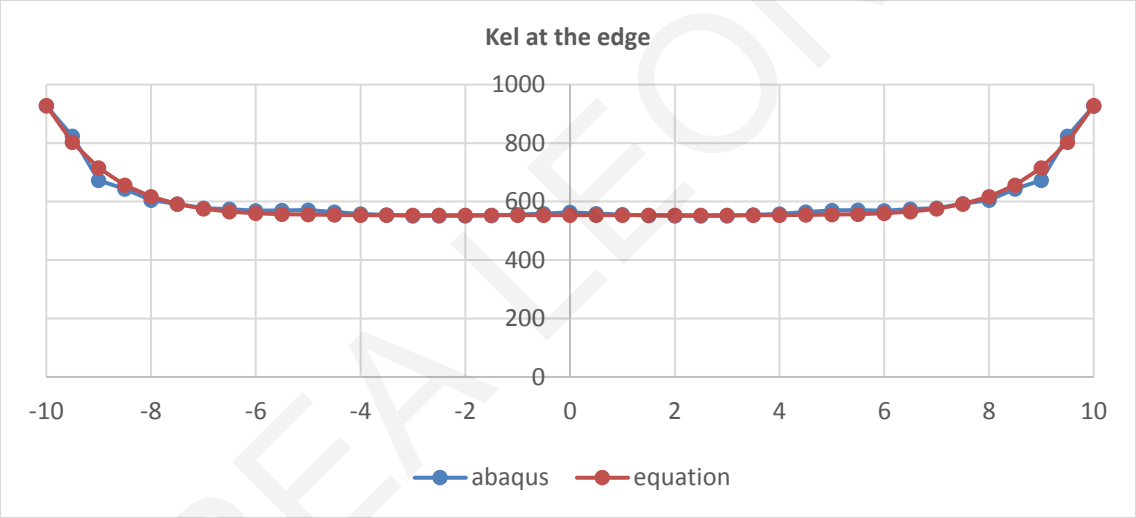

(b)

Figure C32: Comparison of K_{el} from Abaqus and the proposed equation for analysis 32 at (a) the centerline and (b) the edge of the mat.

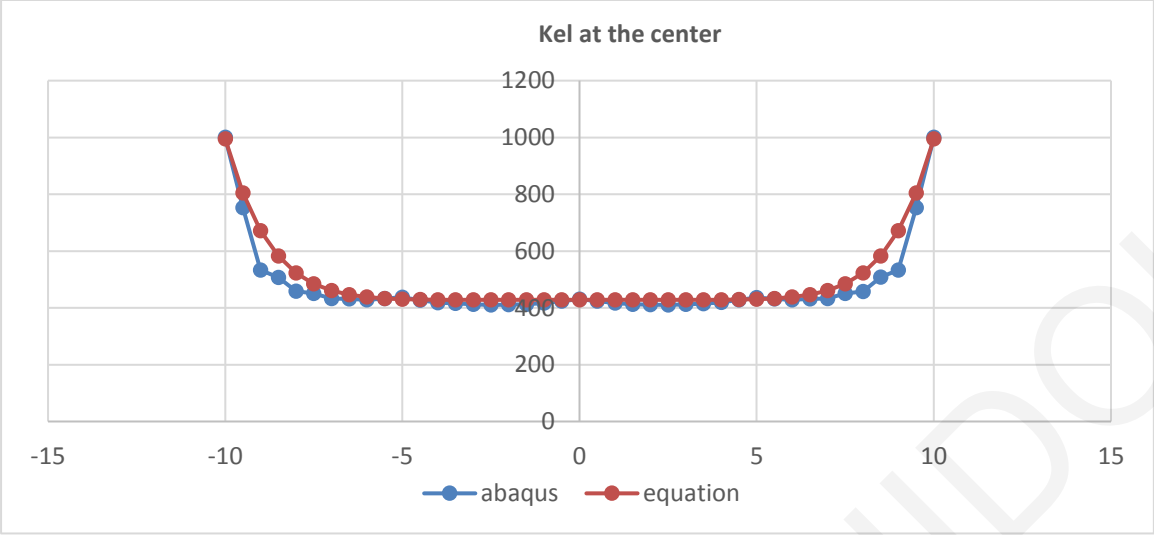

(a)

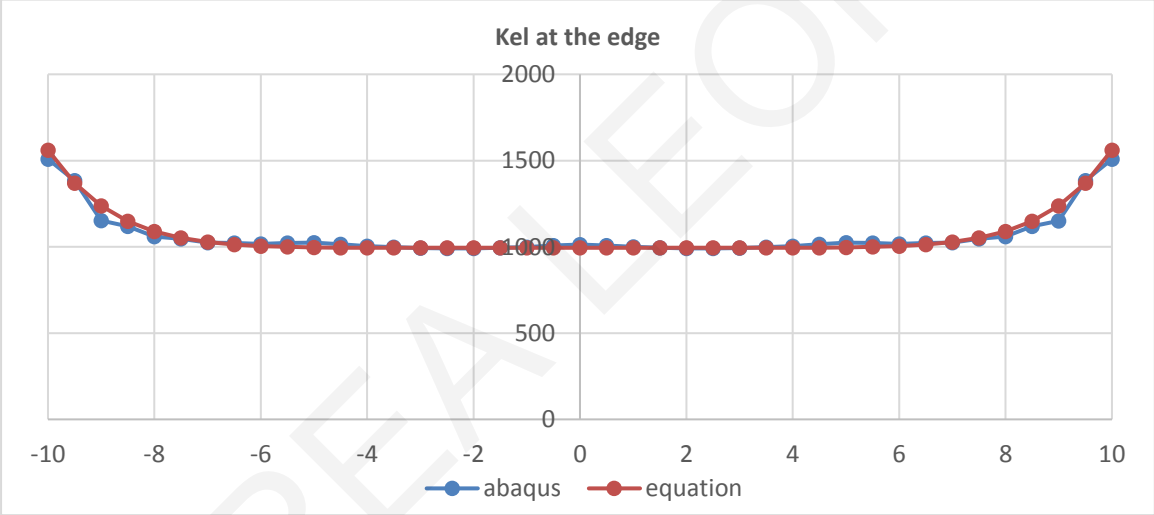

(b)

Figure C33: Comparison of K_{el} from Abaqus and the proposed equation for analysis 33 at (a) the centerline and (b) the edge of the mat.

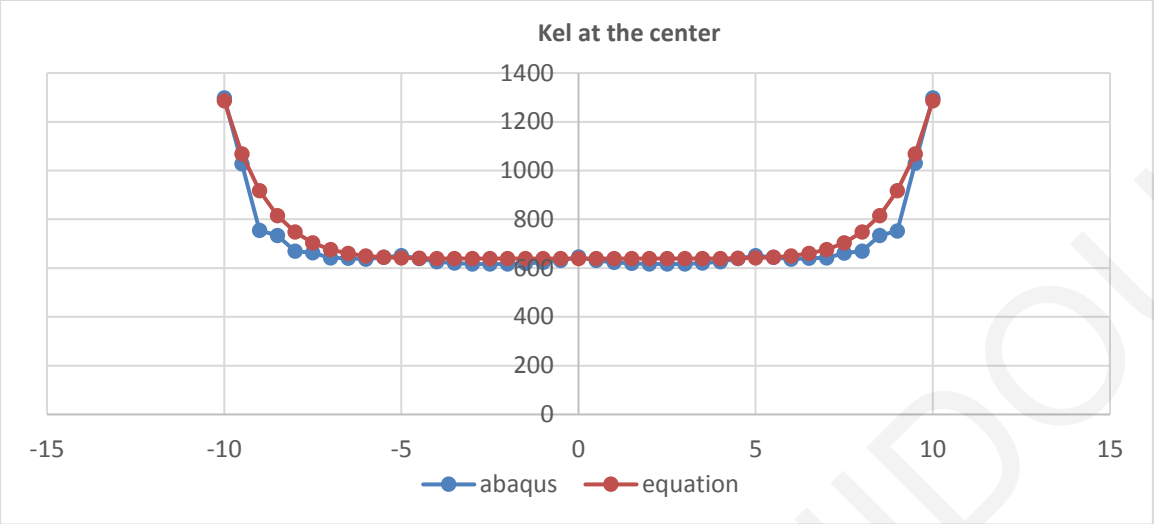

(a)

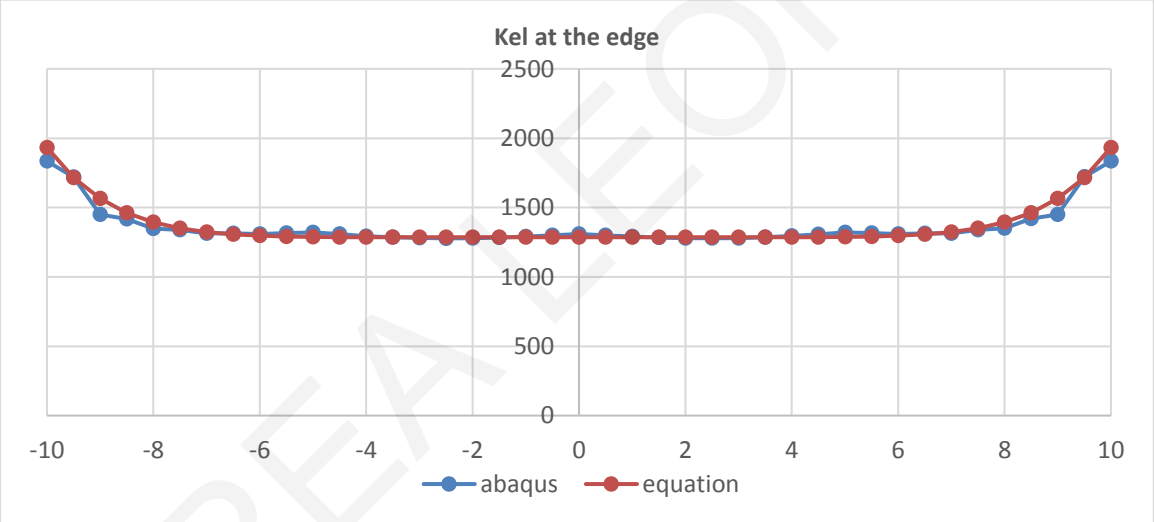

(b)

Figure C34: Comparison of K_{el} from Abaqus and the proposed equation for analysis 34 at (a) the centerline and (b) the edge of the mat.

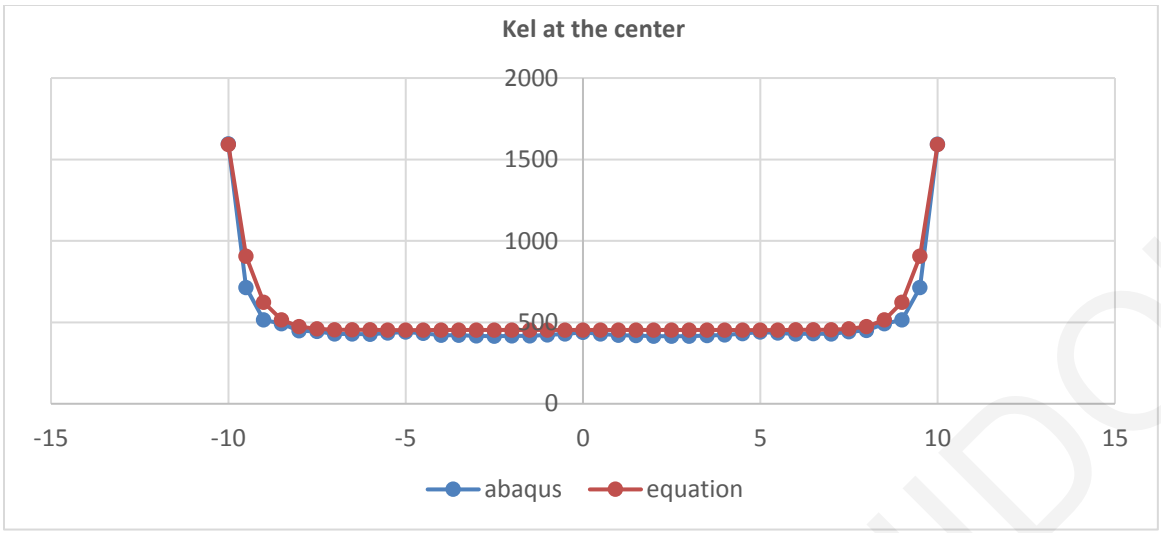

(a)

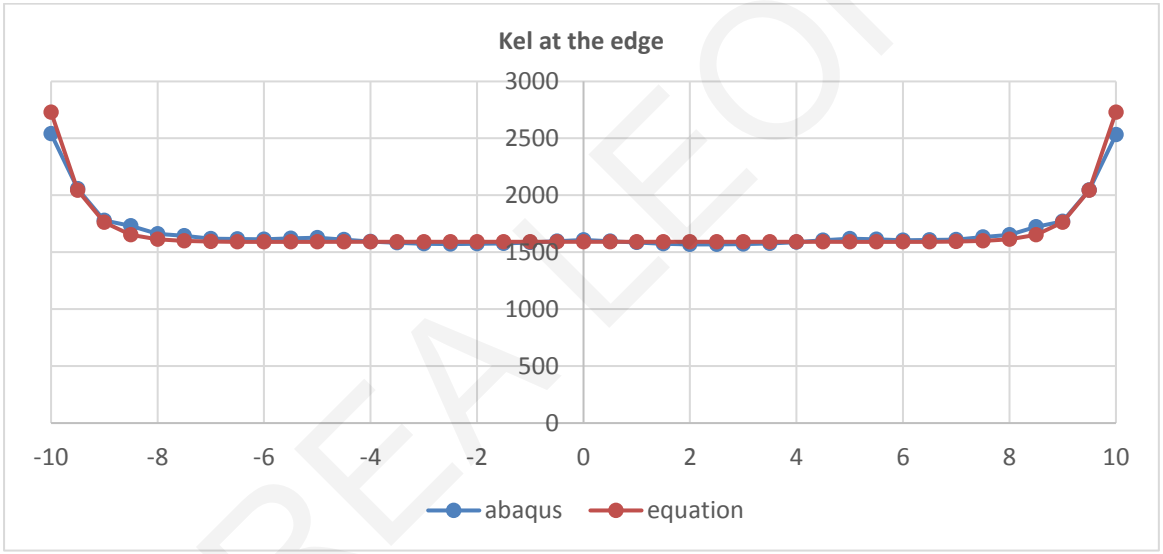

(b)

Figure C35: Comparison of K_{el} from Abaqus and the proposed equation for analysis 35 at (a) the centerline and (b) the edge of the mat.

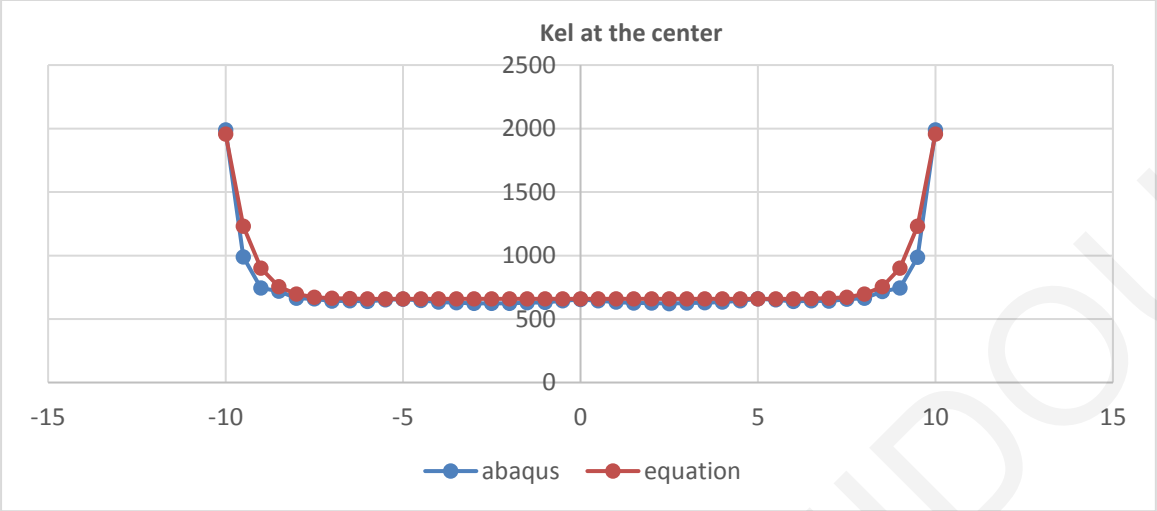

(a)

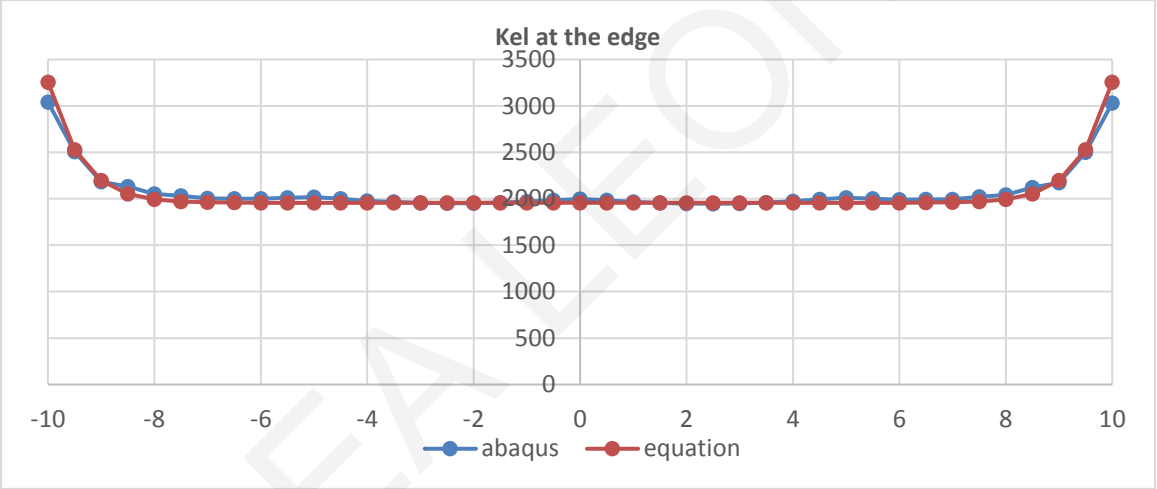

(b)

Figure C36: Comparison of K_{el} from Abaqus and the proposed equation for analysis 36 at (a) the centerline and (b) the edge of the mat.

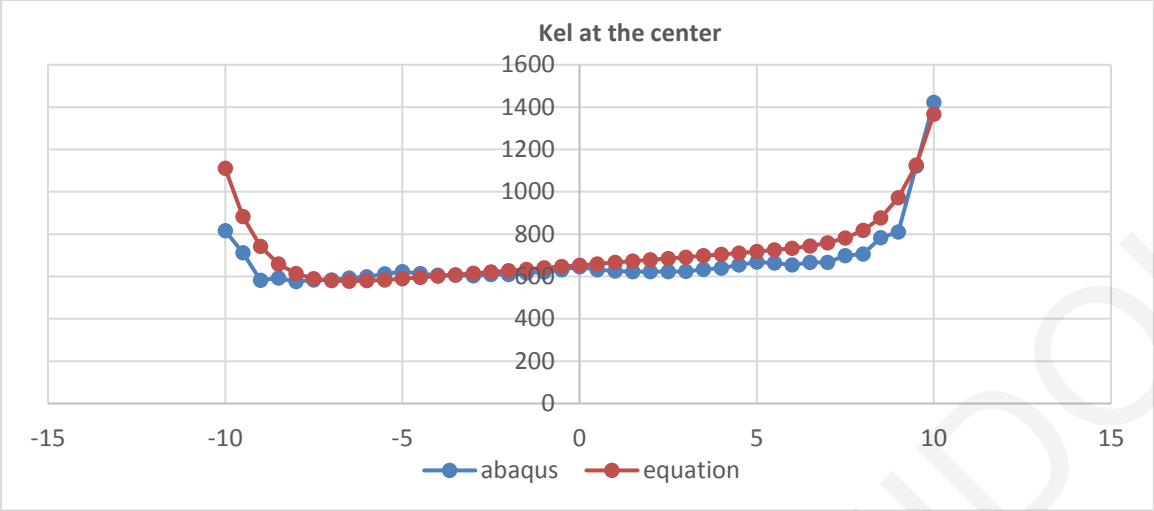

(a)

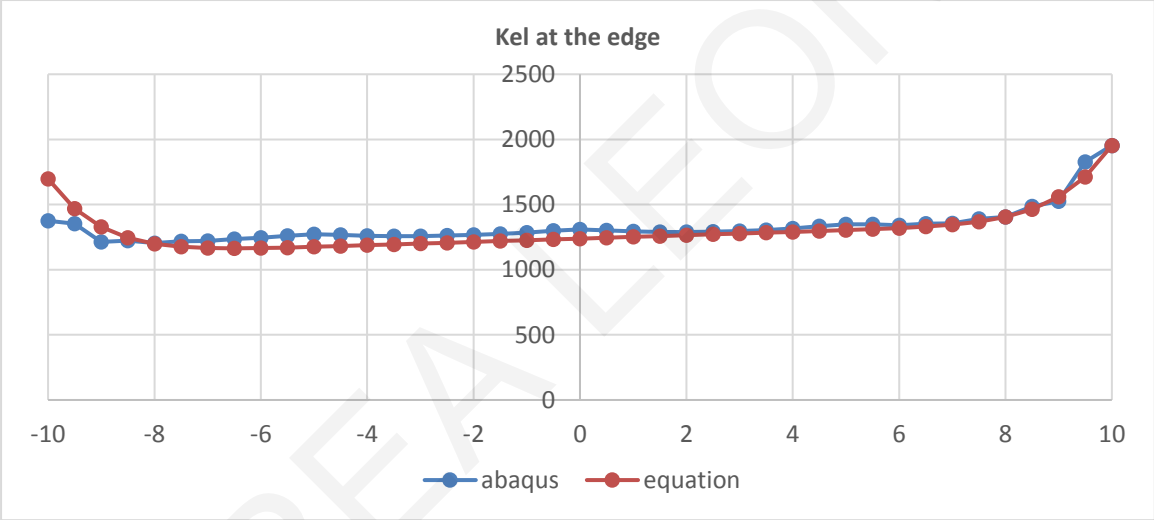

(b)

Figure C37: Comparison of K_{el} from Abaqus and the proposed equation for analysis 37 at (a) the centerline and (b) the edge of the mat.

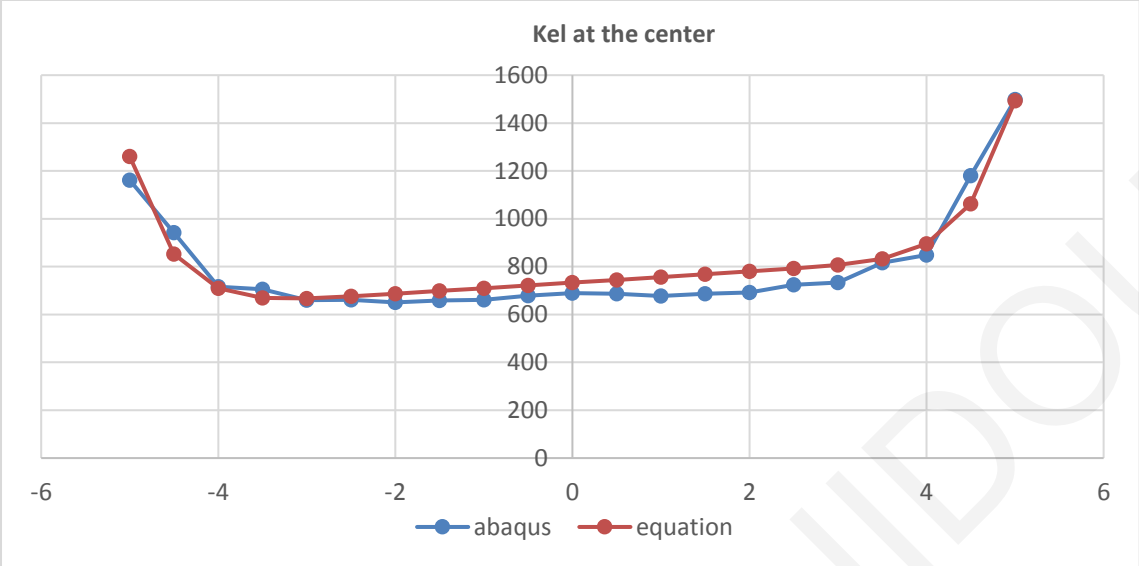

(a)

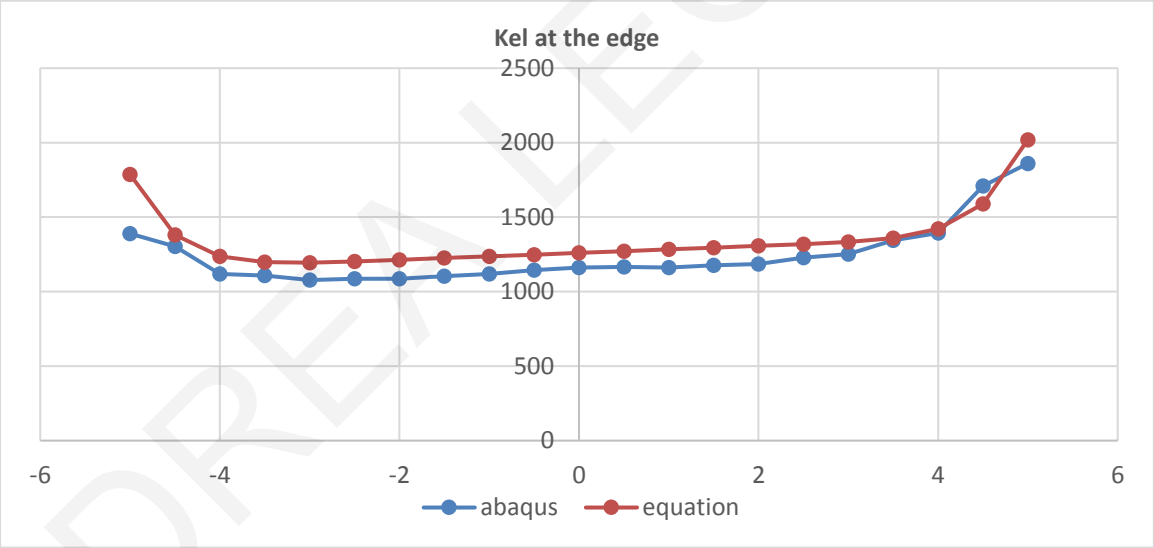

(b)

Figure C38: Comparison of K_{el} from Abaqus and the proposed equation for analysis 38 at (a) the centerline and (b) the edge of the mat.

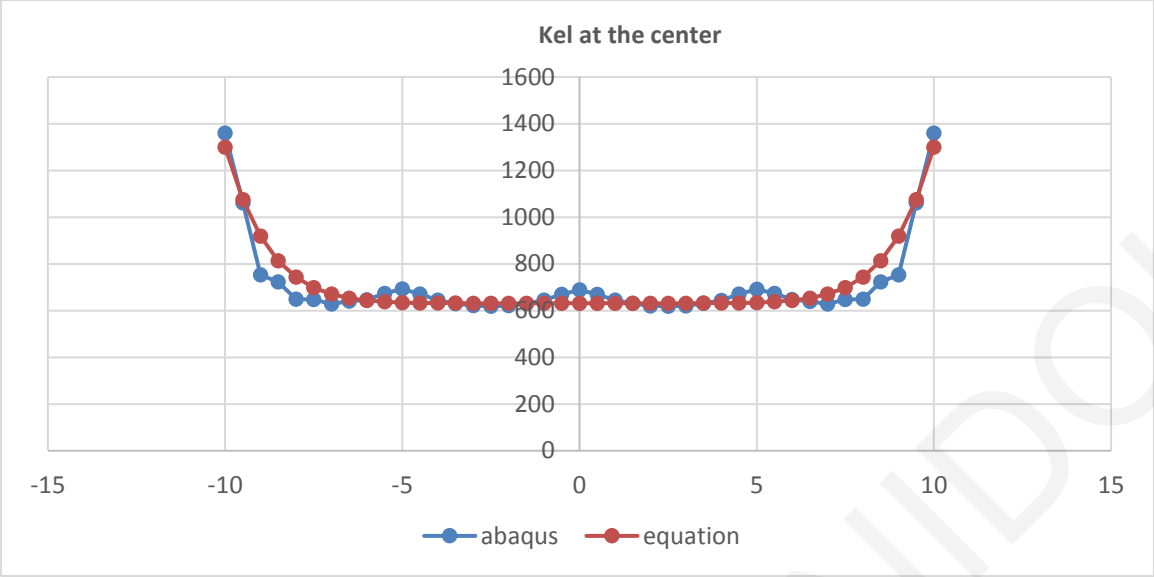

(a)

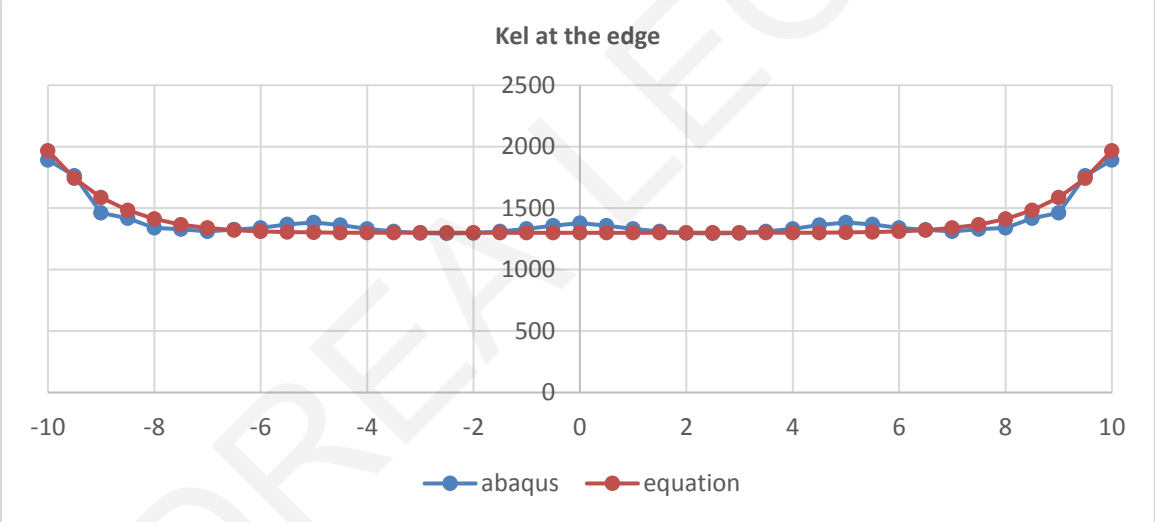

(b)

Figure C39: Comparison of K_{el} from Abaqus and the proposed equation for analysis 39 at (a) the centerline and (b) the edge of the mat.

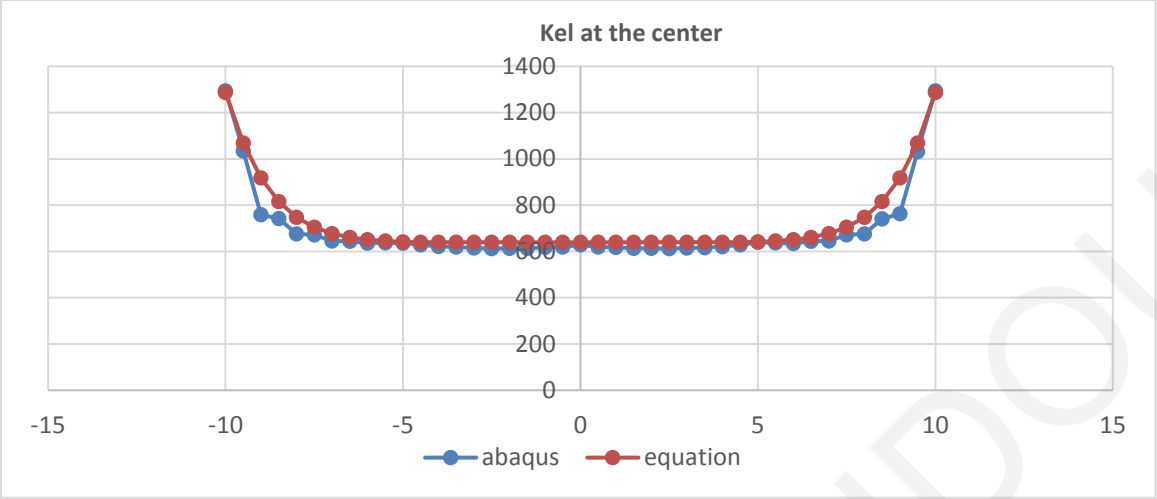

(a)

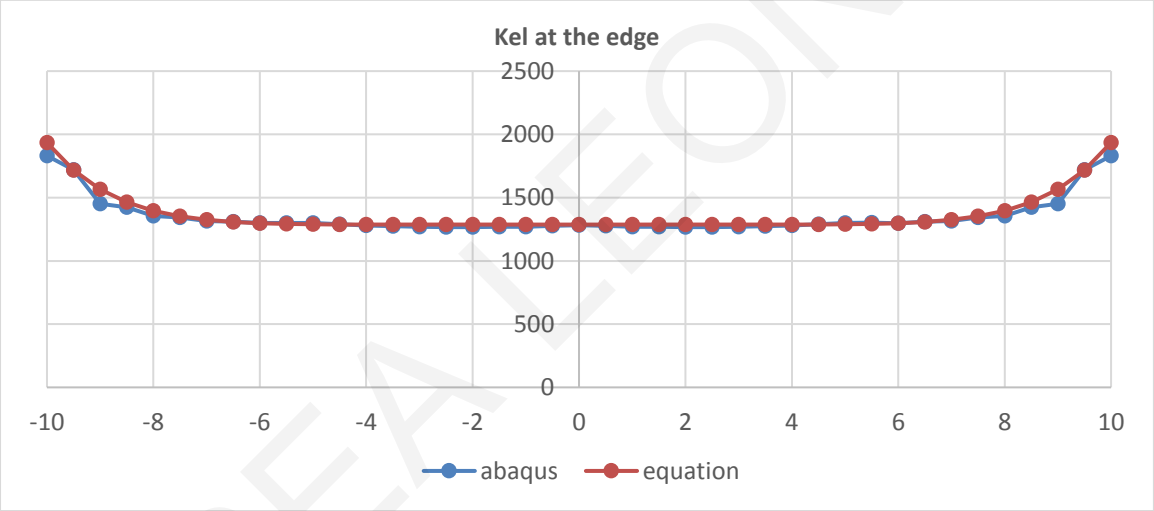

(b)

Figure C40: Comparison of K_{el} from Abaqus and the proposed equation for analysis 40 at (a) the centerline and (b) the edge of the mat.

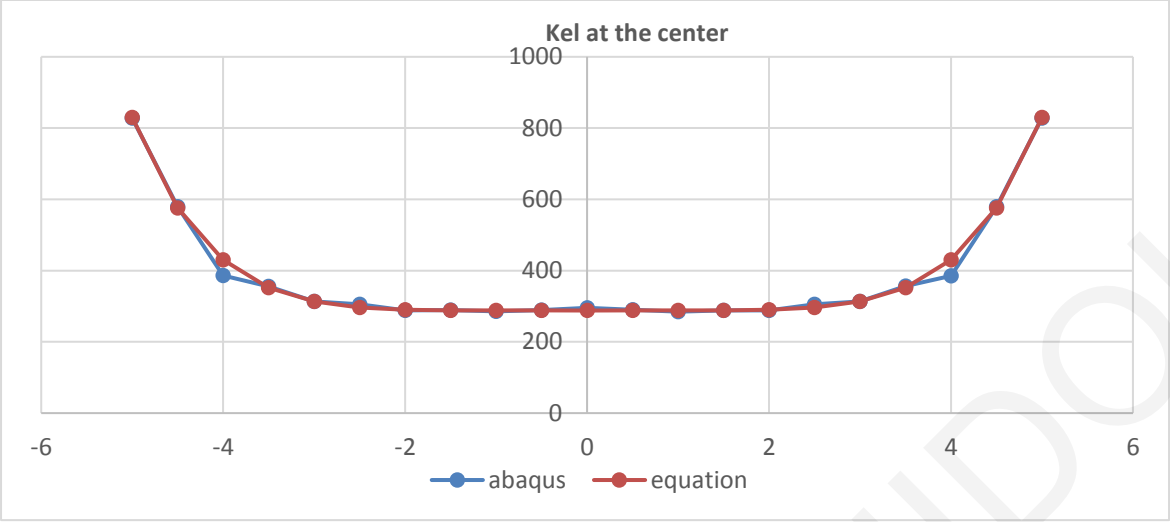

(a)

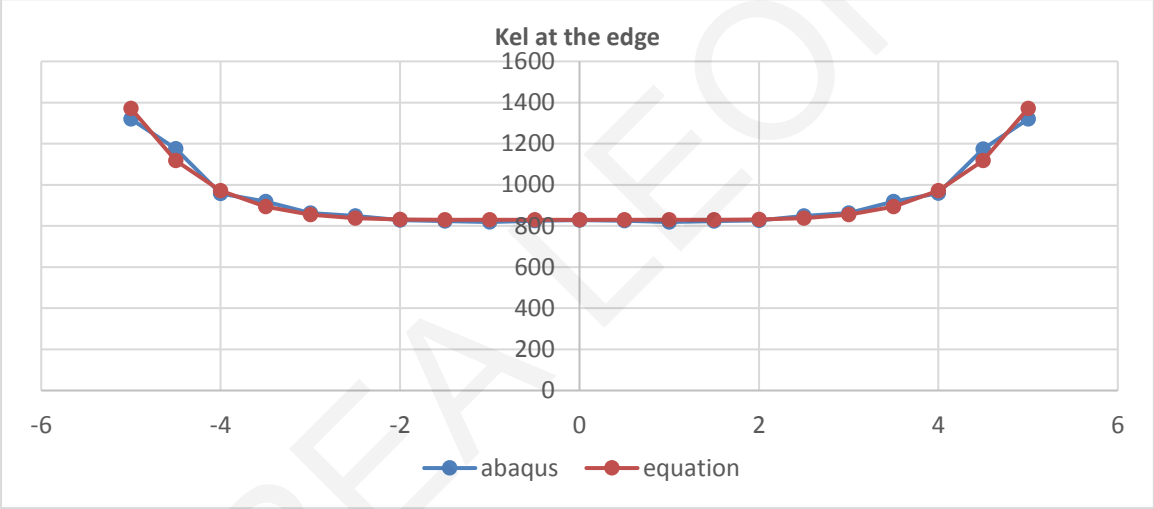

(b)

Figure C41: Comparison of K_{el} from Abaqus and the proposed equation for analysis 41 at (a) the centerline and (b) the edge of the mat.

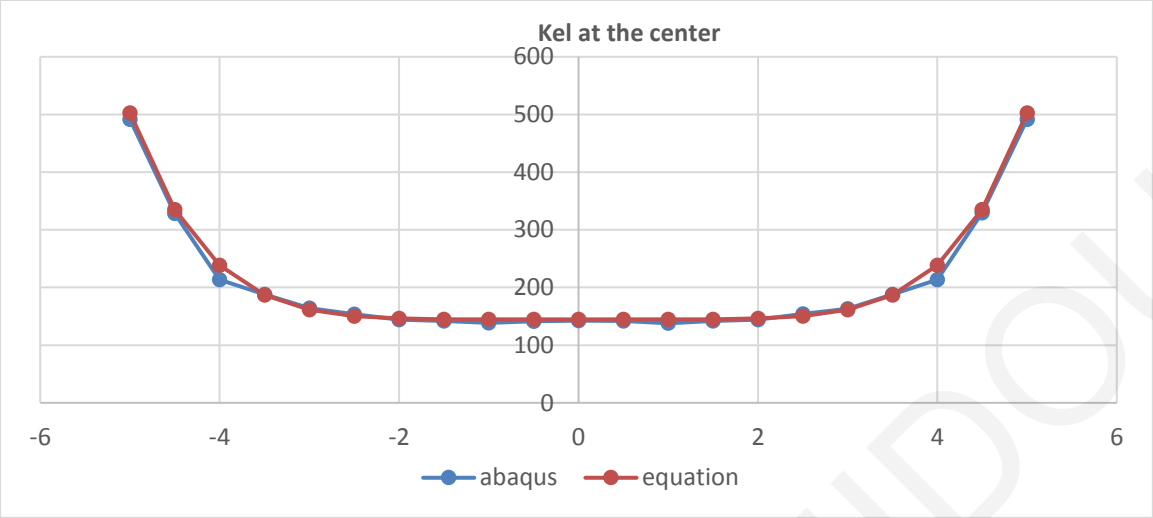

(a)

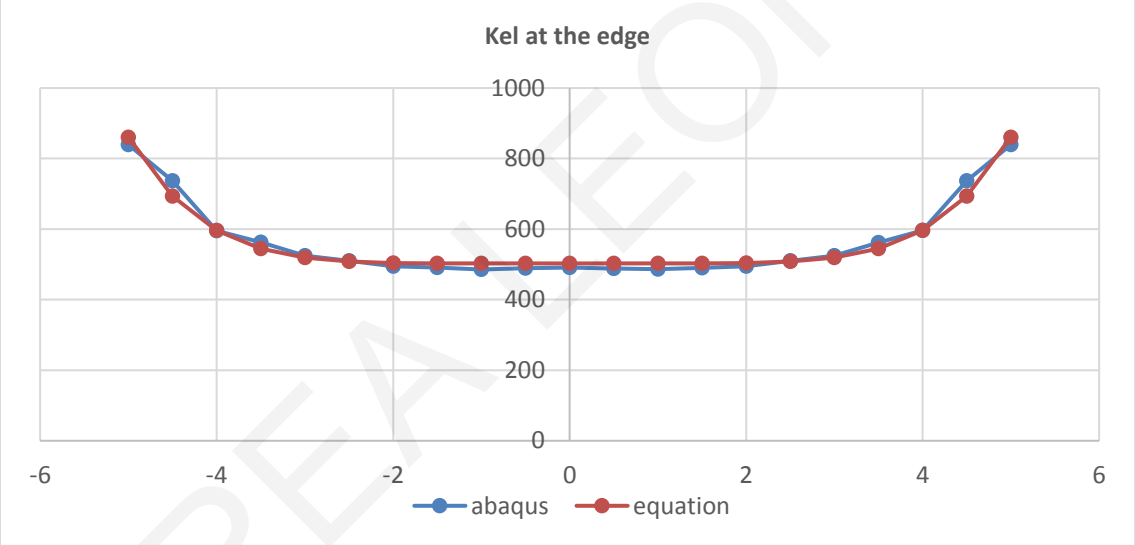

(b)

Figure C42: Comparison of K_{el} from Abaqus and the proposed equation for analysis 42 at (a) the centerline and (b) the edge of the mat.

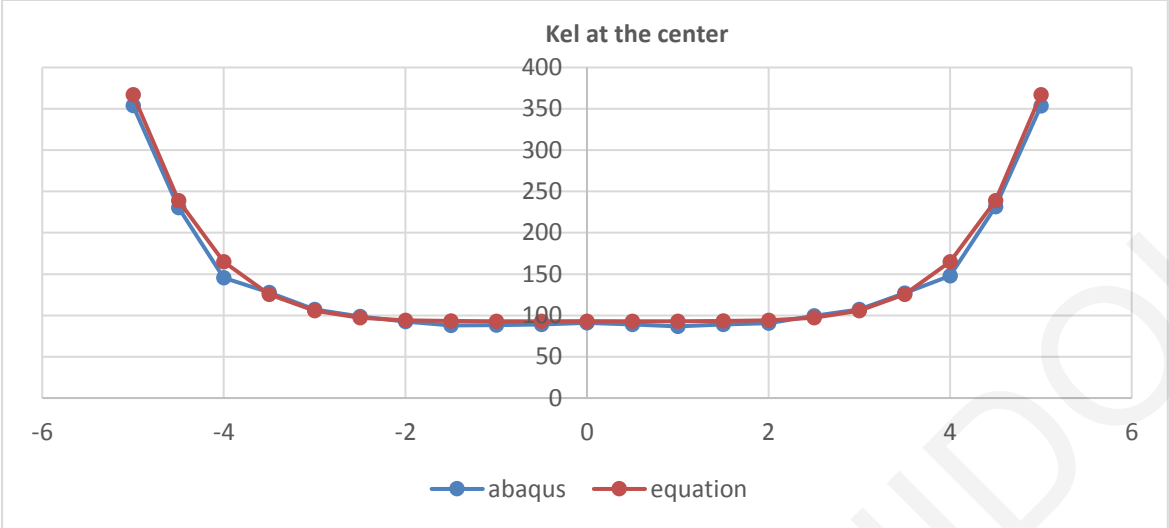

(a)

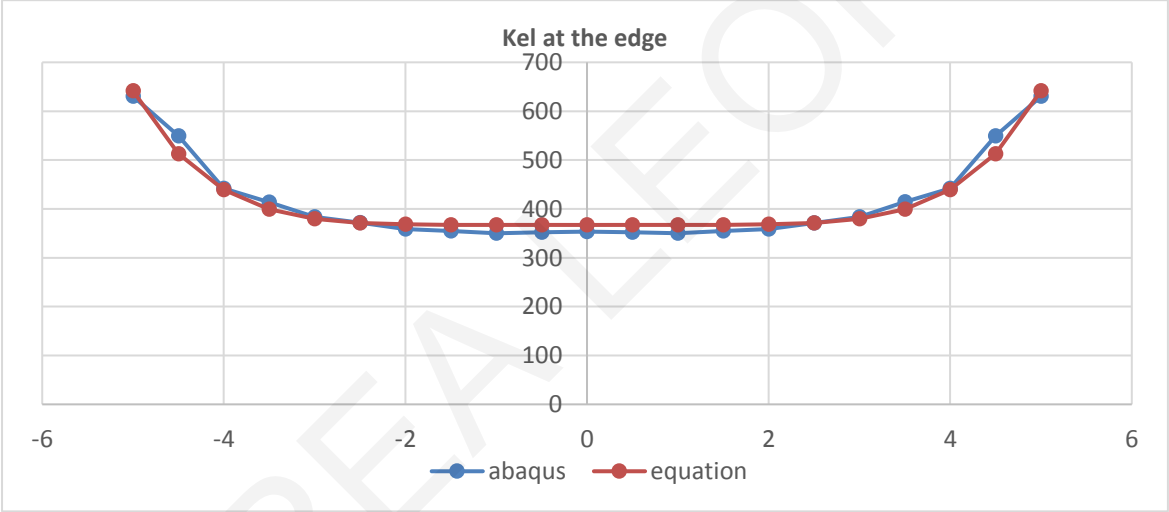

(b)

Figure C43: Comparison of K_{el} from Abaqus and the proposed equation for analysis 43 at (a) the centerline and (b) the edge of the mat.

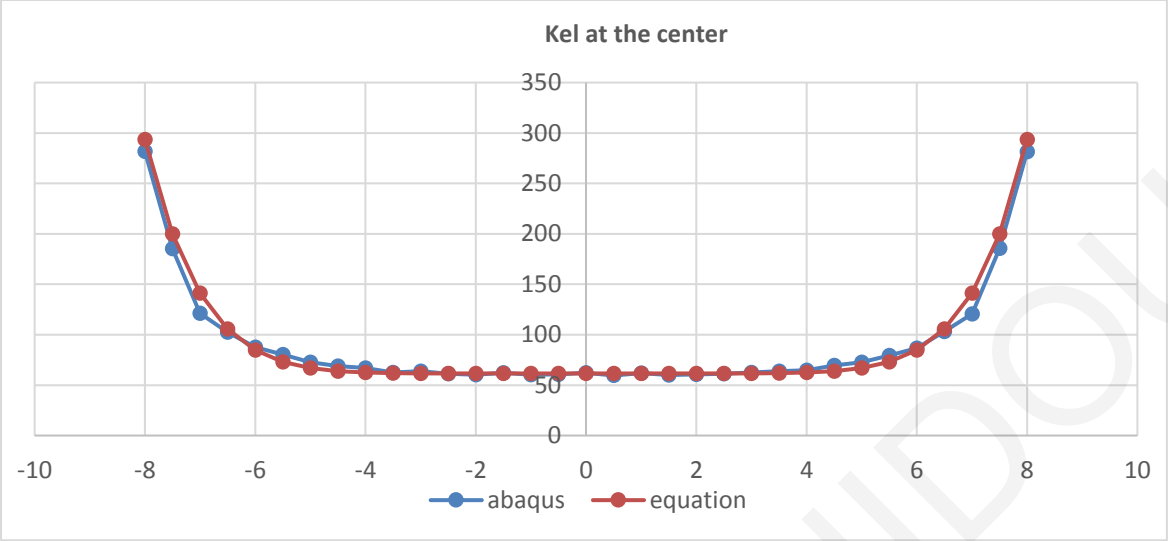

(a)

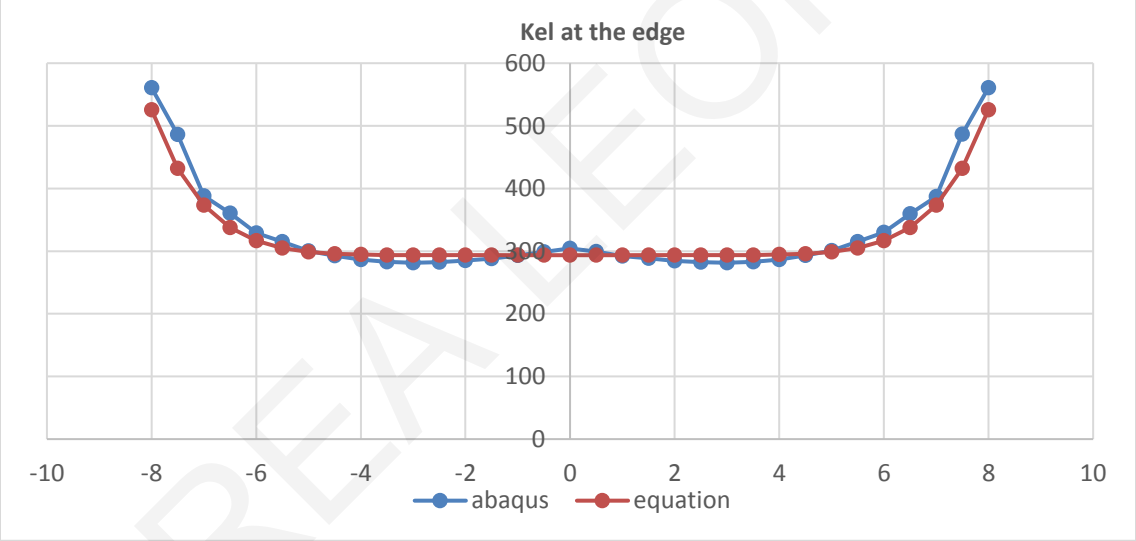

(b)

Figure C44: Comparison of K_{el} from Abaqus and the proposed equation for analysis 44 at (a) the centerline and (b) the edge of the mat.

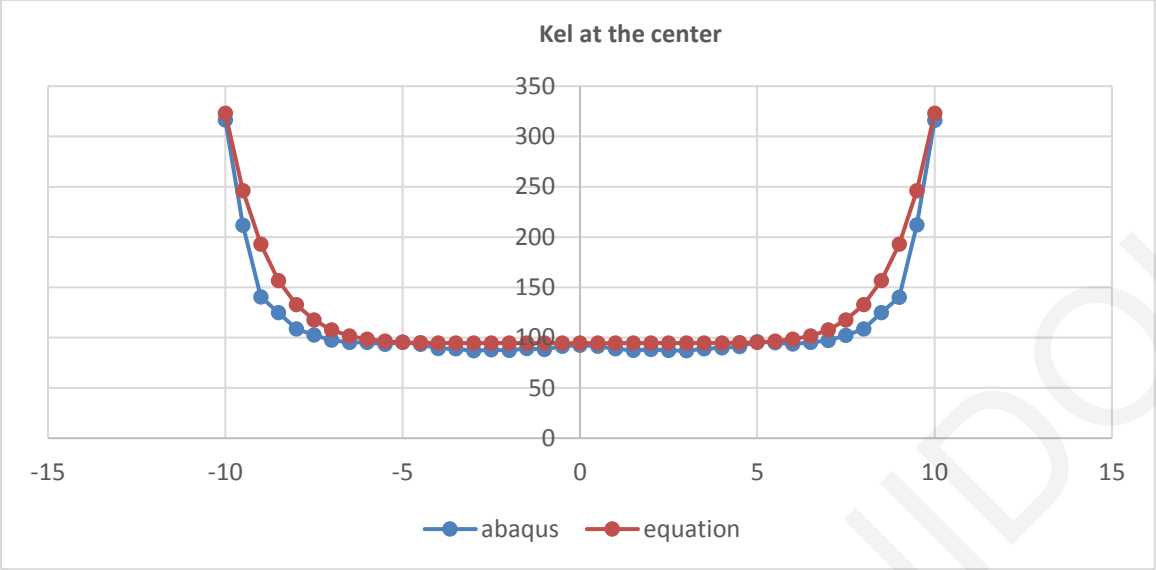

(a)

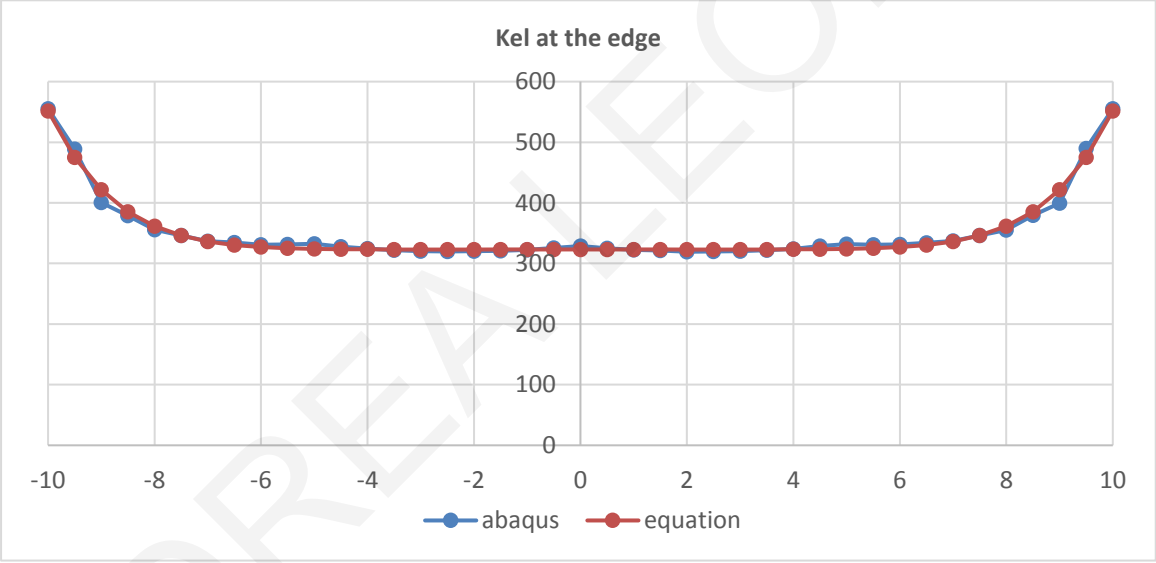

(b)

Figure C45: Comparison of K_{el} from Abaqus and the proposed equation for analysis 45 at (a) the centerline and (b) the edge of the mat.

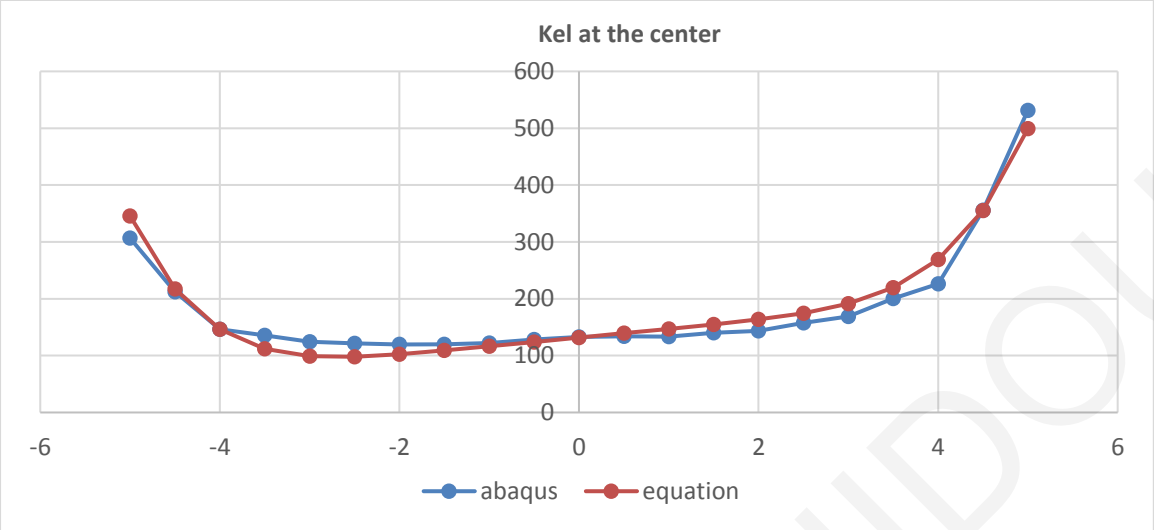

(a)

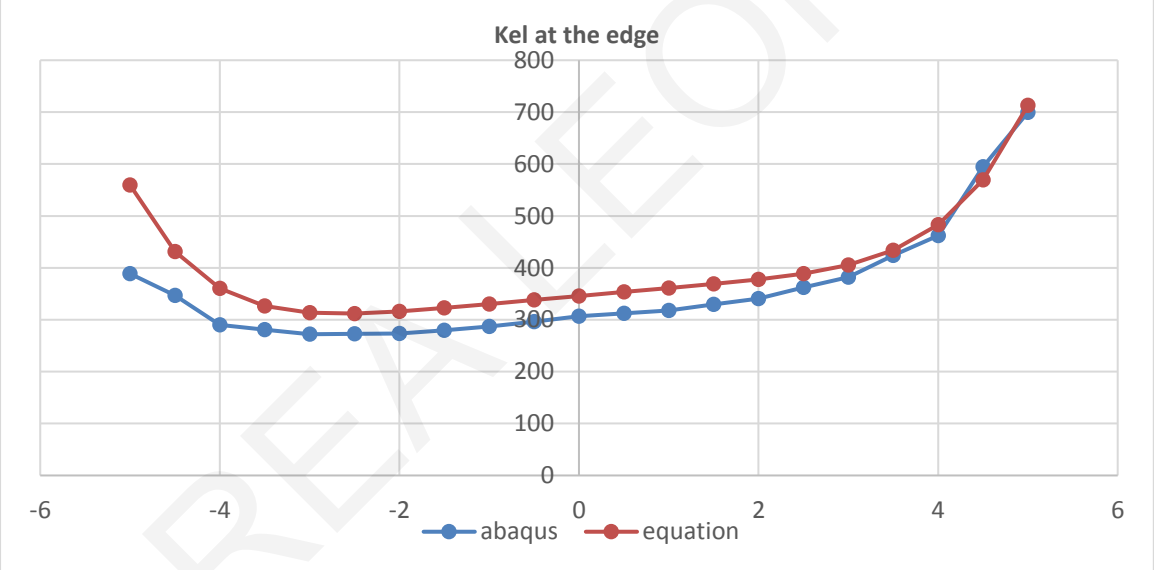

(b)

Figure C46: Comparison of K_{el} from Abaqus and the proposed equation for analysis 46 at (a) the centerline and (b) the edge of the mat.

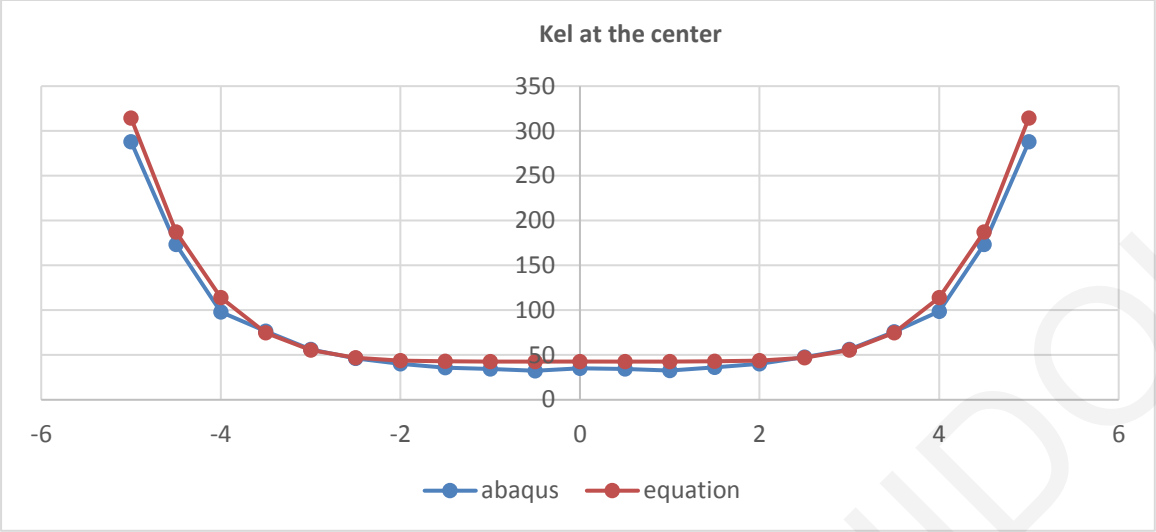

(a)

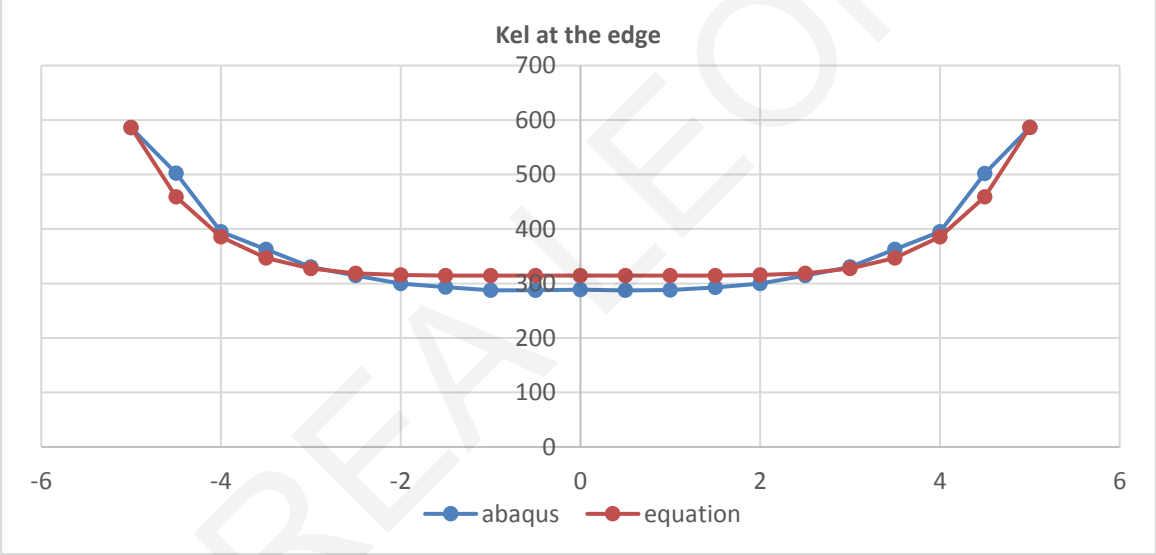

(b)

Figure C47: Comparison of K_{el} from Abaqus and the proposed equation for analysis 47 at (a) the centerline and (b) the edge of the mat.

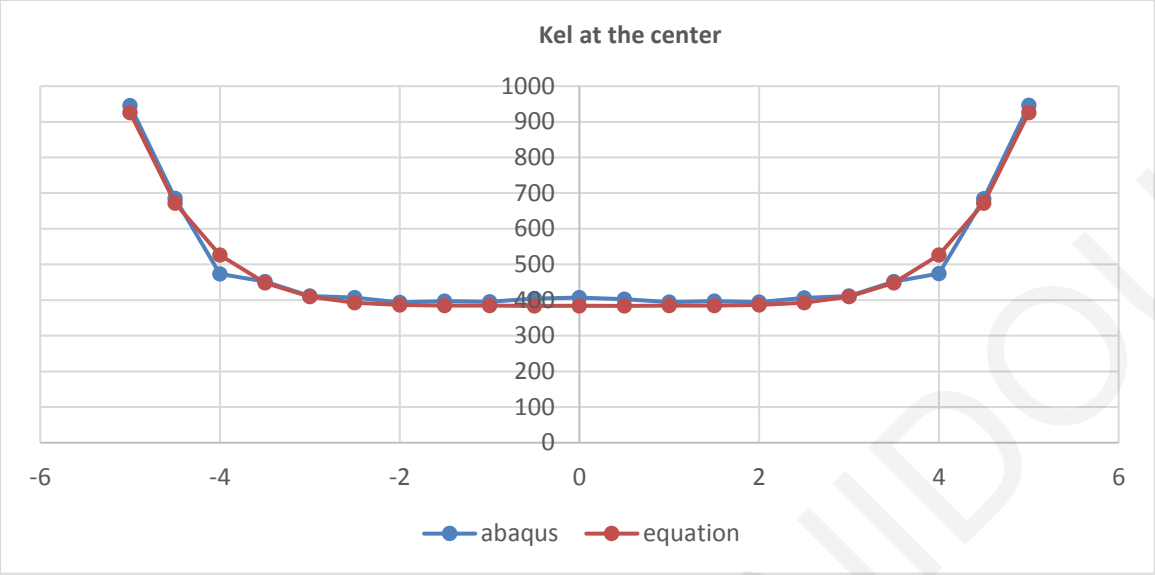

(a)

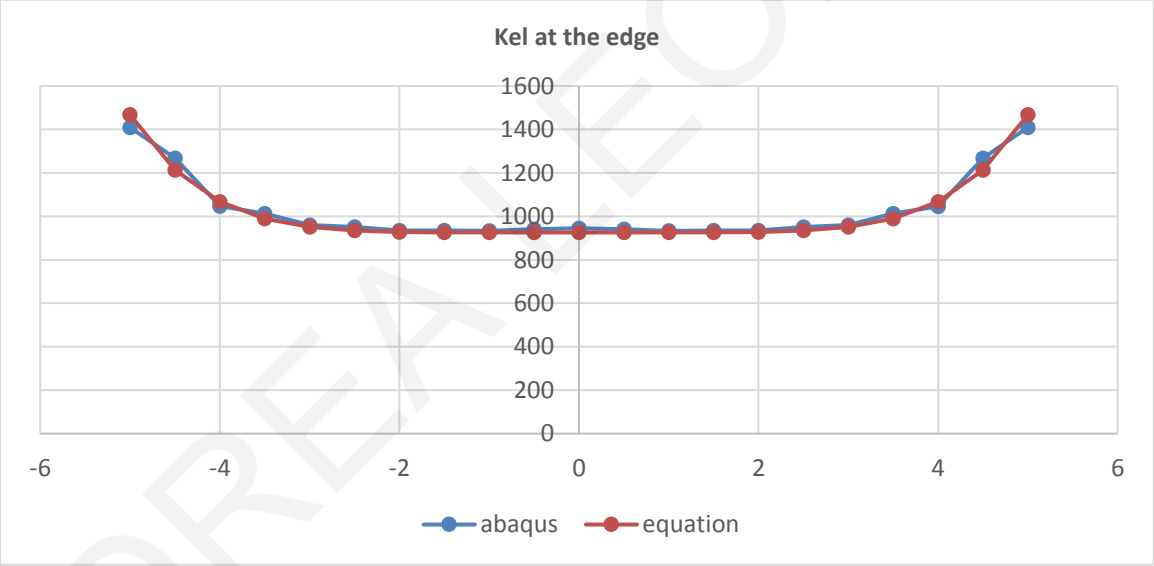

(b)

Figure C48: Comparison of K_{el} from Abaqus and the proposed equation for analysis 48 at (a) the centerline and (b) the edge of the mat.

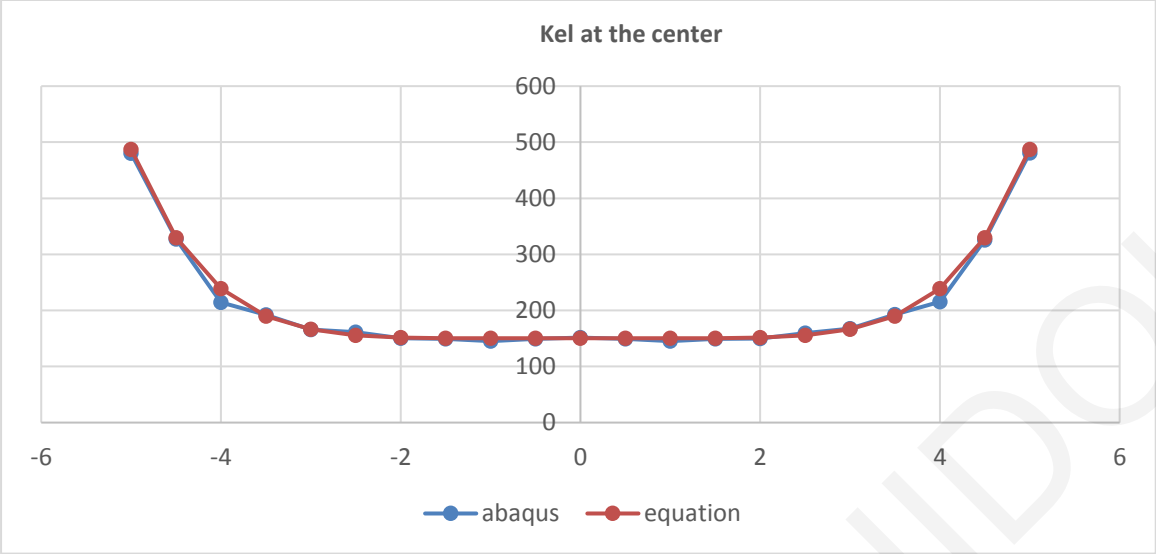

(a)

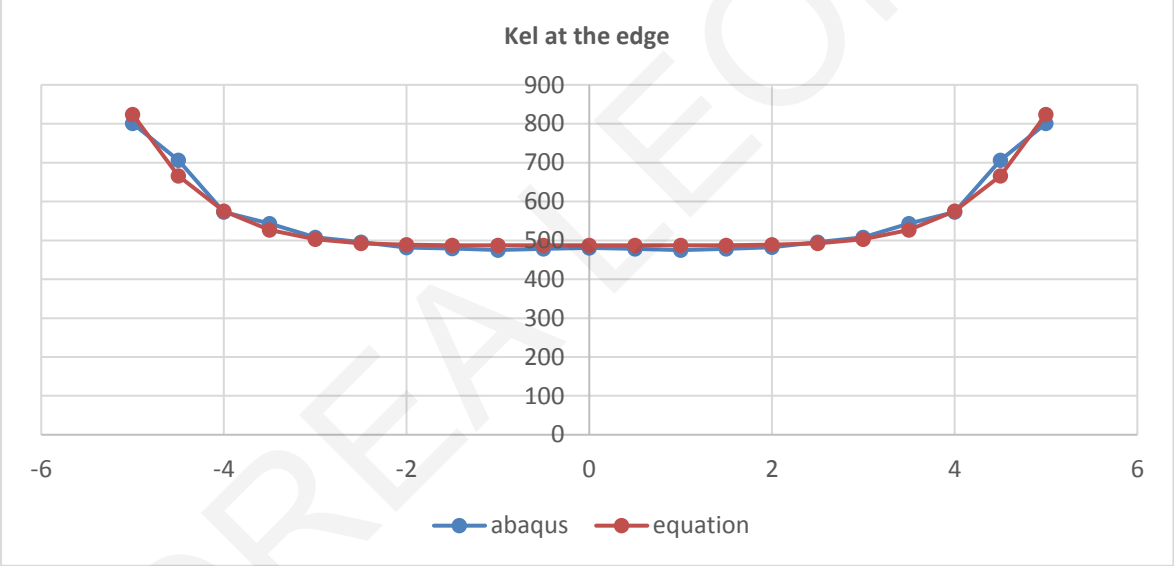

(b)

Figure C49: Comparison of K_{el} from Abaqus and the proposed equation for analysis 49 at (a) the centerline and (b) the edge of the mat.

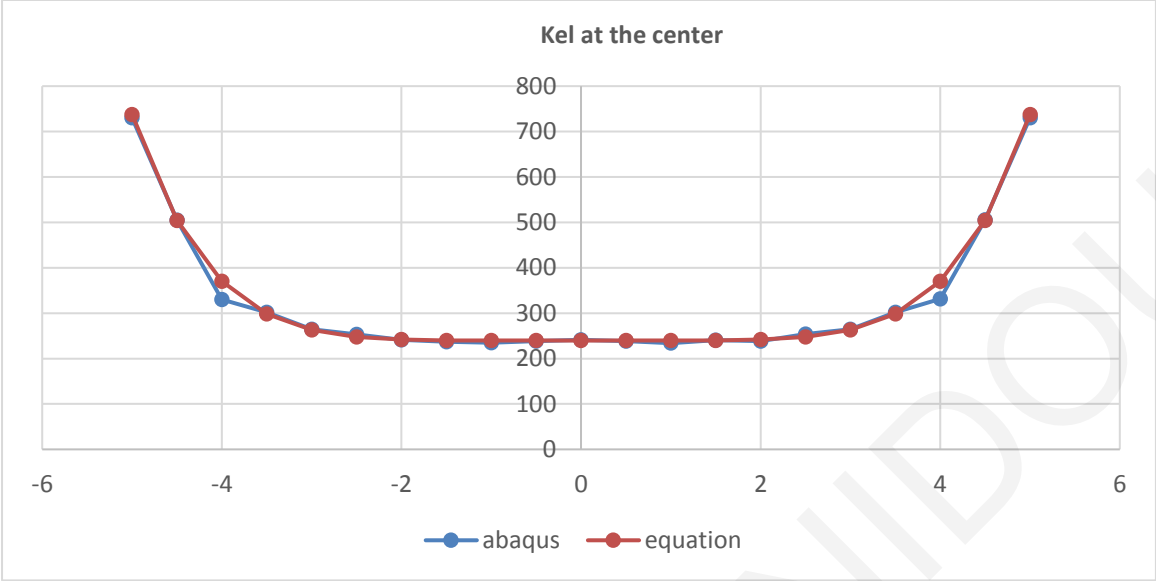

(a)

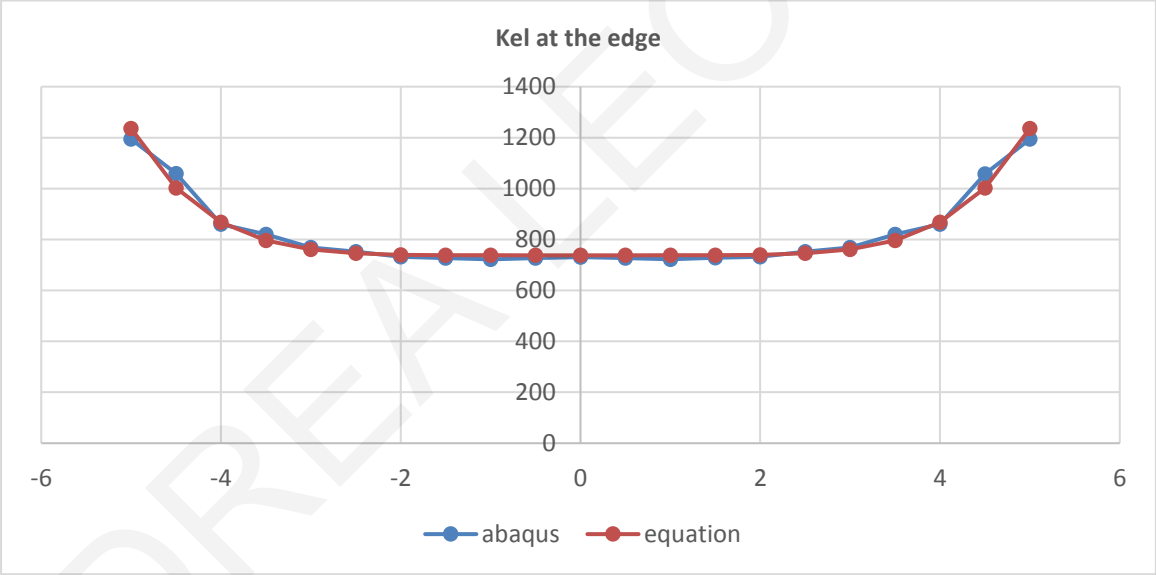

(b)

Figure C50: Comparison of K_{el} from Abaqus and the proposed equation for analysis 50 at (a) the centerline and (b) the edge of the mat.

ANNEX D

MATLAB CODES AND DATA ENTRY FILES

1. Winkler constant spring calculation algorithm with node settlements as input data ("reverse problem") by Tamiolakis (2012)

```
%Clear variables from memory
clear
%Get the name of the input file
inputFile=input('Input File:','s');
fprintf('Reading data from the file: %s',inputFile)

%Διάβασμα αρχείου δεδομένων
eval(inputFile)

%Αποθήκευση συντεταγμένων σε πίνακες
X= NODES(:,2);
Y= NODES(:,3);

%Εύρεση του αριθμού πεπερασμένων στοιχείων
megethos= size(ELEMENTS);
Ar_stoixeiwn= megethos(1);

%Εύρεση του αριθμού των κόμβων του δικτύου
megethos= size(NODES);
Ar_komvwn= megethos(1);

%Εύρεση του αριθμού των φορτίων που ασκούνται στους κόμβους του δυκτίου
megethos= size(LOADS);
Ar_fortiwn= megethos(1);

K=zeros(3*Ar_komvwn,3*Ar_komvwn);
Kel=zeros(3*Ar_komvwn,3*Ar_komvwn);

for m=1:Ar_stoixeiwn

    k=zeros(12,12);
    %Εύρεση των κόμβων του κάθε στοιχείου για τον υπολογισμό των
διαστάσεων
    %του
    komvos1(m)=ELEMENTS(m,2);
    komvos2(m)=ELEMENTS(m,3);
    komvos3(m)=ELEMENTS(m,4);
    komvos4(m)=ELEMENTS(m,5);



    %Σχηματισμός μητρώου δυσκαμψίας στοιχείου abaqus
    k(1,1)=8333287.00;
    k(4,4)=k(1,1);
    k(7,7)=k(1,1);
    k(10,10)=k(1,1);
    k(2,1)=1041660.88;
    k(8,1)=k(2,1);
    k(1,2)=k(2,1);
```

```
k(4,3)=k(2,1);
k(3,4)=k(2,1);
k(5,4)=k(2,1);
k(6,4)=k(2,1);
k(11,4)=k(2,1);
k(4,5)=k(2,1);
k(4,6)=k(2,1);
k(1,8)=k(2,1);
k(10,9)=k(2,1);
k(9,10)=k(2,1);
k(12,10)=k(2,1);
k(4,11)=k(2,1);
k(10,12)=k(2,1);
k(3,1)=-k(2,1);
k(6,1)=-k(2,1);
k(7,2)=-k(2,1);
k(1,3)=-k(2,1);
k(10,5)=-k(2,1);
k(1,6)=-k(2,1);
k(2,7)=-k(2,1);
k(8,7)=-k(2,1);
k(9,7)=-k(2,1);
k(12,7)=-k(2,1);
k(7,8)=-k(2,1);
k(7,9)=-k(2,1);
k(5,10)=-k(2,1);
k(11,10)=-k(2,1);
k(10,11)=-k(2,1);
k(7,12)=-k(2,1);
k(4,1)=-4166643.50;
k(7,1)=k(4,1);
k(1,4)=k(4,1);
k(10,4)=k(4,1);
k(1,7)=k(4,1);
k(10,7)=k(4,1);
k(4,10)=k(4,1);
k(7,10)=k(4,1);
k(5,1)=0;
k(9,1)=0;
k(10,1)=0;
k(11,1)=0;
k(12,1)=0;
k(4,2)=0;
k(10,2)=0;
k(7,3)=0;
k(10,3)=0;
k(2,4)=0;
k(7,4)=0;
k(8,4)=0;
k(9,4)=0;
k(12,4)=0;
k(1,5)=0;
k(7,5)=0;
k(7,6)=0;
k(10,6)=0;
k(3,7)=0;
k(4,7)=0;
```

```
k(5,7)=0;
k(6,7)=0;
k(11,7)=0;
k(4,8)=0;
k(10,8)=0;
k(1,9)=0;
k(4,9)=0;
k(1,10)=0;
k(2,10)=0;
k(3,10)=0;
k(6,10)=0;
k(8,10)=0;
k(1,11)=0;
k(7,11)=0;
k(1,12)=0;
k(4,12)=0;
k(2,2)=673208.19;
k(3,3)=k(2,2);
k(5,5)=k(2,2);
k(6,6)=k(2,2);
k(8,8)=k(2,2);
k(9,9)=k(2,2);
k(11,11)=k(2,2);
k(12,12)=k(2,2);
k(3,2)=-175781.25;
k(2,3)=k(3,2);
k(9,5)=k(3,2);
k(5,9)=k(3,2);
k(8,6)=k(3,2);
k(6,8)=k(3,2);
k(12,11)=k(3,2);
k(11,12)=k(3,2);
k(12,2)=-k(3,2);
k(2,12)=-k(3,2);
k(11,3)=-k(3,2);
k(3,11)=-k(3,2);
k(6,5)=-k(3,2);
k(5,6)=-k(3,2);
k(9,8)=-k(3,2);
k(8,9)=-k(3,2);
k(5,2)=173144.53;
k(9,3)=k(5,2);
k(3,9)=k(5,2);
k(2,5)=k(5,2);
k(12,6)=k(5,2);
k(6,12)=k(5,2);
k(8,11)=k(5,2);
k(11,8)=k(5,2);
k(6,2)=-58593.75;
k(8,3)=k(6,2);
k(3,8)=k(6,2);
k(12,5)=k(6,2);
k(5,12)=k(6,2);
k(2,6)=k(6,2);
k(11,9)=k(6,2);
k(9,11)=k(6,2);
k(9,2)=-k(6,2);
```

```
    k(5,3)=-k(6,2);
    k(3,5)=-k(6,2);
    k(11,6)=-k(6,2);
    k(6,11)=-k(6,2);
    k(12,8)=-k(6,2);
    k(8,12)=-k(6,2);
    k(2,9)=-k(6,2);
    k(8,2)=81997.25;
    k(6,3)=k(8,2);
    k(3,6)=k(8,2);
    k(11,5)=k(8,2);
    k(5,11)=k(8,2);
    k(12,9)=k(8,2);
    k(9,12)=k(8,2);
    k(2,8)=k(8,2);
    k(11,2)=-407519.53;
    k(2,11)=k(11,2);
    k(12,3)=k(11,2);
    k(3,12)=k(11,2);
    k(8,5)=k(11,2);
    k(5,8)=k(11,2);
    k(9,6)=k(11,2);
    k(6,9)=k(11,2);




    disp(k)

    %Δημιουργία των δεικτλων για την εύρεση των βαθμών ελευθερίας
    %προκειμένου να τοποθετηθει το μητρώο δυσκαμψίας του στοιχείου στο
    %μητρώο δυσκαμψίας της πλάκας
    be1=3*komvos1(m)-2;
    be2=3*komvos2(m)-2;
    be4=3*komvos3(m)-2;
    be3=3*komvos4(m)-2;

    %Δημιουργία του μητρώου δυσκαμψίας της πλάκας
    K(be1:be1+2,be1:be1+2)=K(be1:be1+2,be1:be1+2)+k(1:3,1:3);
    K(be2:be2+2,be2:be2+2)=K(be2:be2+2,be2:be2+2)+k(4:6,4:6);
    K(be3:be3+2,be3:be3+2)=K(be3:be3+2,be3:be3+2)+k(7:9,7:9);
    K(be4:be4+2,be4:be4+2)=K(be4:be4+2,be4:be4+2)+k(10:12,10:12);
    K(be1:be1+2,be2:be2+2)=K(be1:be1+2,be2:be2+2)+k(1:3,4:6);
    K(be2:be2+2,be1:be1+2)=K(be2:be2+2,be1:be1+2)+k(4:6,1:3);
    K(be1:be1+2,be3:be3+2)=K(be1:be1+2,be3:be3+2)+k(1:3,7:9);
    K(be3:be3+2,be1:be1+2)=K(be3:be3+2,be1:be1+2)+k(7:9,1:3);
    K(be1:be1+2,be4:be4+2)=K(be1:be1+2,be4:be4+2)+k(1:3,10:12);
    K(be4:be4+2,be1:be1+2)=K(be4:be4+2,be1:be1+2)+k(10:12,1:3);
    K(be2:be2+2,be3:be3+2)=K(be2:be2+2,be3:be3+2)+k(4:6,7:9);
    K(be3:be3+2,be2:be2+2)=K(be3:be3+2,be2:be2+2)+k(7:9,4:6);
    K(be2:be2+2,be4:be4+2)=K(be2:be2+2,be4:be4+2)+k(4:6,10:12);
    K(be4:be4+2,be2:be2+2)=K(be4:be4+2,be2:be2+2)+k(10:12,4:6);
    K(be3:be3+2,be4:be4+2)=K(be3:be3+2,be4:be4+2)+k(7:9,10:12);
    K(be4:be4+2,be3:be3+2)=K(be4:be4+2,be3:be3+2)+k(10:12,7:9);
end
```

```
%Εκτύπωση του μητρώου δυσκαμψίας της πλάκας
fprintf('\n\n Mitrwo dyskampsias plakas: K=\n');
disp(K)

fortio=zeros(3*Ar_komvwn,1);
for i=1:Ar_fortiwn
    fortio(3*LOADS(i,1)-2,1)=LOADS(i,2);
end

disp(fortio)

C=K;
ij=0;
u2=zeros(3*Ar_komvwn,1);
for i=1:3:3*Ar_komvwn
    ij=ij+1;
    C(:,i)=0;
    C(i,i)=u(ij);
    u2(i)=u(ij);
end

Br=fortio-K*u2;
x=inv(C)*(fortio-K*u2);
%x=linsolve(C,Br);
disp(x)

for i=1:3:3*Ar_komvwn
    Kel(i,i)=x(i,1);
end

w=inv(K+Kel)*fortio;
disp(w)
%Εκτύπωση των μετατοπίσεων των βαθμών ελευθερίας της πλάκας
fprintf('\n\n Κελ=\n');
ij=0;
for i=1:3:3*Ar_komvwn
    ij=ij+1;
    uplot(ij,1)=x(i,1);
end
for i=1:3:3*Ar_komvwn
    x(i,1)=u2(i,1);
end
%disp(k)
disp(uplot)
disp(k)
```

2. Example of a data entry file for a Winkler spring export algorithm

```
NODES=[1    -5  -5
2   -5  -4.5
3   -5  -4
4   -5  -3.5
5   -5  -3
6   -5  -2.5
7   -5  -2
8   -5  -1.5
9   -5  -1
10  -5  -0.5
11  -5  0
12  -5  0.5
13  -5  1
14  -5  1.5
15  -5  2
16  -5  2.5
17  -5  3
18  -5  3.5
19  -5  4
20  -5  4.5
21  -5  5
22  -4.5    -5
23  -4.5    -4.5
24  -4.5    -4
25  -4.5    -3.5
26  -4.5    -3
27  -4.5    -2.5
28  -4.5    -2
29  -4.5    -1.5
30  -4.5    -1
31  -4.5    -0.5
32  -4.5    0
33  -4.5    0.5
34  -4.5    1
35  -4.5    1.5
36  -4.5    2
37  -4.5    2.5
38  -4.5    3
39  -4.5    3.5
40  -4.5    4
41  -4.5    4.5
42  -4.5    5
43  -4  -5
44  -4  -4.5
45  -4  -4
46  -4  -3.5
47  -4  -3
48  -4  -2.5
49  -4  -2
50  -4  -1.5
```

```
51  -4  -1
52  -4  -0.5
53  -4  0
54  -4  0.5
55  -4  1
56  -4  1.5
57  -4  2
58  -4  2.5
59  -4  3
60  -4  3.5
61  -4  4
62  -4  4.5
63  -4  5
64  -3.5    -5
65  -3.5    -4.5
66  -3.5    -4
67  -3.5    -3.5
68  -3.5    -3
69  -3.5    -2.5
70  -3.5    -2
71  -3.5    -1.5
72  -3.5    -1
73  -3.5    -0.5
74  -3.5    0
75  -3.5    0.5
76  -3.5    1
77  -3.5    1.5
78  -3.5    2
79  -3.5    2.5
80  -3.5    3
81  -3.5    3.5
82  -3.5    4
83  -3.5    4.5
84  -3.5    5
85  -3  -5
86  -3  -4.5
87  -3  -4
88  -3  -3.5
89  -3  -3
90  -3  -2.5
91  -3  -2
92  -3  -1.5
93  -3  -1
94  -3  -0.5
95  -3  0
96  -3  0.5
97  -3  1
98  -3  1.5
99  -3  2
100 -3  2.5
101 -3  3
102 -3  3.5
103 -3  4
104 -3  4.5
105 -3  5
106 -2.5    -5
107 -2.5    -4.5
```

```
108 -2.5    -4
109 -2.5    -3.5
110 -2.5    -3
111 -2.5    -2.5
112 -2.5    -2
113 -2.5    -1.5
114 -2.5    -1
115 -2.5    -0.5
116 -2.5    0
117 -2.5    0.5
118 -2.5    1
119 -2.5    1.5
120 -2.5    2
121 -2.5    2.5
122 -2.5    3
123 -2.5    3.5
124 -2.5    4
125 -2.5    4.5
126 -2.5    5
127 -2  -5
128 -2  -4.5
129 -2  -4
130 -2  -3.5
131 -2  -3
132 -2  -2.5
133 -2  -2
134 -2  -1.5
135 -2  -1
136 -2  -0.5
137 -2  0
138 -2  0.5
139 -2  1
140 -2  1.5
141 -2  2
142 -2  2.5
143 -2  3
144 -2  3.5
145 -2  4
146 -2  4.5
147 -2  5
148 -1.5    -5
149 -1.5    -4.5
150 -1.5    -4
151 -1.5    -3.5
152 -1.5    -3
153 -1.5    -2.5
154 -1.5    -2
155 -1.5    -1.5
156 -1.5    -1
157 -1.5    -0.5
158 -1.5    0
159 -1.5    0.5
160 -1.5    1
161 -1.5    1.5
162 -1.5    2
163 -1.5    2.5
164 -1.5    3
```

```
165 -1.5    3.5
166 -1.5    4
167 -1.5    4.5
168 -1.5    5
169 -1  -5
170 -1  -4.5
171 -1  -4
172 -1  -3.5
173 -1  -3
174 -1  -2.5
175 -1  -2
176 -1  -1.5
177 -1  -1
178 -1  -0.5
179 -1  0
180 -1  0.5
181 -1  1
182 -1  1.5
183 -1  2
184 -1  2.5
185 -1  3
186 -1  3.5
187 -1  4
188 -1  4.5
189 -1  5
190 -0.5    -5
191 -0.5    -4.5
192 -0.5    -4
193 -0.5    -3.5
194 -0.5    -3
195 -0.5    -2.5
196 -0.5    -2
197 -0.5    -1.5
198 -0.5    -1
199 -0.5    -0.5
200 -0.5    0
201 -0.5    0.5
202 -0.5    1
203 -0.5    1.5
204 -0.5    2
205 -0.5    2.5
206 -0.5    3
207 -0.5    3.5
208 -0.5    4
209 -0.5    4.5
210 -0.5    5
211 0   -5
212 0   -4.5
213 0   -4
214 0   -3.5
215 0   -3
216 0   -2.5
217 0   -2
218 0   -1.5
219 0   -1
220 0   -0.5
221 0   0
```

```
222 0   0.5
223 0   1
224 0   1.5
225 0   2
226 0   2.5
227 0   3
228 0   3.5
229 0   4
230 0   4.5
231 0   5
232 0.5 -5
233 0.5 -4.5
234 0.5 -4
235 0.5 -3.5
236 0.5 -3
237 0.5 -2.5
238 0.5 -2
239 0.5 -1.5
240 0.5 -1
241 0.5 -0.5
242 0.5 0
243 0.5 0.5
244 0.5 1
245 0.5 1.5
246 0.5 2
247 0.5 2.5
248 0.5 3
249 0.5 3.5
250 0.5 4
251 0.5 4.5
252 0.5 5
253 1   -5
254 1   -4.5
255 1   -4
256 1   -3.5
257 1   -3
258 1   -2.5
259 1   -2
260 1   -1.5
261 1   -1
262 1   -0.5
263 1   0
264 1   0.5
265 1   1
266 1   1.5
267 1   2
268 1   2.5
269 1   3
270 1   3.5
271 1   4
272 1   4.5
273 1   5
274 1.5 -5
275 1.5 -4.5
276 1.5 -4
277 1.5 -3.5
278 1.5 -3
```

```
279 1.5 -2.5
280 1.5 -2
281 1.5 -1.5
282 1.5 -1
283 1.5 -0.5
284 1.5 0
285 1.5 0.5
286 1.5 1
287 1.5 1.5
288 1.5 2
289 1.5 2.5
290 1.5 3
291 1.5 3.5
292 1.5 4
293 1.5 4.5
294 1.5 5
295 2   -5
296 2   -4.5
297 2   -4
298 2   -3.5
299 2   -3
300 2   -2.5
301 2   -2
302 2   -1.5
303 2   -1
304 2   -0.5
305 2   0
306 2   0.5
307 2   1
308 2   1.5
309 2   2
310 2   2.5
311 2   3
312 2   3.5
313 2   4
314 2   4.5
315 2   5
316 2.5 -5
317 2.5 -4.5
318 2.5 -4
319 2.5 -3.5
320 2.5 -3
321 2.5 -2.5
322 2.5 -2
323 2.5 -1.5
324 2.5 -1
325 2.5 -0.5
326 2.5 0
327 2.5 0.5
328 2.5 1
329 2.5 1.5
330 2.5 2
331 2.5 2.5
332 2.5 3
333 2.5 3.5
334 2.5 4
335 2.5 4.5
```

```
336 2.5 5
337 3   -5
338 3   -4.5
339 3   -4
340 3   -3.5
341 3   -3
342 3   -2.5
343 3   -2
344 3   -1.5
345 3   -1
346 3   -0.5
347 3   0
348 3   0.5
349 3   1
350 3   1.5
351 3   2
352 3   2.5
353 3   3
354 3   3.5
355 3   4
356 3   4.5
357 3   5
358 3.5 -5
359 3.5 -4.5
360 3.5 -4
361 3.5 -3.5
362 3.5 -3
363 3.5 -2.5
364 3.5 -2
365 3.5 -1.5
366 3.5 -1
367 3.5 -0.5
368 3.5 0
369 3.5 0.5
370 3.5 1
371 3.5 1.5
372 3.5 2
373 3.5 2.5
374 3.5 3
375 3.5 3.5
376 3.5 4
377 3.5 4.5
378 3.5 5
379 4   -5
380 4   -4.5
381 4   -4
382 4   -3.5
383 4   -3
384 4   -2.5
385 4   -2
386 4   -1.5
387 4   -1
388 4   -0.5
389 4   0
390 4   0.5
391 4   1
392 4   1.5
```

```
393 4   2
394 4   2.5
395 4   3
396 4   3.5
397 4   4
398 4   4.5
399 4   5
400 4.5 -5
401 4.5 -4.5
402 4.5 -4
403 4.5 -3.5
404 4.5 -3
405 4.5 -2.5
406 4.5 -2
407 4.5 -1.5
408 4.5 -1
409 4.5 -0.5
410 4.5 0
411 4.5 0.5
412 4.5 1
413 4.5 1.5
414 4.5 2
415 4.5 2.5
416 4.5 3
417 4.5 3.5
418 4.5 4
419 4.5 4.5
420 4.5 5
421 5   -5
422 5   -4.5
423 5   -4
424 5   -3.5
425 5   -3
426 5   -2.5
427 5   -2
428 5   -1.5
429 5   -1
430 5   -0.5
431 5   0
432 5   0.5
433 5   1
434 5   1.5
435 5   2
436 5   2.5
437 5   3
438 5   3.5
439 5   4
440 5   4.5
441 5   5
];

ELEMENTS=[
1   1   2   23  22
2   2   3   24  23
3   3   4   25  24
4   4   5   26  25
5   5   6   27  26
```

6	6	7	28	27
7	7	8	29	28
8	8	9	30	29
9	9	10	31	30
10	10	11	32	31
11	11	12	33	32
12	12	13	34	33
13	13	14	35	34
14	14	15	36	35
15	15	16	37	36
16	16	17	38	37
17	17	18	39	38
18	18	19	40	39
19	19	20	41	40
20	20	21	42	41
21	22	23	44	43
22	23	24	45	44
23	24	25	46	45
24	25	26	47	46
25	26	27	48	47
26	27	28	49	48
27	28	29	50	49
28	29	30	51	50
29	30	31	52	51
30	31	32	53	52
31	32	33	54	53
32	33	34	55	54
33	34	35	56	55
34	35	36	57	56
35	36	37	58	57
36	37	38	59	58
37	38	39	60	59
38	39	40	61	60
39	40	41	62	61
40	41	42	63	62
41	43	44	65	64
42	44	45	66	65
43	45	46	67	66
44	46	47	68	67
45	47	48	69	68
46	48	49	70	69
47	49	50	71	70
48	50	51	72	71
49	51	52	73	72
50	52	53	74	73
51	53	54	75	74
52	54	55	76	75
53	55	56	77	76
54	56	57	78	77
55	57	58	79	78
56	58	59	80	79
57	59	60	81	80
58	60	61	82	81
59	61	62	83	82
60	62	63	84	83
61	64	65	86	85
62	65	66	87	86

63 66 67 88 87
64 67 68 89 88
65 68 69 90 89
66 69 70 91 90
67 70 71 92 91
68 71 72 93 92
69 72 73 94 93
70 73 74 95 94
71 74 75 96 95
72 75 76 97 96
73 76 77 98 97
74 77 78 99 98
75 78 79 100 99
76 79 80 101 100
77 80 81 102 101
78 81 82 103 102
79 82 83 104 103
80 83 84 105 104
81 85 86 107 106
82 86 87 108 107
83 87 88 109 108
84 88 89 110 109
85 89 90 111 110
86 90 91 112 111
87 91 92 113 112
88 92 93 114 113
89 93 94 115 114
90 94 95 116 115
91 95 96 117 116
92 96 97 118 117
93 97 98 119 118
94 98 99 120 119
95 99 100 121 120
96 100 101 122 121
97 101 102 123 122
98 102 103 124 123
99 103 104 125 124
100 104 105 126 125
101 106 107 128 127
102 107 108 129 128
103 108 109 130 129
104 109 110 131 130
105 110 111 132 131
106 111 112 133 132
107 112 113 134 133
108 113 114 135 134
109 114 115 136 135
110 115 116 137 136
111 116 117 138 137
112 117 118 139 138
113 118 119 140 139
114 119 120 141 140
115 120 121 142 141
116 121 122 143 142
117 122 123 144 143
118 123 124 145 144
119 124 125 146 145

120 125 126 147 146
121 127 128 149 148
122 128 129 150 149
123 129 130 151 150
124 130 131 152 151
125 131 132 153 152
126 132 133 154 153
127 133 134 155 154
128 134 135 156 155
129 135 136 157 156
130 136 137 158 157
131 137 138 159 158
132 138 139 160 159
133 139 140 161 160
134 140 141 162 161
135 141 142 163 162
136 142 143 164 163
137 143 144 165 164
138 144 145 166 165
139 145 146 167 166
140 146 147 168 167
141 148 149 170 169
142 149 150 171 170
143 150 151 172 171
144 151 152 173 172
145 152 153 174 173
146 153 154 175 174
147 154 155 176 175
148 155 156 177 176
149 156 157 178 177
150 157 158 179 178
151 158 159 180 179
152 159 160 181 180
153 160 161 182 181
154 161 162 183 182
155 162 163 184 183
156 163 164 185 184
157 164 165 186 185
158 165 166 187 186
159 166 167 188 187
160 167 168 189 188
161 169 170 191 190
162 170 171 192 191
163 171 172 193 192
164 172 173 194 193
165 173 174 195 194
166 174 175 196 195
167 175 176 197 196
168 176 177 198 197
169 177 178 199 198
170 178 179 200 199
171 179 180 201 200
172 180 181 202 201
173 181 182 203 202
174 182 183 204 203
175 183 184 205 204
176 184 185 206 205

177 185 186 207 206
178 186 187 208 207
179 187 188 209 208
180 188 189 210 209
181 190 191 212 211
182 191 192 213 212
183 192 193 214 213
184 193 194 215 214
185 194 195 216 215
186 195 196 217 216
187 196 197 218 217
188 197 198 219 218
189 198 199 220 219
190 199 200 221 220
191 200 201 222 221
192 201 202 223 222
193 202 203 224 223
194 203 204 225 224
195 204 205 226 225
196 205 206 227 226
197 206 207 228 227
198 207 208 229 228
199 208 209 230 229
200 209 210 231 230
201 211 212 233 232
202 212 213 234 233
203 213 214 235 234
204 214 215 236 235
205 215 216 237 236
206 216 217 238 237
207 217 218 239 238
208 218 219 240 239
209 219 220 241 240
210 220 221 242 241
211 221 222 243 242
212 222 223 244 243
213 223 224 245 244
214 224 225 246 245
215 225 226 247 246
216 226 227 248 247
217 227 228 249 248
218 228 229 250 249
219 229 230 251 250
220 230 231 252 251
221 232 233 254 253
222 233 234 255 254
223 234 235 256 255
224 235 236 257 256
225 236 237 258 257
226 237 238 259 258
227 238 239 260 259
228 239 240 261 260
229 240 241 262 261
230 241 242 263 262
231 242 243 264 263
232 243 244 265 264
233 244 245 266 265

234 245 246 267 266
235 246 247 268 267
236 247 248 269 268
237 248 249 270 269
238 249 250 271 270
239 250 251 272 271
240 251 252 273 272
241 253 254 275 274
242 254 255 276 275
243 255 256 277 276
244 256 257 278 277
245 257 258 279 278
246 258 259 280 279
247 259 260 281 280
248 260 261 282 281
249 261 262 283 282
250 262 263 284 283
251 263 264 285 284
252 264 265 286 285
253 265 266 287 286
254 266 267 288 287
255 267 268 289 288
256 268 269 290 289
257 269 270 291 290
258 270 271 292 291
259 271 272 293 292
260 272 273 294 293
261 274 275 296 295
262 275 276 297 296
263 276 277 298 297
264 277 278 299 298
265 278 279 300 299
266 279 280 301 300
267 280 281 302 301
268 281 282 303 302
269 282 283 304 303
270 283 284 305 304
271 284 285 306 305
272 285 286 307 306
273 286 287 308 307
274 287 288 309 308
275 288 289 310 309
276 289 290 311 310
277 290 291 312 311
278 291 292 313 312
279 292 293 314 313
280 293 294 315 314
281 295 296 317 316
282 296 297 318 317
283 297 298 319 318
284 298 299 320 319
285 299 300 321 320
286 300 301 322 321
287 301 302 323 322
288 302 303 324 323
289 303 304 325 324
290 304 305 326 325

291 305 306 327 326
292 306 307 328 327
293 307 308 329 328
294 308 309 330 329
295 309 310 331 330
296 310 311 332 331
297 311 312 333 332
298 312 313 334 333
299 313 314 335 334
300 314 315 336 335
301 316 317 338 337
302 317 318 339 338
303 318 319 340 339
304 319 320 341 340
305 320 321 342 341
306 321 322 343 342
307 322 323 344 343
308 323 324 345 344
309 324 325 346 345
310 325 326 347 346
311 326 327 348 347
312 327 328 349 348
313 328 329 350 349
314 329 330 351 350
315 330 331 352 351
316 331 332 353 352
317 332 333 354 353
318 333 334 355 354
319 334 335 356 355
320 335 336 357 356
321 337 338 359 358
322 338 339 360 359
323 339 340 361 360
324 340 341 362 361
325 341 342 363 362
326 342 343 364 363
327 343 344 365 364
328 344 345 366 365
329 345 346 367 366
330 346 347 368 367
331 347 348 369 368
332 348 349 370 369
333 349 350 371 370
334 350 351 372 371
335 351 352 373 372
336 352 353 374 373
337 353 354 375 374
338 354 355 376 375
339 355 356 377 376
340 356 357 378 377
341 358 359 380 379
342 359 360 381 380
343 360 361 382 381
344 361 362 383 382
345 362 363 384 383
346 363 364 385 384
347 364 365 386 385

```
348 365 366 387 386
349 366 367 388 387
350 367 368 389 388
351 368 369 390 389
352 369 370 391 390
353 370 371 392 391
354 371 372 393 392
355 372 373 394 393
356 373 374 395 394
357 374 375 396 395
358 375 376 397 396
359 376 377 398 397
360 377 378 399 398
361 379 380 401 400
362 380 381 402 401
363 381 382 403 402
364 382 383 404 403
365 383 384 405 404
366 384 385 406 405
367 385 386 407 406
368 386 387 408 407
369 387 388 409 408
370 388 389 410 409
371 389 390 411 410
372 390 391 412 411
373 391 392 413 412
374 392 393 414 413
375 393 394 415 414
376 394 395 416 415
377 395 396 417 416
378 396 397 418 417
379 397 398 419 418
380 398 399 420 419
381 400 401 422 421
382 401 402 423 422
383 402 403 424 423
384 403 404 425 424
385 404 405 426 425
386 405 406 427 426
387 406 407 428 427
388 407 408 429 428
389 408 409 430 429
390 409 410 431 430
391 410 411 432 431
392 411 412 433 432
393 412 413 434 433
394 413 414 435 434
395 414 415 436 435
396 415 416 437 436
397 416 417 438 437
398 417 418 439 438
399 418 419 440 439
400 419 420 441 440];

LOADS=[
   1   100
   11  200
```

```
   21  100
   211 200
   221 400
   231 200
   421 100
   431 200
   441 100];


u=[0.007812780330000
0.007795985790000
0.007790265600000
0.007793796710000
0.007805800530000
0.007825504060000
0.007851588540000
0.007882265370000
0.007914881220000
0.007946472620000
0.007971595040000
0.007946471680000
0.007914880290000
0.007882263510000
0.007851585750000
0.007825501260000
0.007805796810000
0.007793792520000
0.007790260480000
0.007795979730000
0.007812773810000
0.007795986250000
0.007796098940000
0.007798642850000
0.007806572600000
0.007820450700000
0.007839823140000
0.007863640790000
0.007890008390000
0.007916349920000
0.007938289080000
0.007948354820000
0.007938288150000
0.007916348990000
0.007890006530000
0.007863637990000
0.007839819420000
0.007820446980000
0.007806568410000
0.007798637260000
0.007796093360000
0.007795979730000
0.007790266070000
0.007798642850000
0.007807670630000
0.007819370370000
0.007834839630000
```

0.007853996010000
0.007875828070000
0.007898621260000
0.007919610480000
0.007935019210000
0.007940920070000
0.007935019210000
0.007919609550000
0.007898619400000
0.007875825280000
0.007853993210000
0.007834835910000
0.007819365710000
0.007807665500000
0.007798637260000
0.007790259550000
0.007793797650000
0.007806573530000
0.007819370370000
0.007833590730000
0.007850145920000
0.007868986580000
0.007889296860000
0.007909327750000
0.007926743480000
0.007938786410000
0.007943091910000
0.007938785480000
0.007926742550000
0.007909325880000
0.007889294070000
0.007868982850000
0.007850142200000
0.007833586070000
0.007819364780000
0.007806567480000
0.007793791130000
0.007805801930000
0.007820451630000
0.007834840570000
0.007850145920000
0.007867030800000
0.007885505450000
0.007904673000000
0.007923036810000
0.007938478140000
0.007948857730000
0.007952550430000
0.007948856800000
0.007938476280000
0.007923034950000
0.007904670200000
0.007885501720000
0.007867026140000
0.007850141260000
0.007834834980000
0.007820446040000

0.007805794940000
0.007825505920000
0.007839824070000
0.007853996940000
0.007868986580000
0.007885505450000
0.007903417570000
0.007921981630000
0.007939595730000
0.007954352540000
0.007964225490000
0.007967689070000
0.007964224550000
0.007954351600000
0.007939593870000
0.007921978830000
0.007903414780000
0.007885501720000
0.007868981920000
0.007853992280000
0.007839818490000
0.007825499400000
0.007851590400000
0.007863641720000
0.007875829000000
0.007889297790000
0.007904673930000
0.007921981630000
0.007940299810000
0.007958124390000
0.007973264900000
0.007983539250000
0.007987197490000
0.007983538320000
0.007973263970000
0.007958121600000
0.007940297020000
0.007921977900000
0.007904669270000
0.007889292200000
0.007875823420000
0.007863636130000
0.007851583880000
0.007882267240000
0.007890010250000
0.007898623120000
0.007909329610000
0.007923037750000
0.007939596660000
0.007958124390000
0.007976873780000
0.007993550040000
0.008005225100000
0.008009466340000
0.008005224170000
0.007993549110000
0.007976871920000

0.007958121600000
0.007939592940000
0.007923033090000
0.007909324020000
0.007898617540000
0.007890003730000
0.007882260720000
0.007914884020000
0.007916351780000
0.007919612340000
0.007926745340000
0.007938479070000
0.007954353470000
0.007973265830000
0.007993550970000
0.008012705480000
0.008027221080000
0.008032802490000
0.008027220140000
0.008012704550000
0.007993548180000
0.007973263040000
0.007954349740000
0.007938475350000
0.007926740680000
0.007919606750000
0.007916346190000
0.007914877500000
0.007946475410000
0.007938290950000
0.007935022000000
0.007938788270000
0.007948858660000
0.007964226420000
0.007983539250000
0.008005226030000
0.008027221080000
0.008046248000000
0.008055617100000
0.008046247070000
0.008027219210000
0.008005223240000
0.007983537390000
0.007964223620000
0.007948854940000
0.007938782680000
0.007935016420000
0.007938284430000
0.007946468890000
0.007971597840000
0.007948357610000
0.007940922860000
0.007943094710000
0.007952552290000
0.007967690940000
0.007987198420000
0.008009467270000

0.008032803420000
0.008055617100000
0.008076403290000
0.008055616170000
0.008032801560000
0.008009464480000
0.007987195630000
0.007967687210000
0.007952547630000
0.007943089120000
0.007940917280000
0.007948351090000
0.007971591320000
0.007946475410000
0.007938290950000
0.007935022000000
0.007938788270000
0.007948858660000
0.007964226420000
0.007983539250000
0.008005225100000
0.008027221080000
0.008046247070000
0.008055617100000
0.008046247070000
0.008027219210000
0.008005223240000
0.007983536460000
0.007964223620000
0.007948854940000
0.007938782680000
0.007935016420000
0.007938284430000
0.007946467960000
0.007914884020000
0.007916351780000
0.007919612340000
0.007926745340000
0.007938479070000
0.007954353470000
0.007973265830000
0.007993550040000
0.008012705480000
0.008027220140000
0.008032802490000
0.008027220140000
0.008012704550000
0.007993548180000
0.007973263040000
0.007954349740000
0.007938474420000
0.007926740680000
0.007919606750000
0.007916345260000
0.007914876570000
0.007882267240000
0.007890010250000

0.007898622190000
0.007909328680000
0.007923036810000
0.007939596660000
0.007958124390000
0.007976873780000
0.007993550040000
0.008005225100000
0.008009465410000
0.008005224170000
0.007993548180000
0.007976870980000
0.007958121600000
0.007939592940000
0.007923033090000
0.007909324020000
0.007898616600000
0.007890003730000
0.007882259790000
0.007851590400000
0.007863641720000
0.007875829000000
0.007889296860000
0.007904673000000
0.007921980690000
0.007940299810000
0.007958123460000
0.007973264900000
0.007983538320000
0.007987196560000
0.007983537390000
0.007973263970000
0.007958121600000
0.007940297020000
0.007921977900000
0.007904669270000
0.007889292200000
0.007875823420000
0.007863635200000
0.007851582950000
0.007825505920000
0.007839824070000
0.007853996940000
0.007868986580000
0.007885505450000
0.007903417570000
0.007921980690000
0.007939595730000
0.007954352540000
0.007964225490000
0.007967688140000
0.007964224550000
0.007954350670000
0.007939592940000
0.007921977900000
0.007903413850000
0.007885500790000

0.007868981920000
0.007853991350000
0.007839817550000
0.007825498470000
0.007805801460000
0.007820451630000
0.007834839630000
0.007850145920000
0.007867029870000
0.007885504510000
0.007904673000000
0.007923035880000
0.007938477210000
0.007948856800000
0.007952549490000
0.007948855870000
0.007938476280000
0.007923034020000
0.007904670200000
0.007885500790000
0.007867026140000
0.007850140330000
0.007834834050000
0.007820445110000
0.007805794010000
0.007793797180000
0.007806572600000
0.007819369440000
0.007833590730000
0.007850144990000
0.007868985650000
0.007889295930000
0.007909327750000
0.007926743480000
0.007938785480000
0.007943090980000
0.007938784550000
0.007926741610000
0.007909324950000
0.007889293130000
0.007868981920000
0.007850141260000
0.007833585140000
0.007819363850000
0.007806566540000
0.007793790200000
0.007790265600000
0.007798642390000
0.007807670160000
0.007819369440000
0.007834839630000
0.007853996010000
0.007875827140000
0.007898620330000
0.007919609550000
0.007935019210000
0.007940919140000

```
0.007935018280000
0.007919608620000
0.007898618470000
0.007875824350000
0.007853992280000
0.007834834980000
0.007819364780000
0.007807664570000
0.007798635870000
0.007790258150000
0.007795985320000
0.007796098480000
0.007798641920000
0.007806572130000
0.007820449770000
0.007839822210000
0.007863639850000
0.007890007460000
0.007916348990000
0.007938287220000
0.007948353890000
0.007938287220000
0.007916348060000
0.007890005600000
0.007863637060000
0.007839818490000
0.007820446040000
0.007806567010000
0.007798636330000
0.007796091960000
0.007795978340000
0.007812779400000
0.007795984860000
0.007790264670000
0.007793795780000
0.007805799600000
0.007825503130000
0.007851587610000
0.007882264440000
0.007914880290000
0.007946471680000
0.007971594110000
0.007946470750000
0.007914879360000
0.007882261650000
0.007851584810000
0.007825499400000
0.007805795410000
0.007793791130000
0.007790259090000
0.007795978340000
0.007812771950000];
```

3. Algorithm for extracting moments diagrams for mat analysis using the Abaqus-based springs

```
%Clear variables from memory
clear
%Get the name of the input file
inputFile=input('Input File:','s');
fprintf('Reading data from the file: %s',inputFile)

%Διάβασμα αρχείου δεδομένων
eval(inputFile)

%Αποθήκευση συντεταγμένων σε πίνακες
X= NODES(:,2);
Y= NODES(:,3);

%Εύρεση του αριθμού πεπερασμένων στοιχείων
megethos= size(ELEMENTS);
Ar_stoixeiwn= megethos(1);

%Εύρεση του αριθμού των κόμβων του δυκτίου
megethos= size(NODES);
Ar_komvwn= megethos(1);

%Εύρεση του αριθμού των φορτίων που ασκούνται στους κόμβους του δυκτίου
megethos= size(LOADS);
Ar_fortiwn= megethos(1);

K=zeros(3*Ar_komvwn,3*Ar_komvwn);

for m=1:Ar_stoixeiwn

    k=zeros(12,12);
    %Εύρεση των κόμβων του κάθε στοιχείου για τον υπολογισμό των
διαστάσεων
    %του
    komvos1(m)=ELEMENTS(m,2);
    komvos2(m)=ELEMENTS(m,3);
    komvos3(m)=ELEMENTS(m,4);
    komvos4(m)=ELEMENTS(m,5);



    %Σχηματισμός μητρώου δυσκαμψίας στοιχείου abaqus
    k(1,1)=8333287.00;
    k(4,4)=k(1,1);
```

```
k(7,7)=k(1,1);
k(10,10)=k(1,1);
k(2,1)=1041660.88;
k(8,1)=k(2,1);
k(1,2)=k(2,1);
k(4,3)=k(2,1);
k(3,4)=k(2,1);
k(5,4)=k(2,1);
k(6,4)=k(2,1);
k(11,4)=k(2,1);
k(4,5)=k(2,1);
k(4,6)=k(2,1);
k(1,8)=k(2,1);
k(10,9)=k(2,1);
k(9,10)=k(2,1);
k(12,10)=k(2,1);
k(4,11)=k(2,1);
k(10,12)=k(2,1);
k(3,1)=-k(2,1);
k(6,1)=-k(2,1);
k(7,2)=-k(2,1);
k(1,3)=-k(2,1);
k(10,5)=-k(2,1);
k(1,6)=-k(2,1);
k(2,7)=-k(2,1);
k(8,7)=-k(2,1);
k(9,7)=-k(2,1);
k(12,7)=-k(2,1);
k(7,8)=-k(2,1);
k(7,9)=-k(2,1);
k(5,10)=-k(2,1);
k(11,10)=-k(2,1);
k(10,11)=-k(2,1);
k(7,12)=-k(2,1);
k(4,1)=-4166643.50;
k(7,1)=k(4,1);
k(1,4)=k(4,1);
k(10,4)=k(4,1);
k(1,7)=k(4,1);
k(10,7)=k(4,1);
k(4,10)=k(4,1);
k(7,10)=k(4,1);
k(5,1)=0;
k(9,1)=0;
k(10,1)=0;
k(11,1)=0;
k(12,1)=0;
k(4,2)=0;
k(10,2)=0;
k(7,3)=0;
k(10,3)=0;
k(2,4)=0;
k(7,4)=0;
k(8,4)=0;
k(9,4)=0;
k(12,4)=0;
k(1,5)=0;
```

```
k(7,5)=0;
k(7,6)=0;
k(10,6)=0;
k(3,7)=0;
k(4,7)=0;
k(5,7)=0;
k(6,7)=0;
k(11,7)=0;
k(4,8)=0;
k(10,8)=0;
k(1,9)=0;
k(4,9)=0;
k(1,10)=0;
k(2,10)=0;
k(3,10)=0;
k(6,10)=0;
k(8,10)=0;
k(1,11)=0;
k(7,11)=0;
k(1,12)=0;
k(4,12)=0;
k(2,2)=673208.19;
k(3,3)=k(2,2);
k(5,5)=k(2,2);
k(6,6)=k(2,2);
k(8,8)=k(2,2);
k(9,9)=k(2,2);
k(11,11)=k(2,2);
k(12,12)=k(2,2);
k(3,2)=-175781.25;
k(2,3)=k(3,2);
k(9,5)=k(3,2);
k(5,9)=k(3,2);
k(8,6)=k(3,2);
k(6,8)=k(3,2);
k(12,11)=k(3,2);
k(11,12)=k(3,2);
k(12,2)=-k(3,2);
k(2,12)=-k(3,2);
k(11,3)=-k(3,2);
k(3,11)=-k(3,2);
k(6,5)=-k(3,2);
k(5,6)=-k(3,2);
k(9,8)=-k(3,2);
k(8,9)=-k(3,2);
k(5,2)=173144.53;
k(9,3)=k(5,2);
k(3,9)=k(5,2);
k(2,5)=k(5,2);
k(12,6)=k(5,2);
k(6,12)=k(5,2);
k(8,11)=k(5,2);
k(11,8)=k(5,2);
k(6,2)=-58593.75;
k(8,3)=k(6,2);
k(3,8)=k(6,2);
k(12,5)=k(6,2);
```

```
k(5,12)=k(6,2);
k(2,6)=k(6,2);
k(11,9)=k(6,2);
k(9,11)=k(6,2);
k(9,2)=-k(6,2);
k(5,3)=-k(6,2);
k(3,5)=-k(6,2);
k(11,6)=-k(6,2);
k(6,11)=-k(6,2);
k(12,8)=-k(6,2);
k(8,12)=-k(6,2);
k(2,9)=-k(6,2);
k(8,2)=81997.25;
k(6,3)=k(8,2);
k(3,6)=k(8,2);
k(11,5)=k(8,2);
k(5,11)=k(8,2);
k(12,9)=k(8,2);
k(9,12)=k(8,2);
k(2,8)=k(8,2);
k(11,2)=-407519.53;
k(2,11)=k(11,2);
k(12,3)=k(11,2);
k(3,12)=k(11,2);
k(8,5)=k(11,2);
k(5,8)=k(11,2);
k(9,6)=k(11,2);
k(6,9)=k(11,2);




disp(k)

%Δημιουργία των δεικτλων για την εύρεση των βαθμών ελευθερίας
%προκειμένου να τοποθετηθει το μητρώο δυσκαμψίας του στοιχείου στο
%μητρώο δυσκαμψίας της πλάκας
be1=3*komvos1(m)-2;
be2=3*komvos2(m)-2;
be4=3*komvos3(m)-2;
be3=3*komvos4(m)-2;

%Δημιουργία του μητρώου δυσκαμψίας της πλάκας
K(be1:be1+2,be1:be1+2)=K(be1:be1+2,be1:be1+2)+k(1:3,1:3);
K(be2:be2+2,be2:be2+2)=K(be2:be2+2,be2:be2+2)+k(4:6,4:6);
K(be3:be3+2,be3:be3+2)=K(be3:be3+2,be3:be3+2)+k(7:9,7:9);
K(be4:be4+2,be4:be4+2)=K(be4:be4+2,be4:be4+2)+k(10:12,10:12);
K(be1:be1+2,be2:be2+2)=K(be1:be1+2,be2:be2+2)+k(1:3,4:6);
K(be2:be2+2,be1:be1+2)=K(be2:be2+2,be1:be1+2)+k(4:6,1:3);
K(be1:be1+2,be3:be3+2)=K(be1:be1+2,be3:be3+2)+k(1:3,7:9);
K(be3:be3+2,be1:be1+2)=K(be3:be3+2,be1:be1+2)+k(7:9,1:3);
K(be1:be1+2,be4:be4+2)=K(be1:be1+2,be4:be4+2)+k(1:3,10:12);
K(be4:be4+2,be1:be1+2)=K(be4:be4+2,be1:be1+2)+k(10:12,1:3);
K(be2:be2+2,be3:be3+2)=K(be2:be2+2,be3:be3+2)+k(4:6,7:9);
K(be3:be3+2,be2:be2+2)=K(be3:be3+2,be2:be2+2)+k(7:9,4:6);
K(be2:be2+2,be4:be4+2)=K(be2:be2+2,be4:be4+2)+k(4:6,10:12);
```

```
    K(be4:be4+2,be2:be2+2)=K(be4:be4+2,be2:be2+2)+k(10:12,4:6);
    K(be3:be3+2,be4:be4+2)=K(be3:be3+2,be4:be4+2)+k(7:9,10:12);
    K(be4:be4+2,be3:be3+2)=K(be4:be4+2,be3:be3+2)+k(10:12,7:9);
end

%Εκτύπωση του μητρώου δυσκαμψίας της πλάκας
fprintf('\n\n Mitrwo dyskampsias plakas: K=\n');
disp(K)

fortio=zeros(3*Ar_komvwn,1);
for i=1:Ar_fortiwn
    fortio(3*LOADS(i,1)-2,1)=LOADS(i,2);
end

disp(fortio)

Meso1=(Y(Ar_komvwn)-Y(1))/2;
Meso2=(X(Ar_komvwn)-X(1))/2;

%kel=zeros(Ar_komvwn,1);
%for i=1:Ar_komvwn

 %   kel(i,1)=336.4134*0.55*(1+2*((X(i,1)/Meso2-1)^6+(Y(i,1)/Meso1-1)^6));
%end

I=zeros(3*Ar_komvwn);
for i=1:Ar_komvwn
    I(3*i-2,3*i-2)=kel(i,1);
end
Kol=K+I;


u=inv(Kol)*fortio;

%Εκτύπωση των μετατοπίσεων των βαθμών ελευθερίας της πλάκας
fprintf('\n\n Μετατοπίσεις: u=\n');
ij=0;
for i=1:3:3*Ar_komvwn
    ij=ij+1;
    uplot(ij,1)=u(i,1);
end

ij=0;
for i=1:3:3*Ar_komvwn
    ij=ij+1;
    fortioplot(ij,1)=fortio(i,1);
end

disp(uplot)

disp(u)
%disp(k)
```

```
for i=1:Ar_komvwn
    if NODES(i,2)==0 && NODES(i,3)==Meso1
        simeio=NODES(i,1);
    end
end

for i=1:Ar_stoixeiwn
    if ELEMENTS(i,2)==simeio
        stoixio=ELEMENTS(i,1);
    end
end

jk=(X(Ar_komvwn)-X(1))/0.5+1;
M=zeros(jk,1);
V=zeros((jk-1)*2,1);
entmeg=zeros(12,1);
ij=1;
deiktis1=1;
deiktis2=2;
stoixioT=stoixio+(jk-2);



for i=stoixio:stoixioT
   w=zeros(12,1);
   be1=3*komvos1(i)-2;
   be2=3*komvos2(i)-2;
   be4=3*komvos3(i)-2;
   be3=3*komvos4(i)-2;
   w(1:3,1)=u(be1:be1+2,1);
   w(4:6,1)=u(be2:be2+2,1);
   w(7:9,1)=u(be3:be3+2,1);
   w(10:12,1)=u(be4:be4+2,1);
   entmeg=k*w;
   V(ij,1)=entmeg(1,1);
   V(ij+1,1)=entmeg(4,1);
   ij=ij+2;
   if deiktis1==1
      M(1,1)=entmeg(3,1);
      deiktis1=2;
   end
   M(deiktis2,1)=entmeg(6,1);
   deiktis2=deiktis2+1;
end


disp(V)
disp(M)

xp=X-5;
yp=Y-5;

[V,W]=meshgrid(-5:0.02:5,-5:0.02:5);
```

```
figure(2);

Z2=griddata(xp,yp,-uplot*100,V,W,'cubic');

surf(V,W,Z2,'LineStyle','none');

figure(3);

Z3=griddata(xp,yp,kel,V,W,'cubic');

surfc(V,W,Z3,'LineStyle','none');
set(gca,'XTick',[-5 -2.5 0 2.5 5],'YTick',[-5 -2.5 0 2.5 5]);  %
,'Zlim',[0 12500]

colorbar

% Create xlabel
xlabel('x (m)');

% Create ylabel
ylabel('y (m)');

% Create zlabel
zlabel('Ks (kN/m)');

figure(4);

Z3=griddata(xp,yp,fortioplot,V,W,'cubic');

surfc(V,W,Z3,'LineStyle','none');
set(gca,'XTick',[-5 -2.5 0 2.5 5],'YTick',[-5 -2.5 0 2.5 5]);  %
,'Zlim',[0 12500]

colorbar

% Create xlabel
xlabel('x (m)');

% Create ylabel
ylabel('y (m)');

% Create zlabel
zlabel('Ks (kN/m)');
```

4. Example of a data entry file for mat analysis using the Abaqus-based springs

```
 NODES=[
1   0   0
2   0.5 0
3   1   0
4   1.5 0
5   2   0
6   2.5 0
7   3   0
8   3.5 0
9   4   0
10  4.5 0
11  5   0
12  5.5 0
13  6   0
14  6.5 0
15  7   0
16  7.5 0
17  8   0
18  8.5 0
19  9   0
20  9.5 0
21  10  0
22  0   0.5
23  0.5 0.5
24  1   0.5
25  1.5 0.5
26  2   0.5
27  2.5 0.5
28  3   0.5
29  3.5 0.5
30  4   0.5
31  4.5 0.5
32  5   0.5
33  5.5 0.5
34  6   0.5
35  6.5 0.5
36  7   0.5
37  7.5 0.5
38  8   0.5
39  8.5 0.5
40  9   0.5
41  9.5 0.5
42  10  0.5
43  0   1
44  0.5 1
45  1   1
46  1.5 1
```

```
47  2   1
48  2.5 1
49  3   1
50  3.5 1
51  4   1
52  4.5 1
53  5   1
54  5.5 1
55  6   1
56  6.5 1
57  7   1
58  7.5 1
59  8   1
60  8.5 1
61  9   1
62  9.5 1
63  10  1
64  0   1.5
65  0.5 1.5
66  1   1.5
67  1.5 1.5
68  2   1.5
69  2.5 1.5
70  3   1.5
71  3.5 1.5
72  4   1.5
73  4.5 1.5
74  5   1.5
75  5.5 1.5
76  6   1.5
77  6.5 1.5
78  7   1.5
79  7.5 1.5
80  8   1.5
81  8.5 1.5
82  9   1.5
83  9.5 1.5
84  10  1.5
85  0   2
86  0.5 2
87  1   2
88  1.5 2
89  2   2
90  2.5 2
91  3   2
92  3.5 2
93  4   2
94  4.5 2
95  5   2
96  5.5 2
97  6   2
98  6.5 2
99  7   2
100 7.5 2
101 8   2
102 8.5 2
103 9   2
```

```
104 9.5 2
105 10  2
106 0   2.5
107 0.5 2.5
108 1   2.5
109 1.5 2.5
110 2   2.5
111 2.5 2.5
112 3   2.5
113 3.5 2.5
114 4   2.5
115 4.5 2.5
116 5   2.5
117 5.5 2.5
118 6   2.5
119 6.5 2.5
120 7   2.5
121 7.5 2.5
122 8   2.5
123 8.5 2.5
124 9   2.5
125 9.5 2.5
126 10  2.5
127 0   3
128 0.5 3
129 1   3
130 1.5 3
131 2   3
132 2.5 3
133 3   3
134 3.5 3
135 4   3
136 4.5 3
137 5   3
138 5.5 3
139 6   3
140 6.5 3
141 7   3
142 7.5 3
143 8   3
144 8.5 3
145 9   3
146 9.5 3
147 10  3
148 0   3.5
149 0.5 3.5
150 1   3.5
151 1.5 3.5
152 2   3.5
153 2.5 3.5
154 3   3.5
155 3.5 3.5
156 4   3.5
157 4.5 3.5
158 5   3.5
159 5.5 3.5
160 6   3.5
```

```
161 6.5 3.5
162 7   3.5
163 7.5 3.5
164 8   3.5
165 8.5 3.5
166 9   3.5
167 9.5 3.5
168 10  3.5
169 0   4
170 0.5 4
171 1   4
172 1.5 4
173 2   4
174 2.5 4
175 3   4
176 3.5 4
177 4   4
178 4.5 4
179 5   4
180 5.5 4
181 6   4
182 6.5 4
183 7   4
184 7.5 4
185 8   4
186 8.5 4
187 9   4
188 9.5 4
189 10  4
190 0   4.5
191 0.5 4.5
192 1   4.5
193 1.5 4.5
194 2   4.5
195 2.5 4.5
196 3   4.5
197 3.5 4.5
198 4   4.5
199 4.5 4.5
200 5   4.5
201 5.5 4.5
202 6   4.5
203 6.5 4.5
204 7   4.5
205 7.5 4.5
206 8   4.5
207 8.5 4.5
208 9   4.5
209 9.5 4.5
210 10  4.5
211 0   5
212 0.5 5
213 1   5
214 1.5 5
215 2   5
216 2.5 5
217 3   5
```

```
218 3.5 5
219 4   5
220 4.5 5
221 5   5
222 5.5 5
223 6   5
224 6.5 5
225 7   5
226 7.5 5
227 8   5
228 8.5 5
229 9   5
230 9.5 5
231 10  5
232 0   5.5
233 0.5 5.5
234 1   5.5
235 1.5 5.5
236 2   5.5
237 2.5 5.5
238 3   5.5
239 3.5 5.5
240 4   5.5
241 4.5 5.5
242 5   5.5
243 5.5 5.5
244 6   5.5
245 6.5 5.5
246 7   5.5
247 7.5 5.5
248 8   5.5
249 8.5 5.5
250 9   5.5
251 9.5 5.5
252 10  5.5
253 0   6
254 0.5 6
255 1   6
256 1.5 6
257 2   6
258 2.5 6
259 3   6
260 3.5 6
261 4   6
262 4.5 6
263 5   6
264 5.5 6
265 6   6
266 6.5 6
267 7   6
268 7.5 6
269 8   6
270 8.5 6
271 9   6
272 9.5 6
273 10  6
274 0   6.5
```

275 0.5 6.5
276 1 6.5
277 1.5 6.5
278 2 6.5
279 2.5 6.5
280 3 6.5
281 3.5 6.5
282 4 6.5
283 4.5 6.5
284 5 6.5
285 5.5 6.5
286 6 6.5
287 6.5 6.5
288 7 6.5
289 7.5 6.5
290 8 6.5
291 8.5 6.5
292 9 6.5
293 9.5 6.5
294 10 6.5
295 0 7
296 0.5 7
297 1 7
298 1.5 7
299 2 7
300 2.5 7
301 3 7
302 3.5 7
303 4 7
304 4.5 7
305 5 7
306 5.5 7
307 6 7
308 6.5 7
309 7 7
310 7.5 7
311 8 7
312 8.5 7
313 9 7
314 9.5 7
315 10 7
316 0 7.5
317 0.5 7.5
318 1 7.5
319 1.5 7.5
320 2 7.5
321 2.5 7.5
322 3 7.5
323 3.5 7.5
324 4 7.5
325 4.5 7.5
326 5 7.5
327 5.5 7.5
328 6 7.5
329 6.5 7.5
330 7 7.5
331 7.5 7.5

```
332 8   7.5
333 8.5 7.5
334 9   7.5
335 9.5 7.5
336 10  7.5
337 0   8
338 0.5 8
339 1   8
340 1.5 8
341 2   8
342 2.5 8
343 3   8
344 3.5 8
345 4   8
346 4.5 8
347 5   8
348 5.5 8
349 6   8
350 6.5 8
351 7   8
352 7.5 8
353 8   8
354 8.5 8
355 9   8
356 9.5 8
357 10  8
358 0   8.5
359 0.5 8.5
360 1   8.5
361 1.5 8.5
362 2   8.5
363 2.5 8.5
364 3   8.5
365 3.5 8.5
366 4   8.5
367 4.5 8.5
368 5   8.5
369 5.5 8.5
370 6   8.5
371 6.5 8.5
372 7   8.5
373 7.5 8.5
374 8   8.5
375 8.5 8.5
376 9   8.5
377 9.5 8.5
378 10  8.5
379 0   9
380 0.5 9
381 1   9
382 1.5 9
383 2   9
384 2.5 9
385 3   9
386 3.5 9
387 4   9
388 4.5 9
```

```
389 5   9
390 5.5 9
391 6   9
392 6.5 9
393 7   9
394 7.5 9
395 8   9
396 8.5 9
397 9   9
398 9.5 9
399 10  9
400 0   9.5
401 0.5 9.5
402 1   9.5
403 1.5 9.5
404 2   9.5
405 2.5 9.5
406 3   9.5
407 3.5 9.5
408 4   9.5
409 4.5 9.5
410 5   9.5
411 5.5 9.5
412 6   9.5
413 6.5 9.5
414 7   9.5
415 7.5 9.5
416 8   9.5
417 8.5 9.5
418 9   9.5
419 9.5 9.5
420 10  9.5
421 0   10
422 0.5 10
423 1   10
424 1.5 10
425 2   10
426 2.5 10
427 3   10
428 3.5 10
429 4   10
430 4.5 10
431 5   10
432 5.5 10
433 6   10
434 6.5 10
435 7   10
436 7.5 10
437 8   10
438 8.5 10
439 9   10
440 9.5 10
441 10  10];

ELEMENTS=[
1   1   2   23  22
2   2   3   24  23
```

3	3	4	25	24
4	4	5	26	25
5	5	6	27	26
6	6	7	28	27
7	7	8	29	28
8	8	9	30	29
9	9	10	31	30
10	10	11	32	31
11	11	12	33	32
12	12	13	34	33
13	13	14	35	34
14	14	15	36	35
15	15	16	37	36
16	16	17	38	37
17	17	18	39	38
18	18	19	40	39
19	19	20	41	40
20	20	21	42	41
21	22	23	44	43
22	23	24	45	44
23	24	25	46	45
24	25	26	47	46
25	26	27	48	47
26	27	28	49	48
27	28	29	50	49
28	29	30	51	50
29	30	31	52	51
30	31	32	53	52
31	32	33	54	53
32	33	34	55	54
33	34	35	56	55
34	35	36	57	56
35	36	37	58	57
36	37	38	59	58
37	38	39	60	59
38	39	40	61	60
39	40	41	62	61
40	41	42	63	62
41	43	44	65	64
42	44	45	66	65
43	45	46	67	66
44	46	47	68	67
45	47	48	69	68
46	48	49	70	69
47	49	50	71	70
48	50	51	72	71
49	51	52	73	72
50	52	53	74	73
51	53	54	75	74
52	54	55	76	75
53	55	56	77	76
54	56	57	78	77
55	57	58	79	78
56	58	59	80	79
57	59	60	81	80
58	60	61	82	81
59	61	62	83	82

60 62 63 84 83
61 64 65 86 85
62 65 66 87 86
63 66 67 88 87
64 67 68 89 88
65 68 69 90 89
66 69 70 91 90
67 70 71 92 91
68 71 72 93 92
69 72 73 94 93
70 73 74 95 94
71 74 75 96 95
72 75 76 97 96
73 76 77 98 97
74 77 78 99 98
75 78 79 100 99
76 79 80 101 100
77 80 81 102 101
78 81 82 103 102
79 82 83 104 103
80 83 84 105 104
81 85 86 107 106
82 86 87 108 107
83 87 88 109 108
84 88 89 110 109
85 89 90 111 110
86 90 91 112 111
87 91 92 113 112
88 92 93 114 113
89 93 94 115 114
90 94 95 116 115
91 95 96 117 116
92 96 97 118 117
93 97 98 119 118
94 98 99 120 119
95 99 100 121 120
96 100 101 122 121
97 101 102 123 122
98 102 103 124 123
99 103 104 125 124
100 104 105 126 125
101 106 107 128 127
102 107 108 129 128
103 108 109 130 129
104 109 110 131 130
105 110 111 132 131
106 111 112 133 132
107 112 113 134 133
108 113 114 135 134
109 114 115 136 135
110 115 116 137 136
111 116 117 138 137
112 117 118 139 138
113 118 119 140 139
114 119 120 141 140
115 120 121 142 141
116 121 122 143 142

117 122 123 144 143
118 123 124 145 144
119 124 125 146 145
120 125 126 147 146
121 127 128 149 148
122 128 129 150 149
123 129 130 151 150
124 130 131 152 151
125 131 132 153 152
126 132 133 154 153
127 133 134 155 154
128 134 135 156 155
129 135 136 157 156
130 136 137 158 157
131 137 138 159 158
132 138 139 160 159
133 139 140 161 160
134 140 141 162 161
135 141 142 163 162
136 142 143 164 163
137 143 144 165 164
138 144 145 166 165
139 145 146 167 166
140 146 147 168 167
141 148 149 170 169
142 149 150 171 170
143 150 151 172 171
144 151 152 173 172
145 152 153 174 173
146 153 154 175 174
147 154 155 176 175
148 155 156 177 176
149 156 157 178 177
150 157 158 179 178
151 158 159 180 179
152 159 160 181 180
153 160 161 182 181
154 161 162 183 182
155 162 163 184 183
156 163 164 185 184
157 164 165 186 185
158 165 166 187 186
159 166 167 188 187
160 167 168 189 188
161 169 170 191 190
162 170 171 192 191
163 171 172 193 192
164 172 173 194 193
165 173 174 195 194
166 174 175 196 195
167 175 176 197 196
168 176 177 198 197
169 177 178 199 198
170 178 179 200 199
171 179 180 201 200
172 180 181 202 201
173 181 182 203 202

174 182 183 204 203
175 183 184 205 204
176 184 185 206 205
177 185 186 207 206
178 186 187 208 207
179 187 188 209 208
180 188 189 210 209
181 190 191 212 211
182 191 192 213 212
183 192 193 214 213
184 193 194 215 214
185 194 195 216 215
186 195 196 217 216
187 196 197 218 217
188 197 198 219 218
189 198 199 220 219
190 199 200 221 220
191 200 201 222 221
192 201 202 223 222
193 202 203 224 223
194 203 204 225 224
195 204 205 226 225
196 205 206 227 226
197 206 207 228 227
198 207 208 229 228
199 208 209 230 229
200 209 210 231 230
201 211 212 233 232
202 212 213 234 233
203 213 214 235 234
204 214 215 236 235
205 215 216 237 236
206 216 217 238 237
207 217 218 239 238
208 218 219 240 239
209 219 220 241 240
210 220 221 242 241
211 221 222 243 242
212 222 223 244 243
213 223 224 245 244
214 224 225 246 245
215 225 226 247 246
216 226 227 248 247
217 227 228 249 248
218 228 229 250 249
219 229 230 251 250
220 230 231 252 251
221 232 233 254 253
222 233 234 255 254
223 234 235 256 255
224 235 236 257 256
225 236 237 258 257
226 237 238 259 258
227 238 239 260 259
228 239 240 261 260
229 240 241 262 261
230 241 242 263 262

231 242 243 264 263
232 243 244 265 264
233 244 245 266 265
234 245 246 267 266
235 246 247 268 267
236 247 248 269 268
237 248 249 270 269
238 249 250 271 270
239 250 251 272 271
240 251 252 273 272
241 253 254 275 274
242 254 255 276 275
243 255 256 277 276
244 256 257 278 277
245 257 258 279 278
246 258 259 280 279
247 259 260 281 280
248 260 261 282 281
249 261 262 283 282
250 262 263 284 283
251 263 264 285 284
252 264 265 286 285
253 265 266 287 286
254 266 267 288 287
255 267 268 289 288
256 268 269 290 289
257 269 270 291 290
258 270 271 292 291
259 271 272 293 292
260 272 273 294 293
261 274 275 296 295
262 275 276 297 296
263 276 277 298 297
264 277 278 299 298
265 278 279 300 299
266 279 280 301 300
267 280 281 302 301
268 281 282 303 302
269 282 283 304 303
270 283 284 305 304
271 284 285 306 305
272 285 286 307 306
273 286 287 308 307
274 287 288 309 308
275 288 289 310 309
276 289 290 311 310
277 290 291 312 311
278 291 292 313 312
279 292 293 314 313
280 293 294 315 314
281 295 296 317 316
282 296 297 318 317
283 297 298 319 318
284 298 299 320 319
285 299 300 321 320
286 300 301 322 321
287 301 302 323 322

288 302 303 324 323
289 303 304 325 324
290 304 305 326 325
291 305 306 327 326
292 306 307 328 327
293 307 308 329 328
294 308 309 330 329
295 309 310 331 330
296 310 311 332 331
297 311 312 333 332
298 312 313 334 333
299 313 314 335 334
300 314 315 336 335
301 316 317 338 337
302 317 318 339 338
303 318 319 340 339
304 319 320 341 340
305 320 321 342 341
306 321 322 343 342
307 322 323 344 343
308 323 324 345 344
309 324 325 346 345
310 325 326 347 346
311 326 327 348 347
312 327 328 349 348
313 328 329 350 349
314 329 330 351 350
315 330 331 352 351
316 331 332 353 352
317 332 333 354 353
318 333 334 355 354
319 334 335 356 355
320 335 336 357 356
321 337 338 359 358
322 338 339 360 359
323 339 340 361 360
324 340 341 362 361
325 341 342 363 362
326 342 343 364 363
327 343 344 365 364
328 344 345 366 365
329 345 346 367 366
330 346 347 368 367
331 347 348 369 368
332 348 349 370 369
333 349 350 371 370
334 350 351 372 371
335 351 352 373 372
336 352 353 374 373
337 353 354 375 374
338 354 355 376 375
339 355 356 377 376
340 356 357 378 377
341 358 359 380 379
342 359 360 381 380
343 360 361 382 381
344 361 362 383 382

```
345 362 363 384 383
346 363 364 385 384
347 364 365 386 385
348 365 366 387 386
349 366 367 388 387
350 367 368 389 388
351 368 369 390 389
352 369 370 391 390
353 370 371 392 391
354 371 372 393 392
355 372 373 394 393
356 373 374 395 394
357 374 375 396 395
358 375 376 397 396
359 376 377 398 397
360 377 378 399 398
361 379 380 401 400
362 380 381 402 401
363 381 382 403 402
364 382 383 404 403
365 383 384 405 404
366 384 385 406 405
367 385 386 407 406
368 386 387 408 407
369 387 388 409 408
370 388 389 410 409
371 389 390 411 410
372 390 391 412 411
373 391 392 413 412
374 392 393 414 413
375 393 394 415 414
376 394 395 416 415
377 395 396 417 416
378 396 397 418 417
379 397 398 419 418
380 398 399 420 419
381 400 401 422 421
382 401 402 423 422
383 402 403 424 423
384 403 404 425 424
385 404 405 426 425
386 405 406 427 426
387 406 407 428 427
388 407 408 429 428
389 408 409 430 429
390 409 410 431 430
391 410 411 432 431
392 411 412 433 432
393 412 413 434 433
394 413 414 435 434
395 414 415 436 435
396 415 416 437 436
397 416 417 438 437
398 417 418 439 438
399 418 419 440 439
400 419 420 441 440];
```

```
LOADS=[
   1   100
   11  200
   21  100
   211 200
   221 400
   231 200
   421 100
   431 200
   441 100];



kel=[1897.8
1498.3
1270.6
1220.3
1159.6
1138.2
1116.1
1109.6
1107.3
1114.5
1120.8
1114.9
1106.9
1109.6
1116.5
1137.2
1159.8
1220.2
1270.3
1498.7
1897.7
1498
686.4
514.9
492.4
455.4
446.1
432.9
433
430.6
431.5
435.4
433.2
429.9
433
432.9
448.3
455.1
491.2
516.9
685.4
1498.2
1270.7
```

516.1
361.9
336.2
307.9
301.6
289.6
287.7
284.5
286.6
284.2
284.5
284.6
287.7
290.2
299.2
307.8
336.9
361.2
515.2
1270.9
1220.5
490.8
337.7
315.8
283.1
275.5
263.2
264.1
260.3
258.1
259.6
259.7
258.8
264.1
263.2
277
281.4
315.6
338.6
491.5
1220.2
1159.5
455.9
306.1
283.7
252.1
245.4
236.4
231
227.9
227.6
226.1
227.5
230.1
230.4
236.6
246.1

254.6
283.2
307.9
454.5
1160.4
1137.7
446.8
300.6
277.1
246
238.8
224.8
226.1
220
221.6
219
222.3
218.3
225.2
225.5
236.3
244.2
276.8
298.4
446.9
1137.6
1115.7
434.4
290.3
263.3
234.9
226.3
217
211.6
211.5
207.7
208.2
208.7
209.9
215
216.3
227.3
235.6
264.8
291
433
1116
1110.1
432.2
286.9
262.6
232
224.5
213.4
211.6
208.2
208.6

206.7
209.5
207.3
210.2
213.1
224.3
232.5
264.1
286
434.5
1109.8
1106.5
431.4
285.3
259.6
228.6
219.7
210
206.4
207.1
204.8
206
205.7
204.5
209
209.9
221.6
227
258.1
285.7
429
1106.7
1114.1
433.8
284.5
258.9
229.3
221.4
211.1
207.1
206.6
208.4
209.9
208.3
207
208.5
207.8
220
227.6
261.3
283.5
435.4
1113.9
1121.2
434.8
284.2
258

226.1
217
208.1
206.5
204.4
210.8
215.2
211.5
204.1
208.1
208.3
219.1
227.6
258.8
283.1
435.5
1120.4
1114.1
433.8
284.6
259.1
229.5
221.5
210.2
209.4
204.7
210.6
209.1
208.4
207.3
207.8
210.8
219.1
226.8
261.3
283.6
434
1114.6
1106.6
431.3
284.4
258.7
227.9
219.8
209.2
208.9
205.2
207.3
204.4
205.8
203.7
208
209.1
220.7
230.3
257.3
284.5

431.3
1106.5
1110.2
431.5
289.1
263.2
233.3
222.9
213.4
210.2
208
206.1
208.9
207
209.7
212.8
212.6
224.5
231.9
263.3
289.2
431.5
1110.2
1115.9
434.4
288.8
264.7
235.6
228.8
214.8
215.1
210.2
210.3
208.3
210.8
207.5
213.3
215.3
226.5
234.9
264.8
288.8
434.4
1115.9
1137.5
446.9
300
276.1
244.4
236.3
227.8
223.6
219.1
219
220.4
219.2
220.8

226.3
227.1
237.3
246.7
274.7
300
446.9
1137.5
1160.1
453.8
308.7
282.3
253.8
246.8
233.4
233.7
229.6
228.5
226.1
229.1
226.9
231.9
233.1
247.6
251.3
284.7
307.8
454.4
1160.4
1220.3
492.2
339
313.3
284.8
276.2
264.8
261.7
258
259.5
259.5
259.6
259.6
264.3
264
277.2
282.3
315.7
338.5
491.1
1220
1270.5
515.5
360.8
338.4
305.6
299.2
290.3

```
288.5
286
282.8
284.7
284.4
284.5
287.8
290.2
299.3
307.8
336.6
360.8
516.1
1271.1
1498.5
685.5
516.1
490.9
456.7
447.1
433
432.8
429.8
435.3
434.7
433.3
429.8
432.5
432.8
447.7
454.4
492.5
515.7
685.8
1497.8
1897.7
1498.5
1270.5
1220.5
1159.4
1138
1116.1
1109.6
1107.2
1113.9
1120.6
1114.9
1106.4
1110.9
1115.5
1138.3
1159.7
1220.1
1270.5
1498.5
1898];
```

5. Algorithm for extracting moments from mat analysis with proposed equation for K_{el}

```
%Clear variables from memory
clear
%Get the name of the input file
inputFile=input('Input File:','s');
fprintf('Reading data from the file: %s',inputFile)

%Διάβασμα αρχείου δεδομένων
eval(inputFile)

%Αποθήκευση συντεταγμένων σε πίνακες
X= NODES(:,2);
Y= NODES(:,3);

%Εύρεση του αριθμού πεπερασμένων στοιχείων
megethos= size(ELEMENTS);
Ar_stoixeiwn= megethos(1);

%Εύρεση του αριθμού των κόμβων του δυκτίου
megethos= size(NODES);
Ar_komvwn= megethos(1);

%Εύρεση του αριθμού των φορτίων που ασκούνται στους κόμβους του δυκτίου
megethos= size(LOADS);
Ar_fortiwn= megethos(1);

K=zeros(3*Ar_komvwn,3*Ar_komvwn);

for m=1:Ar_stoixeiwn

    k=zeros(12,12);
    %Εύρεση των κόμβων του κάθε στοιχείου για τον υπολογισμό των
διαστάσεων
    %του
    komvos1(m)=ELEMENTS(m,2);
    komvos2(m)=ELEMENTS(m,3);
    komvos3(m)=ELEMENTS(m,4);
    komvos4(m)=ELEMENTS(m,5);



    %Σχηματισμός μητρώου δυσκαμψίας στοιχείου abaqus
    k(1,1)=8333287.00;
    k(4,4)=k(1,1);
    k(7,7)=k(1,1);
    k(10,10)=k(1,1);
```

```
k(2,1)=1041660.88;
k(8,1)=k(2,1);
k(1,2)=k(2,1);
k(4,3)=k(2,1);
k(3,4)=k(2,1);
k(5,4)=k(2,1);
k(6,4)=k(2,1);
k(11,4)=k(2,1);
k(4,5)=k(2,1);
k(4,6)=k(2,1);
k(1,8)=k(2,1);
k(10,9)=k(2,1);
k(9,10)=k(2,1);
k(12,10)=k(2,1);
k(4,11)=k(2,1);
k(10,12)=k(2,1);
k(3,1)=-k(2,1);
k(6,1)=-k(2,1);
k(7,2)=-k(2,1);
k(1,3)=-k(2,1);
k(10,5)=-k(2,1);
k(1,6)=-k(2,1);
k(2,7)=-k(2,1);
k(8,7)=-k(2,1);
k(9,7)=-k(2,1);
k(12,7)=-k(2,1);
k(7,8)=-k(2,1);
k(7,9)=-k(2,1);
k(5,10)=-k(2,1);
k(11,10)=-k(2,1);
k(10,11)=-k(2,1);
k(7,12)=-k(2,1);
k(4,1)=-4166643.50;
k(7,1)=k(4,1);
k(1,4)=k(4,1);
k(10,4)=k(4,1);
k(1,7)=k(4,1);
k(10,7)=k(4,1);
k(4,10)=k(4,1);
k(7,10)=k(4,1);
k(5,1)=0;
k(9,1)=0;
k(10,1)=0;
k(11,1)=0;
k(12,1)=0;
k(4,2)=0;
k(10,2)=0;
k(7,3)=0;
k(10,3)=0;
k(2,4)=0;
k(7,4)=0;
k(8,4)=0;
k(9,4)=0;
k(12,4)=0;
k(1,5)=0;
k(7,5)=0;
k(7,6)=0;
```

```
k(10,6)=0;
k(3,7)=0;
k(4,7)=0;
k(5,7)=0;
k(6,7)=0;
k(11,7)=0;
k(4,8)=0;
k(10,8)=0;
k(1,9)=0;
k(4,9)=0;
k(1,10)=0;
k(2,10)=0;
k(3,10)=0;
k(6,10)=0;
k(8,10)=0;
k(1,11)=0;
k(7,11)=0;
k(1,12)=0;
k(4,12)=0;
k(2,2)=673208.19;
k(3,3)=k(2,2);
k(5,5)=k(2,2);
k(6,6)=k(2,2);
k(8,8)=k(2,2);
k(9,9)=k(2,2);
k(11,11)=k(2,2);
k(12,12)=k(2,2);
k(3,2)=-175781.25;
k(2,3)=k(3,2);
k(9,5)=k(3,2);
k(5,9)=k(3,2);
k(8,6)=k(3,2);
k(6,8)=k(3,2);
k(12,11)=k(3,2);
k(11,12)=k(3,2);
k(12,2)=-k(3,2);
k(2,12)=-k(3,2);
k(11,3)=-k(3,2);
k(3,11)=-k(3,2);
k(6,5)=-k(3,2);
k(5,6)=-k(3,2);
k(9,8)=-k(3,2);
k(8,9)=-k(3,2);
k(5,2)=173144.53;
k(9,3)=k(5,2);
k(3,9)=k(5,2);
k(2,5)=k(5,2);
k(12,6)=k(5,2);
k(6,12)=k(5,2);
k(8,11)=k(5,2);
k(11,8)=k(5,2);
k(6,2)=-58593.75;
k(8,3)=k(6,2);
k(3,8)=k(6,2);
k(12,5)=k(6,2);
k(5,12)=k(6,2);
k(2,6)=k(6,2);
```

```
k(11,9)=k(6,2);
k(9,11)=k(6,2);
k(9,2)=-k(6,2);
k(5,3)=-k(6,2);
k(3,5)=-k(6,2);
k(11,6)=-k(6,2);
k(6,11)=-k(6,2);
k(12,8)=-k(6,2);
k(8,12)=-k(6,2);
k(2,9)=-k(6,2);
k(8,2)=81997.25;
k(6,3)=k(8,2);
k(3,6)=k(8,2);
k(11,5)=k(8,2);
k(5,11)=k(8,2);
k(12,9)=k(8,2);
k(9,12)=k(8,2);
k(2,8)=k(8,2);
k(11,2)=-407519.53;
k(2,11)=k(11,2);
k(12,3)=k(11,2);
k(3,12)=k(11,2);
k(8,5)=k(11,2);
k(5,8)=k(11,2);
k(9,6)=k(11,2);
k(6,9)=k(11,2);



disp(k)

%Δημιουργία των δεικτλων για την εύρεση των βαθμών ελευθερίας
%προκειμένου να τοποθετηθει το μητρώο δυσκαμψίας του στοιχείου στο
%μητρώο δυσκαμψίας της πλάκας
be1=3*komvos1(m)-2;
be2=3*komvos2(m)-2;
be4=3*komvos3(m)-2;
be3=3*komvos4(m)-2;

%Δημιουργία του μητρώου δυσκαμψίας της πλάκας
K(be1:be1+2,be1:be1+2)=K(be1:be1+2,be1:be1+2)+k(1:3,1:3);
K(be2:be2+2,be2:be2+2)=K(be2:be2+2,be2:be2+2)+k(4:6,4:6);
K(be3:be3+2,be3:be3+2)=K(be3:be3+2,be3:be3+2)+k(7:9,7:9);
K(be4:be4+2,be4:be4+2)=K(be4:be4+2,be4:be4+2)+k(10:12,10:12);
K(be1:be1+2,be2:be2+2)=K(be1:be1+2,be2:be2+2)+k(1:3,4:6);
K(be2:be2+2,be1:be1+2)=K(be2:be2+2,be1:be1+2)+k(4:6,1:3);
K(be1:be1+2,be3:be3+2)=K(be1:be1+2,be3:be3+2)+k(1:3,7:9);
K(be3:be3+2,be1:be1+2)=K(be3:be3+2,be1:be1+2)+k(7:9,1:3);
K(be1:be1+2,be4:be4+2)=K(be1:be1+2,be4:be4+2)+k(1:3,10:12);
K(be4:be4+2,be1:be1+2)=K(be4:be4+2,be1:be1+2)+k(10:12,1:3);
K(be2:be2+2,be3:be3+2)=K(be2:be2+2,be3:be3+2)+k(4:6,7:9);
K(be3:be3+2,be2:be2+2)=K(be3:be3+2,be2:be2+2)+k(7:9,4:6);
K(be2:be2+2,be4:be4+2)=K(be2:be2+2,be4:be4+2)+k(4:6,10:12);
K(be4:be4+2,be2:be2+2)=K(be4:be4+2,be2:be2+2)+k(10:12,4:6);
K(be3:be3+2,be4:be4+2)=K(be3:be3+2,be4:be4+2)+k(7:9,10:12);
```

```
    K(be4:be4+2,be3:be3+2)=K(be4:be4+2,be3:be3+2)+k(10:12,7:9);
end

%Εκτύπωση του μητρώου δυσκαμψίας της πλάκας
fprintf('\n\n Mitrwo dyskampsias plakas: K=\n');
disp(K)

fortio=zeros(3*Ar_komvwn,1);
for i=1:Ar_fortiwn
    fortio(3*LOADS(i,1)-2,1)=LOADS(i,2);
end

disp(fortio)

Meso1=(Y(Ar_komvwn)-Y(1))/2;
Meso2=(X(Ar_komvwn)-X(1))/2;

kel=zeros(Ar_komvwn,1);

CH1=0.45*(1-0.65*E1/E2)*exp(-0.74*H1/B);
CH2=((1+5.5*D/B)/(1+1.8*D/B))*(1-2.7*alpha)*exp(-0.4*B/H1*(1-0.6*E1/E2));
if D==0
    n=6;
else
    n=12;
end

for i=1:Ar_komvwn

    Cecc=4*(ecc1/L*(X(i,1)/Meso2-1)+ecc2/B*(Y(i,1)/Meso1-1));

kel(i,1)=kr*(0.55+CH1)*(1+12*alpha)*(1+2*CH2*(((X(i,1)+0.1*ecc1)/Meso2-
1)^n+((Y(i,1)+0.1*ecc2)/Meso1-1)^n)+Cecc);
end

I=zeros(3*Ar_komvwn);
for i=1:Ar_komvwn
    I(3*i-2,3*i-2)=kel(i,1);
end
Kol=K+I;


u=inv(Kol)*fortio;

%Εκτύπωση των μετατοπίσεων των βαθμών ελευθερίας της πλάκας
fprintf('\n\n Μετατοπίσεις: u=\n');
ij=0;
for i=1:3:3*Ar_komvwn
    ij=ij+1;
    uplot(ij,1)=u(i,1);
end

disp(uplot)
```

```
%disp(u)
%disp(k)


for i=1:Ar_komvwn
    if NODES(i,2)==0 && NODES(i,3)==Meso1
        simeio=NODES(i,1);
    end
end

for i=1:Ar_stoixeiwn
    if ELEMENTS(i,2)==simeio
        stoixio=ELEMENTS(i,1);
    end
end

jk=(X(Ar_komvwn)-X(1))/0.5+1;
M=zeros(jk,1);
V=zeros((jk-1)*2,1);
entmeg=zeros(12,1);
ij=1;
deiktis1=1;
deiktis2=2;
stoixioT=stoixio+(jk-2);



for i=stoixio:stoixioT
   w=zeros(12,1);
   be1=3*komvos1(i)-2;
   be2=3*komvos2(i)-2;
   be4=3*komvos3(i)-2;
   be3=3*komvos4(i)-2;
   w(1:3,1)=u(be1:be1+2,1);
   w(4:6,1)=u(be2:be2+2,1);
   w(7:9,1)=u(be3:be3+2,1);
   w(10:12,1)=u(be4:be4+2,1);
   entmeg=k*w;
   V(ij,1)=entmeg(1,1);
   V(ij+1,1)=entmeg(4,1);
   ij=ij+2;
   if deiktis1==1
     M(1,1)=entmeg(3,1);
     deiktis1=2;
   end
   M(deiktis2,1)=entmeg(6,1);
   deiktis2=deiktis2+1;
end

disp(V)
disp(M)
```

6. Example of a data entry file for mat analysis with proposed K_{el} equation

```
 NODES=[
1   0   0
2   0.5 0
3   1   0
4   1.5 0
5   2   0
6   2.5 0
7   3   0
8   3.5 0
9   4   0
10  4.5 0
11  5   0
12  5.5 0
13  6   0
14  6.5 0
15  7   0
16  7.5 0
17  8   0
18  8.5 0
19  9   0
20  9.5 0
21  10  0
22  0   0.5
23  0.5 0.5
24  1   0.5
25  1.5 0.5
26  2   0.5
27  2.5 0.5
28  3   0.5
29  3.5 0.5
30  4   0.5
31  4.5 0.5
32  5   0.5
33  5.5 0.5
34  6   0.5
35  6.5 0.5
36  7   0.5
37  7.5 0.5
38  8   0.5
39  8.5 0.5
40  9   0.5
41  9.5 0.5
42  10  0.5
43  0   1
44  0.5 1
45  1   1
46  1.5 1
47  2   1
48  2.5 1
```

```
49  3   1
50  3.5 1
51  4   1
52  4.5 1
53  5   1
54  5.5 1
55  6   1
56  6.5 1
57  7   1
58  7.5 1
59  8   1
60  8.5 1
61  9   1
62  9.5 1
63  10  1
64  0   1.5
65  0.5 1.5
66  1   1.5
67  1.5 1.5
68  2   1.5
69  2.5 1.5
70  3   1.5
71  3.5 1.5
72  4   1.5
73  4.5 1.5
74  5   1.5
75  5.5 1.5
76  6   1.5
77  6.5 1.5
78  7   1.5
79  7.5 1.5
80  8   1.5
81  8.5 1.5
82  9   1.5
83  9.5 1.5
84  10  1.5
85  0   2
86  0.5 2
87  1   2
88  1.5 2
89  2   2
90  2.5 2
91  3   2
92  3.5 2
93  4   2
94  4.5 2
95  5   2
96  5.5 2
97  6   2
98  6.5 2
99  7   2
100 7.5 2
101 8   2
102 8.5 2
103 9   2
104 9.5 2
105 10  2
```

```
106 0   2.5
107 0.5 2.5
108 1   2.5
109 1.5 2.5
110 2   2.5
111 2.5 2.5
112 3   2.5
113 3.5 2.5
114 4   2.5
115 4.5 2.5
116 5   2.5
117 5.5 2.5
118 6   2.5
119 6.5 2.5
120 7   2.5
121 7.5 2.5
122 8   2.5
123 8.5 2.5
124 9   2.5
125 9.5 2.5
126 10  2.5
127 0   3
128 0.5 3
129 1   3
130 1.5 3
131 2   3
132 2.5 3
133 3   3
134 3.5 3
135 4   3
136 4.5 3
137 5   3
138 5.5 3
139 6   3
140 6.5 3
141 7   3
142 7.5 3
143 8   3
144 8.5 3
145 9   3
146 9.5 3
147 10  3
148 0   3.5
149 0.5 3.5
150 1   3.5
151 1.5 3.5
152 2   3.5
153 2.5 3.5
154 3   3.5
155 3.5 3.5
156 4   3.5
157 4.5 3.5
158 5   3.5
159 5.5 3.5
160 6   3.5
161 6.5 3.5
162 7   3.5
```

```
163 7.5 3.5
164 8   3.5
165 8.5 3.5
166 9   3.5
167 9.5 3.5
168 10  3.5
169 0   4
170 0.5 4
171 1   4
172 1.5 4
173 2   4
174 2.5 4
175 3   4
176 3.5 4
177 4   4
178 4.5 4
179 5   4
180 5.5 4
181 6   4
182 6.5 4
183 7   4
184 7.5 4
185 8   4
186 8.5 4
187 9   4
188 9.5 4
189 10  4
190 0   4.5
191 0.5 4.5
192 1   4.5
193 1.5 4.5
194 2   4.5
195 2.5 4.5
196 3   4.5
197 3.5 4.5
198 4   4.5
199 4.5 4.5
200 5   4.5
201 5.5 4.5
202 6   4.5
203 6.5 4.5
204 7   4.5
205 7.5 4.5
206 8   4.5
207 8.5 4.5
208 9   4.5
209 9.5 4.5
210 10  4.5
211 0   5
212 0.5 5
213 1   5
214 1.5 5
215 2   5
216 2.5 5
217 3   5
218 3.5 5
219 4   5
```

```
220 4.5 5
221 5   5
222 5.5 5
223 6   5
224 6.5 5
225 7   5
226 7.5 5
227 8   5
228 8.5 5
229 9   5
230 9.5 5
231 10  5
232 0   5.5
233 0.5 5.5
234 1   5.5
235 1.5 5.5
236 2   5.5
237 2.5 5.5
238 3   5.5
239 3.5 5.5
240 4   5.5
241 4.5 5.5
242 5   5.5
243 5.5 5.5
244 6   5.5
245 6.5 5.5
246 7   5.5
247 7.5 5.5
248 8   5.5
249 8.5 5.5
250 9   5.5
251 9.5 5.5
252 10  5.5
253 0   6
254 0.5 6
255 1   6
256 1.5 6
257 2   6
258 2.5 6
259 3   6
260 3.5 6
261 4   6
262 4.5 6
263 5   6
264 5.5 6
265 6   6
266 6.5 6
267 7   6
268 7.5 6
269 8   6
270 8.5 6
271 9   6
272 9.5 6
273 10  6
274 0   6.5
275 0.5 6.5
276 1   6.5
```

277 1.5 6.5
278 2 6.5
279 2.5 6.5
280 3 6.5
281 3.5 6.5
282 4 6.5
283 4.5 6.5
284 5 6.5
285 5.5 6.5
286 6 6.5
287 6.5 6.5
288 7 6.5
289 7.5 6.5
290 8 6.5
291 8.5 6.5
292 9 6.5
293 9.5 6.5
294 10 6.5
295 0 7
296 0.5 7
297 1 7
298 1.5 7
299 2 7
300 2.5 7
301 3 7
302 3.5 7
303 4 7
304 4.5 7
305 5 7
306 5.5 7
307 6 7
308 6.5 7
309 7 7
310 7.5 7
311 8 7
312 8.5 7
313 9 7
314 9.5 7
315 10 7
316 0 7.5
317 0.5 7.5
318 1 7.5
319 1.5 7.5
320 2 7.5
321 2.5 7.5
322 3 7.5
323 3.5 7.5
324 4 7.5
325 4.5 7.5
326 5 7.5
327 5.5 7.5
328 6 7.5
329 6.5 7.5
330 7 7.5
331 7.5 7.5
332 8 7.5
333 8.5 7.5

```
334 9   7.5
335 9.5 7.5
336 10  7.5
337 0   8
338 0.5 8
339 1   8
340 1.5 8
341 2   8
342 2.5 8
343 3   8
344 3.5 8
345 4   8
346 4.5 8
347 5   8
348 5.5 8
349 6   8
350 6.5 8
351 7   8
352 7.5 8
353 8   8
354 8.5 8
355 9   8
356 9.5 8
357 10  8
358 0   8.5
359 0.5 8.5
360 1   8.5
361 1.5 8.5
362 2   8.5
363 2.5 8.5
364 3   8.5
365 3.5 8.5
366 4   8.5
367 4.5 8.5
368 5   8.5
369 5.5 8.5
370 6   8.5
371 6.5 8.5
372 7   8.5
373 7.5 8.5
374 8   8.5
375 8.5 8.5
376 9   8.5
377 9.5 8.5
378 10  8.5
379 0   9
380 0.5 9
381 1   9
382 1.5 9
383 2   9
384 2.5 9
385 3   9
386 3.5 9
387 4   9
388 4.5 9
389 5   9
390 5.5 9
```

```
391 6   9
392 6.5 9
393 7   9
394 7.5 9
395 8   9
396 8.5 9
397 9   9
398 9.5 9
399 10  9
400 0   9.5
401 0.5 9.5
402 1   9.5
403 1.5 9.5
404 2   9.5
405 2.5 9.5
406 3   9.5
407 3.5 9.5
408 4   9.5
409 4.5 9.5
410 5   9.5
411 5.5 9.5
412 6   9.5
413 6.5 9.5
414 7   9.5
415 7.5 9.5
416 8   9.5
417 8.5 9.5
418 9   9.5
419 9.5 9.5
420 10  9.5
421 0   10
422 0.5 10
423 1   10
424 1.5 10
425 2   10
426 2.5 10
427 3   10
428 3.5 10
429 4   10
430 4.5 10
431 5   10
432 5.5 10
433 6   10
434 6.5 10
435 7   10
436 7.5 10
437 8   10
438 8.5 10
439 9   10
440 9.5 10
441 10  10];

ELEMENTS=[
1   1   2   23  22
2   2   3   24  23
3   3   4   25  24
4   4   5   26  25
```

5	5	6	27	26
6	6	7	28	27
7	7	8	29	28
8	8	9	30	29
9	9	10	31	30
10	10	11	32	31
11	11	12	33	32
12	12	13	34	33
13	13	14	35	34
14	14	15	36	35
15	15	16	37	36
16	16	17	38	37
17	17	18	39	38
18	18	19	40	39
19	19	20	41	40
20	20	21	42	41
21	22	23	44	43
22	23	24	45	44
23	24	25	46	45
24	25	26	47	46
25	26	27	48	47
26	27	28	49	48
27	28	29	50	49
28	29	30	51	50
29	30	31	52	51
30	31	32	53	52
31	32	33	54	53
32	33	34	55	54
33	34	35	56	55
34	35	36	57	56
35	36	37	58	57
36	37	38	59	58
37	38	39	60	59
38	39	40	61	60
39	40	41	62	61
40	41	42	63	62
41	43	44	65	64
42	44	45	66	65
43	45	46	67	66
44	46	47	68	67
45	47	48	69	68
46	48	49	70	69
47	49	50	71	70
48	50	51	72	71
49	51	52	73	72
50	52	53	74	73
51	53	54	75	74
52	54	55	76	75
53	55	56	77	76
54	56	57	78	77
55	57	58	79	78
56	58	59	80	79
57	59	60	81	80
58	60	61	82	81
59	61	62	83	82
60	62	63	84	83
61	64	65	86	85

62 65 66 87 86
63 66 67 88 87
64 67 68 89 88
65 68 69 90 89
66 69 70 91 90
67 70 71 92 91
68 71 72 93 92
69 72 73 94 93
70 73 74 95 94
71 74 75 96 95
72 75 76 97 96
73 76 77 98 97
74 77 78 99 98
75 78 79 100 99
76 79 80 101 100
77 80 81 102 101
78 81 82 103 102
79 82 83 104 103
80 83 84 105 104
81 85 86 107 106
82 86 87 108 107
83 87 88 109 108
84 88 89 110 109
85 89 90 111 110
86 90 91 112 111
87 91 92 113 112
88 92 93 114 113
89 93 94 115 114
90 94 95 116 115
91 95 96 117 116
92 96 97 118 117
93 97 98 119 118
94 98 99 120 119
95 99 100 121 120
96 100 101 122 121
97 101 102 123 122
98 102 103 124 123
99 103 104 125 124
100 104 105 126 125
101 106 107 128 127
102 107 108 129 128
103 108 109 130 129
104 109 110 131 130
105 110 111 132 131
106 111 112 133 132
107 112 113 134 133
108 113 114 135 134
109 114 115 136 135
110 115 116 137 136
111 116 117 138 137
112 117 118 139 138
113 118 119 140 139
114 119 120 141 140
115 120 121 142 141
116 121 122 143 142
117 122 123 144 143
118 123 124 145 144

```
119 124 125 146 145
120 125 126 147 146
121 127 128 149 148
122 128 129 150 149
123 129 130 151 150
124 130 131 152 151
125 131 132 153 152
126 132 133 154 153
127 133 134 155 154
128 134 135 156 155
129 135 136 157 156
130 136 137 158 157
131 137 138 159 158
132 138 139 160 159
133 139 140 161 160
134 140 141 162 161
135 141 142 163 162
136 142 143 164 163
137 143 144 165 164
138 144 145 166 165
139 145 146 167 166
140 146 147 168 167
141 148 149 170 169
142 149 150 171 170
143 150 151 172 171
144 151 152 173 172
145 152 153 174 173
146 153 154 175 174
147 154 155 176 175
148 155 156 177 176
149 156 157 178 177
150 157 158 179 178
151 158 159 180 179
152 159 160 181 180
153 160 161 182 181
154 161 162 183 182
155 162 163 184 183
156 163 164 185 184
157 164 165 186 185
158 165 166 187 186
159 166 167 188 187
160 167 168 189 188
161 169 170 191 190
162 170 171 192 191
163 171 172 193 192
164 172 173 194 193
165 173 174 195 194
166 174 175 196 195
167 175 176 197 196
168 176 177 198 197
169 177 178 199 198
170 178 179 200 199
171 179 180 201 200
172 180 181 202 201
173 181 182 203 202
174 182 183 204 203
175 183 184 205 204
```

176 184 185 206 205
177 185 186 207 206
178 186 187 208 207
179 187 188 209 208
180 188 189 210 209
181 190 191 212 211
182 191 192 213 212
183 192 193 214 213
184 193 194 215 214
185 194 195 216 215
186 195 196 217 216
187 196 197 218 217
188 197 198 219 218
189 198 199 220 219
190 199 200 221 220
191 200 201 222 221
192 201 202 223 222
193 202 203 224 223
194 203 204 225 224
195 204 205 226 225
196 205 206 227 226
197 206 207 228 227
198 207 208 229 228
199 208 209 230 229
200 209 210 231 230
201 211 212 233 232
202 212 213 234 233
203 213 214 235 234
204 214 215 236 235
205 215 216 237 236
206 216 217 238 237
207 217 218 239 238
208 218 219 240 239
209 219 220 241 240
210 220 221 242 241
211 221 222 243 242
212 222 223 244 243
213 223 224 245 244
214 224 225 246 245
215 225 226 247 246
216 226 227 248 247
217 227 228 249 248
218 228 229 250 249
219 229 230 251 250
220 230 231 252 251
221 232 233 254 253
222 233 234 255 254
223 234 235 256 255
224 235 236 257 256
225 236 237 258 257
226 237 238 259 258
227 238 239 260 259
228 239 240 261 260
229 240 241 262 261
230 241 242 263 262
231 242 243 264 263
232 243 244 265 264

233 244 245 266 265
234 245 246 267 266
235 246 247 268 267
236 247 248 269 268
237 248 249 270 269
238 249 250 271 270
239 250 251 272 271
240 251 252 273 272
241 253 254 275 274
242 254 255 276 275
243 255 256 277 276
244 256 257 278 277
245 257 258 279 278
246 258 259 280 279
247 259 260 281 280
248 260 261 282 281
249 261 262 283 282
250 262 263 284 283
251 263 264 285 284
252 264 265 286 285
253 265 266 287 286
254 266 267 288 287
255 267 268 289 288
256 268 269 290 289
257 269 270 291 290
258 270 271 292 291
259 271 272 293 292
260 272 273 294 293
261 274 275 296 295
262 275 276 297 296
263 276 277 298 297
264 277 278 299 298
265 278 279 300 299
266 279 280 301 300
267 280 281 302 301
268 281 282 303 302
269 282 283 304 303
270 283 284 305 304
271 284 285 306 305
272 285 286 307 306
273 286 287 308 307
274 287 288 309 308
275 288 289 310 309
276 289 290 311 310
277 290 291 312 311
278 291 292 313 312
279 292 293 314 313
280 293 294 315 314
281 295 296 317 316
282 296 297 318 317
283 297 298 319 318
284 298 299 320 319
285 299 300 321 320
286 300 301 322 321
287 301 302 323 322
288 302 303 324 323
289 303 304 325 324

290 304 305 326 325
291 305 306 327 326
292 306 307 328 327
293 307 308 329 328
294 308 309 330 329
295 309 310 331 330
296 310 311 332 331
297 311 312 333 332
298 312 313 334 333
299 313 314 335 334
300 314 315 336 335
301 316 317 338 337
302 317 318 339 338
303 318 319 340 339
304 319 320 341 340
305 320 321 342 341
306 321 322 343 342
307 322 323 344 343
308 323 324 345 344
309 324 325 346 345
310 325 326 347 346
311 326 327 348 347
312 327 328 349 348
313 328 329 350 349
314 329 330 351 350
315 330 331 352 351
316 331 332 353 352
317 332 333 354 353
318 333 334 355 354
319 334 335 356 355
320 335 336 357 356
321 337 338 359 358
322 338 339 360 359
323 339 340 361 360
324 340 341 362 361
325 341 342 363 362
326 342 343 364 363
327 343 344 365 364
328 344 345 366 365
329 345 346 367 366
330 346 347 368 367
331 347 348 369 368
332 348 349 370 369
333 349 350 371 370
334 350 351 372 371
335 351 352 373 372
336 352 353 374 373
337 353 354 375 374
338 354 355 376 375
339 355 356 377 376
340 356 357 378 377
341 358 359 380 379
342 359 360 381 380
343 360 361 382 381
344 361 362 383 382
345 362 363 384 383
346 363 364 385 384

```
347 364 365 386 385
348 365 366 387 386
349 366 367 388 387
350 367 368 389 388
351 368 369 390 389
352 369 370 391 390
353 370 371 392 391
354 371 372 393 392
355 372 373 394 393
356 373 374 395 394
357 374 375 396 395
358 375 376 397 396
359 376 377 398 397
360 377 378 399 398
361 379 380 401 400
362 380 381 402 401
363 381 382 403 402
364 382 383 404 403
365 383 384 405 404
366 384 385 406 405
367 385 386 407 406
368 386 387 408 407
369 387 388 409 408
370 388 389 410 409
371 389 390 411 410
372 390 391 412 411
373 391 392 413 412
374 392 393 414 413
375 393 394 415 414
376 394 395 416 415
377 395 396 417 416
378 396 397 418 417
379 397 398 419 418
380 398 399 420 419
381 400 401 422 421
382 401 402 423 422
383 402 403 424 423
384 403 404 425 424
385 404 405 426 425
386 405 406 427 426
387 406 407 428 427
388 407 408 429 428
389 408 409 430 429
390 409 410 431 430
391 410 411 432 431
392 411 412 433 432
393 412 413 434 433
394 413 414 435 434
395 414 415 436 435
396 415 416 437 436
397 416 417 438 437
398 417 418 439 438
399 418 419 440 439
400 419 420 441 440];

LOADS=[
   1   100
```

```
   11  200
   21  100
   211 200
   221 400
   231 200
   421 100
   431 200
   441 100];

E1=10000;
E2=100000000000000000;
pois=0.49;

B=10;
L=10;
D=6;

alpha=0;

ecc1=0;
ecc2=0;

H1=100;

Cf=0.85*(L/B)^0.45/(1+0.1*(2+L/B)*B/H1)^(1+exp(5*pois^3));
Df=1+(0.27-0.12*log(pois))*(1-exp(-0.83*(D/B)^0.83));
kr=E1*0.5^2*Df/Cf/(1-pois^2)/B;
```